Novel Aspects of Distributed Antenna Systems in 5G and Beyond

Von der Fakultät für Ingenieurwissenschaften,
Abteilung Elektrotechnik und Informationstechnik
der Universität Duisburg-Essen

zur Erlangung des akademischen Grades

Doktor der Ingenieurwissenschaften (Dr.-Ing.)

genehmigte Dissertation

von

Sundar Daniel Victor Peethala

aus

Rajahmundry, Indien

Gutachter:
Prof. Dr.-Ing. Thomas Kaiser
Prof. Dr.-Ing. Andreas Czylwik
Dr. Tao Chen

Tag der mündlichen Prüfung: 08.12.2020

ACKNOWLEDGEMENTS

I am deeply indebted to my ”Doktorvater”, Prof. Dr.-Ing. Thomas Kaiser, for his fundamental role in my doctoral work. My sincere gratitude to Thomas for giving me this opportunity to pursue my Ph.D. work at DSV. I am much thankful for his continuous trust in my abilities, which has given me immense motivation and focus to give my very best in my professional career and research work. I appreciate the freedom he has given to me in selecting the areas of my interest and his support towards my ideas related to implementation and building of real-time standard complaint prototypes for novel technologies. In the past 12 years of my association with Thomas both professionally and personally, I have always known him as a highly energetic and motivating person, who is also a great visionary with an innate ability to constructively guide and help in making correct and sustainable decisions. His innate abilities and very strong expertise in signal processing and wireless communication technologies have been of a great value in selecting, formulating and pursuing my research work. Without his continuous support, motivation and trust I simply could not have completed my thesis.

I am grateful to Prof. Dr.-Ing. Andreas Czylwik, Professor in Nachrichtentechnische Systeme (NTS) at Universität Duisburg-Essen, Duisburg, for his efforts and interest to diligently and constructively evaluate my thesis.

I am very much grateful to Dr. Tao Chen, Senior researcher at VTT Finland and Honorary Professor at University of Kent, who has accepted my request to be the third evaluator of my thesis. Tao was the project coordinator of flagship 5GPPP COHERENT project, where I was involved for more than 3 years.Tao’s recognition of the COHERENT work published in this thesis is a great honour for my work.

I express my gratitude and appreciation to Mr. Theo Kreul, with whom I have closely worked for 6 years on European Commission funded research projects, FP7 ABSOLUTE and 5GPPP-H2020-COHERENT. Theo spent a lot of his time in technical discussions for real-time

testbed implementations, reviewing my publications and thesis, and sharing his invaluable insights from his vast experience. Theo is best known in DSV for his diligence, patience and foresightedness, which have greatly benefited me in my research work and thesis.

My sincere thanks to my close colleague Mr. Marc Hoffmann for his constant support and help in reviewing my thesis. I would also like to thank Dr. Feng Zheng for spending his time to review my thesis and research work.

My appreciation and gratitude to Mrs. Sabine Jankowski for her care in planing and advising me of many important things starting from Day 1 at DSV.

I am grateful to all the partners of 5GPPP COHERENT project for the 3 years of endless interesting brainstorming sessions for COHERENT solution and COHERENT architecture, which have benefited much to my research work. In this regard, I express my appreciation to my colleague Mr. Nidal Zarifeh for the interesting discussions and help.

I am also thankful to my former colleagues Dr. Ali Ramadan Ali and Mr. Ammar Kabbani for their hardwork and support in building up of LTE based real-time testbed for ABSOLUTE project.

I would like to convey my gratitude to all other colleagues at DSV for providing a nice, friendly, motivating and supportive atmosphere for research activities.

My heartfelt thanks to my dearest wife Olive and my little daughters Eliana and Shiloh for their endurance, encouragement and persistent support, which has made my thesis completion possible. I am also grateful to my parents and brother for their encouragement and support. Above all, I thank my Lord and Saviour Jesus Christ, giver of eternal life, for HIS grace and favour all through this time.

ABSTRACT

Mobile communications technology has been revolutionizing people's life and work. To meet the ever-increasing demands for varied wireless services, the International Telecommunication Union (ITU) has recently defined challenging requirements for Fifth Generation (5G) and Beyond mobile networks. This thesis work is motivated by the flagship 5G enhanced Mobile Broad Band (eMBB) *hotspot* scenario, which represents crowded or dense mobile devices scenarios such as stadiums, shopping malls and marketplaces. Hotspot scenario sets very high requirement on one of the key capabilities of 5G, *Area traffic capacity* (10 Mbit/s/m^2), which is the total throughput served per coverage area. In the recent years, centralized processing architecture with distributed Remote Radio Heads (RRHs) called Centralized Radio Access Network (C-RAN) or Cloud-RAN has emerged as a very viable and fitting solution for hotspots. At lower layers, Distributed Antenna System (DAS) technology is well known to offer significant benefits over the conventional cellular systems such as improved coverage, improved throughput and connection density. Driven by the huge potential of C-RAN architecture and DAS technology, this thesis focuses at first on designing a *novel* lower layer framework for DAS, corresponding to the key design principles of 5G and Beyond systems, namely *reliability* and *flexibility*. In this thesis, *reliability* is defined as the probability of achieving a minimum required Signal-to-Interference-plus-Noise-Ratio (SINR) at the User Equipment (UE) location. In this regard, a *novel* RRH distribution model is presented, besides deriving lower layers reliability in Non-Line-Of-Sight (NLOS) and Line-Of-Sight (LOS) channel conditions.

In order to address the challenging requirements set forth in hotspot scenario, a pertinent DAS transmission scheme called paired selection transmission is investigated. Based on the novel reliability framework, three key challenges utilizing this transmission scheme are identified, formulated and analyzed. These key challenges are: formation of (UE, RRH) pairs, rapid frequency reuse and Downlink (DL) transmit power allocation among RRHs within a frequency

reuse group. In order to achieve effective frequency reuse, based on the users' *reliability* and throughput requirements, a *novel* minimum reuse distance is derived. DL transmit power allocation among the reuse RRHs is addressed by using optimum solutions from cooperative game theory in conjunction with *reliability* based *novel* utility function. In this regard, the existence, uniqueness and fairness of the formulated cooperative game are proved analytically by validating all the Nash conditions and proved the existence of an optimal and unique Nash Bargaining Solution (NBS). Furthermore, iterative Nash bargaining algorithms are developed and implemented using MATLAB simulation models which are shown to converge to a Pareto-optimal equilibrium. The simulation results show how the reduction in RRH coverage area decreases the reuse distance which helps to achieve multifold improvement in throughput and area traffic capacity.

The latter part of the thesis aims at investigating the challenges faced by C-RAN / DAS in a realistic ultra-dense Heterogeneous Mobile Networks (HMN). HMN pose challenges to C-RAN / DAS primarily because of the coexistence of C-RAN / DAS with high radiating power base stations. Consequently, a *novel* flexible and programmable Software Defined Networking (SDN) based RAN architecture is presented, which is shown to have the ability to efficiently perform the control and coordination in HMN. The *novel* Network Graphs (NG) based abstraction and control framework methodologies for efficient pairing and scheduling of resources in C-RAN / DAS systems in HMN are outlined. Lastly, the system design and implementation aspects of Long Term Evolution (LTE) based real-time C-RAN / DAS testbed, which is implemented on a Software Defined Radio (SDR) platform, are presented. The validation of some of the aspects of *reliability* based solutions presented in this thesis is achieved by observing Error Vector Magnitude (EVM) measurements on a commercial LTE test equipment.

In this thesis, based on *novel reliability* framework and the proposed solutions for 5G and Beyond eMBB *hotspot* scenarios and practical ultra-dense HMN, it will be shown that C-RAN / DAS technology has the potential to meet the challenging capabilities of multifold increase in system throughput and area traffic capacity via dense deployment of RRHs and rapid frequency reuse while maintaining *reliability* and *fairness* among UEs.

ZUSAMMENFASSUNG

Die mobile Kommunikation hat das Leben und die Arbeit der Menschen stark verändert. Um die stetig steigende Nachfrage nach drahtlosen Diensten zu befriedigen, hat die Internationale Fernmeldeunion (engl. International Telecommunication Union, ITU) kürzlich herausfordernde Vorgaben für 5G und die zukünftigen Mobilfunknetze aufgestellt. Die vorliegende Dissertation ist durch das 5G enhanced Mobile Broad Band (deutsch erweiterte mobile Breitband, eMBB) *Hotspot* Szenario motiviert worden, in dem viele mobile Geräte auf engem Raum unterstützt werden sollen, wie z.B. in Stadien, Einkaufszentren oder auf Marktplätzen. Diese Szenarien stellen die hohe Anforderung von 10 Mbit/s/m^2 an den Datendurchsatz pro Quadratmeter (engl. Area traffic capacity), hierbei handelt es sich um eine Schlüsselfähigkeit von 5G. In den letzten Jahren sind zentralverarbeitende Architekturen mit entfernt installierten Sende- und Empfangseinheiten (engl. Remote Radio Heads, RRHs), genannt zentralisiertes Funkzugangsnetz (engl. Centralized Radio Access Network, C-RAN or Cloud-RAN), als praktikable Lösung für Hotspot Szenarien erschienen. Für die unteren Protokollschichten ist bekannt, dass die Technik der verteilten Antennensysteme (engl. Distributed Antenna Systems, DAS) entscheidende Vorteile gegenüber herkömmlichen Zellennetzen aufweist, wie z.B. verbesserte Abdeckung, höhere Datenraten und eine höhere Verbindungsdichte. Getrieben durch das enorme Potenzial von C-RAN Architektur und DAS Technologie, konzentriert sich diese Dissertation zunächst auf die Entwicklung eines DAS-Lösungsansatzes für die unteren Protokollschichten, entsprechend den Schlüsselprinzipien für den Entwurf von 5G und zukünftigen Systemen, nämlich *Zuverlässigkeit* und *Flexibilität*. In dieser Arbeit ist *Zuverlässigkeit* durch die Wahrscheinlichkeit, einen minimalen Signal-Störer-Rauschabstand (engl. Signal-to-Interference-plus-Noise-Ratio, SINR) am Ort des Endnutzers (engl. User Equipment, UE) erreichen zu können, definiert. Dafür wird neben der Herleitung der *Zuverlässigkeit* bei Funkkanälen mit und ohne Sichtverbindung (engl. Line-Of-Sight, LOS, Non-Line-Of-Sight, NLOS) für die unteren Protokollschichten ein *neuartiges* RRH Verteilungs-Model präsentiert.

Um die anspruchsvollen Vorgaben für Hotspot Szenarien zu erfüllen, wird ein geeignetes DAS Übertragungsschema, genannt Paired Selection Transmission, untersucht. Basierend auf dem neu entwickelten Gerüst für die *Zuverlässigkeit* werden drei wesentliche Herausforderungen identifiziert, beschrieben und analysiert. Diese sind: die Identifizierung geeigneter UE-RRH-Paare, räumlich dichte Wiederverwendung gleicher Frequenzen und die Zuweisung der Sendeleistung auf der Abwärtsstrecke (engl. Downlink, DL) innerhalb der RRHs einer Gruppe der wiederverwendeten Frequenz. Es wird ein *neuer* Ansatz für die minimale Wiederverwendungsdistanz entwickelt, um basierend auf den Anforderungen an die *Zuverlässigkeit* und den Durchsatz beim Nutzer eine wirkungsvolle Frequenzwiederverwendung zu erreichen. Die Zuweisung der DL Sendeleistung innerhalb der RRHs wird mit Hilfe von optimalen Lösungsansätzen aus der Kooperativen Spieltheorie unter Berücksichtigung einer *neuen*, auf *Zuverlässigkeit* basierenden Nutzenfunktion (engl. utility function) ermittelt. In diesem Fall werden die Existenz, die Eindeutigkeit und die Fairness des formulierten kooperativen Spiels analytisch durch die Erfüllung aller von Nash aufgestellten Bedingungen überprüft und die Existenz einer optimalen und eindeutigen Nash'schen Verhandlungslösung (engl. Nash Bargaining Solution, NBS) bewiesen. Dazu werden iterative Algorithmen der Nash-Verhandlung entwickelt und in MATLAB simuliert, und es wird gezeigt, dass diese zu einem pareto-optimalen Gleichgewicht konvergieren. Die Simulationsergebnisse zeigen, dass die Reduzierung der Abdeckungsfläche durch die RRH auch die Wiederverwendungsdistanz verkleinert, was Verbesserungen im Gesamtdatendurchsatz und im Datendurchsatz pro Quadratmeter bringt.

Der nächste Teil dieser Dissertation beschäftigt sich mit den Herausforderungen, die sich in einem realen, ultra-dichten heterogenen Mobilfunknetz (engl. Heterogeneous Mobile Network, HMN) für C-RAN / DAS ergeben. Dabei liegt die wesentliche Herausforderung in der Koexistenz von C-RAN / DAS und Basisstationen mit hoher Sendeleistung. In der Folge wird eine *neuartige* flexible und über ein softwarebasiertes Netzwerk (engl. Software Defined Network, SDN) programmierbare RAN Architektur vorgestellt, die die Fähigkeit einer effizienten Kontrolle und Koordinierung im HMN aufweist. Es wird ein *neuartiger*, auf Netzwerkgraphen (engl. Network Graphs, NG) aufbauender Abstraktions- und Kontrollansatz für die effiziente Paarung und Verteilung (engl. Scheduling) der Ressourcen in C-RAN / DAS Systemen für HMN präsentiert. Zum Schluss werden Systementwurf und Implementierungsaspekte für eine LTE

basierte, echtzeitfähige C-RAN / DAS Testumgebung an Hand einer Implementierung auf einer Software definierten Funkplattform (engl. Software Defined Radio, SDR) gezeigt. Die Gültigkeit einiger der auf *Zuverlässigkeit* basierenden Lösungen, die in dieser Dissertation diskutiert werden, wird exemplarisch mit Hilfe von EVM (engl. Error Vector Magnitude) Messungen mit einem kommerziellen LTE Testgerät nachgewiesen.

In dieser Arbeit wird gezeigt, dass die C-RAN / DAS Technologie das Potenzial hat, die Herausforderungen in Bezug auf Gesamtdatendurchsatz und Datendurchsatz pro Quadratmeter durch dichten Einsatz von RRHs und Frequenz-Wiederverwendung, unter Wahrung von *Zuverlässigkeit* und *Fairness* zwischen den Nutzern, zu lösen.

Contents

1 State of the Art and Motivation **1**

1.1 5G and Beyond 1

1.2 Motivation 6

1.2.1 C-RAN / DAS 6

1.2.2 Reliability and Flexibility 9

1.3 Outline and Main Contributions 11

2 Novel Framework for C- RAN / DAS in 5G and Beyond **15**

2.1 Hexagonal Circle Packing 16

2.2 System Model 18

2.3 Reliability 20

2.3.1 Non-Line-Of-Sight 21

2.3.2 Line-Of-Sight 22

2.4 Simulation Results 26

2.4.1 Simulation Model 26

2.4.2 Reliability 27

2.5 Conclusion 32

3 Key Challenges in C-RAN / DAS for 5G and Beyond **35**

3.1 Key Challenges 35

3.2 System Model and Methodology 38

3.2.1 System Model 38

3.2.2 Reliability 38

3.3 Pairing 39

3.4 Frequency Reuse 40

3.4.1 Problem Formulation . . . 40
3.4.2 Minimum Reuse Distance . . . 41
3.5 Power Allocation . . . 43
3.5.1 Problem Formulation . . . 43
3.5.2 Problem Definition . . . 44
3.5.3 Design of Novel Utility Function . . . 46
3.5.4 Derivation of Nash Bargaining Solution . . . 50
3.6 Simulation Results . . . 55
3.6.1 Simulation Model . . . 55
3.6.2 Frequency Reuse . . . 57
3.6.3 Power Allocation . . . 59
3.6.4 Throughput Improvement . . . 61
3.7 Conclusion . . . 64

4 C-RAN / DAS in 5G and Beyond Heterogeneous Mobile Networks 67
4.1 5G and Beyond Heterogeneous Mobile Networks . . . 67
4.1.1 Introduction and Challenges . . . 67
4.1.2 COHERENT Solution . . . 72
4.2 COHERENT Architecture . . . 78
4.2.1 Terminology . . . 79
4.2.2 Overview . . . 80
4.2.3 Control and Coordination . . . 83
4.2.4 Abstraction and Network Graphs . . . 84
4.3 C-RAN / DAS in HMN . . . 89
4.3.1 Motivation and Goals . . . 89
4.3.2 Generation and Usage of Network Graphs . . . 92
4.3.3 Abstracted Parameters . . . 94
4.3.4 Simulation Results . . . 95
4.4 Conclusion . . . 101

5 Real-time C-RAN / DAS Testbed and Measurement Results 103
5.1 System Design . . . 103

5.1.1 TMS320C6670 DSP . . . 105
5.1.2 Antenna Interface 2 (AIF2) . . . 108
5.1.3 Radio Front-end . . . 113
5.2 Adaptations in LTE for C-RAN / DAS . . . 115
5.2.1 Introduction - LTE PHY Downlink . . . 116
5.2.2 Adaptations - LTE PHY Downlink . . . 119
5.2.3 Adaptations - LTE Procedures . . . 122
5.3 Implementation and Validation . . . 124
5.3.1 DAS Engine . . . 125
5.3.2 Mapper . . . 126
5.3.3 AIF2 . . . 128
5.3.4 Validation . . . 128
5.4 Testbed and Measurement setup . . . 129
5.4.1 Testbed . . . 129
5.4.2 Measurement setup . . . 131
5.5 Measurement Scenarios and Results . . . 132
5.5.1 Measurement Scenario 1 . . . 136
5.5.2 Measurement Scenario 2 . . . 139
5.5.3 Measurement Scenario 3 . . . 143
5.5.4 Measurement Scenario 4 . . . 145
5.6 Conclusion . . . 148

6 Conclusions and Future Work **149**
6.1 Conclusions . . . 149
6.2 Future Work . . . 152

List of Publications **155**

Bibliography **158**

List of Figures

1.1 Envisioned use case scenarios of IMT for 2020 and Beyond [1] 1

1.2 Work flow diagram and inter-relation between chapters in this thesis 11

2.1 DAS RRHs distribution based on Hexagonal circle packing 17

2.2 Total Tx Power saved in DAS w.r.t. CAS for the same coverage 18

2.3 C-RAN system model with distributed RRHs and CU 19

2.4 DAS distribution with 61 RRHs 27

2.5 DAS distribution with 169 RRHs 29

2.6 Reliability in case of $\mathbf{K}_{\mathbf{ri}}^{\mathbf{k,N}} = -\infty$ dB, varying $\mathbf{K}_{\mathbf{ri}}^{\mathbf{k,r_k}}$ 30

2.7 Reliability in case of $\mathbf{K}_{\mathbf{ri}}^{\mathbf{k,r_k}}$ = 12dB, varying $\mathbf{K}_{\mathbf{ri}}^{\mathbf{k,N}}$ 30

2.8 Reliability in case of varying the distances of interferers, with $\mathbf{K}_{\mathbf{ri}}^{\mathbf{k,r_k}}$ = 12 dB, $\mathbf{K}_{\mathbf{ri}}^{\mathbf{k,N}} = -\infty$ dB 31

3.1 DAS distribution with 169 RRHs 56

3.2 RRH reuse distance factor (in terms of RRH coverage radius) Vs Number of reuse RRHs, varying SINR requirement of UE k. UE j, k are at RRH coverage edge. Reliability, SINR requirements of $(j, k) = (0.8, 0.8), (20dB, 20dB)$ . . . 57

3.3 RRH reuse distance factor (in terms of RRH coverage radius) Vs UE k distance factor, varying UE j distance factor. Reliability, SINR requirements of $(j, k) = (0.8, 0.8), (20dB, 20dB)$ 58

3.4 Convergence of transmit power allocation among reuse RRHs in iterative NBS in $Algorithm1$ and $Algorithm2$ 59

3.5 Convergence of reliability (utility) functions of UEs served by reuse RRHs in $Algorithm1$ and $Algorithm2$ 60

3.6 Figure showing number of reuse RRHs for different channels in the case of 127 RRHs 61

3.7 Figure showing number of reuse RRHs for different channels in the case of 271 RRHs 62
3.8 X fold Throughput improvement in comparison with single cell Vs Targeted SINR for different number of RRHs packed 63
3.9 Reuse distance in meters Vs Targeted SINR for different number of RRHs packed 64

4.1 Example of Heterogeneous Mobile Network Scenario 68
4.2 Block diagram showing control split in COHERENT, i.e., Network wide control and real-time control [2, 3] 76
4.3 COHERENT Architecture [2, 3] 81
4.4 Control and coordination functional architecture for HMN [2, 3] 83
4.5 An example downlink Network Graph showing interference [2, 4] 87
4.6 Abstraction flow for the formulation of network graph in C3 instance [4] 88
4.7 Abstraction flow for the network graph in RTC instance [4] 89
4.8 C-RAN / DAS in 5G and Beyond HMN: Coexistence with LTE CAS 90
4.9 C-RAN / DAS in 5G and Beyond HMN: NG representation based on definition 93
4.10 C-RAN / DAS in 5G and Beyond HMN: Generation of NG in NIF for the communication from RTC to CU and CAS eNodeB 93
4.11 MATLAB based GUI for generation of NGs in C-RAN / DAS 96
4.12 NG formulated for pairing of $UE1$, for a targeted SINR of 20 dB 97
4.13 NG formulated for pairing of $UE5$, for a targeted SINR of 15 dB 98
4.14 NG formulated for pairing of $UE5$, for a targeted SINR of 20 dB 98
4.15 C-RAN / DAS in HMN: Efficient scheduling of resources in Interference scenario 99
4.16 NG for efficient scheduling 100

5.1 Hardware blocks and Software Partition on DSP [5] 104
5.2 TMS320C6670 relevant functional blocks [6] 106
5.3 Functional block diagram of Dual 6670 AMC module [7] 108
5.4 LTE frame timing 110
5.5 CPRI 4x Basic Frame Vs. LTE Bandwidth [8] 111
5.6 CPRI 2x Basic Frame Vs. LTE Bandwidth [8] 112
5.7 Table showing CPRI number of AxCs per link Vs. LTE Bandwidth [8] 112

5.8 Front panel of HHI's Radio Front-end [9] . . . 113
5.9 Block diagram of SDR Transceiver [9] . . . 114
5.10 GUI for Radio Front-end Configuration [9] . . . 115
5.11 LTE PHY Downlink Channels structure in a subframe . . . 117
5.12 PDSCH processing chain adaptations for DAS [10] . . . 120
5.13 PDSCH bit level processing . . . 121
5.14 Central Unit DL PHY processing Architecture . . . 125
5.15 DAS Engine Functional layout . . . 126
5.16 Mapper Functional layout . . . 127
5.17 LTE based DAS eNodeB setup with 2 RRHs [11] . . . 129
5.18 Micro-TCA Chassis with AMC modules and interfaces [12] . . . 130
5.19 Keysight's MXA Measurement equipment with 89600 VSA software [12] . . . 131
5.20 LTE based C-RAN / DAS Central Unit with 2 RRHs [12] . . . 132
5.21 Indoor lab layout. Pictorial representation of signals transmitted from RRH1 and RRH2 [12] . . . 133
5.22 RRHs and UE positions in Measurement scenario 1 [12] . . . 136
5.23 Scenario 1: EVM measurements and constellation diagrams [12] . . . 137
5.24 Scenario 1: NG showing Reliability for 20 dB SINR at UE position with varying SINR level experienced at UE location [12] . . . 138
5.25 RRHs and UE postions in Measurement scenario 2 [12] . . . 139
5.26 scenario 2: EVM measurements and constellation diagrams [12] . . . 141
5.27 Scenario 2: NG showing Reliability for 20 dB SINR at UE position with varying SINR level experienced at UE location [12] . . . 142
5.28 RRHs and UE positions in Measurement scenarios 3 and 4 [12] . . . 143
5.29 Scenario 3: EVM measurements and constellation diagrams [12] . . . 144
5.30 scenario 4: EVM measurements and constellation diagrams [12] . . . 146
5.31 Scenarios 3 and 4: NG showing Reliability for 15 dB SINR at UE position with varying SINR level experienced at UE location [12] . . . 147

List of Tables

1.1 Key Capabilities of 5G and Beyond for eMBB use case 3
1.2 Key Capabilities of 5G and Beyond for URLLC use case 4
1.3 Key capabilities of 5G and Beyond for mMTC use case 4

2.1 Simulation Parameters for Reliability analysis 28

3.1 Simulation Parameters for Power allocation 56
3.2 NBS Algorithm Parameters 59

4.1 Exposed Parameters [13] 95
4.2 Controlled Parameters [13] 95

5.1 LTE configuration parameters [12] 134
5.2 3GPP LTE EVM Requirements [14] 135
5.3 Scenario 1: CRC and EVM measurement results [12] 136
5.4 Scenario 2: CRC and EVM measurement results [12] 140
5.5 Scenario 3: CRC and EVM measurement results [12] 143
5.6 Scenario 4: CRC and EVM measurement results [12] 145

LIST OF ACRONYMS

3GPP	The 3rd Generation Partnership Project
4G	The 4th Generation mobile communications
5G	The 5th Generation mobile communications
5GPPP	The 5th Generation Public Private Partnership
ADC	Analog to Digital Converter
AIF2	Antenna Interface module 2
ARQ	Automatic Repeat reQuest
BRAN	Boadband Radio Access Network
BS	Base station
C3	Central Controller and Coordinator
C-RAN	Centralized Radio Access Network
CCE	Control Channel Element
CNV	Centralized Network View
CP	Cyclic Prefix
CPRI	Common Public Radio Interface
CRC	Cyclic Redundancy Check
CQI	Channel Quality Indicator
CU	Central Unit
D2D	Device to Device communication
DAS	Distributed Antenna System
DL	Downlink transmission
DMA	Direct Memory Access
DSP	Digital Signal Processor
EARFCN	E-UTRA Absolute Radio Frequency Channel Number

eICIC	enhanced Inter-Cell Interference Coordination
eMBB	enhanced Mobile Broadband
EPC	Evolved Packet Core
ETSI	European Telecommunications Standards Institute
EVM	Error Vector Magnitude
FFT	Fast Fourier Transform
FR1	Feature Release 1
FR2	Feature Release 2
FSPL	Free Space Path Loss
GSM	Global System for Mobile communications
H2020	HORIZON 2020
HMN	Heterogeneous Mobile Networks
ICIC	Inter-Cell Interference Coordination
IMT	International Mobile Telecommunications
IoT	Internet of Things
ITU	International Telecommunication Union
LAA	Licensed Assisted Access
LOS	Line of Sight
LSA	Licensed Spectrum Access
LTE	Long Term Evolution
M2M	Machine to Machine Communication
MIMO	Multiple Input Multiple Output
mMTC	massive Machine to Machine Communication
mmWave	millimeter Wave Communication
MAC	Medium Access Control layer
MCS	Modulation and Coding Scheme
MXA	Mixed Signal Analyzer
NBi	North Bound interface
NIF	Network Information Function
NFV	Network Function Virtualization
NG	Network Graphs

NLOS	Non Line of Sight
NR	5G New Radio
OBSAI	Open Base Station Architecture Initiative
OFDM	Orthogonal Frequency Division Multiplexing
OFDMA	Orthogonal Frequency Division Multiple Access
PBCH	Physical Broadcast Channel
PCFICH	Physical Control Format Indicator Channel
PDCCH	Physical Downlink Control Channel
PDSCH	Physical Downlink Shared Channel
PHICH	Physical Hybrid ARQ Indicator Channel
PHY	Physical layer
PSS	Primary Synchronization Sequence
QAM	Quadrature Amplitude Modulation
QOS	Quality of Service
QPSK	Quadrature Phase Shift Keying
RAN	Radio Access Network
RAT	Radio Access Technology
RB	Resource Block
RF	Radio Frequency
RLC	Radio Link Control layer
RRC	Radio Resource Control layer
RRH	Remote Radio Head
RSSI	Received Signal Strength Indicator
RT	Radio Transceiver
RTC	Real Time Controller
R-TP	Radio Transmission Point
SFR	Soft Frequency Reuse
SDR	Software Defined Radio
SDN	Software Defined Network
SINR	Signal to Interference plus Noise Ratio
SNR	Signal to Noise Ratio

SNR	Slice specific Network View
SON	Self Organizing Network
SSS	Secondary Synchronization Sequence
ST	Selection Transmission
TI	Texas Instruments
UE	User Equipment
URLLC	Ultra Reliable Low Latency Communication
UL	Uplink transmission
UMTS	Universal Mobile Telecommunications Service
V2X	Vehicle to Everything Communication
VRP	Virtual Radio Processing
VSA	Vector Signal Analyzer
WAS	Wireless Access Systems
WiFi	Wireless Fidelity

NOTATION

x	Scalar
$\mathbf{x}$	Vector
$\mathbf{X}$	Matrix
$\mathbf{X}^T$	Transpose of matrix $\mathbf{X}$
$E(\mathbf{x})$	Expected value of random variable $\mathbf{x}$
$\mathbb{R}_{++}$	represents the set of positive reals
$\mathbb{R}^N$	real coordinate space of N dimensions
$\mathbb{R}^N_{++}$	positive real coordinate space of N dimensions
$\{K\}$	represents a set of K
$k \in \{K\}$	k belongs to a set K
$\arg\max$	arguments of the maxima
$:=$	equal to by definition
$\ln$	natural logarithmic function
$\max$	the maxima
$\frac{dy}{dx}$	first order derivative of y w.r.t. x
$\frac{dy}{d^2x}$	second order derivative of y w.r.t. x
$\int_a^b f(x)dx$	Integration of $f(x)$ w.r.t. x over limits $[a, b]$

1 State of the Art and Motivation

1.1 5G and Beyond

In the recent years, mobile communication technologies have been advancing at an incredible pace. It is beyond doubt that mobile communication technologies are enriching people's lives, besides significantly impacting most of the businesses and industries thereby advancing global socio-economic development [15]. Consequently, there is an ever growing demand for novel mobile communication technologies. In order to meet the ever rising demand for higher data rates, novel services with very high quality of service and reliability, massive connectivity of smart devices etc., in recent years International Telecommunication Union (ITU) defined challenging requirements and key capabilities for International Mobile Telecommunications (IMT) for 2020 and Beyond mobile communication technologies [1].

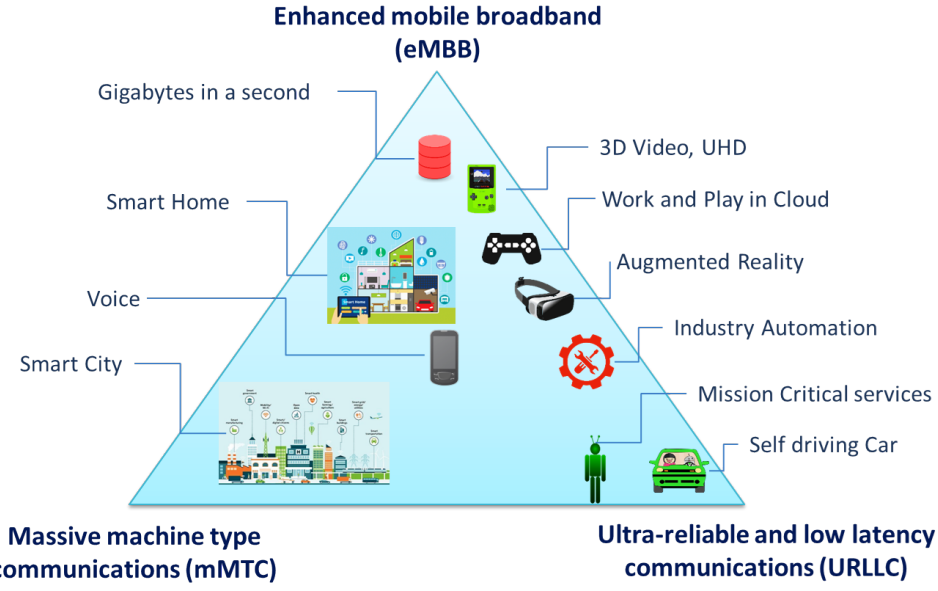

Fig. 1.1: Envisioned use case scenarios of IMT for 2020 and Beyond [1]

IMT for 2020 and Beyond [1], which serve as guidelines for 5G and Beyond systems, is conceptualized to extend the support of diverse novel services and applications, which will continue beyond the Fourth Generation mobile communications system (4G) IMT standards [1]. Fig.1.1 depicts the envisioned use case scenarios for IMT for 2020 and Beyond [1], besides showing some practical applications of the use case scenarios. As shown in the figure, varied novel technologies and services will be introduced in 5G and Beyond. Furthermore, the three corners of the pyramid, shown in the Fig.1.1, represent the three broadly classified use case scenarios defined by ITU Radiocommunication sector (ITU-R).
The use case scenarios and the key capabilities for IMT for 2020 and Beyond include [1]:

The use case scenarios presented below are extracted from ITU-R's "IMT Vision – Framework and overall objectives of the future development of IMT for 2020 and beyond" [1]

- *Enhanced Mobile Broadband (eMBB) [1]*:

  Mobile broadband use case primarily focuses on people-centered services and applications requiring broadband access to multimedia services and high speed data transfer. ITU-R envisioned that in the near future, novel applications demanding ultra fast broadband access will steadily increase, consequently a novel use case scenario called enhanced Mobile Broadband is defined. Besides supporting the current mobile broadband applications, the enhanced Mobile Broadband use case scenario comprises of novel services and requirements targeting enhanced performance and an improved consistent user experience. eMBB use case scenario focuses on a broad range of services with diverse requirements such as, wide-area coverage and hotspot [2]. *Hotspot* represents a service area comprising of high user density requiring very high throughput density, defined in 5G as *Area Traffic Capacity* [2]. Whereas, in the wide-area coverage scenario, the user data rate requirement is not so high as in the hotspot but the mobility requirement is high. Therefore, eMBB use case scenario targets to cater applications demanding very high data rates, enhanced and seamless coverage, medium to high mobility [2].

  Table 1.1 describes the key capabilities and the requirements, defined in IMT for 2020 and Beyond [1] which are tightly coupled to eMBB use case scenario. The key capabilities which are much relevant to eMBB use case scenario are peak data rate, user experienced data rate, spectrum efficiency, area traffic capacity and mobility [1]. However, the impor-

Table 1.1: Key Capabilities of 5G and Beyond for eMBB use case

(*This table is extracted from the publication "5G: A Tutorial Overview of Standards, Trials, Challenges, Deployment, and Practice" published in IEEE Journal on Selected Areas in Communications, year 2017, by M. Shafi et. al [16] and ITU-R's "IMT Vision – Framework and overall objectives of the future development of IMT for 2020 and beyond" [1]*)

Key capability	**Description**	**Targets**
Peak data rate	Maximum rate achievable per user / device	DL / UL: 20 / 10 Gbit/s
User experienced data rate	Achievable rate per user / device across coverage area	DL / UL: 100 / 50 Mbit/s (Dense Urban)
Mobility	Maximum speed of communication transfer between radio nodes with a specified QoS achieved	Up to 500 km/h
Spectrum efficiency	Average throughput per unit of spectrum resource and per cell	3 - 4 times 4G data rate
Area traffic capacity	Total throughput served per coverage / geographic area	10 Mbits/s/m^2 (Hotspot)

tance of each of the key capabilities can vary starkly in various application scenarios. For example, in indoor *hotspot* scenarios, the requirement set on user experienced data rate is very high compared to the requirement set on mobility [1]. On the other hand, the mobility is a more relevant requirement for wide area coverage case.

- *Ultra-reliable and low latency communications (URLLC) [1]*: This use case sets stringent requirements on the key capabilities, latency and reliability. Very stringent requirements are set on these key capabilities because of the mission critical services covered under this use case [2]. As shown in Fig.1.1, some services and applications that represent this use case are, tactile internet services, intelligent transport systems or autonomous driving, vehicle-to-everything (V2X) and transportation safety, remote medical surgery, disaster relief and remote control in industrial manufacturing [1].

  Table 1.2 shows the key capabilities and the target values for URLLC use case scenarios. In mission critical URLLC applications, the requirement on the latency is of very high importance. Some of the mission critical applications such as autonomous driving would require high mobility in addition to very low latency requirement [1].

- *Massive machine type communications (mMTC) [1]*: It is envisioned that there will be a

Table 1.2: Key Capabilities of 5G and Beyond for URLLC use case

(*This table is extracted from the publication "5G: A Tutorial Overview of Standards, Trials, Challenges, Deployment, and Practice" published in IEEE Journal on Selected Areas in Communications, year 2017, by M. Shafi et. al [16] and ITU-R's "IMT Vision – Framework and overall objectives of the future development of IMT for 2020 and beyond" [1]*)

Key capability	**Description**	**Targets**
Latency	Radio network contribution to packet travel time	User Plane - 1 ms
Reliability	Percentage of sent packets successfully delivered to the destination within the time constraint required by the targeted service	99.999%

huge number of connected smart devices primarily in industrial and smart city applications. Therefore, mMTC use case scenario addresses these applications and services. Connected smart devices typically transmit intermittently at a very low data rate. These applications typically have very low requirements set for latency and reliability, which implies that these low data rate transmissions are not time critical. However, because of the rapid deployment of smart devices in industrial and smart city scenarios, the use case scenario should support longer battery life of these devices.

Table 1.3: Key capabilities of 5G and Beyond for mMTC use case

(*This table is extracted from the publication "5G: A Tutorial Overview of Standards, Trials, Challenges, Deployment, and Practice" published in IEEE Journal on Selected Areas in Communications, year 2017, by M. Shafi et. al [16] and ITU-R's "IMT Vision – Framework and overall objectives of the future development of IMT for 2020 and beyond" [1]*)

Key capability	**Description**	**Targets**
Connection density	The number of connected devices per unit coverage area / geographical area	10^6 devices / km^2
Energy efficiency	The amount of data transmitted / received (in bits per second) per unit energy consumed by device / network	Equal to 4G

Table 1.3 shows the key capabilities and target values for mMTC use case scenarios. This use case scenario sets very high requirement on the key capability, *connection density*, which

is targeted to support connectivity to a very large number of devices with very low mobility. Furthermore, these connected devices are designed to be less expensive with a very long battery life, therefore this use case scenario should address these additional requirements.

The key capabilities which feature IMT 2020 and Beyond systems are *peak data rate* targeting upto 20 Gbit/s and *user experienced data rate* in dense deployments touching 100 Mbit/s [1]. In real-life crowded environments such as stadiums, shopping malls and marketplaces, requirements are set on achieving very high total throughput density and connection density. Therefore, in these scenarios, the requirements on total transmission rate reaches that of optical fiber in order to support multimedia applications such as live streaming of high quality videos and high speed gaming applications [15]. At present, 4G systems are not able to satisfy these challenging requirements in these crowded / dense scenarios [15]. As defined in Table 1.1, ITU-R has defined a new key capability called *user experienced data rate*, which helps to control and monitor the users' requirements in different use case scenarios. To satisfy users' experience in diverse services, applications and requirements, a combination of various novel technologies or approaches is needed [15]. In general, the various technologies or approaches which can significantly improve the users' experience can be classified into:

The following description of various technologies is extracted from the book "5G Wireless Systems: Simulation and Evaluation Techniques (Wireless Networks)" published by Springer in year 2017, authored by "Yang Yang et. al" [15]

- *Large Scale Antenna Technology*: Massive Multi-Input Multi-Output (MIMO) can be effective in achieving high spectral efficiency via the usage of massive number of antennas. Therefore, it has a huge potential in 5G and Beyond systems to meet the requirements on eMBB key capabilities, which are *peak data rate*, *connection density* and *user experienced data rate* [15].

- *Flexible Spectrum Usage*: In order to effectively address the highly challenging and diverse requirements of various use case scenarios, introducing novel radio access technologies is inevitable, while continuing to support the existing technologies and applications. Consequent to the rapid increase in novel mobile communication technologies such as, 5G NR, D2D, V2X, NB-IoT etc., and various novel applications, the problem of shortage of available spectral resources becomes more and more vivid. In order to effectively tackle

this problem, on one hand, the provision of expanded spectrum, e.g. using millimeter wave frequency range ($>$ 30 GHz) is needed. On other hand, there exists a need to improve efficiency in the utilization of existing spectral resources. This can be achieved by defining fair and efficient spectrum sharing between operators and via the existing 4G LTE in Unlicensed band (LTE-U) [15].

- *Ultra-Dense Wireless Network*: Ultra-dense networks can offer promising solutions to address eMBB $hotspot$ requirements on the key capabilities, *user experienced data rate*, *area traffic capacity* and *connection density*, by dense deployment of base stations of very less coverage area, which enables rapid frequency reuse. The focus of the work presented in this thesis is to employ this approach using Centralized Radio Access Networks (C-RAN) / Distributed Antenna Systems (DAS).

1.2 Motivation

1.2.1 C-RAN / DAS

The following text is derived from author's published work "Reliability Analysis of Centralized Radio Access Networks in Non-Line-of-Sight and Line-of-Sight Scenarios" published in IEEE Access, year 2019 [5]

From the physical (PHY) and medium-access-control (MAC) layers of Radio Access Network (RAN) perspective, the key capabilities of this broad set of 5G and Beyond use cases can be evaluated in terms of the well known lower layer metrics: capacity, coverage, user throughput, energy consumption, latency and *reliability* [17]. In the recent years, centralized processing architecture in RAN called as centralized RAN (C-RAN) or Cloud-RAN [18] has been proposed by researchers as one of the potential solutions for 5G and Beyond [5]. C-RAN architecture is shown in the literature [19] to have the ability to increase coverage, network capacity and energy-efficiency [5]. C-RAN primarily constitutes of two entities, a group of remote radio heads (RRHs) distributed over the serving area and a central unit (CU) [5]. In C-RAN, CU typically executes all the RAN layers functionality including baseband processing, whereas the RRHs function generally as Radio Frequency (RF) transceivers [20]. Distributed RRHs are connected to the CU through real-time fronthaul links, which are either dedicated

optical cables or Ethernet links [5]. As a lower layer technology, the centralized processing with distributed antennas has been existing in the literature as Distributed Antenna System (DAS) [21, 22]. Therefore, the lower layers DAS techniques can always be incorporated within the 5G and Beyond C-RAN architecture view. This thesis primarily focuses on the lower layers challenges in 5G and Beyond C-RAN / DAS. Therefore, the terms "C-RAN" or "DAS" are mentioned interchangeably in this thesis.

In conventional cellular systems, also called as co-located antenna systems (CAS), the antennas of the serving base station are typically co-located at the base station processing, where all the RAN layers are processed. Therefore, in CAS, the base station along with its antennas are typically co-located at the center of the cell to achieve uniform cell coverage. CAS can employ various multi-antenna techniques to improve coverage such as beamforming or sectoring, but the focus here is on the placement of antennas, which are co-located at the base station. Nevertheless, dead spots exist within the coverage area due to the effect of shadowing, which can significantly degrade the received signal strength, thereby limiting the throughput and system performance [23]. Consequently, the performance degradation is most harsh on cell-edge users experiencing shadowing because of relatively weaker signal strength received due to higher path-losses and stronger inter-cell interference [23]. In DAS, the base station antennas are distributed over the coverage area and more specifically in the dead spots. The distributed antennas are connected to the base station processing, called as central unit (CU), which can be located anywhere. Owing to the flexibility of deploying the basestation antennas distributedly, the received signal strength and in turn the system throughput can be significantly improved [23]. As a promising solution to this problem, in the literature, DAS has been proven to have the potential to improve the overall system performance by improving coverage and capacity of cellular networks [21, 23].

Significant work [24–26] on DAS to understand the benefits over conventional CAS exists in the literature. In order to illustrate the significant advantages of DAS over CAS, a DAS with M RRHs distributed over a given area, and a conventional base station with co-located antennas, is considered. For the sake of exemplification, a practical scenario with the number of RRHs set to $M = 64$, and a path loss exponent $\alpha = 3$ is considered. Now, a summary of potential benefits of DAS over CAS is presented below:

This following text is based on the publication "Performance advantages of distributed

antennas in indoor wireless communication systems", Proceedings of IEEE Vehicular Technology Conference (VTC)' 1994 by P. Chow et. al - in [27]

- *Improved Coverage area*: It is proven in [27], that for a given radiated power, a M RRHs DAS will have improved coverage area given by the expression: $Coverage\_Area_{DAS(M)} = M^{1-\frac{2}{\alpha}} Coverage\_Area_{CAS}$, where α stands for the path loss exponent. In the illustration considered, i.e., $M = 64$ and $\alpha = 3$, the improvement in DAS is by a factor 4. Therefore for the same coverage, fewer cells are required in DAS. The main advantage of using fewer cells is less hand-offs, thereby significantly improving the system latency.

- *Minimized Radiated Power*: For the same coverage, a M RRHs DAS achieves reduction in radiated power, which is given in [27] by the expression: $P^{rad}_{DAS(M)} = M^{1-\frac{\alpha}{2}} P^{rad}_{CAS}$ [27]. In the illustration scenario considered above, the reduction in total radiated power is 9 dB. The power reduction factor has a positive impact on RF hardware design and thereby cost and interference can be reduced. Similarly, the radiated power reduced per RRH is given by: $P^{rad}_{RRH} = M^{-\frac{\alpha}{2}} P^{rad}_{Antenna}$. Similarly in the illustration, the radiated power saved by a RRH is 27 dB, which is a very significant improvement. This improvement reduces the cost of RRH, allows compact hardware design and increased battery life.

- *Minimized Path Loss*: For the same coverage, a M RRHs DAS achieves reduction in maximum path loss, which is given in [27] by, $PathLoss_{DAS(M)} = M^{-\frac{\alpha}{2}} PathLoss_{CAS}$. In the illustration scenario considered above, the path loss is reduced by 27 dB, which is an advantage because the coverage is more uniform.

- *Minimized Interference*: For the same coverage, a M RRHs DAS reduces the interference power propagated, which is given in [27] by, $Intf_{DAS(M)} = M^{1-\frac{\alpha}{2}} Intf_{CAS}$. In the same example considered above, the reduction in interference power is about 9 dB compared to CAS. This reduction in interference power propagated helps to improve the spectral efficiency by rapid frequency reuse.

- *Improved Signal quality / Reliability*: Based on the above mentioned significant reductions in interference power propagated and path loss, reception of much improved Signal to Interference plus Noise Ratio (SINR) can therefore be achieved in DAS. Furthermore,

by deploying RRHs in dead spots, it is shown in [23] that DAS can effectively provide solutions for shadowing and scenarios having higher penetration losses.

- *Improved Connection density*: Since many RRHs can pair with different users independently, the number of connected users to cell can be significantly improved in DAS.
- *Improved Area traffic Capacity*: As a result of the potential reduction in interference, the scheduling resources of RRHs can be reused at shorter distances, thereby improving the total throughput per coverage area.
- *Minimized Latency*: Overall system latency can be significantly improved because of decrease in the number of handovers, as the distributed RRHs belong to the same cell. Hence, moving from one coverage area of a RRH to another doesn't require a handover, in contrast to the conventional small-cell base stations.

Consequently, C-RAN architecture and DAS schemes offer compelling benefits, which can potentially meet the key capabilities of 5G and Beyond usecase scenarios. Specifically for the eMBB indoor hotspot scenarios like stadiums, market places and shopping malls, where the area traffic capacity requirement is very high, the DAS can provide viable solutions to meet this key capability of 5G and Beyond systems via rapid frequency reuse. In this thesis, we will analyze DAS in the 5G's flagship eMBB usecase scenario.

1.2.2 Reliability and Flexibility

The following text is derived from author's published work "Reliability Analysis of Centralized Radio Access Networks in Non-Line-of-Sight and Line-of-Sight Scenarios" published in IEEE Access, year 2019 [5]

The key design principles of 5G and Beyond mobile networks, which guide all the key capabilities are, *flexibility* and *reliability* [1, 17, 28]. In 5G and Beyond systems, *flexibility* is necessary in order to effectively serve emerging use cases and services with a wide range of requirements. Therefore, *flexibility* is addressed in 5G and Beyond networks primarily at architecture level via control plane and user plane separation, programmability across the layers and network slicing based on Software Defined Networking (SDN) [29, 30] principles. On the other hand, *reliability* in 5G architectures sets the requirement on the *flexibility* and qualifies

it. This implies that, for all the use cases, services and UEs the Quality of Service (QoS) requirements can be reliably met within the allowable latency. The term $reliability$ in 5G and Beyond systems is defined at higher layers as the probability of packets delivered successfully to the destination within the required time of the service or application [28]. The $reliability$ requirement can vary much widely from service to service and use case to use case. In 5G and Beyond, the targeted $reliability$ in 5G for some mission critical usecases is set to 99.999% [28], which implies that the probability of packet failure is to be around 10^{-5}.

Considering the versatility of the use cases and their requirements in 5G and Beyond mobile networks, it is quite interesting and significant to formulate a $flexible$ and $reliable$ framework with the goal to analyze, monitor and reliably control the versatile requirements of diverse use cases. The work presented in this thesis is predominantly driven by the two key design principles of 5G and Beyond, $flexibility$ and $reliability$. In this regard, firstly, a novel lower layer focused C-RAN / DAS framework is developed. This framework is based on lower level *reliability*, which is defined in terms of the *"probability of achieving a required signal-to-interference-plus-noise-ratio (SINR) at user location" [5].* Therefore, the derived *reliability* portrays a reasonable estimate of lower layers *reliability* in the overall system *reliability*.

Secondly, driven by the other key design aspect in 5G and Beyond, $flexibility$, RAN architecture level solutions for the key challenges emerging out of a practical 5G eMBB ultra-dense Heterogeneous Mobile Networks (HMN) in coexistence with C-RAN / DAS are investigated. In 5G and Beyond, it is anticipated to see a coexistence of currently existing Radio Access Technologies (RATs) such as GSM, UMTS, LTE, WiFi, and novel emerging technologies, 5G New Radio (NR), Massive MIMO, mmWave etc., and varied deployment scenarios such as ultra dense multi-layer networks consisting of cells of various topologies. Consequently, HMN poses challenges to C-RAN / DAS primarily because of the coexistence of C-RAN / DAS with conventional base station topologies which radiate very high power. In these scenarios, without an effective control and coordination of resources in HMN, the high power radiating base stations can severely limit the compelling benefits of DAS. Therefore, there arises a need for $flexible$ and $programmable$ architecture for 5G and Beyond HMN. Consequently, in this thesis, a novel $flexible$ software defined networking (SDN) based architecture is presented. Furthermore, the solutions for C-RAN / DAS in HMN, based on the novel SDN architecture, are presented.

1.3 Outline and Main Contributions

In this section, the outline and main contributions of the novel aspects of C-RAN / DAS in 5G and Beyond systems investigated in this thesis are presented. Fig.1.2 depicts the work flow diagram starting with the requirements of 5G and Beyond, the novel aspects of C-RAN / DAS addressed within each chapter and the inter-relation between chapters.

The thesis is organized as follows:

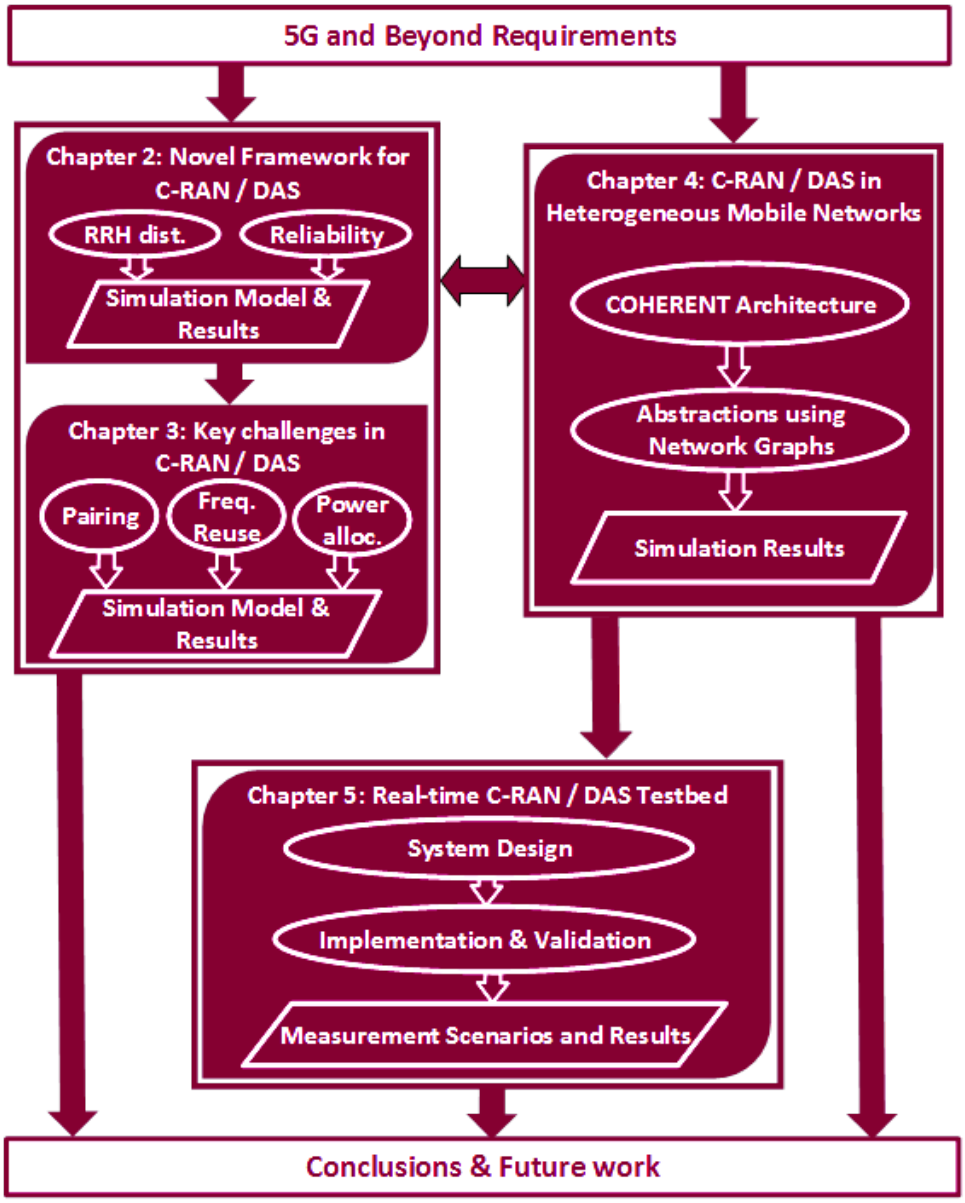

Fig. 1.2: Work flow diagram and inter-relation between chapters in this thesis

- **Chapter 2 : Novel Framework for C- RAN / DAS in 5G and Beyond**

This chapter describes a *novel* lower layer focused framework for C-RAN / DAS in 5G and Beyond systems. This novel framework comprises of:

- firstly, a *novel* placement of RRHs, which is based on the mathematical solution of optimum hexagonal packing of circles is conceptualized. This novel method provides the highest packing density. According to this model, given the coverage radius requirement the number of RRHs and the RRHs placement locations can be determined. The analysis, usage and benefits of this novel method are presented
- secondly, at lower layers, a *novel* lower layer *reliability* in C-RAN / DAS for Non-Line-Of-Sight (NLOS) and Line-Of-Sight (LOS) scenarios is derived.

Furthermore, the simulation model, validation of the derivations and discussion of results are presented.

- **Chapter 3 : Key Challenges in C-RAN / DAS for 5G and Beyond**
  In this chapter, the following key challenges at lower layers in C-RAN / DAS for 5G and Beyond are addressed:
  - firstly, the problem of forming effective (UE, RRH) pairs is formulated and an effective solution based on the nearest distance is presented
  - secondly, the problem of frequency reuse is formulated, and a *novel* reuse distance is derived, based on the *reliability*, in order to *reliably* achieve rapid frequency reuse
  - lastly, the problem of DL power allocation among the RRHs belonging to same reuse group is formulated. Since, the RRHs within the same reuse group transmit on the same scheduling resources, each transmission link is considered as a player in a general interference game. In the interference channel, the cooperative game theory provides optimal solutions by maintaining *efficiency* and *fairness* among the players. In this work, both *fairness* and *reliability* for all the users is addressed, by employing a *novel* utility function. The existence, fairness and uniqueness of the cooperative game, based on *novel* utility function, are proved analytically, by validating all the Nash conditions. Thereby, proving the existence of an unique Nash Bargaining Solution (NBS). In this regard, the derived solutions for optimum transmit

power allocation solution using Lagrange multipliers is presented. In this regard, the developed iterative Nash bargaining algorithms are presented.

The chapter concludes with a description of the simulation model, verification of the derived solutions and discussion of results.

- **Chapter 4 : C-RAN / DAS in 5G and Beyond Heterogeneous Mobile Networks**
  Flexibility, one of the key design principle of 5G and Beyond is addressed in this chapter by presenting the features of a *novel* software defined networking (SDN) based architecture of radio access network in Heterogeneous Mobile Networks (HMN) scenarios. In 5G and Beyond, it is much anticipated to see the coexistence of legacy RATs such as, GSM, UMTS, LTE, and novel technologies such as, 5G New Radio (NR), Massive MIMO and mmWave, and also ultra dense deployments of cells of diverse coverage areas. Here, the challenges encountered by C-RAN / DAS in HMN, especially in ultra-dense eMBB use case scenarios is analyzed. The need for $flexible$ and $programmable$ architecture for 5G and Beyond in HMN is presented. Consequently, a novel $flexible$ software defined networking (SDN) based architecture, which was jointly achieved under COHERENT, a 5GPPP research project, is outlined. Based on the *novel* abstraction framework, the control framework methodologies for addressing the challenges of C-RAN / DAS in HMN are presented. In this regard, the formulation of NGs for C-RAN / DAS using the derived PHY layer *reliability*, for efficient pairing and scheduling of resources of C-RAN / DAS in HMN is presented.

- **Chapter 5 : Real-time C-RAN / DAS Testbed and Measurement Results**
  This chapter presents the system design of Long Term Evolution (LTE) based real-time testbed, which is implemented on Software Defined Radio (SDR) platform. The analysis of the required adaptations in LTE MAC layer and LTE PHY DL processing chains for the deployment of C-RAN / DAS is presented. Moreover, the software implementation details of the new adaptations for C-RAN / DAS and LTE processing channels are presented. The methodology used for validating the real-time testbed is described. Lastly, the validation of some of the feasible aspects of $reliability$ based solutions presented in this thesis is achieved in various measurement scenarios using a commercial LTE test equipment. A detailed analysis of the validation results and the measurement scenarios is presented,

besides providing the insights into the practical deployment of these scenarios.

- **Chapter 6 : Conclusions and Future Work**

  The chapter provides a summary of the different novel aspects addressed in this thesis, besides presenting the conclusions drawn from the investigations, verification and validation of novel aspects. Finally, some recommendations for feasible extensions of the work is presented.

2 Novel Framework for C- RAN / DAS in 5G and Beyond

The work presented in this chapter is copied / derived from author's published work "Reliability Analysis of Centralized Radio Access Networks in Non-Line-of-Sight and Line-of-Sight Scenarios" published in "IEEE Access", year 2019 [5] and "Probability of coverage based analysis of distributed antenna system and its implementation on LTE based real-time-testbed" published in "9th International Congress on Ultra Modern Telecommunications and Control Systems and Workshops (ICUMT)", year 2017 [10]

In this chapter, a *novel* lower layer centric C-RAN / DAS framework is presented. This framework is designed on the key design principles of 5G systems, which are *flexibility* and *reliability* [1, 17]. The work presented in this chapter addresses *flexibility* by formulating a *novel* RRH distribution in C-RAN / DAS, which is based on the optimum hexagonal packing of circles. This arrangement provides the highest packing density, as it is based on the optimum hexagonal circular packing [31]. This method provides an easier way of controlling the RRH coverage radius, depending on the requirements of the scenario, which also provides the information about number of RRHs required for the scenario. In addition to that, based on this RRH distribution model, an analysis of overall transmission power saved in C-RAN / DAS in comparison with conventional co-located antenna system (CAS) is presented.

Secondly in this chapter, *reliability* in 5G systems is addressed. *Reliability* in 5G is defined at higher layers as the percentage ratio of successfully delivered packets to the destination to the total number of packets transmitted, within a time constraint set by the service [28]. In 5G, for some mission critical use cases belonging to URLLC, the targeted *reliability* is set to 99.999%. Therefore in this work, in order to reasonably estimate reliability at lower layers, a measure of *reliability* is defined as the probability of achieving a minimum required SINR at a UE location.

The work in this chapter is presented as follows: firstly, the hexagonal circle packing method for RRH distribution is described. Secondly, the C-RAN / DAS system model is described. Thirdly, *reliability* in C-RAN / DAS using Rayleigh and Rician Fading channel models, which cover the non-line-of-sight (NLOS) [32] and line-of-sight (LOS) conditions, is derived. Finally, the simulation model with results and discussion is presented.

2.1 Hexagonal Circle Packing

Different RRH distributions for DAS have been proposed in the literature [33–35]. Most of these methods are stochastic based models targeted to improve the ergodic channel capacity of DAS. However, mathematical models for RRH deployment which can provide solutions of less complexity are not much reported in the literature. Therefore, in this work, the distribution of RRHs based on hexagonal packing of circles in a hexagonal cell is considered. In geometry, circle packing studies various alignments of non-overlapping uniform circles on a plane [31]. The best arrangement of uniform circles on a horizontal plane provides the highest density, so that the circles are packed as closely as possible to each other [31]. This implies that in a hexagonal cell, the best possible arrangement of uniform circles also provides the best coverage of the hexagonal area. According to Axel Thue's theorem [31], the hexagonal packing of uniform circles gives the densest circle packing in the plane. The density of hexagonal circle packing is $\frac{\pi}{\sqrt{12}} \approx 0.9$. Where packing density η is given by $\eta = \frac{Sum\ of\ the\ areas\ of\ circles}{Area\ of\ hexgonal\ cell}$.

Let R be the side length of the hexagonal cell, then the length of any diagonal in the hexagon would be $2R$. Now we consider the RRH coverage area, which is represented by the uniform circles, will have a radius r which is a factor of R, i.e., $r = \frac{R}{C}$, where C represents the packing factor. Fig.2.1 shows an illustration of the proposed distribution of RRHs, where the radius of the cell is 10 m and the RRH coverage radius is 1.4 m. Based on the hexagonal circle packing arrangement, we have in the center a circle and around the center circle the centers of the first set of circles form the vertices of a hexagon of side length $2R/C$. The centers of the second, third and further sets of circles also form hexagons with side lengths of $4R/C$, $6R/C$ and so on. From this arrangement, the number of circles M that can packed efficiently within the hexagon is derived to be $M = 1 + 0.75(C^2 - 1)$.

Now, the effective transmit power saved in the case of distributed antenna system w.r.t.

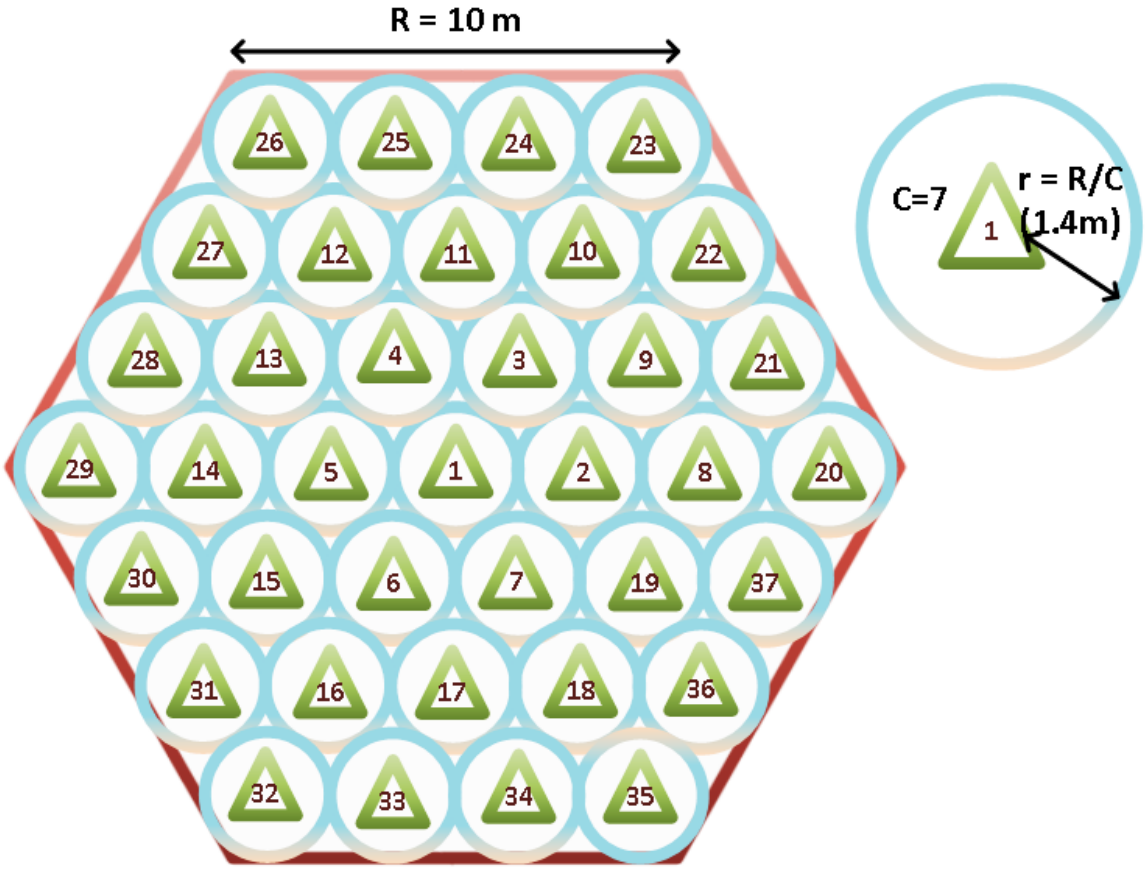

Fig. 2.1: DAS RRHs distribution based on Hexagonal circle packing

conventional collocated antenna system (CAS) is presented. The received power at the cell edge using pathloss model in CAS and DAS is given by,

$$\begin{aligned} P_{r_{CAS}} &= P_{t_{CAS}} K_{FS} \left(\frac{d_0}{R}\right)^{\alpha} \\ P_{r_{DAS}} &= \frac{P_{t_{DAS}}}{M} K_{FS} \left(\frac{d_0}{r}\right)^{\alpha}, \end{aligned} \tag{2.1}$$

where α is the path loss exponent. K_{FS} is a constant which equals to free-space path loss, assuming omni-directional antennas, at a reference distance d_0. The total transmit power of DAS is represented by $P_{t_{DAS}}$, while $\frac{P_{t_{DAS}}}{M}$ represents the transmit power of each RRH within DAS. Since $r = \frac{R}{C}$, (2.1), can be written as,

$$P_{r_{DAS}} = \frac{P_{t_{DAS}}}{M} C^{\alpha} \frac{P_{r_{CAS}}}{P_{t_{CAS}}}. \tag{2.2}$$

Now, the total transmit power saved in DAS compared to CAS for the same cell-edge coverage

can be derived from (2.2) as,

$$\mathbf{P}_{\mathbf{t\ Saved}}^{\mathbf{DAS}}(\mathbf{dB}) = 10\log_{10}\left(\frac{P_{t_{CAS}}}{P_{t_{DAS}}}\right) = 10\alpha\log_{10}(C) - 10\log_{10}(M). \tag{2.3}$$

Fig.2.2 shows the potential saving in the transmission power in C-RAN / DAS, compared to

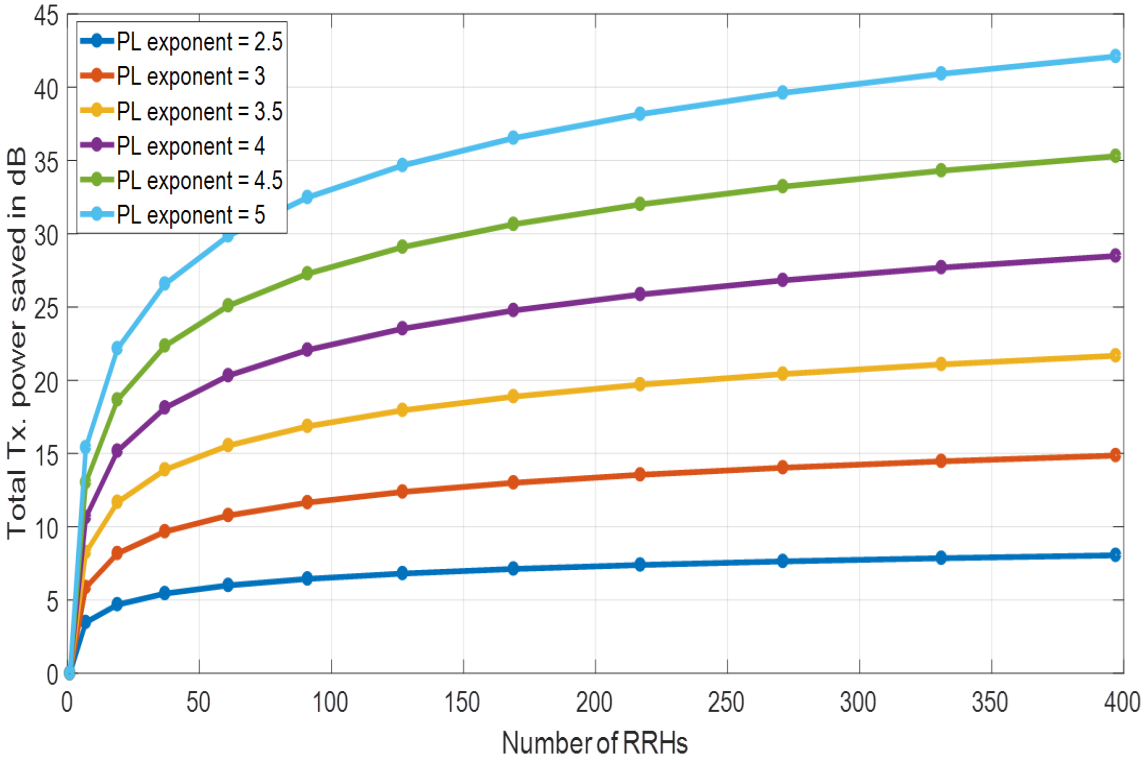

Fig. 2.2: Total Tx Power saved in DAS w.r.t. CAS for the same coverage

CAS, by increasing the number of RRHs, considering the same coverage at cell edge. The effect of variation of pathloss exponent on the transmit power saving is also shown in the figure. Fig.2.2 shows the overall transmit power in C-RAN / DAS that can be saved, which positively influences the system throughput because of its huge potential to decrease interference in the system and thereby promoting rapid frequency reuse.

2.2 System Model

Fig.2.3 shows a typical C-RAN / DAS system where the Central Unit (CU) does the centralized Radio Access Technology (RAT) processing and sends the baseband signals to the distributed RRHs. The distributed RRHs and CU are interconnected via optical cables using baseband

transmission standards like Common Public Radio Interface (CPRI) or Open Base Station Architecture Initiative (OBSAI). The RRHs usually perform as radio frequency (RF) transceivers, but depending on the requirements, RRHs can perform some part of baseband processing as well in order to decrease the baseband transmission rate through the fronthaul links.

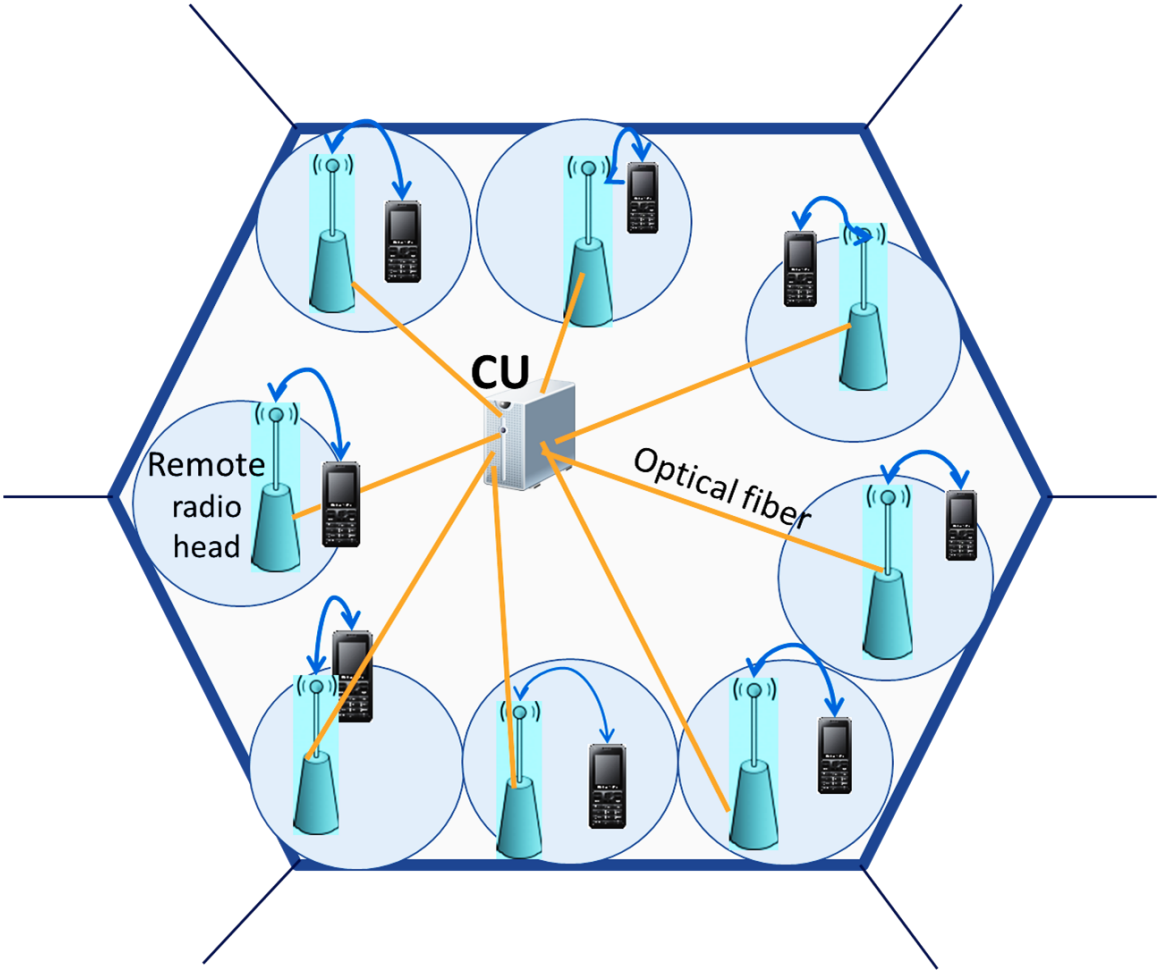

Fig. 2.3: C-RAN system model with distributed RRHs and CU

For the system model, a scenario, which consists of M RRHs and K UEs distributed over the coverage area, is considered. Each RRH can have multiple antennas, but here for the sake of simplicity we have considered the case of single antennas at RRHs and UEs. Let UE k be paired with its nearest RRH called r_k, where $r_k \in \{1, 2, ., M\}$. The received signal at UE k can be expressed as,

$$y_k = h_{k,r_k} x_k + \sum_{r_j \in [1,M], r_j \neq r_k} h_{k,r_j} x_j + z_k, \tag{2.4}$$

where h_{k,r_j} represents the channel coefficient between UE k and RRH r_j. The transmitted signal

from the RRH r_j is represented by x_j. The noise at the receiver of UE k is represented by z_k. The intended signal for UE k is given by x_k which is transmitted by its paired RRH r_k.

2.3 Reliability

One of the key design principles of the design of 5G wireless networks is *reliability*. Therefore, in this section, the expression for lower layer *reliability* in C-RAN / DAS is derived. In this thesis, *reliability* at lower layers is defined in terms of probability of achieving a minimum required SINR at a UE location, which is a also the probability of coverage. In general the minimum required SINR at a UE location is determined by various metrics such as, Quality of Service (QoS) requirements targeted by the service, UE priority, conformance requirements of a communication standard etc.. For example, in 3GPP LTE standard, the minimum required SINR at UE can be derived from the error vector magnitude (EVM) requirements [36] for different modulation schemes. Similarly one can as well deduce the UE's minimum SINR requirement from its different requirements like, block error rate (BLER), bit error rate (BER) and average throughput. Based on the minimum SINR requirement, reliability can help in monitoring and controlling different UE requirements, which in turn helps in efficient scheduling of time, frequency, space and power resources. Deriving SINR requirements for UEs and employing *reliability* in addressing the following challenges in C-RAN / DAS: pairing of RRHs with UEs, finding frequency reuse pairs, and scheduling of time, frequency and space resources; can significantly help to improve the system efficiency. Furthermore, this analysis can assist in determining the effective placements of RRHs depending on the user distribution and use case requirements.

In the following subsections, *reliability* in C-RAN / DAS in Non-Line-Of-Sight (NLOS) scenarios [22], considering Rayleigh fading channel model is derived. In Line-Of-Sight (LOS) scenarios [21] the $reliability$ based on Rician fading channel model is derived. In practical application, LOS scenarios are more pertinent to real-life scenarios like stadiums, theaters and shopping mals, where the LOS component is dominant.

2.3.1 Non-Line-Of-Sight

This subsection is copied / derived from author's published work "Probability of coverage based analysis of distributed antenna system and its implementation on LTE based real-time-testbed" published in "2017 9th International Congress on Ultra Modern Telecommunications and Control Systems and Workshops (ICUMT)" [10]"

In the case of NLOS scenario, the probability distribution function of the received power p_r^{k,r_k} at UE k from the RRH r_k in Rayleigh fading channel [10] is given by,

$$f_{P_r}(p_r^{k,r_k}) = \frac{1}{2\gamma_{k,r_k}^2} \exp(-\frac{p_r^{k,r_k}}{2\gamma_{k,r_k}^2}), \tag{2.5}$$

where $2\gamma_{k,r_k}^2 = P_t^{r_k} K_{FS} (\frac{d_0}{d_{k,r_k}})^\alpha$ represents the mean received power of the signal from the RRH r_k at UE k based on pathloss model. The mean transmitted power of RRH r_k is given by $P_t^{r_k}$, which equals to $E(x_k x_k^*)$, where $E()$ represents the expectation operation. The distance between the RRH port r_k and UE k is given by d_{k,r_k} and α is the path loss exponent. The free-space path loss, assuming an omni-directional antenna, is given by K_{FS} at a reference distance d_0.
Let $A_k^{r_k} = \frac{1}{2\gamma_{k,r_k}^2}$, then pdf of the received power at UE k from it's paired RRH r_k as given in (2.5) can be expressed as,

$$f_{P_r}(p_r^{k,r_k}) = A_k^{r_k} \exp(-A_k^{r_k} p_r^{k,r_k}), \tag{2.6}$$

In an interference and noise limited system, when N interfering RRHs are transmitting in the same time-frequency resources as that of (UE,RRH) pair (k, r_k), the SINR at k^{th} UE is given by,

$$SINR_{k,r_k} = \frac{p_r^{k,r_k}}{p_N^k + \eta}, \tag{2.7}$$

where η is the noise power at the receiver and p_N^k is the interference power observed at k^{th} UE from N interfering RRHs. The interference power, p_N^k, can be expressed as $\sum_{r_j \in \{N\}, r_j \neq r_k} p_r^{k,r_j}$. Reliability, R^k at UE k location, for a minimum required SINR, γ_k, is given by,

$$R^k = P\big(SINR_{k,r_k} \geq \gamma_k\big) = P\bigg(\frac{p_r^{k,r_k}}{p_N^k + \eta} \geq \gamma_k\bigg) = P\bigg(p^{k,r_k} \geq \gamma_k (p_N^k + \eta)\bigg), \tag{2.8}$$

$$= E_{P_N^k}\Big(\int_{\gamma_k(p_N^k+\eta)}^{\infty} A_k^{r_k} \exp\Big(- A_k^{r_k} p_r^{k,r_k} \Big)\, dp^{k,r_k} \Big), \tag{2.9}$$

where $E_{P_N^k}$ represents the expectation over the interference at k^{th} UE and $A_k^{r_k} = \frac{1}{2\gamma_{k,r_k}^2}$. Since the received interference is independent of the received power from the paired RRH r_k and the interferers are independent as well, (2.7) can be derived as given in [10] as,

$$R^k = \int_0^{\infty} ... \int_0^{\infty} \exp\Big(- A_k^{r_k}\gamma_k\Big(\sum_{r_j\in[1,M], r_j\neq r_k} p_r^{k,r_j} + \eta\Big)\Big) \prod_{r_j\in[1,M], r_j\neq r_k} f(p_r^{k,r_j})\, dp_r^{k,r_j}. \tag{2.10}$$

Now,(2.7) can be expressed as,

$$R^k = \exp\Big(- A_k^{r_k}\eta\gamma_k\Big) \prod_{r_j\in[1,M], r_j\neq r_k} \int_0^{\infty} \exp\Big(- A_k^{r_k}\gamma_k p_r^{k,r_j}\Big) f(p_r^{k,r_j}) dp_r^{k,r_j}. \tag{2.11}$$

Using (2.5) in (2.11) gives,

$$R^k = \exp\Big(- A_k^{r_k}\eta\gamma_k\Big) \prod_{r_j\in[1,M], r_j\neq r_k} A_k^{r_j} \int_0^{\infty} \exp\Big(- \Big(A_k^{r_k}\gamma_k + A_k^{r_j}\Big) p_r^{k,r_j}\Big) dp_r^{k,r_j}. \tag{2.12}$$

The integral in (2.12) can be solved as,

$$\int_0^{\infty} \exp\Big(- \Big(A_k^{r_k}\gamma_k + A_k^{r_j}\Big) p_r^{k,r_j}\Big) dp_r^{k,r_j} = \frac{1}{A_k^{r_k}\gamma_k + A_k^{r_j}}. \tag{2.13}$$

Using the result from (2.13) in (2.12) gives the expression for $reliability$ at UE k in NLOS as,

$$R^k(rayleigh) = \exp\Big(- A_k^{r_k}\eta\gamma_k\Big) \prod_{r_j\in[1,M], r_j\neq r_k} \frac{1}{\frac{A_k^{r_k}}{A_k^{r_j}}\gamma_k + 1}. \tag{2.14}$$

2.3.2 Line-Of-Sight

The work presented in this subsection is copied / derived from author's published work "Reliability Analysis of Centralized Radio Access Networks in Non-Line-of-Sight and Line-of-Sight Scenarios" published in "IEEE Access", year 2019 [5]

In this subsection, we derive $reliability$ in case of received signal with LOS component. The probability density function (pdf) of received signal power based on Rician fading channel is given by [37],

$$f_{P_r}(p_r^{k,r_j}) = \frac{1}{P_{S_{k,r_j}}} \exp(-K_{ri}^{k,r_j}) \exp\left(- \frac{p_r^{k,r_j}}{P_{S_{k,r_j}}} \right) I_0\left(2\sqrt{K_{ri}^{k,r_j} \frac{p_r^{k,r_j}}{P_{S_{k,r_j}}}} \right), \tag{2.15}$$

$$f_{P_r}(p_r^{k,r_k}) = \frac{1}{P_{S_{k,r_k}}} \exp(-K_{ri}^{k,r_k}) \exp\left(- \frac{p_r^{k,r_k}}{P_{S_{k,r_k}}} \right) I_0\left(2\sqrt{K_{ri}^{k,r_k} \frac{p_r^{k,r_k}}{P_{S_{k,r_k}}}} \right), \tag{2.16}$$

where $K_{ri}^{k,r_k} = \frac{P_{D_{k,r_k}}}{P_{S_{k,r_k}}}$ is the Rician factor and $I_0(\,)$ is the modified Bessel function of first kind and zero order [38]. In this channel model, the total mean power received at UE k is equal to sum of the average power received by the LOS component, $P_{D_{k,r_j}}$, and mean of total received power over the scattered paths, $P_{S_{k,r_j}}$. According to the pathloss model, the sum of the mean received powers via LOS and NLOS is given by,

$$P_{D_{k,r_k}} + P_{S_{k,r_k}} = P_t^{r_k} K_{FS} (\frac{d_0}{d_{k,r_k}})^{\alpha}. \tag{2.17}$$

Let $A_k^{r_k} = \frac{1}{P_{S_{k,r_k}}}$ and $B_k^{r_k} = \frac{K_{ri}^{k,r_k}}{P_{S_{k,r_k}}}$, then the pdf of the received signal power at UE k due to RRH r_k is represented by,

$$f_{P_r}(p_r^{k,r_k}) = A_k^{r_k} \exp(k, r_k) \exp\left(- A_k^{r_k} p_r^{k,r_k} \right) I_0\left(2\sqrt{B_k^{r_k} p_r^{k,r_k}} \right). \tag{2.18}$$

The $reliability$, R^k, at k^{th} UE location for a minimum SINR required, γ_k, where UE k is paired

to RRH r_k and having N number of interfering RRHs is given by,

$$\begin{aligned} R^k = P\bigg(SINR_{k,r_k} \geq \gamma_k\bigg) &= P\bigg(\frac{p_r^{k,r_k}}{p_N^k + \eta} \geq \gamma_k\bigg) \\ &= P\bigg(p_N^k \leq \frac{p_r^{k,r_k}}{\gamma_k} - \eta\bigg) \\ = \int_0^\infty \bigg(\int_0^{(\frac{p_r^{k,r_k}}{\gamma_k} - \eta)} f_{P_N^k}(p_N^k)\, dp_N^k \bigg) f_{P_r}(p_r^{k,r_k})\, dp_r^{k,r_k}. \end{aligned} \tag{2.19}$$

The double integral in (2.19) can be solved by changing the order of integration as,

$$R^k = \int_0^\infty \bigg(\int_{(p_N^k+\eta)\gamma_k}^\infty f_{P_r}(p_r^{k,r_k}) dp_r^{k,r_k} \bigg) f_{P_N^k}(p_N^k)\, dp_N^k. \tag{2.20}$$

At first we solve the inner integral in (2.20), which results in,

$$\begin{aligned} \int_{(p_N^k+\eta)\gamma_k}^\infty f_{P_r}(p_r^{k,r_k}) dp_r^{k,r_k} &= A_k^{r_k} \exp(-K_{ri}^{k,r_k}) \\ \sum_{n=0}^\infty \frac{(B_k^{r_k})^n}{(n!)^2} \int_{(p_N^k+\eta)\gamma_k}^\infty (p_r^{k,r_k})^n \exp(-A_k^{r_k} p_r^{k,r_k}) dp_r^{k,r_k} \\ = \exp\big(-K_{ri}^{k,r_k}\big) \sum_{n=0}^\infty \frac{(K_{ri}^{k,r_k})^n}{(n!)^2} \Gamma\big(n+1, A_k^{r_k}(p_N^k+\eta)\gamma_k\big), \end{aligned} \tag{2.21}$$

where $\Gamma\big(a, b\big)$ is the upper incomplete gamma function, which can be expressed as series expansion according to [38] as

$$\begin{aligned} \Gamma\big(n+1, A_k^{r_k}(p_N^k+\eta)\gamma_k\big) &= \Gamma(n+1) \\ \exp\big(-A_k^{r_k}(p_N^k+\eta)\gamma_k\big) \sum_{k=0}^n \frac{(A_k^{r_k}(p_N^k+\eta)\gamma_k)^k}{k!}. \end{aligned} \tag{2.22}$$

Using (2.22) in (2.21) gives the solution for the inner integral of (2.20) as

$$\begin{aligned} \int_{(p_N^k+\eta)\gamma_k}^\infty f_{P_r}(p_r^{k,r_k}) dp_r^{k,r_k} &= \exp\big(-K_{ri}^{k,r_k}\big) \exp\big(-A_k^{r_k}\eta\gamma_k\big) \\ \sum_{n=0}^\infty \frac{(K_{ri}^{k,r_k})^n}{n!} \sum_{m=0}^n \frac{(A_k^{r_k}\gamma_k)^m}{m!} \exp(-A_k^{r_k} p_N^k \gamma_k)(p_N^k+\eta)^m. \end{aligned} \tag{2.23}$$

In order to solve the pdf of p_N^k, which is sum of the received powers at UE k from N reuse

RRHs, we assume Rician fading channel model for the interfering channels. For the sake of simplicity of derivation, we assume all the interfering RRHs are placed equidistantly to the UE k and equal transmit powers from RRHs. It is to be noted that, owing to the high mathematical complexity involved, to the best of my knowledge the derived closed form expressions with these approximations is still the first work in finding reliability in rician fading channels. Furthermore, these assumptions apply very well to one of the key challenges addressed in this thesis which is, formation of RRH reuse groups. Where the same frequencies are reused within the coverage area. It is expected that these reuse RRHs are most likely located equidistant to the UE, as it results in optimal power allocation and throughput. In this case, the pdf of p_N^k is solved in [37] to be,

$$f_{P_N^k}(p_N^k) = \exp(-NK_{ri}^{k,N}) \exp\big(-(A_N^k)^N\big)\big(\frac{1}{NB_N^k}\big)^{\frac{N-1}{2}}(p_N^k)^{\frac{N-1}{2}} I_{N-1}\big(2\sqrt{NB_N^k p_N^k}\big), \tag{2.24}$$

where I_{N-1} is the modified $N-1^{th}$ order Bessel function of first kind. Using the series expansion of I_{N-1} [38], (2.24) can be expressed as,

$$f_{P_N^k}(p_N^k) = \exp(-NK_{ri}^{k,N})(A_N^k)^N \exp(-A_N p_N^k \gamma_k) \sum_{l=0}^{\infty} \frac{(NB_N^k)^l}{l!\Gamma(l+N)}(p_N^k)^{l+N-1}. \tag{2.25}$$

Using (2.23), (2.25) in (2.20), results in,

$$R^k = \exp\big(-(NK_{ri}^{k,N} + K_{ri}^{k,r_k})\big)\exp(-A_k^{r_k}\eta\gamma_k)(A_N^k)^N \sum_{n=0}^{\infty}\frac{(K_{ri}^{k,r_k})^n}{n!}\sum_{m=0}^{n}\frac{(A_k^{r_k}\gamma_k)^m}{m!}\sum_{l=0}^{\infty}\frac{(NB_N^k)^l}{l!\Gamma(l+N)} \int_0^{\infty}\exp(-p_N^k(A_k^{r_k}\gamma_k + A_N^k)(p_N^k)^{m+l+N-1}\big(1+\frac{\eta}{p_N^k}\big)^m dp_N^k. \tag{2.26}$$

Since in practical cellular scenarios, the received interference power p_N^k is much greater than noise power η, the integral in (2.26) can be approximated according to [38] as,

$$\frac{1}{(A_k^{r_k}\gamma_k + A_N^k)^{m+l+N}}\Gamma(m+l+N). \tag{2.27}$$

Now, using the result from (2.27) in (2.26) derives the $reliability$ at UE k for LOS scenarios, which is given by,

$$R^k(rician) = \exp\big(-(NK_{ri}^{k,N} + K_{ri}^{k,r_k})\big)\exp(-A_k^{r_k}\eta\gamma_k) \sum_{n=0}^{\infty}\frac{(K_{ri}^{k,r_k})^n}{n!}\sum_{m=0}^{n}\left(\frac{A_k^{r_k}}{A_N^k}\right)^m \frac{(\gamma_k)^m}{m!\left(\frac{A_k^{r_k}}{A_N^k}\gamma_k+1\right)^m}\sum_{l=0}^{\infty}\frac{(NK_{ri}^{k,N^k})^l}{l!} \frac{1}{\left(\frac{A_k^{r_k}}{A_N^k}\gamma_k+1\right)^{l+N}}\frac{\Gamma(m+l+N)}{\Gamma(l+N)}. \tag{2.28}$$

As a corollary, if $K_{ri}^{k,N} = 0$, $K_{ri}^{k,r_k} = 0$ and the interfering RRHs are equidistant to UE k, the $R^k(rician)$ in (2.28) and $R^k(rayleigh)$ in (2.14) becomes equal to that of NLOS scenario, which is given by,

$$R^k(rician) = R^k(rayleigh) = \exp(-A_k^{r_k}\eta\gamma_k)\frac{1}{\left(\frac{A_k^{r_k}}{A_N^k}\gamma_k+1\right)^N}. \tag{2.29}$$

2.4 Simulation Results

The work presented in this subsection is copied / derived from author's published work "Reliability Analysis of Centralized Radio Access Networks in Non-Line-of-Sight and Line-of-Sight Scenarios" published in "IEEE Access", year 2019 [5]

2.4.1 Simulation Model

In order to evaluate the performance of the proposed metrics and algorithms, we consider a simulation model consisting of various RRH distributions based on the proposed DAS hexagonal packing, which is described in Section 2.1. The UEs are distributed uniformly over the coverage area. Figures 2.4 and 2.5 represents the positioning of RRHs in case of packing factors 9 and 15 respectively. The packing factor C directly relates to RRH coverage radius by $r = R/C$. The number of RRHs in these two cases are 61 and 169. The numbers in the center of each dotted circle represents the RRH number, which increases concentrically. The dotted small circles around the RRHs represent the radial coverage area r. The UEs are uniformly distributed over

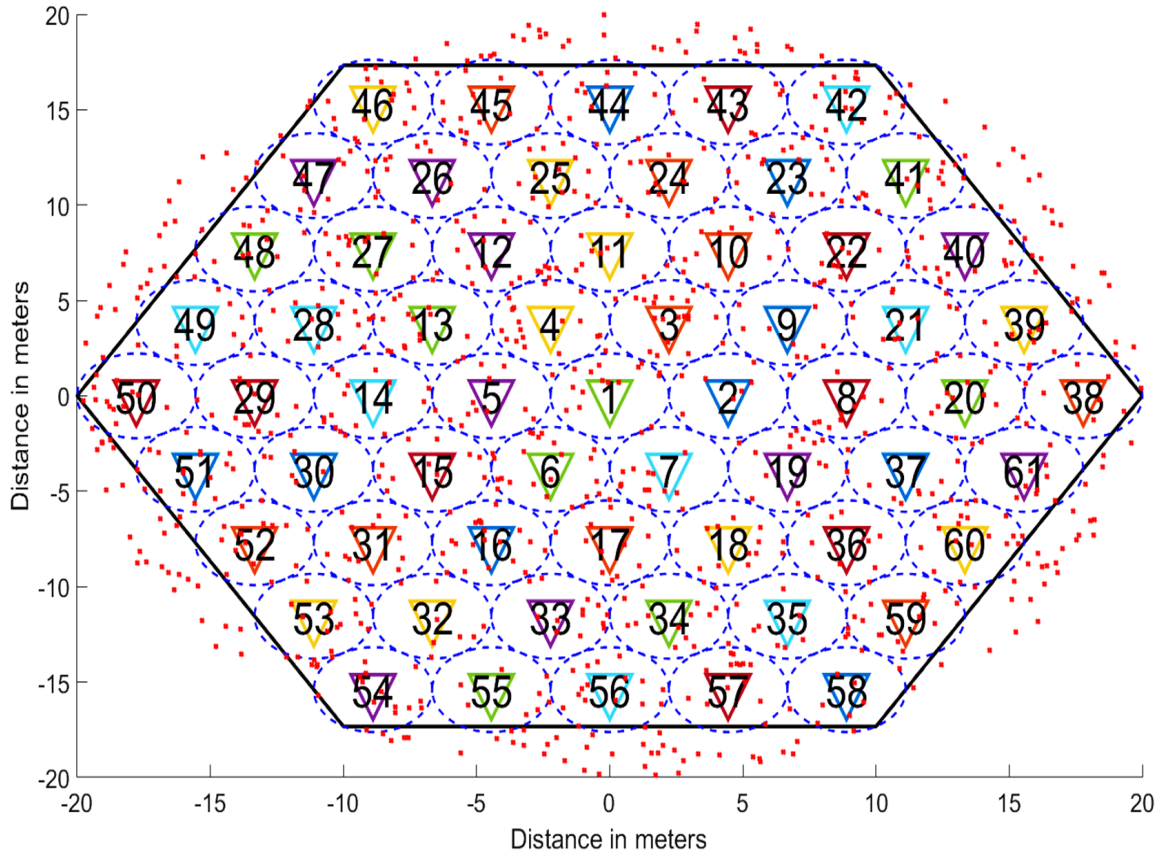

Fig. 2.4: DAS distribution with 61 RRHs

the complete cellular area, which are represented by red dots.

The simulation parameters considered in the simulation model implemented in MATLAB are given in Table 2.1.

2.4.2 Reliability

The derived $reliability$ in Section 2.3, which are Eq. (2.14) and Eq. (2.28), are validated using extensive simulations, around 10 million simulation runs, in MATLAB using Rayleigh and Rician distribution empirical models provided by MATLAB. We have verified the derived $reliability$ extensively by varying: the number of RRHs, UE locations and SINR requirements. Within the constraint set based on the assumptions made in the derivation, i.e. equidistant interferers and equal transmit powers of the interferers, we have observed perfect match between MATLAB based empirical models and derived expressions, which implies that the error is less than 10^{-5}. Hence the correctness of the derivations is verified.

Table 2.1: Simulation Parameters for Reliability analysis

Parameters	**Values**
Carrier frequency DL	2.655 GHz
Channel bandwidth DL	20 MHz
subcarrier spacing Δf	15 KHz
Num of subcarriers	1200
Cellular radius (R)	20 m
RRH packing factors (C)	$\{9, 13, 19, 25, 29, 35\}$
RRH coverage radius (r = R/C)	$\{2.2, 1.5, 1.1, 0.8, 0.7, 0.6\}$ m
Num of RRHs	$\{61, 127, 271, 469, 631, 919\}$
Num of UEs	2000
Noise level	-100 dBm
Pathloss exponent	3
Baseband transmission	OFDM
Transmit power	Equal for all RRHs
Rx and Tx Antenna Gain	0 dB
min. required SINR	$>$ 0 dB (application specific)

To evaluate the $reliability$, we have considered an UE k with 6 equidistantly placed interferers, and all the RRHs are transmitting equal power. We have assumed that the interferers are located at a distance of 7 times the RRH coverage radius from the UE k location, which implies that the interferers are adequately distant to reuse the time frequency resources of UE k. At first we investigate the effect of LOS components of the interfering and desired signals on the *reliability*, and later we present the effect of interferers distance on the *reliability*.

In Fig.2.6, we have simulated a case where the Rician factor of each interfering channels are set, $\mathbf{K_{ri}^{k,N}} = -\infty$ dB, and the Rician factor $\mathbf{K_{ri}^{k,r_k}}$ of the desired signal at UE k varies between $-\infty$ dB to 12 dB. NLOS scenario is represented by the Rician factor being $-\infty$ and Rician factor of 12 dB represents a very strong LOS signal. From the results we can observe that, for practical $reliability$ level of 0.8, the minimum required SINR at a UE location increases from 11 dB to 16 dB, as the power in LOS component increases. This scenario has a direct practical relevance for C-RAN / DAS in shopping malls. In shopping malls, the probability of receiving LOS signal from serving RRH is significantly higher than that of interfering signals because of

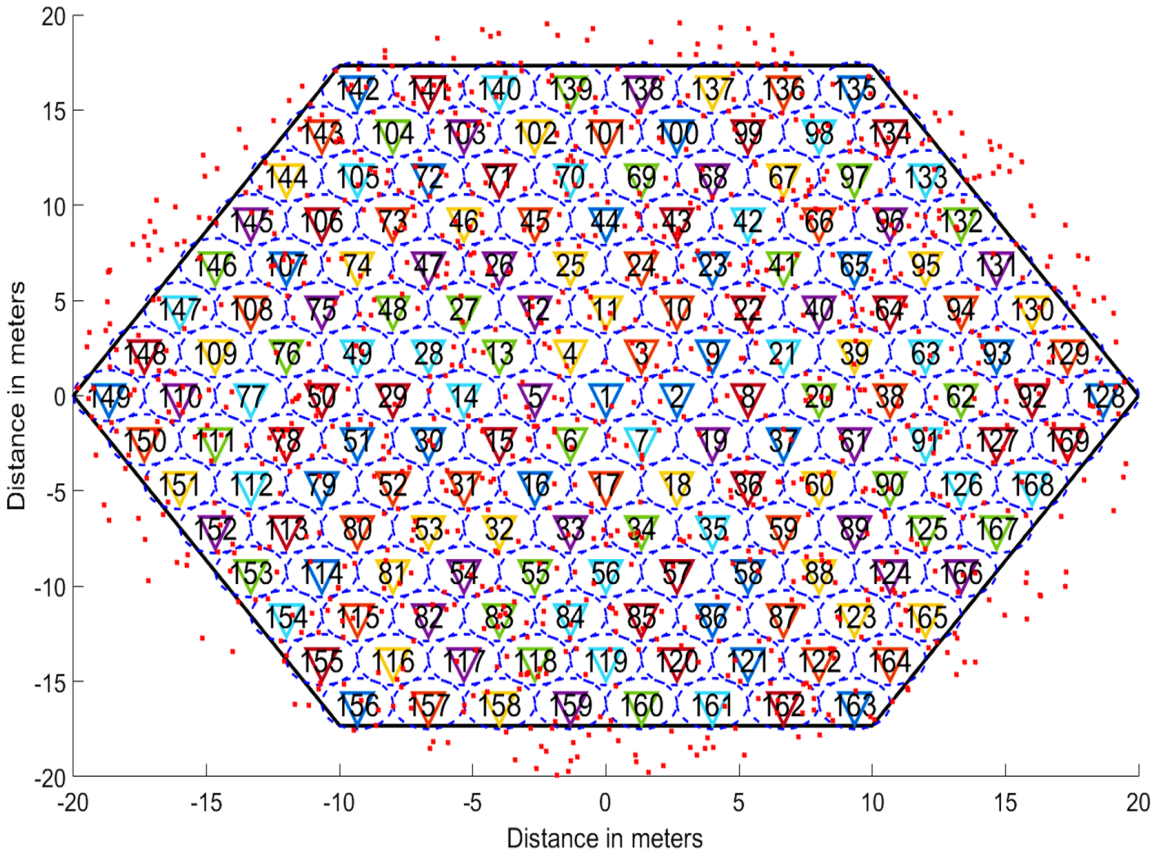

Fig. 2.5: DAS distribution with 169 RRHs

many obstructions.

Fig.2.7 represents the impact of interferer's LOS component on the reliability of UE k, which has a strong LOS component (12 dB) from its serving RRH. From this result, $reliablity$ is not much affected by increase in the intensity of LOS components of the interfering signals until a certain level, which is around 8 dB. But, when intensity of LOS components of the interfering signals is above 9 dB, its impact on the reliability of UE k is significant, which makes it non-practical to reuse the time-frequency resources with the interfering RRHs. Hence $reliability$ provides statistically a good insight in these scenarios for RRH placements and finding frequency reuse opportunities.

Fig.2.8 shows the effect of variation of location of interferers on the $reliability$ of UE k. When the interfering RRHs are located exactly at the same distance to the UE as that of its serving RRH, the $reliability$ is very small for the simulated target SINRs. This is because the 6 interfering RRHs are located equidistant to the UE, which results in very high interference at UE compared to the desired received signal. But, for all other cases there is always some

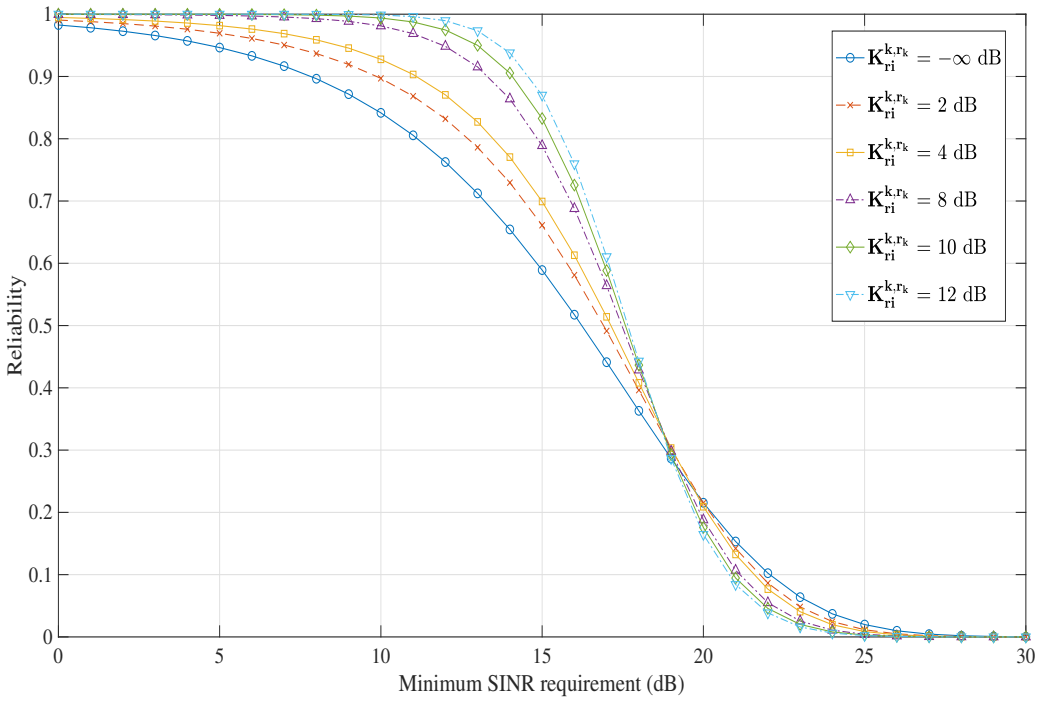

Fig. 2.6: Reliability in case of $\mathbf{K}_{\mathbf{ri}}^{\mathbf{k},\mathbf{N}} = -\infty$ dB, varying $\mathbf{K}_{\mathbf{ri}}^{\mathbf{k},\mathbf{r_k}}$

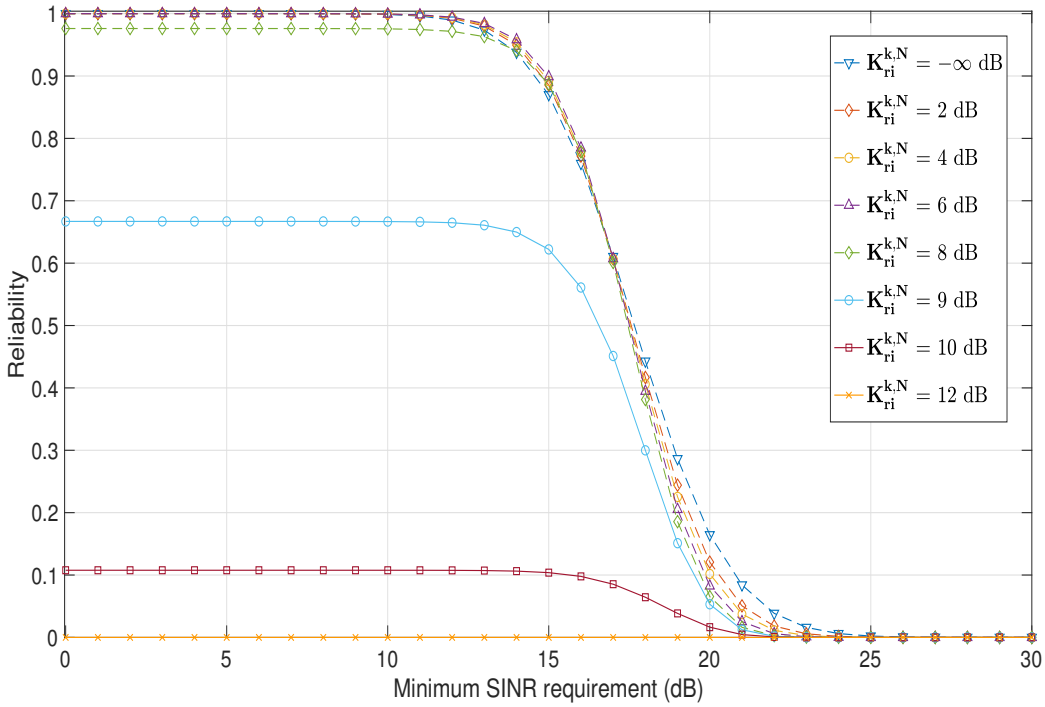

Fig. 2.7: Reliability in case of $\mathbf{K}_{\mathbf{ri}}^{\mathbf{k},\mathbf{r_k}} = 12$dB, varying $\mathbf{K}_{\mathbf{ri}}^{\mathbf{k},\mathbf{N}}$

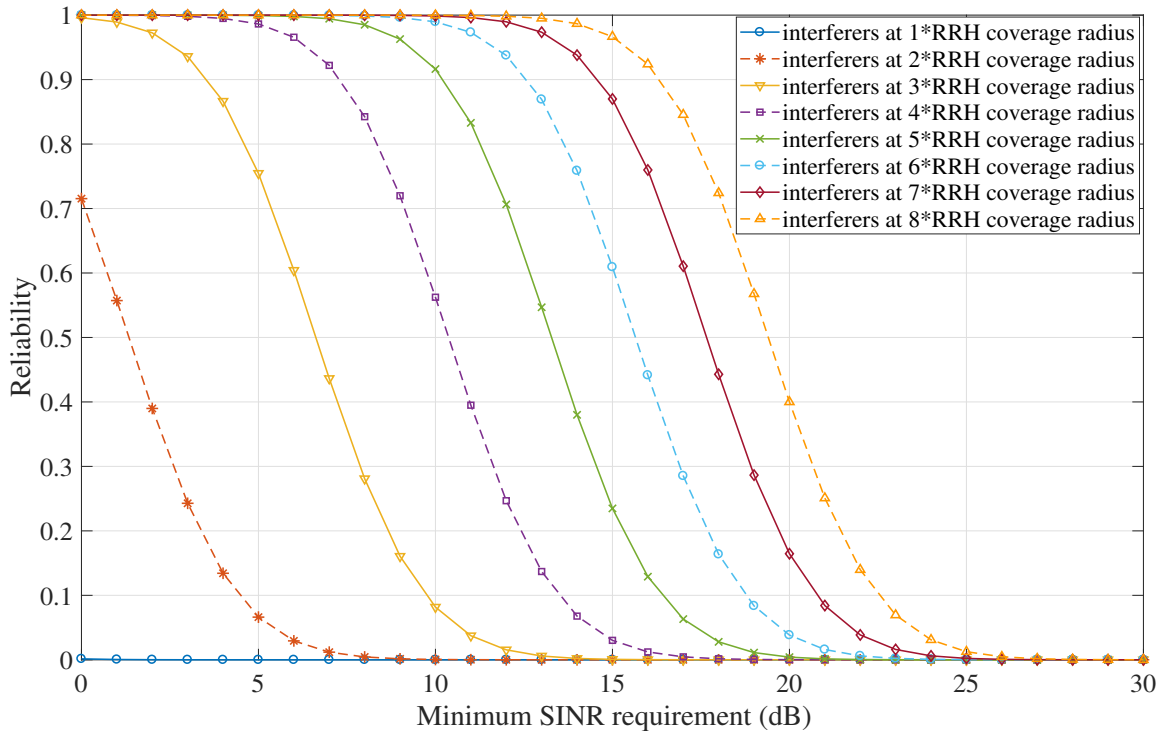

Fig. 2.8: Reliability in case of varying the distances of interferers, with $\mathbf{K}_{\mathbf{ri}}^{\mathbf{k},\mathbf{r_k}}$ = 12 dB, $\mathbf{K}_{\mathbf{ri}}^{\mathbf{k},\mathbf{N}} = -\infty$ dB

achievable $reliability$ at different targeted SINR levels at UE location. This can be exploited by the formation of dynamic frequency reuse RRH groups. Since in a practical wireless system, different UEs have different throughput and reliability requirements, the results here show the possibilities of forming dynamic frequency reuse RRH groups, thereby improving the system throughput and as well meeting the varied requirements of UEs.

Furthermore, at lower layers, *reliability* provides a statistical estimate of the system *reliability*, which is one of the key capabilities defined in 5G. In some mission critical applications belonging to 5G URLLC usecase, the *reliability* requirement is set to a very high value, which is $1 - 10^{-5}$ [28]. As shown in the results from different scenarios, the minimum SINR requirement at the device location can be determined based on the location of the device, transmitted powers, reliability requirement and LOS components strengths. In order to achieve the minimum SINR requirement of these mission critical applications, MAC scheduler can effectively schedule time, frequency and power resources among the devices or users reusing the same time-frequency resources. Therefore, *reliability* addresses the lower layer key capability requirement of 5G systems, besides providing minimum SINR requirements of different users and devices, which

can significantly help in reliable and efficient scheduling of resources.

2.5 Conclusion

In this chapter, a lower layers centric C-RAN / DAS framework inspired by the key design principles of 5G and Beyond, which are *reliability* and *flexibility* is presented. Firstly, a *novel* flexible distribution of RRHs based on the optimum method of hexagonal packing of circles, which has the highest packing density, is presented. *Flexibility* is achieved by presenting a easier way of controlling the RRH coverage radius, $r = \frac{R}{C}$, by the introduction of C called packing factor. A relation between the number of RRHs required, N, and the packing factor, C, is derived to be $N = 1 + 0.75(C^2 - 1)$. In this regard, a comparison of the total transmit power saved DAS in comparison with CAS for the same cell-edge coverage, while varying the number of RRHs and path loss exponent is shown. From this comparison, it is shown that DAS has the potential to save more than 25 dB of transmit power, in some practical scenarios.

Secondly, in this chapter, the lower layers *reliability* in C-RAN / DAS is defined as the probability of achieving a minimum required SINR at a UE location. Based on this definition, the mathematical expressions for *reliability* in NLOS scenarios using Rayleigh fading model and LOS scenarios using Rician fading channel model are derived. The main *novelty* here is the derivation of *reliability* in Rician fading channels. In order to ensure the correctness of derived analytical approximations presented in this chapter, extensive simulations are performed within the constraint set of assumptions mentioned in the derivations. The results of derived Reliability are compared against simulations using Rayleigh and Rician distribution empirical models in MATLAB. The observed error in all the simulated cases, within the constraint set of equidistant interferers and equal transmit powers of the interferers, is less than 10^{-5}. Hence the correctness of derivations is verified. Through simulation results, it is shown how the intensity of LOS component of interferers and desired signals effects the *reliability*. An analysis of simulation results in the view of realistic C-RAN / DAS deployment scenarios like stadiums and shopping malls, besides presenting the benefits of *reliability* analysis.

In the next chapter, it will be shown how this *novel* reliability based C-RAN / DAS is utilized to address key challenges of C-RAN / DAS with focus on 5G and Beyond *hotspot* scenario. Further in this thesis, it will be shown how this framework continues to form the basis

for addressing different novel aspects of C-RAN / DAS dealt in this thesis.

3 KEY CHALLENGES IN C-RAN / DAS FOR 5G AND BEYOND

Some parts of the work presented in this chapter is copied / derived from author's published work "Probability of coverage based analysis of distributed antenna system and its implementation on LTE based real-time-testbed" published in "9th International Congress on Ultra Modern Telecommunications and Control Systems and Workshops (ICUMT)", year 2017 [10] and "Reliability Analysis of Centralized Radio Access Networks in Non-Line-of-Sight and Line-of-Sight Scenarios" published in "IEEE Access", year 2019 [5]

3.1 Key Challenges

In order to understand the advantages and possible deployment strategies for C-RAN / DAS, significant work [24–26] is done. Further, much work is reported, in analyzing the performance in DAS [39–41] and in finding the RRH locations which improve the performance. In order to improve the coverage of cell edge users, some transmission schemes [42] in DAS such as, blanket transmission and selection transmission, are proposed in the literature. The general idea of selection transmission in DAS is to select the RRH for the transmission to all the UEs in the cellular coverage area in order to achieve the best system performance. In the case of multi-user DL DAS, a study on different selection transmission schemes to increase the sum rate is presented [41]. The idea of *paired selection transmission* technique, where more than one RRH serving different sets of UEs is first described in [41]. The present work is based on this approach of paired selection transmission. The motivation of the work presented here comes from real-life environments, where the UEs / mobile users are mostly stationary or having very low mobility where the sum rate requirement is very high due to high user density, e.g. in stadiums, theaters and shopping malls. 5G and Beyond defines these scenarios under eMBB use

case scenario as *hotspots* [1]. *Hotspot* scenario sets very high requirements on the key capability, *Area traffic capacity* (10 Mbit/s/m^2), which is defined in IMT 2020 [1] as the total throughput served per geographical area. Driven by the promising benefits due to very low transmit power in DAS, in this chapter, the key challenges in C-RAN / DAS will be identified and addressed in these scenarios to meet the above set challenging requirements. Therefore, this work aims to efficiently pair the UEs with the RRHs, i.e. to form (UE, RRH) pairs, so that the scheduling resources of these pairs can be reused at other reasonably distant pairs depending on sum rate requirement, user throughput requirements, user priorities and user services.

In the Chapter 2, the *novel* reliability based C-RAN / DAS framework is presented. This framework forms the basis of the work addressed in this chapter. This chapter analyzes the key challenges in C-RAN / DAS in the *hotspot* scenarios described above, which basically require *reliability* and high throughput density. The key challenges addressed in this work are: exploring efficient strategies for pairing, formation of frequency reuse RRH groups and efficient DL power allocation in order to meet UEs' expected throughput *reliability* and *fairness*. We utilize the lower layer *reliability*, definition presented in Chapter 2, which is defined in terms of *"the probability of achieving a minimum required signal-to-interference-plus-noise (SINR) at a UE location" [5]*. In 5G and Beyond, system reliability is defined as the ratio of number of successfully delivered packets to the destination within the time constraint to the total number of packets sent to the destination, expressed in percentage. In 5G, the reliability requirement depends on the service and use case. The targeted reliability in 5G for some mission critical use cases is set to 99.999% [28]. Hence, the *reliability* definition utilized in this work, provides a reasonable estimate of $reliability$ at lower layers of the overall system *reliability*.

In order to tackle the challenging requirements in *hotspot* use cases, a novel frequency reuse method which considers both of these requirements is proposed. In this regard, the problem of finding frequency reuse RRH groups is formulated based on a derivation of RRH reuse distance. This derivation is based on the UEs' lower layer requirements of *reliability* and throughput. Furthermore, the problem of downlink (DL) power allocation among the RRHs belonging to the same frequency reuse RRH group is formulated based on the cooperative game theory technique. An optimal solution for the DL power allocation is achieved using nash bargaining solution (NBS) [43].

The main contributions of this work can be summarized as follows: firstly, the problem of

forming (UE, RRH) pairs, which is based on the minimum pathloss, is formulated. Secondly, the minimum frequency reuse distance is derived, which is based on the *reliability* and throughput requirements of UEs.

Lastly, based on the cooperative game theory the problem of DL power allocation among the RRHs belonging to the same frequency reuse group is formulated. Since, the RRHs within the same reuse group transmit on the same scheduling resources, each transmission link is considered a player in a common interference game. In these scenarios, common non-cooperative solutions such as iterative water-filling [44], which lead to optimal solutions for multiple access and broadcast channels, can be highly sub-optimal in interference limited scenarios [45]. As a result, in the interference limited scenarios, cooperative game theory provides optimal solutions by maintaining efficiency and $fairness$ among the players. The Pareto-optimality property in game theory guarantees the efficiency, and the proportional fairness property arising from the Nash conditions ensures user fairness [45]. Most of the previous approaches in the literature [46, 47] study were targeted to maximize the total transmission rate or SINR of users, mainly using non-cooperative games. But the $fairness$ and $reliability$ issues have been mostly ignored.

In this work, both $fairness$ and $reliability$ for all the UEs is addressed, by employing a novel utility function based on $reliability$, besides optimizing the system to achieve the high sum rate using Nash Bargaining Solution (NBS). The DL power allocation problem among the RRHs in the frequency reuse group based on cooperative game theory is formulated. Further, the existence, uniqueness, and fairness conditions for the cooperative game based on novel utility function are proved analytically, by validating all the Nash conditions, and will prove the existence of an unique NBS. Furthermore, we derive equations for optimum transmit power allocation solution using Lagrange multipliers. Accordingly, an iterative Nash bargaining algorithm is developed, which shows its convergence to a Pareto-optimal equilibrium for the proposed cooperative game. To the best of our knowledge we haven't found any prior work in finding the unique NBS for DL power allocation problem in C-RAN / DAS using the novel $reliability$ based utility functions.

The chapter is organized as follows: first section focuses on the system model of C-RAN / DAS along with $reliability$. The derived $reliability$ expression in Chapter 2 is briefly presented here; Second section presents the first key issue called Pairing; Third section at first formulates the second key issue i.e., the formation of frequency reuse RRH groups in C-RAN / DAS. In this

regard, a novel solution for finding the minimum frequency reuse distance is presented; Fourth section deals with the issue of power allocation among the RRHs belonging to a reuse RRH group, which is addressed by using cooperative game theory methods; Finally, the simulation results to validate the proposed techniques and discussion of results are presented.

3.2 System Model and Methodology

3.2.1 System Model

We consider a scenario, which consists of M RRHs and K UEs distributed over the coverage area. Each RRH can have multiple antennas, but here without loss of generality we consider single antennas at RRHs and UEs. Let the UE k be paired with one of its nearest RRH called r_k, where $r_k \in \{1, 2, .., M\}$ of RRHs. The received signal at UE k can be expressed as:

$$y_k = h_{k,r_k} x_k + \sum_{r_j \in [1,M], r_j \neq r_k} h_{k,r_j} x_j + z_k, \tag{3.1}$$

where h_{k,r_j} represents the channel coefficient between UE k and RRH r_j. The transmitted signal from RRH r_j is represented by x_j. The only intended signal for UE k is represented by x_k, which is transmitted by its paired RRH r_k. The noise at the receiver of UE k is represented by z_k.

3.2.2 Reliability

In 5G URLLC use cases, for e.g. in mission critical applications, determining $reliability$ based on channel models, provides a statistical estimate of the reliable throughput achievable at the UEs. In the succeeding sections, we show how the $reliability$ based analysis can improve system efficiency through, pairing of RRHs with UEs, formation of frequency reuse RRH groups and scheduling of time, frequency, space and power resources. In this subsection, we define the $reliability$ for lower layers in C-RAN / DAS, which is the probability of achieving the UE's minimum required SINR at its location. A non-line of sight (NLOS) scenario based on Rayleigh fading channel model is considered. This derivation is already presented in Section 2.3.1 of Chapter 2. For the sake of continuity, the definition and result from this derivation is given.

In a interference and noise limited system, when N interfering RRHs are transmitting in the

same time, frequency resources as that of (UE, RRH) pair, which is given by (k, r_k), the signal to interference plus noise ratio (SINR) at k^{th} UE is given by,

$$SINR_{k,r_k} = \frac{p_r^{k,r_k}}{p_N^k + \eta}, \tag{3.2}$$

where η is the noise power at the receiver and p_N^k is the interference power observed at k^{th} UE from N interfering RRHs, which reuse the same time-frequency resources. The interference power, p_N^k, can be expressed as $\sum_{r_j \in \{N\}, r_j \neq r_k} p_r^{k,r_j}$.
$Reliability$, R^k, at UE k is given by,

$$R^k = P\big(SINR_{k,r_k} \geq \gamma_k\big) = P\bigg(p^{k,r_k} \geq \gamma_k(p_N^k + \eta)\bigg). \tag{3.3}$$

In Section 2.3.1 of Chapter 2, $Reliability$ is derived to be,

$$R^k(rayleigh) = \exp\Big(-A_k^{r_k}\eta\gamma_k\Big) \prod_{r_j \in [1,M], r_j \neq r_k} \frac{1}{\frac{A_k^{r_k}}{A_k^{r_j}}\gamma_k + 1}, \tag{3.4}$$

where,

$$A_k^{r_k} = \frac{1}{P_t^{r_k} K_{FS}} \Big(\frac{d_{k,r_k}}{d_0}\Big)^{\alpha}, \tag{3.5}$$

represents the inverse of mean received power of the signal from the RRH r_k at UE k based on the Pathloss model. The mean transmitted power of RRH r_k is represented by $P_t^{r_k}$. The distance between the RRH port r_k and UE k is given by d_{k,r_k}. The path loss exponent is given by α. The constant K_{FS} equals to free-space path loss at a reference distance d_0, assuming omni-directional antennas.

3.3 Pairing

(UE, RRH) pairing or association plays an important role in C-RAN design. This aspect has been well investigated in the literature [48, 49]. In C-RAN / DAS, various pairing methods can be employed in order to make use of the potential of the multiple RRHs. However, much care needs to be taken in pairing the UEs with RRHs as the sum rate can be significantly reduced because of the interference arising from multiple RRHs.

In C-RAN / DAS, pairing of RRHs and UEs based on nearest distance has practical significance. As a result of the distributed RRH placements in the coverage area, it is expected that UEs find multiple RRHs at almost the same radial distances. This ensures that there is a very high probability that a UE finds the RRH with the strongest received signal, or minimum path loss, which will most likely be one of the nearest RRHs. This is one of the significant benefits of distributed RRHs, otherwise high power transmission from RRHs distant from UE in order to achieve the targeted SINR at the UE can cause significant increase in interference, which outweighs the benefits of DAS. Therefore, in our investigations we safely assume pairing UE with one of its nearest RRHs, which will most likely result in the minimum pathloss measured at the UE. Selecting the serving eNodeB is achieved in LTE systems [50] by UE performing cell search procedure to find out the best eNodeB before camping on the cell. In C-RAN / DAS the RRH search procedure can be achieved by allocating sub-cell IDs to the RRHs. A UE then can detect the sub-cell ID / RRH ID based on synchronization signals from nearest surrounding RRHs to find the best possible RRH to be paired. Based on the pathloss model described in (3.5), the pathloss between UE k and RRH r_j is given by,

$$PL(k, r_j) = \frac{1}{K_{FS}} \Big(\frac{d_{k,r_j}}{d_0} \Big)^{\alpha}. \tag{3.6}$$

Let (k, r_k) denote the (UE, RRH) pair for k^{th} UE from the set of K UEs and RRH r_k from the set of M RRHs, which is selected according to minimum pathloss, which is given by, $r_k = \arg\min_{r_j \in [1,M]} PL(k, r_j)$.

3.4 Frequency Reuse

3.4.1 Problem Formulation

In order to meet the stringent throughput demands in *hotspot* scenarios like stadiums and shopping malls, where the required throughput density, which is total throughput per square meter area, is very high, rapid frequency reuse becomes inevitable. Many techniques of frequency reuse for CAS are available in literature [51–53], such as: hard frequency reuse, soft frequency reuse, fine frequency reuse and fractional frequency reuse of resources. In the high system rate density scenarios, applying the conventional static frequency resources sharing methods among

RRHs will not meet this requirement. On the contrary, not much work has been reported in the literature about reuse techniques for C-RAN / DAS. In our work, we consider frequency reuse at very small quantized scheduling [51] time-frequency resource, as it provides more opportunities and flexibility in forming reuse pairs. For e.g. in 3GPP LTE the smallest scheduling resource is called as resource block (RB), which is around 180 KHz and 0.5 ms in time. In this work we use the term RB generically for the smallest quantized scheduling resource. As different UEs within the RRH coverage can be located at different distances from RRH, the transmitted power levels from the RRH can be different in the different RBs. This dynamic nature of transmitted power levels and scheduling resources over UEs provide opportunities for finding dynamic reuse sets of RRHs for different RBs, instead of using a fixed reuse set of RRHs based on traditional frequency reuse techniques.

Finding the set of $\{N_b\}$ pairs that can reuse the RB b, involves exhaustive search over the all the possible (UE, RRH) pairs, which will involve high computational complexity. Therefore, in Section 3.4.2, we have derived a novel, reliable and low complexity method of finding the RB reuse pairs by deriving the minimum RRH reuse distance based on the UE positions, SINR requirements and $reliability$ requirements of the UEs.

3.4.2 Minimum Reuse Distance

In this section, in order to derive the minimum reuse distance between two RRHs, we have considered the $reliability$ based on Rayleigh Fading channel. Let $\{N_b\}$ be the set of reuse RRHs of RB b with a total of N_b RRHs, where the bandwidth of each RB is Δf. Let B denotes the total number of RBs in the DAS bandwidth W, therefore $W = B\Delta f$. Let R^k represents the minimum required reliability at k^{th} UE for a specific SINR requirement γ_k, which is the required rate for the UE. The reliability R^k sets a requirement on the probability of coverage which is derived in (3.4). This implies that,

$$R^k \leq \exp\Big(-A_k^{r_k}\eta\gamma_k\Big) \prod_{r_j\in\{N_b\}, r_j\neq r_k} f(k, r_j) \tag{3.7}$$

where $f(k,j) = \frac{1}{\frac{A_k^{r_k}}{A_j^{r_k}}\gamma_k+1}$ represents the effect on the probability of coverage at UE k because of the transmission from RRH r_j. In order to meet the reliability requirement of UE k fairly

among the N_b reuse RRHs, we can impose the condition $f(k, r_j) \geq (R^k)^{\frac{1}{N_b}}$. Similarly at UE $j \in \{N_b\}, j \neq k$, we have the condition $f(j, r_k) \geq (R^j)^{\frac{1}{N_b}}$. In deriving $f(k, r_j)$ and $f(j, r_k)$ expressions, the exponential term in (3.7) is ignored, as it tends to 1 in C-RAN / DAS. This is because in C-RAN / DAS the received SNR is much higher compared to the SINR requirement due to the very small coverage area of RRH. As $f(j, r_k)$ and $f(k, r_j)$ are functions of transmit powers $P_t^{r_k}$, $P_t^{r_j}$ of RRHs r_k, r_j and the distances between UEs k, j and RRHs r_k, r_j, the following conditions are derived:

$$\begin{aligned} \frac{P_t^{r_j}}{P_t^{r_k}} &\geq \gamma_k \Big(\frac{d_{j,r_j}}{d_{j,r_k}}\Big)^{\alpha} \frac{(R_j)^{\frac{1}{N_b}}}{1-(R_j)^{\frac{1}{N_b}}}, \\ \frac{P_t^{r_j}}{P_t^{r_k}} &\leq \frac{1}{\gamma_k} \Big(\frac{d_{k,r_j}}{d_{k,r_k}}\Big)^{\alpha} \frac{(R_k)^{\frac{1}{N_b}}}{1-(R_k)^{\frac{1}{N_b}}}. \end{aligned} \tag{3.8}$$

From the conditions in (3.8) we can derive that

$$\Big(\frac{d_{k,r_j} d_{j,r_k}}{d_{k,r_k} d_{j,r_j}}\Big)^{\alpha} \geq \gamma_k \gamma_j \Bigg(\frac{(R_k R_j)^{\frac{1}{N_b}}}{(1-(R_k)^{\frac{1}{N_b}})(1-(R_j)^{\frac{1}{N_b}})}\Bigg). \tag{3.9}$$

Let,

$$S_{kj} = \Bigg(\gamma_k \gamma_j \frac{(R_k R_j)^{\frac{1}{N_b}}}{(1-(R_k)^{\frac{1}{N_b}})(1-(R_j)^{\frac{1}{N_b}})}\Bigg)^{\frac{1}{\alpha}}. \tag{3.10}$$

Let D_{r_k,r_j} represent be the separation distance between RRHs r_k and r_j, which is given by

$$D_{r_k,r_j}^2 = d_{k,r_j}^2 + d_{k,r_k}^2 - 2 d_{k,r_j} cos(\theta) \tag{3.11}$$

where θ represents the angle between vectors $\overline{d}_{k,r_k}$ and $\overline{d}_{k,r_j}$. We have assumed the worst case scenario where both the UEs are at edge of RRH coverage radius,for the RRH reuse distance calculation. This condition implies to consider the minima of D_{r_k,r_j} in (3.11). So, (3.9) can be reformulated as

$$\Big(\frac{D_{r_k,r_j}}{d_{k,r_k}} - 1\Big)\Big(\frac{D_{r_k,r_j}}{d_{j,r_j}} - 1\Big) \geq S_{kj}. \tag{3.12}$$

On solving (3.12), it gives a feasible solution which is

$$\begin{aligned} D_{r_k,r_j} &\geq \frac{1}{2}\Big(d_{k,r_k} + d_{j,r_j} + \sqrt{(d_{k,r_k} - d_{j,r_j})^2 + 4S_{kj}d_{k,r_k}d_{j,r_j}}\Big) \\ D^{min}_{r_k,r_j} &= \frac{1}{2}\Big(d_{k,r_k} + d_{j,r_j} + \sqrt{(d_{k,r_k} - d_{j,r_j})^2 + 4S_{kj}d_{k,r_k}d_{j,r_j}}\Big). \end{aligned} \tag{3.13}$$

The significance of this novel expression is that, $D^{min}_{r_k,r_j}$ in (3.13) depends only on the distances between the UEs and their serving RRHs and not on the distances between all other RRHs. This reduces the complexity and overhead of collecting information about distances between all RRHs and all UEs besides significantly reducing the computational complexity. The UE $reliability$ and throughput requirements have been considered in S_{kj} parameter. For illustration, in a practical scenario with $R_k = R_j = 0.8$ and $\gamma_k = \gamma_j = 15dB$ with pathloss exponent $\alpha = 3$ and $N_b = 6$, $S_kj \approx 180$ and UEs k, j are locate at rrh coverage edge then, $D^{min}_{r_k,r_j} = 1 + \sqrt{S_{kj}}$= 10 times the RRH coverage radius.

3.5 Power Allocation

3.5.1 Problem Formulation

The other main challenge we will address in this work is the problem of optimal DL power allocation among the RB reuse RRHs within a RB reuse group $\{N_b\}$. Among the set of $\{N_b\}$ reuse pairs of RB b, in order to reliably and fairly meet the varied users' quality of service (QOS) requirements such as: UE priority, SINR and reliability, an effective and fast power allocation of RRHs is indispensable. Our work addresses both user-reliability requirements and user-fairness by making use of cooperative game theory.

Game theory [54] is a well established mathematical tool, which can be very beneficial in analyzing complex decision making problems where the decision of each decision maker affects others involved in the game. The participants in the game or the decision makers are called players in game theory. In this work, N_b stands for number of players in the game, which are the number of (UE, RRH) pairs which reuse the same Resource Block (RB) b. The basic component of game theory is a game, $G = \langle \mathcal{K}_b, \{\mathcal{P}^b_k\}_{k\in\mathcal{K}_b}, \{u^b_k\}_{k\in\mathcal{K}_b}\rangle$, where: $\mathcal{K}_b \in \{1, 2, ..., N_b\}$ is the set of (UE, RRH) pairs that are selected for reuse of RB b, where N_b represents the number of (UE, RRH) pairs reusing RB b. $\mathcal{P}^b_k$ is the set of transmit power allocation strategies for

each RRH $r_k \in \{N_b\}$; and $u_k^b(\mathbf{p})$ is the utility function of the UE k, in the (k, r_k) UE pair. The combination of DL power allocation strategies is given by $\mathbf{p} = \{p_t^{r_1}, p_t^{r_2}, ..., p_t^{r_{N_b}}\}$, where $\mathbf{p} \in \{\mathcal{P}_k^b\}$. We assume that the set of power allocation strategies, $\{\mathcal{P}_k^b\}$, be a closed and convex subset of $\mathbb{R}_{++}^{N_b}$. In general, the game outcome $u_k^b(\mathbf{p})$ for UE k depends on all the RRHs' power choices through $\mathbf{p}$. Let $u_k^{b\ min}$ be the minimum payoff the k^{th} UE would expect. Hence, $U_k^{b\ min} = \{u_1^{b\ min}, u_2^{b\ min}..., u_{N_b}^{b\ min}\}$.

In this section, a cooperative bargaining game model is formulated, where the goal is to maximize a function (3.14) of individual utility functions $\{u_k^b\}_{k\in\mathcal{K}_b}$ of UEs belonging to the $\{N_b\}$ reuse pairs. As given in Eq. (3.15) we have considered two scenarios for constraining the transmit power for practical implementation: firstly, total transmit power of RRHs, secondly, individual transmit power of each RRH. In addition, the minimum reliability requirements (3.16) of each UE are constrained to provide efficient management of QOS requirements of UEs. With these considerations, we formulate a DL power allocation optimization problem that determines $\mathbf{p} = \{p_t^{r_1}, p_t^{r_2}, ..., p_t^{r_{N_b}}\}$ as,

$$\max_{\mathbf{p}=(p_1,p_2,...,p_{N_b})} f\Big(u_1^b(\mathbf{p}), u_2^b(\mathbf{p}), ..., u_{N_b}^b(\mathbf{p})\Big), \tag{3.14}$$

$$subject\ to \sum_{r_k=1}^{N_b} p_k \leq P_{max}\ or\ p_k \leq P_{max}, \tag{3.15}$$

$$u_k \geq u_k^{b\ min}, \qquad k = 1, 2, ..., N_b. \tag{3.16}$$

This problem will be defined, analyzed and solved in the next subsection.

3.5.2 Problem Definition

In this section, the Nash bargaining solution (NBS) [43]for the game formulated in subsection 3.5.1 is presented. Firstly, a novel $reliability$ utility function for the cooperative game model given in (3.14) is proposed. Secondly, function (3.14) of the cooperative game, which maximizes

the utility functions of all the UEs is proposed. Thirdly, the existence, fairness and uniqueness properties of the solution for the formulated game are proved. Finally, an iterative Nash bargaining algorithm for optimum power allocation is developed in order to achieve optimum and fair DL power allocation among the set of $\{N_b\}$ RRHs which reuse RB b. Furthermore, a novel utility function for (3.14) is formulated, which is based on the derived $reliability$.

The following text and "Definition 1" is derived from "Nash bargaining between friends for cooperative data distribution in a social peer-to-peer swarming system" published in "2013 International Conference on Machine Learning and Cybernetics" by IEEE, year 2013 authored by G. Wang [55]

In game theory, an *agreement point* is any strategy vector $\mathbf{p} \in \{\mathcal{P}_k^b\}$, which belongs to one of the possible outcomes of the bargaining process. A *disagreement point* is any strategy vector $\mathbf{p} \in \{\mathcal{P}_{r_k}^b\}$ that is usually a result of non-cooperative play in which all the players disagree. Therefore, the utility achieved by every player at the *agreement point* should be better than or equal to every player's utility at the *disagreement point*. Nash proposed the following conditions for the game in order to reach Pareto-optimal NBSs [43, 54].

Definition 1: **Nash Bargaining Solution [56]**. Let $U^b = \{\{u_k^b(\mathbf{p}) | \mathbf{p} \in \{\mathcal{P}_k^b\}\}\}$ be a convex, closed and upper bounded subset of $\mathbb{R}_{++}^{N_b}$. Let $\mathbf{p}_d$ be the disagreement point, $u_k^{b\,min} = u_k^b(\mathbf{p}_d)$ be utility of UE k at the disagreement point, and $U_a^b = \{\mathbf{u}^b \in U | \mathbf{u}^b \geq \mathbf{u}_{min}^b\}$ be the set of achievable utilities. Then $\mathbf{u}^{b\star} = \phi(U^b, \mathbf{u}_{min}^b)$ is a NBS if it fulfills the following necessary conditions:

1. Individual rationality (IR): $u_k^{b\star} \geq u_k^{b\,min}$, implying $\mathbf{u}^{b\star} \in U_a^b$.
2. Pareto optimality (PO): If there exists $\mathbf{u}^{b\prime} \in U_a^b$ such that $u_k^{b\prime} \geq u_k^{b\star}$, then $u_k^{b\prime} = u_k^{b\star}, \forall k$.
3. Invariance to affine transformations (INV): if $\psi : \mathbb{R}^{N_b} \rightarrow \mathbb{R}^{N_b}$, $\psi(\mathbf{u}^b) = \mathbf{u}_\prime^b$ with $u_k^{b\prime} = c_k u_k^b + d_k,\ c_k, d_k \in \mathbb{R}, c_k > 0, \forall k$, then $\phi(\psi(U^b), \psi(\mathbf{u}_{min}^b)) = \psi(\phi(U^b, \mathbf{u}_{min}^b)$.
4. Independence of irrelevant alternatives (IIA): if $\mathbf{u}_\prime^b \in V \subset U$ and $\mathbf{u}_\prime^b = \phi(U, \mathbf{u}_{min}^b)$ then $\phi(V, \mathbf{u}_{min}^b) = \mathbf{u}_\prime^b$.
5. Symmetry (SYM): if U^b is symmetric with respect to k and l, $u_k^{b\,min} = u_l^{b\,min}$, and $\mathbf{u}_\prime^b = \phi(U, \mathbf{u}_{min}^b)$, then $u_k^{b\prime} = u_l^{b\prime}$.

The following text is derived from "Cooperative Game Theory for Distributed Spectrum

Sharing" published in "2007 IEEE International Conference on Communications" by IEEE, authored by J. E. Suris [57]

From the above conditions, INV, IIA and SYM, ensure the fairness aspect of NBS [57]. IIA condition makes sure that if the domain of game is reduced to a subset which constitutes the NBS, then the NBS will be the same, which implies the invariance of NBS. SYM condition ensures that NBS is not bound to the player positions or labels, which implies that if two players have the same disagreement utility belonging to the same utility set, then they will always arrive at the same NBS . INV condition always ensure that the NBS is invariant if the utility function is affinely transformed.

The following text and "Lemma 1" is extracted from "Nash bargaining between friends for cooperative data distribution in a social peer-to-peer swarming system" published in "2013 International Conference on Machine Learning and Cybernetics" by IEEE, year 2013 authored by G. Wang [55]

The following lemma, *Lemma 1*, which helps to find an unique NBS in case of convex utility spaces [58], was first postulated for a two-player games by Nash [59]. This lemma is then later extended for more than two players in [56].

Lemma 1 (Extended Nash Theorem) [56]: Let $K_b = \{k \in 1, ..., N_b | \mathbf{u}^b \in U_a^b, u_k^b > u_k^{b\,min}\}$ be the set of players that can achieve a utility strictly greater the utility at the disagreement point, which is $u_k^{b\,min}$, then the unique NBS, $\mathbf{u}^{b\star}$, is the maximizer of the Nash product (NP):

$$\mathbf{u}^{b\star}(\mathbf{p}^\star) = \arg \max_{\mathbf{u} \in U_a^b} \prod_{k \in K_b} (u_k^b(\mathbf{p}) - u_k^{b\,min}), \tag{3.17}$$

where $\mathbf{p}^\star$ is the unique and fair NBS for DL power allocation among the reuse RRHs of RB b.

Therefore,Lemma 1 states that the sufficient condition to get an unique NBS is the convexity of the utility space U^b [56].

3.5.3 Design of Novel Utility Function

In order to make *Lemma 1* relevant for our DL power allocation problem, a decisive step is design of utility function. The key here is to find utility expressions which not only comprehensively represent the requirements of players but also mathematically feasible expressions which ensure

global convergence to the NBS. In this work, a novel utility function u_k^b which is the required reliability R_k of the targeted SINR γ_k at UE k is employed, where $(k, r_k) \in \{K_b\}$. We make use of a set of minimum required reliability thresholds $\{R_k^{min}\}_{k\in\{K_b\}}$ as the disagreement points, which reflect the minimum QOS requirement in terms of reliability of the targeted SINR. In this analysis, the $reliability$ over Rayleigh fading channel, which is derived in (2.14) Section 3.2, is used as the utility function. Therefore we can express the utility function as,

$$u_k^b(\mathbf{p}) = \exp\Big(-A_k^{r_k}\eta\gamma_k\Big) \prod_{r_j\in\{N_b\}, r_j\neq r_k} \frac{1}{\frac{A_k^{r_k}}{A_k^{r_j}}\gamma_k + 1}, \tag{3.18}$$

where $A_k^{r_k} = \frac{1}{p_t^{r_k} K_{FS}}(\frac{d_{k,r_k}}{d_0})^\alpha$ and $A_k^{r_j} = \frac{1}{p_t^{r_j} K_{FS}}(\frac{d_{k,r_j}}{d_0})^\alpha$ as described in (3.5).

Definition 2: It has been shown in [60] that the standard NBS framework can be extended to certain "log convex" utility sets, which is based on transformation of utility functions as given by, $q_k^b(\mathbf{p}) := \ln\big(u_k^b(\mathbf{p})\big), \forall k \in \{N_b\}$, which denote the logarithmic transformation of the utility function u_k^b, which is given by,

$$q_k^b(\mathbf{p}) = \Big(-A_k^{r_k}\eta\gamma_k\Big) - \sum_{r_j\in\{N_b\}, r_j\neq r_k} \ln\left(\frac{A_k^{r_k}}{A_k^{r_j}}\gamma_k + 1\right). \tag{3.19}$$

This approach is a common technique in order to exploit the "hidden convexity" [61, 62]. It is proved in [63] that the product maximizer of (3.17) is the single-valued NBS if the set of transformed utilites $\{q_k^b(\mathbf{p})\}$ is a *strictly convex, compact* and *comprehensive* set.

Using this utility set, the DL power allocation game which was presented in (3.14) can be now represented as,

$$\begin{aligned} \mathbf{q}^{b\star}(\mathbf{p}^\star) &= \arg\max_{\mathbf{q}\in Q_a^b} \sum_{k\in K_b} q_k^b(\mathbf{p}) \\ subject\ to \sum_{k=1}^{N_b} p_k &\leq P_{max} \\ u_k &\geq u_k^{b\ min}, \qquad k = 1, 2, ..., N_b. \end{aligned} \tag{3.20}$$

In order to find that the Nash conditions for the utility set are met, to have a unique NBS, for the sake of convenience without loss of generality, we have assumed $\{u_k^{b\ min}\} = \{0\}$ in (3.20).

This assumption for the sake of verification of the existence of unique NBS is valid because the existence of a unique NBS is always guaranteed by the properties of the utility set only [63].

Theorem 1: The log-transformed feasible utility set $Q^b = \{\mathbf{q}^b(\mathbf{p}) = \ln(\mathbf{u}^b(\mathbf{p}))| \sum_{k=1}^{N_b} p_t^{r_k} \leq P_{max}, \mathbf{u}^b(\mathbf{p}) \in U^b\}$ is *non-empty*, *compact*, *comprehensive* and *convex*.

Proof: U^b is a *non-empty* subset of $\mathbb{R}_{++}^{N_b}$, where $\mathbb{R}_{++}$ is the set of positive reals, which implies that in the RB reuse scenario considered, all the $\{N_b\}$ set of (UE, RRH) pairs participate, i.e., they have non-zero utility. U^b is *compact* because of the constraint on the sum of the transmit powers, which is $\sum_{k=1}^{N_b} p_t^{r_k} \leq P_{max}$. U_b is *comprehensive*, that means that for all $\mathbf{u}^b(\mathbf{p}) \in U^b$ and $\mathbf{u}^{b\prime}(\mathbf{p}) \in \mathbb{R}_{++}^{N_b}$, the component-wise inequality $\mathbf{u}^{b\prime}(\mathbf{p}) < \mathbf{u}^b(\mathbf{p})$ implies $\mathbf{u}^{b\prime}(\mathbf{p}) \in U^b$. Since *compactness* and *comprehensiveness* of U^b are preserved by the log-transformation, the log-transformed utility set $Q_b \in \mathbb{R}^{N_b}$ is also *compact* and *comprehensive* in addition to *non-empty*.

In order to prove the *convexity* of Q_b, we assume that, $\frac{A_k^{r_k}}{A_k^{r_j}}\gamma_k << 1$, which is a valid assumption in the bounds of reliability considered in our investigations. Usual reliability requirements are typically greater than 0.8. Consequently, $\ln(1 + \frac{A_k^{r_k}}{A_k^{r_j}}\gamma_k) \approx \frac{A_k^{r_k}}{A_k^{r_j}}\gamma_k$. Based on the Taylor series expansion of $\ln(1+x)$ the error due to the approximation is quite negligible for the reliability bounds considered. With this approximation, (3.19) can be rewritten as,

$$\begin{aligned} q_k^b(\mathbf{p}) \approx \hat{q}_k^b(\mathbf{p}) &= \Big(- A_k^{r_k}\eta\gamma_k \Big) - \sum_{r_j \in \{N_b\}, r_j \neq r_k} \left(\gamma_k \frac{A_k^{r_k}}{A_k^{r_j}} \right), \\ \hat{q}_k^b(\mathbf{p}) &= \Big(- A_k^{r_k}\eta\gamma_k \Big) - \frac{1}{p_t^{r_k}} \sum_{r_j \in \{N_b\}, r_j \neq r_k} \gamma_k p_t^{r_j} \left(\frac{d_{k,r_k}}{d_{k,r_j}} \right)^{\alpha}. \end{aligned} \tag{3.21}$$

Therefore, log-transformed feasible set can be represented as,

$$\begin{aligned} Q^b &= \{\hat{q}_1^b(\mathbf{p}), \hat{q}_2^b(\mathbf{p}) ... \hat{q}_{N_b}^b(\mathbf{p}))| \sum_{k=1}^{N_b} p_t^{r_k} \leq P_{max}\}, \\ Q^b &= \{\hat{q}_1^b(\mathbf{p}), ... \hat{q}_{N_b}^b(\mathbf{p}))| - \sum_{k=1}^{N_b} \frac{\gamma_k p_t^{r_j} \left(\frac{d_{k,r_k}}{d_{k,r_j}} \right)^{\alpha}}{\hat{q}_k^b(\mathbf{p}) + \Big(A_k^{r_k}\eta\gamma_k \Big)} \leq P_{max}\}. \end{aligned} \tag{3.22}$$

Let $\hat{q}_k^{b1}(\mathbf{p}), \hat{q}_k^{b2}(\mathbf{p}) \in Q^b$ and $\xi \in [0, 1]$, in order to prove that any point on the line $\xi\hat{q}_k^{b1}(\mathbf{p}) + (1 -$

$\xi)\hat{q}_k^{b2}(\mathbf{p})$ is also in Q^b, which is represented as,

$$-\sum_{k=1}^{N_b} \frac{\gamma_k p_t^{r_j} \left(\frac{d_{k,r_k}}{d_{k,r_j}}\right)^{\alpha}}{\xi\hat{q}_k^{b1}(\mathbf{p}) + (1-\xi)\hat{q}_k^{b2}(\mathbf{p}) + \left(A_k^{r_k}\eta\gamma_k\right)} \leq P_{max}. \tag{3.23}$$

Let us define,

$$h_k(\xi) = \frac{\gamma_k p_t^{r_j} \left(\frac{d_{k,r_k}}{d_{k,r_j}}\right)^{\alpha}}{\xi\hat{q}_k^{b1}(\mathbf{p}) + (1-\xi)\hat{q}_k^{b2}(\mathbf{p}) + \left(A_k^{r_k}\eta\gamma_k\right)}. \tag{3.24}$$

Then,

$$\frac{d}{d^2\xi}h_k(\xi) = \frac{2\gamma_k p_t^{r_j} \left(\frac{d_{k,r_k}}{d_{k,r_j}}\right)^{\alpha}}{\left(\xi\hat{q}_k^{b1}(\mathbf{p}) + (1-\xi)\hat{q}_k^{b2}(\mathbf{p}) + \left(A_k^{r_k}\eta\gamma_k\right)\right)^2}(\hat{q}_k^{b1} - \hat{q}_k^{b2})^2 \geq 0, \tag{3.25}$$

which proves the *convexity* of Q_b. Therefore, *Theorem 1* is proved, which confirms the existence of NBS.

In order to prove the uniqueness of NBS, *strict convexity* [63] of the log-transformed set $\{Q_b\}$ plays an important role.

Theorem 2 (Uniqueness): The log-transformed feasible utility set $Q^b = \{\mathbf{q}^b(\mathbf{p}) = \ln(\mathbf{u}^b(\mathbf{p}))|$ $\sum_{k=1}^{N_b} p_t^{r_k} \leq P_{max}, \mathbf{u}^b(\mathbf{p}) \in U^b\}$ is *strictly convex*, hence there exists an unique NBS.

Proof: In order to prove the *strict convexity* of Q_b on its strategy set $\mathcal{P}_k^b$, according to [43] the following condition is to be met: for any $\mathbf{p}^{(0)} \neq \mathbf{p}^{(1)}$ with $\mathbf{p}^{(k)} = [p_t^{r_1\,(k)}, p_2^{r_2\,(k)}, ..., p_{N_b}^{r_1\,(k)}] \in \mathcal{P}_k^b$ for $k = 0, 1$ and for $\mathbf{v} = [v_1, v_2, ..., v_{N_b}]^T$, then

$$\left(\mathbf{p}^{(0)} - \mathbf{p}^{(1)}\right)^T U\left(\mathbf{p}^{(0)}, \mathbf{v}\right) + \left(\mathbf{p}^{(1)} - \mathbf{p}^{(0)}\right)^T U\left(\mathbf{p}^{(1)}, \mathbf{v}\right) < 0 \tag{3.26}$$

where $U\big(\mathbf{p},\mathbf{v}\big)=\Big[v_1\frac{\partial q_1^b(\mathbf{p})}{\partial p_t^{r_1}},...,v_{N_b}\frac{\partial q_{N_b}^b(\mathbf{p})}{\partial p_t^{r_{N_b}}}\Big]^T$. To prove this condition, (3.26) can be written as,

$$\begin{aligned}\big(\mathbf{p}^{(0)}-\mathbf{p}^{(1)}\big)^T U\big(\mathbf{p}^{(0)},\mathbf{v}\big)+\big(\mathbf{p}^{(1)}-\mathbf{p}^{(0)}\big)^T U\big(\mathbf{p}^{(1)},\mathbf{v}\big)=\\ \sum_{k=1}^{N_b} v_k\big(p_t^{r_k\ (0)}-p_t^{r_k\ (1)}\big)\left(\frac{\partial q_k^b(\mathbf{p})}{\partial p_t^{r_k\ (0)}}-\frac{\partial q_k^b(\mathbf{p})}{\partial p_t^{r_k\ (1)}}\right).\end{aligned} \tag{3.27}$$

According to (3.21), $\frac{\partial q_k^b(\mathbf{p})}{\partial p_t^{r_k\ (0)}}=\left(\frac{1}{p_t^{r_k\ (0)}}\right)^2 C_k^{(0)}$, where $C_k^{(0)}=\sum_{r_j\in\{N_b\},r_j\neq r_k}\gamma_k p_t^{r_j}\left(\frac{d_{k,r_k}}{d_{k,r_j}}\right)^{\alpha}>0$. As $\frac{\partial q_k^b(\mathbf{p})}{\partial p_t^{r_k\ (0)}}$ is monotonically decreasing with respect to $p_t^{r_k\ (0)}$, we have $\left(p_t^{r_k\ (0)}-p_t^{r_k\ (1)}\right)\left(\frac{\partial q_k^b(\mathbf{p})}{\partial p_t^{r_k\ (0)}}-\frac{\partial q_k^b(\mathbf{p})}{\partial p_t^{r_k\ (1)}}\right)<0$ for $p_t^{r_k\ (1)}>p_t^{r_k\ (0)}$. Using this result in the summation of (3.26), results always in a negative value, which proves the $Theorem2$ and hence the $uniqueness$ condition is fulfilled.

Because of the one-to-one logarithmic mapping between the sets Q_b and U_b, all Nash conditions: IR, PO, INV, IIA, SYM in the utility set U_b corresponds directly to log-transformed utility set Q_b. Furthermore, it has been proven in [60, 63] that the solution outcome in the log-transformed set Q_b satisfies all the Nash conditions if and only if it is the unique maximizer of

$$\mathbf{q}^{b\star}(\mathbf{p}^{\star})=\arg\max_{\mathbf{q}\in Q_a^b}\sum_{k\in K_b}\hat{q}_k^b(\mathbf{p}). \tag{3.28}$$

Consequently, for all U_b the optimizer of (3.28) in the log-transformed domain Q_b leads to the unique optimizer in U_b [63].

3.5.4 Derivation of Nash Bargaining Solution

Having established the existence and uniqueness of NBS in the log-transformed set and the direct correspondence of the optimization in the non-transformed set U_b, we can now safely introduce the disagreement points $\{u_k^{b\ min}\}$, as the existence of NBS is dependent only on the properties of utility sets.

Case 1: Sum of transmit powers constrained

We now solve for the unique solution of the constrained optimization problem, in case of the sum transmit power constrained, given as,

$$\begin{aligned} \mathbf{u}^{b\star}(\mathbf{p}^{\star}) = &\max_{\mathbf{u}\in U_a^b} \sum_{k\in K_b} \alpha_k \ln(u_k^b(\mathbf{p}) - u_k^{b\,min}) \\ subject\ to &\sum_{r_k=1}^{N_b} p_t^{r_k} \leq P_{max} \\ &u_k \geq u_k^{b\,min}, \qquad k = 1, 2, ..., N_b. \end{aligned} \tag{3.29}$$

In order to enhance the flexibility, in (3.29) we have additionally included the utility weights $\{\alpha_k\}$, which reflect the different priorities or fairness policies of UEs to be used in NBS. $\{\alpha_k\}$s' in NBS are also called as users' bargaining powers.

We make use of Lagrange multipliers [43] method for solving the problem of constrained optimization . Let λ and $\{\mu\} := (\mu_1, \mu_2, ..., \mu_{N_b})$ be the Lagrange multipliers for the multiple constraints given in (3.29). Then, the optimum solution of (3.29) can be equivalently solved by maximizing the equation

$$\begin{aligned} L(\{u_k^b(\mathbf{p})\}, \lambda, \{\mu\}) = &\sum_{k\in K_b} \alpha_k \ln(u_k^b(\mathbf{p}) - u_k^{b\,min}) \\ &-\lambda\left(\left(\sum_{k\in K_b} p_t^{r_k}\right) - P_{max}\right) + \sum_{k\in K_b} \mu_k (u_k^b(\mathbf{p}) - u_k^{b\,min}). \end{aligned} \tag{3.30}$$

In order to find the maximizer,

$$\frac{dL}{dp_t^{r_k}} = \frac{\alpha_k}{(u_k^b(\mathbf{p}) - u_k^{b\,min})} \frac{du_k^b(\mathbf{p})}{dp_t^{r_k}} - \lambda + \mu_k \frac{du_k^b(\mathbf{p})}{dp_t^{r_k}} = 0, \tag{3.31}$$

which results in,

$$\frac{du_k^b(\mathbf{p})}{dp_t^{r_k}} = \frac{\lambda}{\frac{\alpha_k}{(u_k^b(\mathbf{p}) - u_k^{b\,min})} + \mu_k}. \tag{3.32}$$

since $\frac{du_k^b(\mathbf{p})}{dp_t^{r_k}} = u_k^b(\mathbf{p})\frac{d\ln(u_k^b(\mathbf{p}))}{dp_t^{r_k}}$ and finding $\frac{d\ln(u_k^b(\mathbf{p}))}{dp_t^{r_k}}$ using (3.21) results in,

$$\frac{d\ln(u_k^b(\mathbf{p}))}{dp_t^{r_k}} = \frac{\gamma_k \eta (d_{k,r_k})^\alpha}{(p_t^{r_k})^2} + \sum_{r_j \in \{N_b\}, r_j \neq r_k} \gamma_k p_t^{r_j} \left(\frac{d_{k,r_k}}{d_{k,r_j}}\right)^\alpha. \tag{3.33}$$

Using the result of (3.33) in (3.32) gives,

$$\begin{aligned}(p_t^{r_k})^2 = \frac{u_k^b(\mathbf{p})}{\lambda}\Big(\frac{\alpha_k}{(u_k^b(\mathbf{p}) - u_k^{b\ min})} + \mu_k\Big)\Big(\gamma_k \eta (d_{k,r_k})^\alpha) + \\ \sum_{r_j \in \{N_b\}, r_j \neq r_k} \gamma_k p_t^{r_j} \left(\frac{d_{k,r_k}}{d_{k,r_j}}\right)^\alpha\Big).\end{aligned} \tag{3.34}$$

Using Karush-Kuhn-Tucker condition [64] can encounter the NP-hard problem. Therefore, based on the derived (3.34), we develop here an iterative procedure that updates the transmit power allocation among the $\{N_b\}$ reuse RRHs of RB b given by

$$p_t^{r_k(itr)} = \sqrt{\left[\frac{1}{\lambda^{(itr-1)}}\left((\gamma_k \eta (d_{k,r_k})^\alpha + \sum_{r_j \in \{N_b\}, r_j \neq r_k} \gamma_k p_t^{r_j(itr-1)}\right)}{\left(\frac{d_{k,r_k}}{d_{k,r_j}}\right)^\alpha\right)\left(\frac{\alpha_k u_k^b(\mathbf{p}^{(itr-1)})}{u_k^b(\mathbf{p}^{(itr-1)}) - u_k^{b\ min}}\right) + \mu_k^{(itr-1)}\right)\Bigg]_0^+} \tag{3.35}$$

where $[x]_0^+ = x$ if $x > 0$, and $[x]_0^+ = 0$ if $x < 0$. In this iterative procedure for power allocation, the utility function $u_k^b(\mathbf{p}^{(itr-1)})$ values are calculated based on (3.18). In general one can make use of dynamic $u_k^b(\mathbf{p}^{(itr-1)})$ based on measurements as well. The reuse RRHs $\{N_b\}$ cooperate through the selection of $\lambda^{(itr)}$, which is common in all $p_t^{r_k(itr)}$ such that $\sum_{k=1}^{N_b} p_t^{r_k} \leq P_{max}$. Based on the cooperation and total transmit constraint, equation (3.35) gives rise to an iterative water-filling interpretation. The power allocation is adjusted according to proportional fairness factor $\frac{u_k^b(\mathbf{p}^{(itr-1)})}{u_k^b(\mathbf{p}^{(itr-1)}) - u_k^{b\ min}}$, as well as the UE priorities reflected by their bargaining powers $\{\alpha_k\}$, and the adjustable water-filling level factor λ.

The Lagrange multipliers $\lambda^{(itr)}$ and $\{\mu_k^{(itr)}\}$ are to be carefully initialized to ensure fast

convergence. We used *subgradient* method [65] to calculate the multipliers as given below:

$$\begin{aligned} \lambda^{(itr)} &= \Big[\lambda^{(itr-1)} - \beta\Big(P_{max} - \sum_{r_k \in K_b} p_t^{r_k(itr)}\Big)\Big]_0^+, \\ \mu_k^{(itr)} &= \Big[\mu_k^{(itr-1)} - \beta\Big(u_k^b(\mathbf{p}^{(itr)}) - u_k^{b\ min}\Big)\Big]_0^+ \end{aligned} \tag{3.36}$$

where β is a very small step size. The Algorithm 1 below describes the implementation steps NBS for optimal power allocation:

Algorithm 1: NBS for optimal power allocation with sum transmit power constraint

1. *Initialization*: For each UE $k := 1 : N_b, \forall\{K_b\}$

   a) minimum required SINR : γ_k

   b) minimum required reliability : $u_k^{b\ min}$

   c) priority / bargaining power : α_k

   d) minimum transmit power : $p_t^{r_k(0)}$

   e) UE specific Lagrange mutliplier : $\mu_k^{(0)}$

   Initialize the reuse RRHs cooperation multiplier $\lambda^{(0)}$ with a large value. The maximum sum transmit power P_{max} is initialized based on the RRHs capabilities and conformance requirements.

2. *Iteration*:

   a) calculate the utility functions $u_k^b(\mathbf{p}^{(itr-1)})$ using (3.18)

   b) update the power allocation values $p_t^{r_k(itr)}$ using (3.35)

   c) update the multipliers $\lambda^{(itr)}$ and $\mu_k^{(itr)}$ using (3.36)

3. *Convergence check*:

   After step 2) converges, the power allocation decisions $p_t^{r_k(itr)}$ reach the optimal NBS

Case 2: Individual transmit power constrained

Here we consider the case in which the transmit power of each RRH is constrained. This case is of more practical value as each RRH is usually limited by hardware design to a maximum

transmit power $P_{max}^{r_k}$. The constrained optimization problem is given as,

$$\begin{aligned} \mathbf{u}^{b\star}(\mathbf{p}^{\star}) = &\max_{\mathbf{u}\in U_a^b} \sum_{k\in K_b} \alpha_k \ln(u_k^b(\mathbf{p}) - u_k^{b\ min}) \\ subject\ to: p_t^{r_k} \leq P_{max}^{r_k}, &\qquad r_k = 1, 2, ..., N_b \\ u_k \geq u_k^{b\ min}, &\qquad k = 1, 2, ..., N_b. \end{aligned} \tag{3.37}$$

The constrained problem in (3.37) using Lagrange multipliers $\{\lambda_k\}$ and $\{\mu_k\}$ can be represented as,

$$\begin{aligned} L(\{u_k^b(\mathbf{p})\}, \lambda, \{\mu\}) = &\sum_{k\in K_b} \alpha_k \ln(u_k^b(\mathbf{p}) - u_k^{b\ min}) \\ &- \sum_{k\in K_b} \lambda_k \big(p_t^{r_k} - P_{max}^{r_k}\big) + \sum_{k\in K_b} \mu_k \big(u_k^b(\mathbf{p}) - u_k^{b\ min}\big). \end{aligned} \tag{3.38}$$

Following the steps described above for finding optimal power allocation based on NBS in case 1, where the sum transmit power is constrained, we get the power allocation among $\{N_b\}$ reuse RRHs of RB b based on iterative procedure as,

$$p_t^{r_k(itr)} = \sqrt{\left[\frac{1}{\lambda_k^{(itr-1)}}\left((\gamma_k \eta (d_{k,r_k})^{\alpha} + \sum_{r_j\in\{N_b\}, r_j\neq r_k} \gamma_k p_t^{r_j(itr-1)}\right.\right.} \\ \left.\left.\frac{}{\left(\frac{d_{k,r_k}}{d_{k,r_j}}\right)^{\alpha}\right)\left(\frac{\alpha_k u_k^b(\mathbf{p}^{(itr-1)})}{u_k^b(\mathbf{p}^{(itr-1)}) - u_k^{b\ min}}\right) + \mu_k^{(itr-1)}\right)\Bigg]_0^+}. \tag{3.39}$$

Using *subgradient* method [65] the multipliers are updated as:

$$\begin{aligned} \lambda_k^{(itr)} &= \Big[\lambda_k^{(itr-1)} - \beta\Big(P_{max}^{r_k} - p_t^{r_k(itr)}\Big)\Big]_0^+, \\ \mu_k^{(itr)} &= \Big[\mu_k^{(itr-1)} - \beta\Big(u_k^b(\mathbf{p}^{(itr)}) - u_k^{b\ min}\Big)\Big]_0^+ \end{aligned} \tag{3.40}$$

where β is a very small step size.

Algorithm 2: NBS for optimal power allocation with individual transmit power constraint

1. *Initialization*: For each UE $k := 1 : N_b, \forall\{K_b\}$

   a) minimum required SINR : γ_k

   b) minimum required reliability : $u_k^{b\ min}$

c) priority / bargaining power : α_k

d) maximum transmit power : $P_{max}^{r_k}$

e) minimum transmit power : $p_t^{r_k(0)}$

f) UE specific Lagrange mutliplier : $\mu_k^{(0)}$

f) UE specific Lagrange mutliplier : $\lambda_k^{(0)}$

The maximum transmit power of each RRH $P_{max}^{r_k}$ is initialized based on each RRH capability and conformance requirements.

2. *Iteration*:

   a) calculate the utility functions $u_k^b(\mathbf{p}^{(itr-1)})$ using (3.18)

   b) update the power allocation values $p_t^{r_k(itr)}$ using (3.39)

   c) update the multipliers $\lambda_k^{(itr)}$ and $\mu_k^{(itr)}$ using (3.40)

3. *Convergence check*:

   After step 2) converges, the power allocation decisions $p_t^{r_k(itr)}$ reach the optimal NBS

3.6 Simulation Results

3.6.1 Simulation Model

In order to evaluate the performance of the proposed metrics and algorithms, we consider a simulation model consisting of various RRH distributions based on the proposed DAS hexagonal packing having multiple-users distributed uniformly. Figure 3.1 presents the positioning of RRHs in case of packing factor 15. The advantage of this analysis is that the packing factor C directly relates to RRH coverage radius by $r = R/C$ and the number of RRHs, which corresponds to 169 RRHs. The numbers in the center of each dotted circle represents the RRH number, which increase concentrically. The downward pointed triangles represent the positions of RRHs. It should be noted that the colors of RRHs are used only for better presentation. The blue dotted small circles around the RRHs represent the radial coverage area r. The UEs are uniformly distributed over the complete cellular area, which are represented by red dots. The simulation parameters considered in the simulation model implemented in MATLAB are given in Table 3.1.

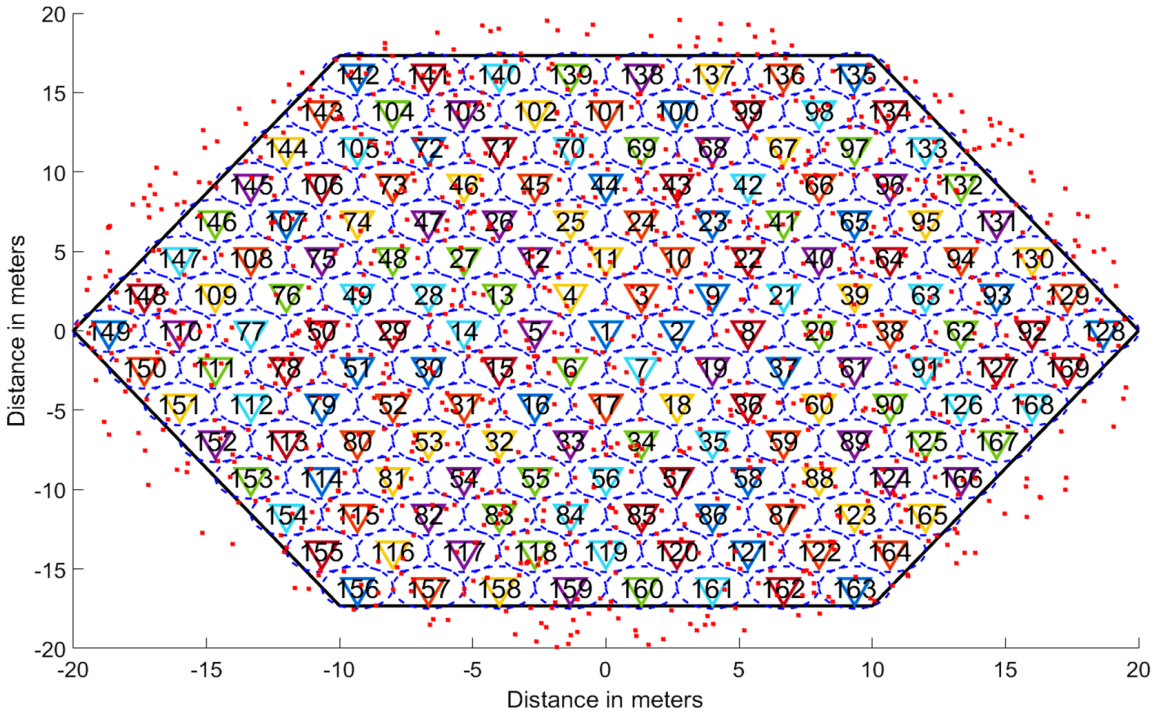

Fig. 3.1: DAS distribution with 169 RRHs

Table 3.1: Simulation Parameters for Power allocation

Parameters	**Values**
Carrier frequency DL	2.655 GHz
Channel bandwidth DL	20 MHz
subcarrier spacing Δf	15 KHz
Num of subcarriers	1200
Cellular radius (R)	20 m
RRH packing factors (C)	$\{9, 13, 19, 25, 29, 35\}$
RRH coverage radius (r = R/C)	$\{2.2, 1.5, 1.1, 0.8, 0.7, 0.6\}$ m
Num of RRHs	$\{61, 127, 271, 469, 631, 919\}$
Num of UEs	2000
Noise level	-100 dBm
Pathloss exponent	3

3.6.2 Frequency Reuse

In this section, we evaluate how the minimum reuse distance between RRHs is impacted by different UE requirements like SINR requirement, reliability and UE's radial distance from the serving RRH. This study provides us the insights into the opportunities to explore the formation of very high reuse rate RRHs groups for different RBs. Minimum RRH reuse distance, between any pair of RRHs (r_j, r_k) within a reuse group of N_b RRHs, where b represents the b^{th} RB, is described and derived in Section 3.4.2. The UEs (j, k) represent the connected UEs to the RRHs (r_j, r_k), which reuse the b^{th} RB. In this section, the derived minimum RRH reuse distance in Section 3.4.2 equation (3.13) is simulated, based on the different reliability requirements of the UEs (j, k), locations of the UEs, where the RRHs are transmitting equal power.

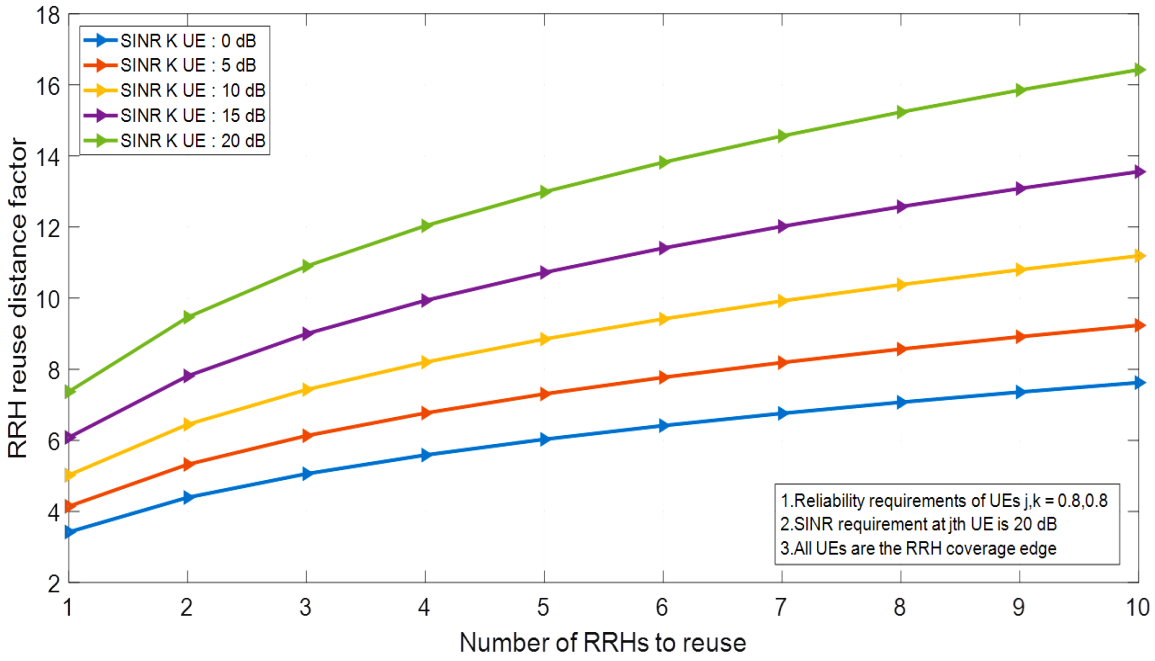

Fig. 3.2: RRH reuse distance factor (in terms of RRH coverage radius) Vs Number of reuse RRHs, varying SINR requirement of UE k. UE j, k are at RRH coverage edge. Reliability, SINR requirements of $(j, k) = (0.8, 0.8), (20dB, 20dB)$

Fig.3.2 shows how the RRH reuse distance factor, which is expressed in terms of the multiple of RRH coverage radius r, varies with respect to the number of reuse RRHs and SINR requirement of the UE k. Here we assume that all UEs are at cell edge and having the same minimum reliability requirement. For example in case of the total number of reuse RRHs equals to 2 with 20 dB SINR and 0.8 reliability requirements, the top most curve shows that

the minimum RRH reuse distance is around 9 times the RRH coverage radius. This implies that when the RRH coverage radius reduces, the RRH reuse distance also reduces, so that the frequency reuse-rate density can be increased in the given cellular area.

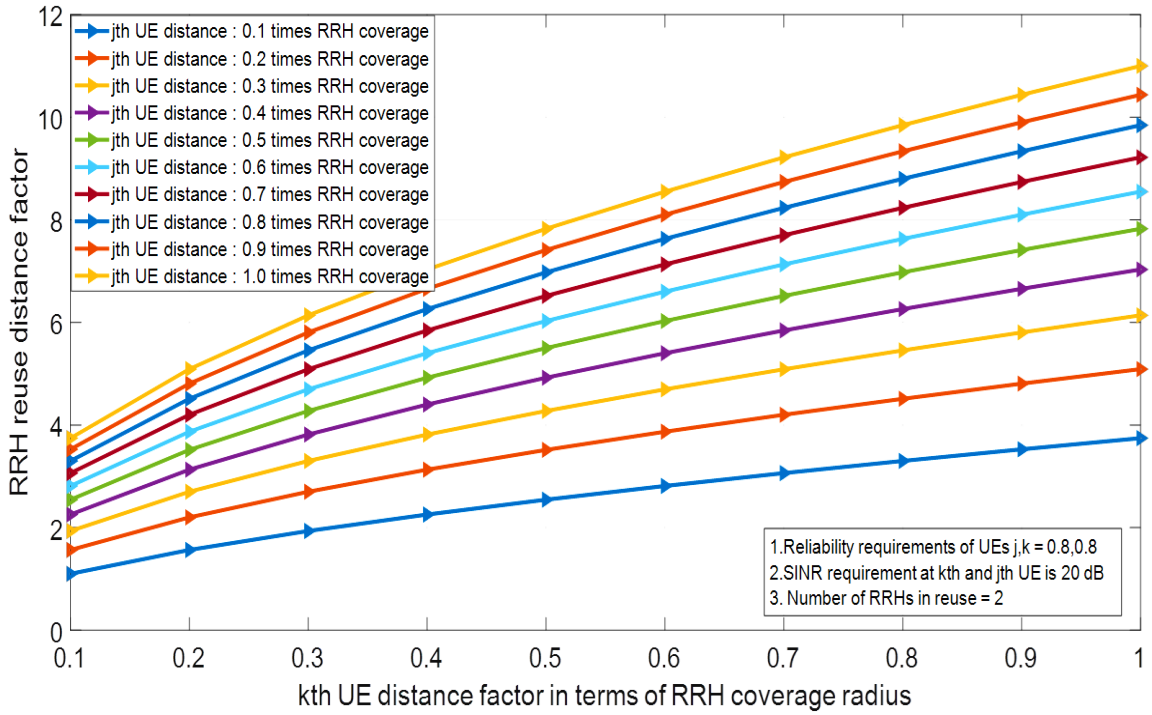

Fig. 3.3: RRH reuse distance factor (in terms of RRH coverage radius) Vs UE k distance factor, varying UE j distance factor. Reliability, SINR requirements of $(j,k) = (0.8, 0.8), (20dB, 20dB)$

Fig.3.3 depicts the possibilities of forming different reuse RRH groups based on: UE locations, which is the radial distance of UEs from the serving RRHs, and different UE requirements, in order to achieve the optimum system throughput via forming reuse RRHs groups with minimum RRH reuse distances. In this case, the number of reuse RRHs considered is 2, and the UEs have the SINR requirement, $\mathbf{\Gamma_k}$, of 20 dB with a reliability of 0.8, but the location of UEs (j,k) in terms of the coverage radius is varied. We can see from the curves how variable the RRH reuse distance is depending on locations of the UEs. In a real cellular system the UEs require different services in turn different data rates, different reliability and latency requirements, this analysis provides details in different dimensions to achieve very high system throughput by using efficient and fine granular frequency reuse, which can be at RB level.

3.6.3 Power Allocation

This section validates our proposed NBS algorithms $Algorithm1$ and $Algorithm2$ for optimal power allocation among the RRHs within the reuse RRH group as described in Section 3.5.2. Fig.3.4 and Fig.3.5 validate the convergence of the proposed algorithms, with regard to transmit power allocation and $reliability$ respectively. As shown in Fig.3.4, the RRHs are initialized with equal power, which is the minimum transmit power given in the Table 3.2. Furthermore, it is observed that the algorithms converge very fast, which is between five to ten iterations.

Table 3.2: NBS Algorithm Parameters

Parameters	**Values**
min. required SINR $\mathbf{\Gamma_k}$	$\{0, 5, 10, 15, 20\}dB$
min. required reliability $u_k^{b\ min}$	0.8
UE priority / bargaining power α_k	$\{equal, random\}$
min. transmit Power per RRH $\mathbf{P_t^{r_k(0)}}$	-30 dBm
Max. Tx. Power per RRH $\mathbf{P_{max}^{r_k}}$	0 dBm

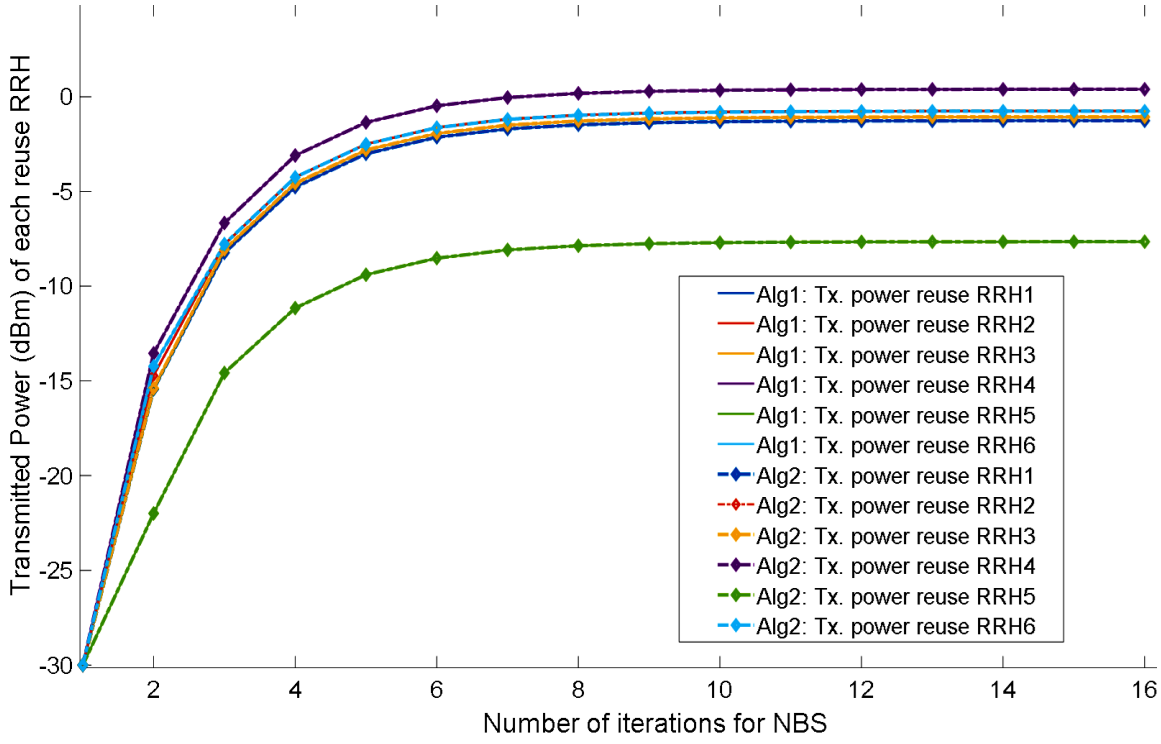

Fig. 3.4: Convergence of transmit power allocation among reuse RRHs in iterative NBS in $Algorithm1$ and $Algorithm2$

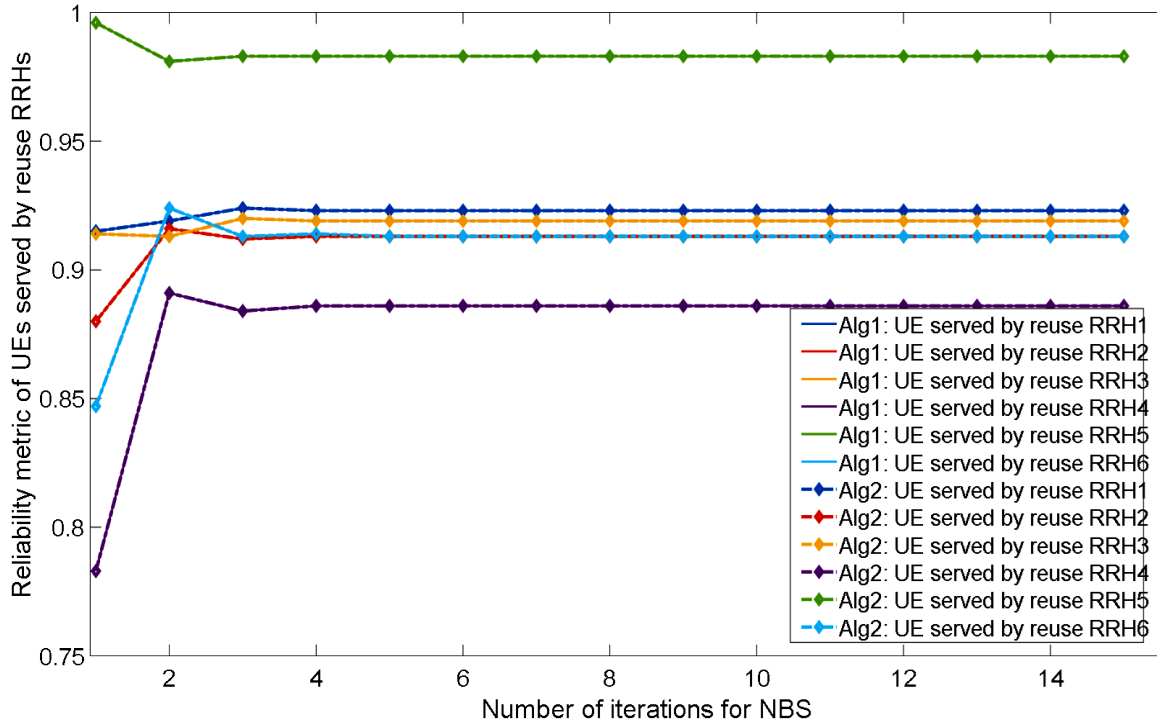

Fig. 3.5: Convergence of reliability (utility) functions of UEs served by reuse RRHs in $Algorithm1$ and $Algorithm2$

It is also observed that the choice of the Lagrange multipliers $\mu_k^{(0)}$ and $\lambda_k^{(0)}$ and $\lambda^{(0)}$ is crucial for convergence. We have noticed that initializing the Lagrange multipliers with large values $\mu_k^{(0)} = 10^5$, $\lambda_k^{(0)} = 10^8$ and $\lambda^{(0)} = 10^8$ is required due to very restricted feasible transmit power requirements. Table 3.2 provides the information about the NBS initialization, UE requirements in terms of reliability and SINR, and feasible transmit power requirements of RRHs.

In Fig.3.5 shows $reliability$ UEs belonging to the reuse RRH group at a scheduling snapshot. Each of UE has the same minimum reliability requirement which is 0.8 and same SINR requirement, $\mathbf{\Gamma_k}$, which is 20 dB. Reuse RRH4 represents symbolically the RRH in the fourth reuse (UE, RRH) pair within the same reuse group. We can see from Fig.3.5 that, at the initialisation time, where all the RRHs transmit with equal transmit power, UE served by RRH4 has not achieved the minimum required reliability of 0.8. The UE being served by RRH4 is the farthest UE of all the UEs being currently being served by the reuse RRH group. Therefore it has started with a achieved reliability value which is less the minimum required reliability value. We can also see for this UE in Fig.3.4, the transmit power allocation of reuse RRH4 increases to the maximum value and stabilizes after 8 iterations. We can also see from Fig.3.5 that the $reliability$

of this UE converges synchronously to that of its paired RRH power allocation. For all other UEs the reliability values and transmit power allocation of serving RRHs have been optimally selected and fairness among the multiple UEs is achieved as well. Hence the promised $fairness$ and minimum required SINR and $reliablity$ of NBS solution have been validated successfully. In all other trials performed under varied combinations of UE requirements, very fast convergence and optimal power allocation maintaining fairness and minimum required reliability is observed. It is noteworthy to mention that both the algorithms have resulted in the same transmit power values, which also proves the optimality and uniqueness of NBS solution, which is achieved by both the algorithms. As mentioned above, the equal power allocation method forms the baseline for validating our optimal power allocation algorithms.

3.6.4 Throughput Improvement

In this subsection, the throughput improvements results based on the RRH reuse distance and power allocation methods is presented.

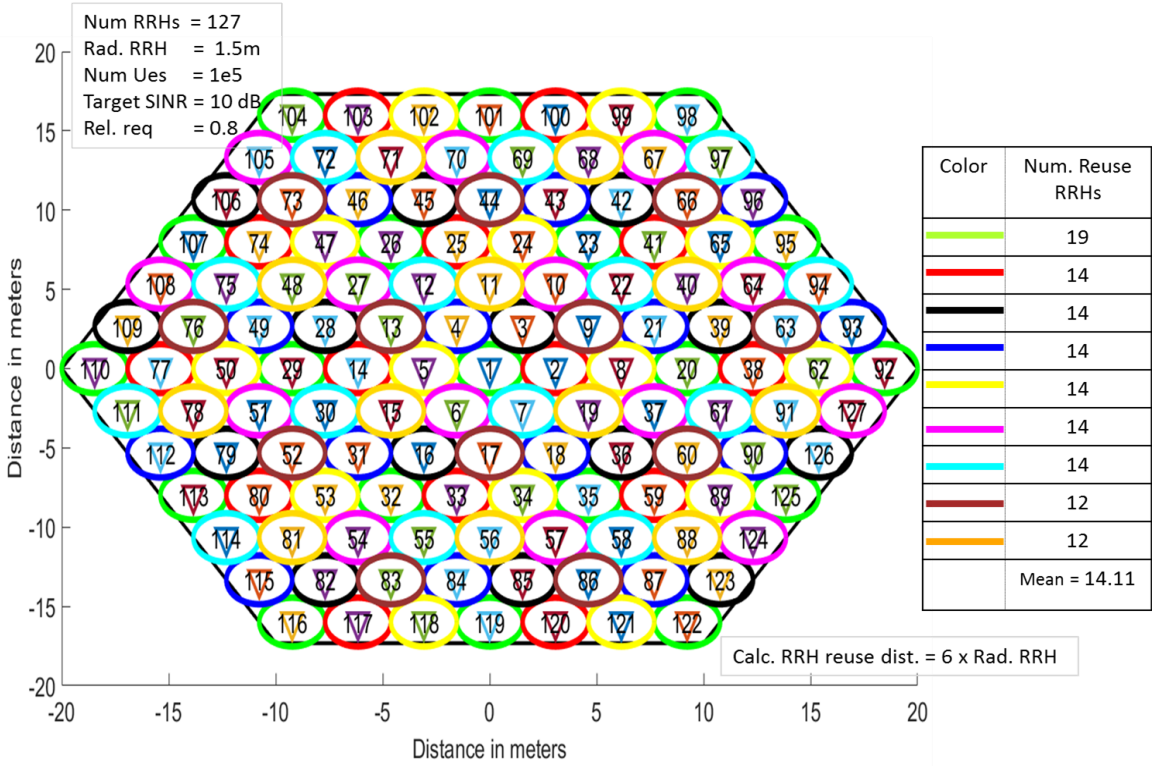

Fig. 3.6: Figure showing number of reuse RRHs for different channels in the case of 127 RRHs

Fig.3.6 depicts the number of reuse RRHs possible for different frequency channels /

resource blocks (RBs) in the case of C-RAN / DAS with 127 RRHs, where the colours on each RRH radial coverage area represent a specific frequency channel. The downward pointed triangle in the center of each RRH coverage circle represents the RRH location. It should be noted that the colours of RRHs are used only for the sake of better presentation, otherwise have no significance. As shown in the figure, the coverage radius of each RRH is 1.5 m. The targeted SINR is 10 dB and the $reliability$ requirement of all the UEs is 0.8. In this scenario, as shown the maximum number of reuse RRHs is 19, in the case of reusing the RBs allocated to $RRH1$. The mean number reuse RRHs is 14.11. Therefore, the throughput in C-RAN / DAS can be significantly improved by a factor, which is the mean number of reuse RRHs, 14.11 in comparison with a single cell without frequency reuse.

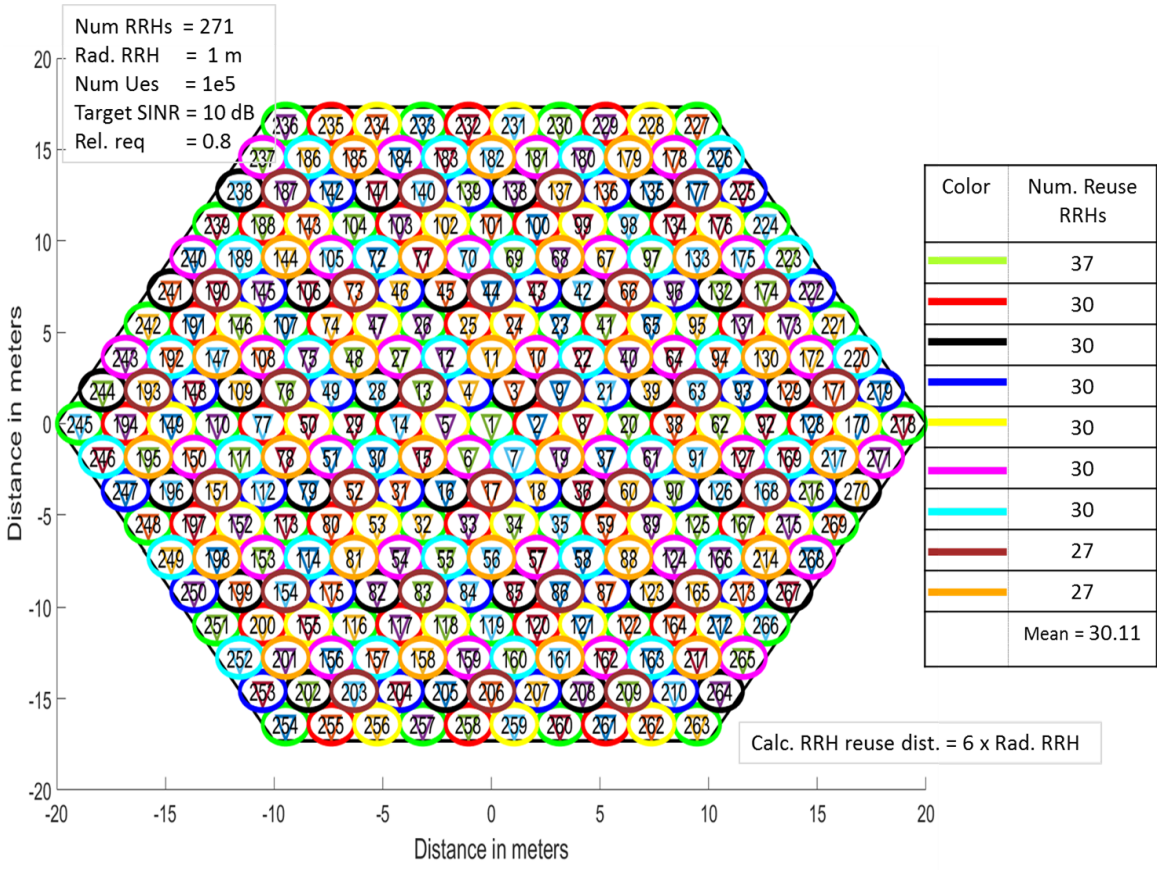

Fig. 3.7: Figure showing number of reuse RRHs for different channels in the case of 271 RRHs

Similarly, Fig.3.7 shows the results of the number of reuse RRHs in the case of 271 RRHs. As shown in the figure, the coverage radius of each RRH is 1 m, the targeted SINR of each UE is 10 dB and requested $reliability$ is 0.8. In this scenario, the maximum number of reuse RRHs for the RBs utilized by $RRH1$ is 37, and the mean number of reuse RRHs is 30.11. Therefore,

the throughput in C-RAN / DAS can be significantly improved by a factor, which is the mean number of reuse RRHs, 30.11 in comparison with a single cell without frequency reuse.

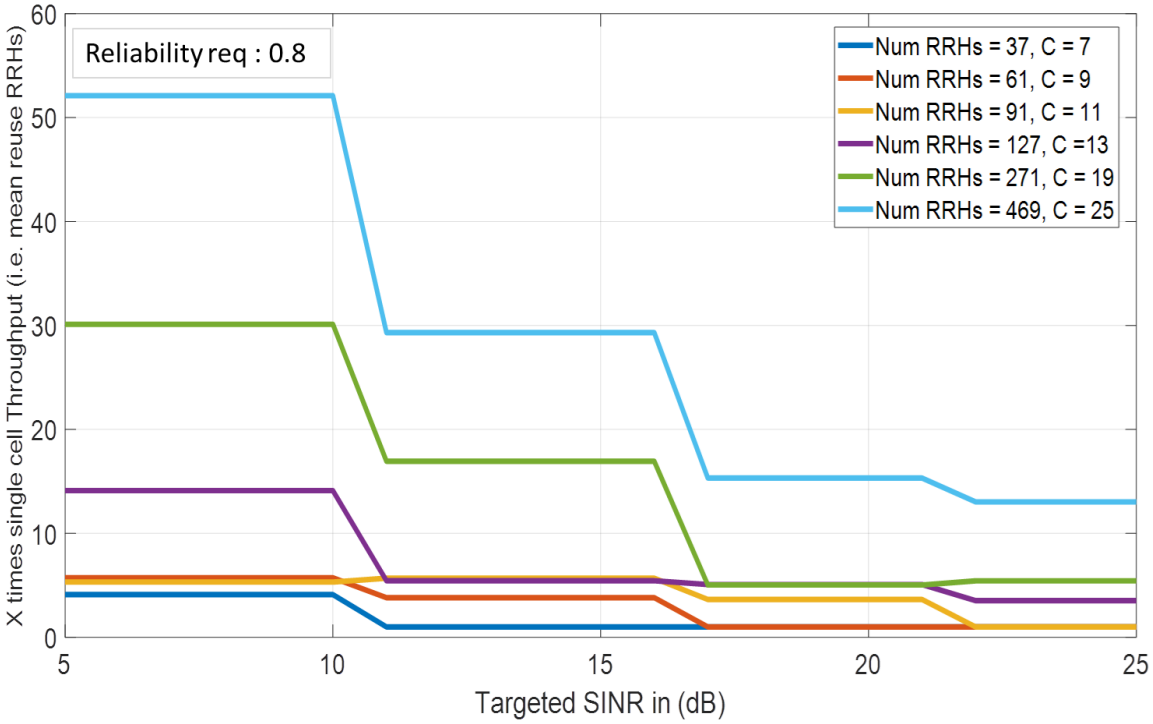

Fig. 3.8: X fold Throughput improvement in comparison with single cell Vs Targeted SINR for different number of RRHs packed

In Fig.3.8 the potential throughput improvement in C-RAN / DAS in comparison to single cell scenario, by varying the different SINR requirements, in varied number of RRHs packed within the same area is presented. The $reliability$ requirement for all the UEs is set at 0.8. As shown in the figure, for very low SINR requirement use cases, the potential throughput improvement in 469 RRH case is more than 50 fold. For other cases, the potential throughput improvement is also high. It is also shown that for very high SINR requirement the throughput improvement is not so high as that of low SINR requirement case, but still one can $reliably$ achieve 5 - 15 fold increase.

Fig.3.9 shows the reuse distance for the case of the throughput improvement results shown in Fig.3.8. The cell radius is set at 20 m for all the investigations, which implies that for the scenarios with number of RRHs: 37 and 61, the RRH reuse distance is greater than cell radius, therefore there is no chance to win any throughput improvement at high SINR required use cases via frequency reuse. For the RRHs packing factor (C) above 11, in the use cases where the SINR

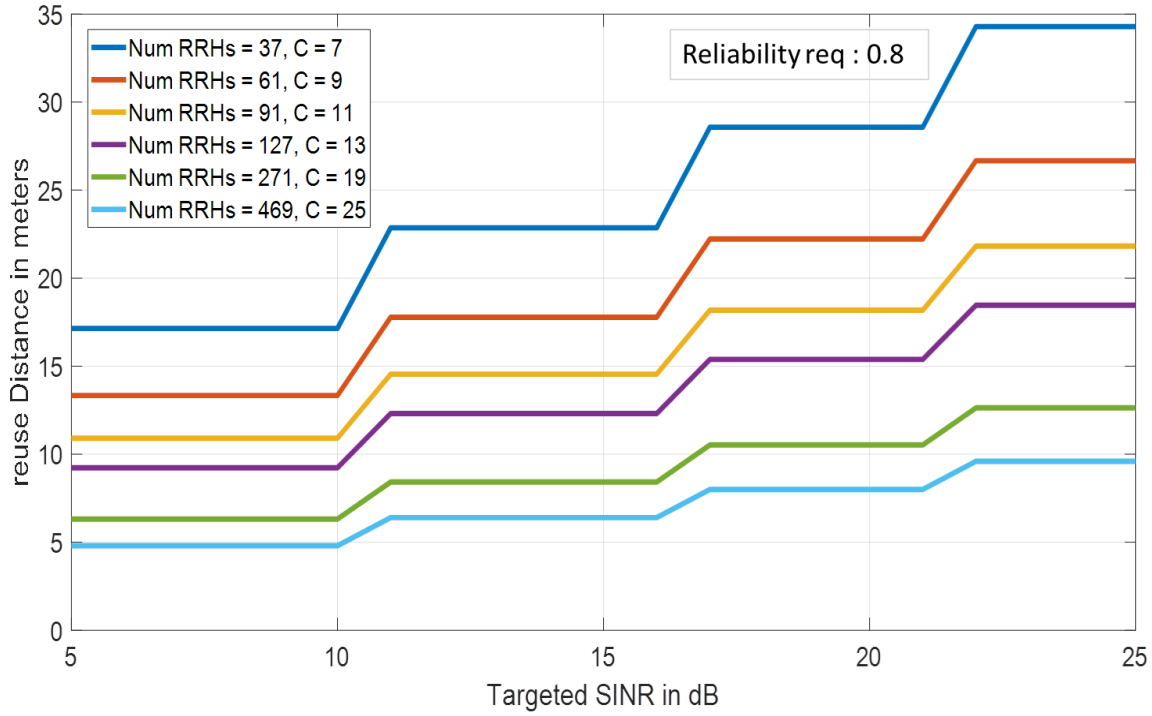

Fig. 3.9: Reuse distance in meters Vs Targeted SINR for different number of RRHs packed

requirement is below 20 dB, we can see that the RRH reuse distance is below cell radius. This enables the throughput improvement as shown in Fig.3.8. Similarly, for all other use cases with different SINR requirements, the results show significant potential for throughput improvement via frequency reuse. In addition to the significant potential for throughput improvement the $reliability$ and $fairness$ of the UE requirements are met, because of the usage of $reliability$ expression and $fair$ NBS power allocation methods.

3.7 Conclusion

In this chapter, the key challenges in C-RAN / DAS, in order to meet the high requirements of 5G and Beyond in eMBB *hotspot* scenario, are investigated. The novel *reliability* framework, which was described in chapter 2 forms the basis of the analysis of these key challenges. The key challenges addressed in this scenario investigated are: efficient pairing of UEs and RRHs, effective and low complexity solution of achieving frequency reuse, and fair DL power allocation among the RRHs within a reuse RRH group.

Firstly, it is shown that (UE, RRH) pairing or association plays a significant role in C-RAN

/ DAS design. Pairing of RRHs and UEs based on least pathloss has practical significance. This is primarily because high power transmission from RRHs distant from UE in order to achieve the targeted SINR at the UE can cause significant increase in interference, which outweighs the benefits of DAS. Therefore, pairing based on the measured pathloss is preferred, as the target of this work is to rapid frequency reuse.

Secondly, an efficient and low complexity method of find frequency reuse RRH groups in C-RAN / DAS taking into consideration the UE requirements on $reliability$ and throughput is presented. In this regard, a novel expression for the minimum reuse distance is derived. The significance of the derived expression is that, the minimum reuse distance depends only on the distances between the UEs and their serving RRHs and not on the distances between all other RRHs. This significantly reduces the overhead of collecting information about distances between all RRHs and all UEs besides remarkably lowering the computational complexity. Using MATLAB simulation model, it is shown how the reuse distance varies based on the UE locations and UE requirements. Through simulation results, it is shown that, using this novel reuse distance, one can exploit the reuse opportunities, available due to different requirements of UEs, in order to find the best fitting set of dynamic reuse RRH groups in a given scenario.

Thirdly, the problem of downlink (DL) power allocation among the RRHs belonging to same reuse group is formulated. Since, the RRHs within the same reuse group transmit on the same scheduling resources, each transmission link is considered a player in a general interference game. In this work, the intention to meet *fairness* and *reliability* for all the users is shown by employing a novel utility function, which is based on the $reliability$. The existence, uniqueness,and fairness for the cooperative game based on novel utility function are proven in detail using mathematical analysis of validation of all Nash conditions. In this regard, two theorems are postulated and proven to show the existence of an unique Nash Bargaining Solution (NBS). Based on the existence of unique NBS, the optimum DL power allocation solution using Lagrange multipliers is presented. Accordingly, iterative Nash bargaining algorithms developed, which are validated to converge to Pareto-optimal solution, in a very less number of iterations (around 5-10 iterations). Finally, the overall potential in C-RAN /DAS for multifold throughput increase based on the mean number of RRHs is presented, via simulation results. In some simulated scenarios, it is even shown that, around 50 fold improvement in throughput and *Area traffic capacity* can be potentially achieved.

In the next Chapter, the challenges faced by C-RAN / DAS in a realistic ultra-dense Heterogeneous Mobile Networks (HMN), and the solutions for efficient control and coordination of resources in these scenarios are presented.

4 C-RAN / DAS IN 5G AND BEYOND HETEROGENEOUS MOBILE NETWORKS

4.1 5G and Beyond Heterogeneous Mobile Networks

4.1.1 Introduction and Challenges

The work presented in this subsection is derived from Deliverables "D2.1 - Use Cases and Architecture [2]" and "D2.2 - System Architecture and Abstractions for Mobile Networks [3]" of European Commission funded COHERENT H2020 5G-PPP project (July 2015 - March 2018). The work described in these deliverables is a cooperative work of various project partners where the author made significant contributions to the project results.

In the future 5G and Beyond wireless systems it is necessary to envision and address the challenges and concerns that arise due to coexistence of varied technologies and networks. The heterogeneous mobile networks can be broadly classified in two classes, firstly due to the coexistence of currently deployed RATs such as GSM, UMTS, LTE, WiFi and novel emerging technologies such as 5G New Radio, Massive MIMO, mmWave. Secondly, due to envisioned coexistence of extremely dense multi-layer networks of diverse sizes and topologies.

Fig.4.1 shows an example of coexistence in heterogeneous mobile networks which includes macro base stations, C-RAN / DAS CU with distributed RRHs and Femto base stations, serving different sets of UEs with diverse requirements. In essence, the coexistence of manifold cellular networks and varied technologies in 5G and Beyond systems poses challenges of very high complexity in order to meet the demanding requirements of 5G and Beyond use case scenarios. In this chapter, the focus is to depict an overview of the multidimensional problems that arise in HMN due to coexistence. Further on, the need for a novel and comprehensive solution for efficient and fair control and coordination of radio resources and requirements is presented,

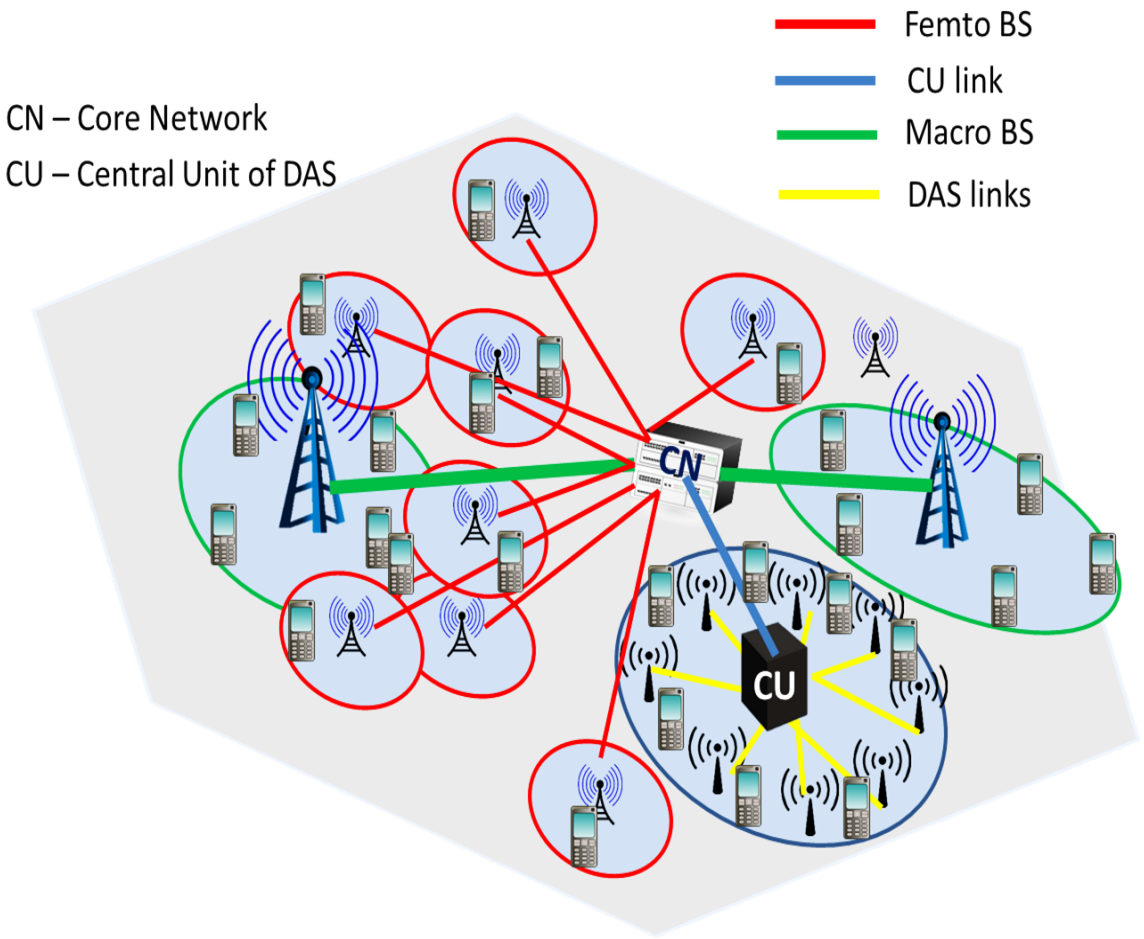

Fig. 4.1: Example of Heterogeneous Mobile Network Scenario

in order to comprehensively deal the challenges of coexistence in different cellular network topologies like Macro, Micro, Femto, Pico and different RATs: GSM, UMTS, LTE, 5G NR and future technologies in 5G and Beyond.

5G and Beyond systems promise novel multifaceted human and machine oriented services. These varied services require novel technologies at all layers. The focus of the work presented here is centered on lower MAC and PHY layers. According to [66], there are many novel and emerging technologies considered in 5G and Beyond at lower layers. A nice summary of these technologies is given in [67–70]. From the topology perspective they include Macro, Micro, Femto and Pico cells. From the view of RATs, they include massive or very large Multiple-Input Multiple-Output (MIMO) antenna technology, 5G New Radio, mmWave etc.. From machine centric networks perspective they include smart devices, Internet of Things (IoT) connectivity and Device to Device (D2D) or machine-to-machine (M2M) communications. As a result of, versatile

services spanning broad areas of human and industrial applications, novel technologies and various mobile network topologies, the challenges arising out of novel scenarios, which comprise of diverse combinations of the new features in 5G and Beyond, can achieve multidimensional complexity. Therefore, in view of understanding the multidimensional complexity in HMN, a brief introduction to the challenging requirements of some of the key technology enablers in 5G and Beyond mobile networks is presented below:

The work presented below is derived from Section 2.3 "Trends in enabling technologies" of COHERENT deliverable "D2.1 - Use Cases and Architecture [2]". The work described in this deliverable is a cooperative work of various project partners where the author made significant contributions to the project results.

- *ultra-dense small cells*: Deployment of ultra-dense small cells has been by far the most significant approach to enhance system throughput because of low transmission power of radio waves [68, 71] resulting in rapid frequency reuse. Nevertheless in small cells, high interference limits the rapid frequency reuse deployments [72]. In order to deal with interference, a large set of solutions suitable at different RAN layers are proposed in the literature. They range from interference avoidance and cancellation techniques at PHY / L1 layer to interference coordination at Radio Resource Mangement (RRM) layer such as enhanced Inter-Cell Interference Coordination (eICIC) methods.

  In addition, the new technologies in 5G and Beyond such as Device to Device (D2D) and Vehicle to Anything (V2X) communications in conjunction with ultra-dense small-cell deployments may result in new challenges primarily emerging out of the new interference patterns, which need to be measured, analyzed and characterized. Therefore, ultra-dense small-cell deployments in 5G and Beyond HMN pose novel challenges in interference management and characterization.

- *smart technology*: In 5G and Beyond HMN it is anticipated that, the communication networks and devices will be equipped with smart technology. Smart technology implies that the devices and networks will be more adaptive, self-organizing and autonomous. In case of Self-Organizing Network (SON), SON can change its topology [73] based on the learning methods employed. Ad hoc networks are an example of self-organizing networks. In 5G and Beyond HMN, self-organization of networks is considered as an key

enabler of smart technology. Typical applications where smart technology benefits 5G and Beyond technologies and services, which include device-centric / D2D connectivity, distributed services, local caching and interference management [68]. In cellular systems, D2D communication is an example of smart technology, as it enables direct device to device communication, which facilitates the user-plane communication between connected devices without involving the complete network layers [70]. The main challenge that needs to be addressed in smart systems is robustness. Generally because of the flexibility and adaptability offered by smart systems, typically they are not energy efficient. Therefore, robustness in smart systems implies that these systems should be operated at right level of automation ensuring high energy efficiency.

- *machine to machine*: The other major area included in 5G and Beyond HMN is massive Machine to Machine (M2M) communication. M2M includes mission critical services such as autonomous driving and massive deployments of sensors in public safety, medical and emergency services. Moreover, M2M includes the existing Internet of Things (IoT) devices with a wide and varied range of applications spread along various industrial fields such as automotive, smart metering and industrial automation [70]. The M2M services vary widely in requirements, which primarily depend on the targeted application. For example, in some mission critical applications such as connected cars, where the requirement on data rate may be minimal but they require very high and consistent reliability all the duration of service. In other applications such as vehicle to anything (V2X), very low latency with real-time functionality is required. In massive M2M applications such as IoT applications, for e.g. the industrial IoT devices require very low power and long battery life requirement, which may be up to 10-15 years [28].

- *flexible spectrum usage*: The need for spectrum in 5G and Beyond HMN for cellular communications increases due to ever increase in demand for higher data rates and reliable coverage. One of the solutions to meet this need is the usage of higher frequencies. In this regard, 3GPP in 5G New Radio (NR) standardized some frequency bands (FR2) in mmWave spectrum. Nevertheless, development of Radio Frequency (RF) components in mmWave frequencies is more challenging due to high cost, high loss of transmission power, enhanced jitter and leakages, which require few more years to reach the required

maturity. Therefore, one of feasible solutions which is currently been explored in 3GPP standardization is the efficient usage of unlicensed spectrum. It is foreseen in 5G and Beyond systems that, the licensed spectrum will become heavily deployed or congested due to deployment of ultra-dense small-cells. Consequently, the utilization of unlicensed spectrum is considered as one of the key enablers for achieving higher date rates. Therefore, there is a high interest among the cellular operators to provide reliable and efficient services by utilizing the unlicensed spectrum. Additionally, the small cells can be deployed effectively in these unlicensed bands as the interference is limited in these bands or the low interference bands can be cognitively sensed and selected before the deployment. The challenges that emerge due to the deployment of small cells in unlicensed spectrum are, developing more effective traffic steering techniques, cognitive channel selection techniques and definition of favorable and amenable policies among the operators using unlicensed band.

Therefore, in the light of the above described multidimensional and varied set of stringent requirements, it is evident that there exist many challenges of high complexity in 5G and Beyond HMN systems. In order to address these challenges that arise due to coexistence of varied set of RATs and types of networks, it is evident that an efficient control and coordination of resources among these networks is necessary. In this regard, over 33 months (July 2015 - March 2018), 15 partners from 9 countries collaborated in the European Commission funded H2020 5G-PPP project, COHERENT (Coordinated cOntrol and spectrum management for 5G HEterogeneous Radio AccEss NeTworks), in order to analyze the complexity of the problems that arise in 5G and Beyond HMN. During this period, COHERENT proposed viable solutions to these problems, of which many of them have been accepted by 3GPP in the standardization. The author, as a member of the project partner, University of Duisburg-Essen, made significant contributions, to the project's success, as a Researcher and a Task leader of the key work package of this project, "Physical and MAC layer Modelling and Abstraction". In this regard, the author has contributed to *European Telecommunications Standards Institute* (ETSI) standards for "Broadband Radio Access Networks (BRAN) - Study of central coordination of wireless access systems (WAS) / radio local area networks (RLANs) operating in the 5 GHz frequency band" [74]. Furthermore, the proposed solutions of this project were rated by European Commission, Brussels, as "Excellence" at the review held in June 2018.

In this chapter, firstly, the required and relevant description of the solutions jointly achieved under COHERENT, namely COHERENT architecture, is briefly presented. Secondly, the challenges faced in C-RAN / DAS in HMN scenarios and the solutions based on the COHERENT architecture and framework are outlined. In this work, the author's contributions are focused mainly on addressing C-RAN / DAS challenges in HMN with an objective to provide solutions at COHERENT architecture level and formulation of required lower layers methodology using COHERENT framework. Accordingly, the author made significant contributions to various aspects of COHERENT architecture such as: Real-Time Controller (RTC) requirements and methods, generation of Network Graphs and abstraction framework methodologies for C-RAN / DAS. In order to have complete details of COHERENT, please refer to the documents on the COHERENT website `http://www.ict-coherent.eu/coherent/?page_id=8081`.

To briefly summarize, the COHERENT solution consists of the design of a novel system level architecture for RAN, control and coordination methodology, and Abstractions. In the next sections, a brief overview of these aspects with their significance is presented. After that, the coexistence problems faced by C-RAN / DAS in HMN are analyzed and the solutions using the COHERENT framework are presented.

4.1.2 COHERENT Solution

The work presented in this subsection is derived from Section - "1.Introduction" of COHERENT deliverable "D2.2 - System Architecture and Abstractions for Mobile Networks [3]". The work described in this deliverable is a cooperative work of various project partners where the author made significant contributions to the project results.

It is expected that 5G and Beyond networks incorporate the state-of-the-art networking features such as Software Defined Networking (SDN), Network Function Virtualisation (NFV) and Mobile Edge Computing (MEC) in the RAN [3]. COHERENT [2, 3] provides a comprehensive solution in order to address the challenges in HMN by proposing a novel *flexible* and *programmable* system level architecture for 5G and Beyond RAN. *Flexibility* in 5G and Beyond is necessary to control and coordinate a varied and huge set of novel 5G and Beyond services, in addition to facilitating the novel concepts such as network slicing in RAN.

In order to design a *flexible* and programmable RAN, many aspects need to be taken into consideration. Firstly, the most significant aspect is the separation of control and data plane [3]. Secondly, appropriating the major concept of Software Defined Networking (SDN) architecture [3], which implies centralized control. Correspondingly, the control and data plane separation facilitates the logically centralized control of the network. This approach is essential in order to achieve a consolidated and comprehensive control framework for 5G and Beyond networks [3]. Nevertheless in RAN, an absolute separation of data and control plane is not possible because of some time critical radio functions such as radio resources scheduling, which are time-critical. The latency sensitive control functions of RAN have to therefore reside very close to the data plane. Therefore, in contrast to typical SDN architecture, in RAN, a provision has to be made for real-time control besides having centralized control.

Thirdly, in order to support flexibility in implementations of different Radio Access Technologies (RATs) architectures, the network functions at the data plane should support flexibility, which implies a flexible split in functionality. Some of the practical applications of flexible network functions can be illustrated in a ultra dense small cell deployment scenario. In this scenario, the multiplexing gain functionality within a set of cooperative base stations can be significantly improved by optimal joint processing of relevant functions in the data plane. Additionally, utilization of NFV techniques will further empower 5G and Beyond RAN to be cost-effective and service-agile.

Fourthly, 5G and Beyond RAN should facilitate highly flexible spectrum management. This implies that, in addition to the licensed spectrum within sub 6 GHz spectrum, the 5G and Beyond RAN should optimally utilize existing spectrum sharing techniques such as Licensed Assisted Access (LAA), Licensed Shared Access (LSA) and flexible duplexing techniques to provide much enhanced network capacity and facilitation of varied services [3]. Therefore, in the design of control plane in 5G and Beyond RAN, flexible spectrum management [3] methodology needs to be considered comprehensively.

Finally, *programmability* is a key requirement in 5G and Beyond RAN. *Programmability* means that flexible adaptation of data and control plane functions depending on the varied network and service requirements is facilitated. In case of network slicing in 5G and Beyond RAN, *programmability* will enable varied control functions implemented on a network slice, which is a key requirement to achieve service isolation.

The key concepts of the COHERENT solution, as described in the deliverable D2.2 [3], are summarized here:

- *Control Separation*: COHERENT architecture is based on the state-of-the-art Software Defined Networking principles in RAN. Therefore, COHERENT solution embraces a centralized control of HMN, which could in theory achieve the global optimum. Nevertheless in centralized control, the intrinsic delay between a control entity and any radio network element poses huge challenges for RAN. The reason is that, RAN needs to support some delay sensitive radio functions such as scheduling of time frequency resources. Hence, the centralized control in COHERENT is further separated into functionalities related to centralized control and real-time control. This split in the centralized control could help the fast changing wireless networks to get adapted to the new conditions within the required time, besides having the benefit of performance gain facilitated by centralized control.

- *Network Abstractions [3]*: A consistent and systematic abstraction of the network, which is represented by its states and resources, is a key requirement which enables programmable control and coordination in 5G and Beyond RAN. In COHERENT, abstractions comprise of models representing network level information such as, network states, resources, average throughput per allocated resources or network slice besides representing RAN information such as, space-time-frequency resources and device capabilities [3]. In COHERENT architecture, due to real-time and non-real time control split, different controller instances manage real-time and centralized control dispensing local and logically centralized view of the network, respectively [3].

- *Network Slicing*: It is well known in the area of computer networking that the principles of SDN and NFV provide promising novel techniques to achieve significant reduction in deployment costs and network operations predominantly in large networks [3]. To make use of SDN and NFV principles in RAN primarily implies that the Network Functions (NFs) not anymore located locally on the dedicated hardware resources but rather distributed on to software instances. These software instances are envisioned to run the NFs on virtual networks and general computational infrastructures. Thereby significantly promoting flexible and scalable RAN [3]. These methodologies expedite the deployment of new

services and applications, which is achieved by significantly faster software development lifecycle compared to hardware development lifecycle. Additionally, sharing of same resources between various NFs can optimize the resource utilization and speed of execution. Therefore, the principles and methodologies of SDN and NFV in mobile networks are set to play a major role in 5G and Beyond HMN.

To elucidate the advantages described above, for example, a business model known as Network-as-a-Service (NaaS) showcases the requirement of providing flexible and scalable interfaces and functions to the operators in order to explore new revenue streams. This can be achieved by the abstraction of available network and radio resources into network slices which are specified by the service. These service based network slices can be even distributed over various Mobile Virtual Network Operators (MVNOs) [3]. In COHERENT, the network slices are conceptualized by providing comprehensive abstraction methodologies which span the physical and hardware layers up to network layer, service layers and applications running above the protocol stack. This approach lines up with the targets of 5G and Beyond HMN for industry and telecom perspective [28, 75] in order to meet the multifaceted requirements of use cases and applications.

Based on the major design considerations for flexible and programmable RAN, COHERENT has proposed a comprehensive SDN based architecture for RAN. The architecture details are presented in the next section. In the following sub-sections, the significance of COHERENT's control and coordination and abstraction in programmable RAN is introduced.

Control and Coordination

The work presented in this subsection is derived from subsection - "4.2 Control Separation to Network-Wide Control and Real-Time Control" of COHERENT deliverable "D2.2 - System Architecture and Abstractions for Mobile Networks [3]". The work described in this deliverable is a cooperative work of various project partners where the author made significant contributions to the project results.

In HMNs, the optimal utilization of resources is a problem of high complexity. This problem even reaches multi-dimensional complexity scale in 5G and Beyond ultra dense HMNs. The existing network control is primarily based on distributed control, which can be easily scalable

and flexible, but the solutions often lead to sub-optimal resource utilization. Therefore, COHERENT embraces state of the art centralized control methodology based on SDN architecture, which could theoretically achieve a global optimum. As described in the previous subsection, concerning the service of non-delay sensitive and delay sensitive control functions, COHERENT architecture supports respectively, network-wide and real-time control.

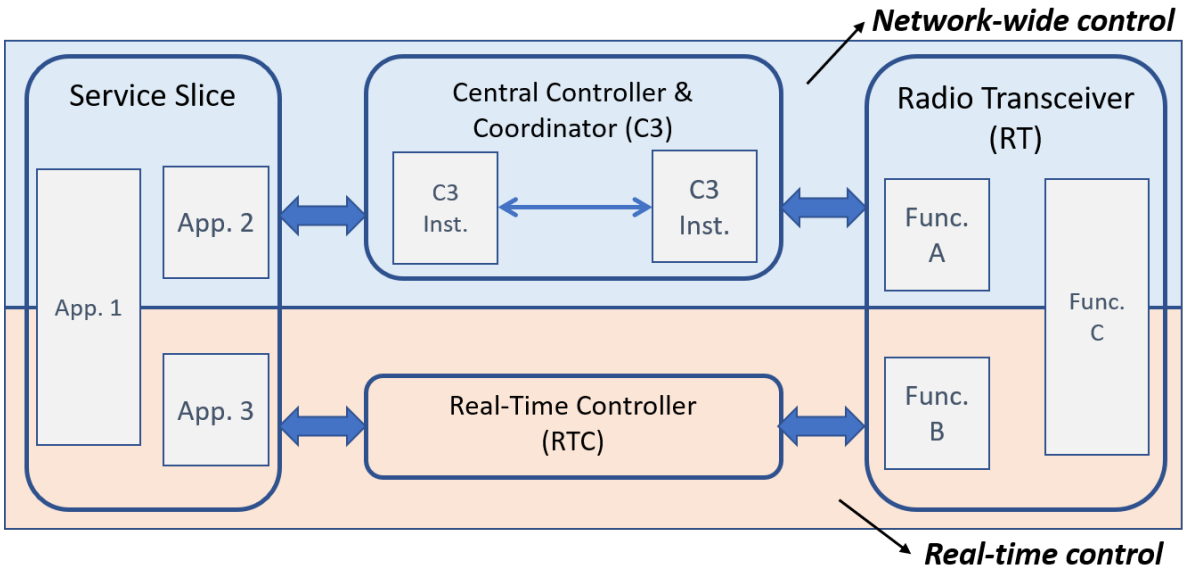

Fig. 4.2: Block diagram showing control split in COHERENT, i.e., Network wide control and real-time control [2, 3]

Fig.4.2 shows the split in control and coordination envisioned in COHERENT for SDN based RAN. In the top portion of the figure, the COHERENT's SDN based network-wide or centralized control is depicted. The entity which facilitates the network-wide control in COHERENT is called *"Central Controller and Coordinator (C3)" [3]*, which is generically a logically centralized entity. In wide area coverage and dense RAN deployments, where size and complexity of centralized control entity rapidly increases or in other words the scalability becomes challenging, the logically centralized C3 solution can be implemented. This logical implementation of C3 could be achieved by distributing the physical control instances using the shared network information. Therefore in COHERENT, C3 instance builds the *" logically centralized network view " [3]*, thereby facilitating logically centralized control.

In the bottom portion of the Fig.4.2, the other major aspect addressed in COHERENT for RAN, the real-time control is depicted. The need for real-time control in SDN based RAN arises

because of the non-deterministic delay between C3 instance and RAN. These non-deterministic delays may cause serious problems to delay sensitive RAN functions such as, MAC layer time frequency resource scheduling, coordinated transmissions such as Coordinated Multi-point (CoMP), handover etc.. Therefore, there arises a necessity that the controller operations for time-critical network functions must be extremely quick and reliable compared to the non time-critical network functions such as load-balancing and traffic steering [3].

Therefore in COHERENT, in order to provide a comprehensive solution for time-critical network functions, the *"Real-Time Controller (RTC)" [3]* shown in Fig.4.2 is conceptualized to facilitate handling of time-critical control functions. Accordingly, RTC must be located in close proximity to the RAN such that RTC could meet the strict latency requirements of these functions in rapidly varying wireless environments and networks. Additionally, it is not envisioned in COHERENT that the RTCs in the RAN coordinate with each other, mainly to ensure the reliable latency requirement handling. Therefore in COHERENT, RTCs in RAN function distributed, in contrast to C3.

Finally to summarize, C3 provides logically centralized control of network states, while RTC provides distributed or localized control, of latency or delay-sensitive network functions in RAT specific entities such as Radio Transceiver (RT), in coordination with C3 but not necessarily in coordination with other RTCs in RAN. The service slices shown in Fig.4.2 depict the network slices where different network applications with varied requirements. This figure illustrates the scenario where some network applications may require the control and coordination of C3 or RTC, while other applications may require overlap of C3 and RTC control.

Abstraction

The work presented in this subsection is derived from subsection - "4.3 Abstraction" of COHERENT deliverable "D2.2 - System Architecture and Abstractions for Mobile Networks [3]". The work described in this deliverable is a cooperative work of various project partners where the author made significant contributions to the project results.

In order to achieve the benefits of SDN concepts in 5G and Beyond RAN, a very well described and coherent abstraction of network states and resources is decisive such that, efficient control, coordination of network resources and programmable services are facilitated. In CO-

HERENT, abstractions comprise of modeling of various network states and resources across the RAN layers, such as, time-frequency resources, UE and eNodeB capabilities, average throughput per slice etc. In COHERENT, the abstracted information is represented using network graphs. Although one can represent the abstracted information by using data structures, network graphs structure the network information being abstracted systematically and mathematically, thereby offering more structured representation. Furthermore, making use of mathematical methods from graph theory can offer very efficient solutions which provide fast convergence and optimized network performance [76, 77].

The network graph comprises of various elements, which basically is a interconnection of graph vertices and graph edges. Network graphs are abstracted from the raw metrics collected from different entities in the network. Typically, the raw data sets from the various network elements are stored in storage networks and databases. It is envisioned in COHERENT that, diverse network graphs, which are primarily targeted for specific goals and layers are created, in order to optimize the data handling and speed of decision making. Typically, the network graphs which are specific to C3 could be more generic or RAT agnostic compared to that of RTC, where the network graphs will be more RAT specific.

Therefore, in this subsection a brief outline of the key concepts that are foundational to the COHERENT Architecture, the control split and abstractions, is presented. For a complete description of COHERENT concepts, please refer to the corresponding sections of COHERENT deliverables [2, 3]. In the next section, a more detailed view of how these key concepts fit inside the COHERENT architecture is presented.

4.2 COHERENT Architecture

The work presented in this section is derived from Section - "5. COHERENT Architecture" of COHERENT deliverable "D2.2 - System Architecture and Abstractions for Mobile Networks [3]". The work described in this deliverable is a cooperative work of various project partners where the author made significant contributions to the project results.

It is foreseen that 5G and Beyond heterogeneous RAN requires highly programmable, flexible and scalable control and coordination, which can support control at coarse to fine granularity with real-time control [3]. As described in section 4.1.2, the key concept which drives

programmability and flexibility in SDN based control and coordination of RAN is abstraction. Therefore, efficient abstraction methods of RAN specific metrics and information will significantly help to optimize the usage of these abstractions at the control and coordination plane, thereby enhancing the speed of decision making. Furthermore, efficient abstraction of RAN resources helps to manage complex networks efficiently, which makes the implementation and deployment of advanced control and coordination functions in the RAN simpler [3].

In the next subsection, firstly, the definition of the terms used with in COHERENT architecture is briefly presented. In the later subsection, the overview of the COHERENT architecture with an overview of some key features is presented. In the last two subsections, the methodology of control and coordination, and abstractions using network graphs is presented.

4.2.1 Terminology

The work presented in this subsection is derived from Section - "4. COHERENT Concept" of COHERENT deliverable "D2.2 - System Architecture and Abstractions for Mobile Networks [3]". The work described in this deliverable is a cooperative work of various project partners where the author made significant contributions to the project results.

This subsection outlines some of the important terminology used in the COHERENT Architecture [3]:

- *"Radio Transmission Point (R-TP)" [3]*: R-TP is a radio access point, where either full or partial functionality of RAN node can be implemented.
- *"Virtual Radio Processing (vRP)" [3]*: vRP represents a pool of computing resources, which supports full or partial processing of RAN node functions.
- *"Radio Transceiver (RT)" [3]*: RT is a logical entity of radio access with a complete set of RAN functions implemented, which can be achieved by a *"flexible combination of R-TP, vRP and RTC functions" [3].*
- *"Real-Time Controller (RTC)" [3]*: A logical control entity with a local or region-wide scope, facilitating delay sensitive or real-time control operations, e.g., MAC time frequency resources scheduling.

- *"Central Controller and Coordinator (C3)" [3]*: A logical control entity managing and controlling logically centralized complete *"network-wide control and coordination" [3]* of RAN entities. C3 has a centralized network view. C3 could be implemented either on a physically centralized computing resources or distributedly on physical instances which share a common network information. Therefore, logically *"centralized view of the network" [3]* at the C3 is accomplished by the common shared network information among the group of C3 instances.

- *"Slice" [3]*: Formally, in networking, a slice is defined by the following aspects:

  - a specific network topology, which comprises of network entities such as network switches, network ports and links
  - a mapping of network topology specified in the slice to physical network entities
  - and a compilation of routing rules

  In COHERENT architecture, a network slice is configured to optimally meet the service or application requirements. Therefore, a network slice constitutes of application specific network services and RAT specific configurations. Hence, it is envisioned in COHERENT that different network slices are created in order to achieve the targeted requirements of various applications. Additionally, to meet the stringent and reliable requirements of latency-critical applications, the network slices which comprise of these applications reside in the RTC.

4.2.2 Overview

The work presented in this subsection and all the sub-subsections including figures is derived from Section - "5. COHERENT Architecture" of COHERENT deliverable "D2.2 - System Architecture and Abstractions for Mobile Networks [3]". The work described in this deliverable is a cooperative work of various project partners where the author made significant contributions to the project results.

Fig.4.3 shows the architecture of SDN based RAN in COHERENT. The architectural diagram shows the split among different planes of the network such as, management plane, control and coordination plane, user plane and service plane [3]. This split enables programmable

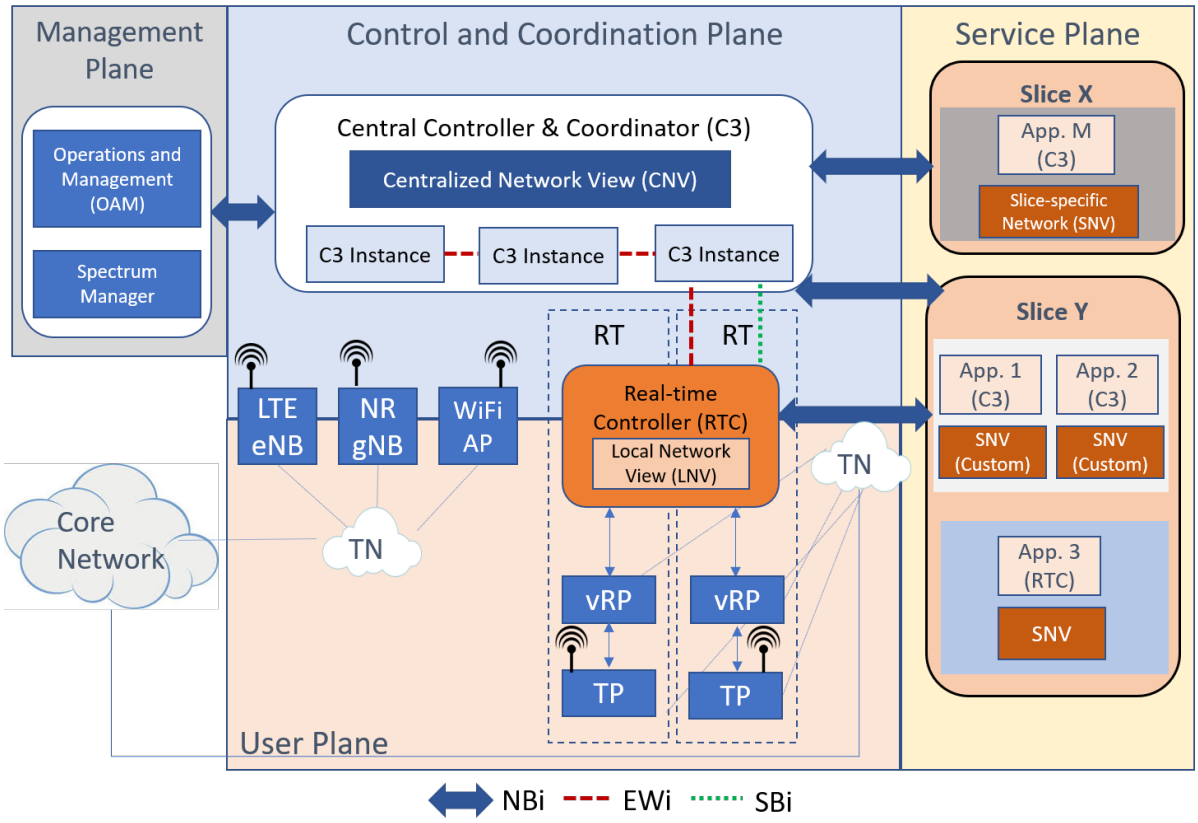

Fig. 4.3: COHERENT Architecture [2, 3]

and scalable control and coordination at very fine granularity and as well facilitating real-time control. Therefore, COHERENT architecture mainly targets to address the two key aspects, scalability and timeliness. Scalability is achieved by the central controller and coordinator (C3), which has the logically centralized view of the network. C3 itself can be a logically centralized entity, which facilitates scalability by distributing the functionalities onto various C3 instances, which share a common network information. Timeliness is vital in RAN due to the strict requirements of certain delay sensitive RAN functions, such as MAC resource scheduler. Timeliness is facilitated by the real-time controller, which is tightly coupled or even co-located with the vRP, R-TP and RT of RAT. Therefore, it is necessary that all delay-sensitive or time-critical control functionalities, which are primarily belong to RAT specific functions, will be handed over by C3 to RTC.

The programmability is basically achieved by using efficient abstractions through the formulation of diverse network graphs. The centralized network view of the network elements is maintained at C3 by metrics and status reports continuously received from the network elements

being controlled.

Interfaces

Different interfaces for communication between the entities are defined in the COHERENT architecture as shown in Fig.4.3. The communication interface between controllers *"(RTC-C3, C3-C3)" [3]* is called as *"east-west interface (EWi)" [3].* This interface is used to share the abstracted network information and also to transfer the control functions between the controllers. The interface which connects the network elements to the C3 and RTC is called as *"southbound interface (SBi)" [3].* Some examples for practical SBi protocols include OpenFlow [78], NETCONF [79], CAPWAP [80] (for WiFi) and LWAPP [81] (for WiFi).

The *"northbound interface (NBi)" [3]* provides the interface between the control instances (C3, RTC) and the service plane. The *"slice-specific network view (SNV)" [3]* for the slices is provided by the control instances via the NBi. Furthermore, the network slices could communicate the expected characteristics of network via the NBi to the control instances. The expected network characteristics are programmable at the network slice, which hides the hardware details and required changes in the network from the service plane.

Service Plane

The service plane depicted in Fig.4.3 hosts varied application specific network slices. A network slice, as defined in COHERENT, comprises of a set of applications and the relevant RAT specific settings for the applications. Some examples of network slices are shown in Fig.4.3. *"Slice specific network view (SNV)" [3]* is logical view of the network, which is provided by the control and coordination plane for the network slices. SNV at the network slices facilitate the programmability so that the slices can communicate the expected network behavior, completely agnostic of the real physical hardware or implementation details, to the control and coordination plane. Additionally, in order to cater the latency-sensitive application specific network slices, necessary modules which handle these time critical services are present in the RTC.

In the next subsection, the functionality of control and coordination plane of the COHERENT architecture is described in detail.

4.2.3 Control and Coordination

COHERENT control and coordination plane is proposed in COHERENT primarily to facilitate coordinated control in HMN. Control and coordination plane [2,3] as shown in Fig.4.3 is depicted in Fig.4.4 to elaborate its functionality.

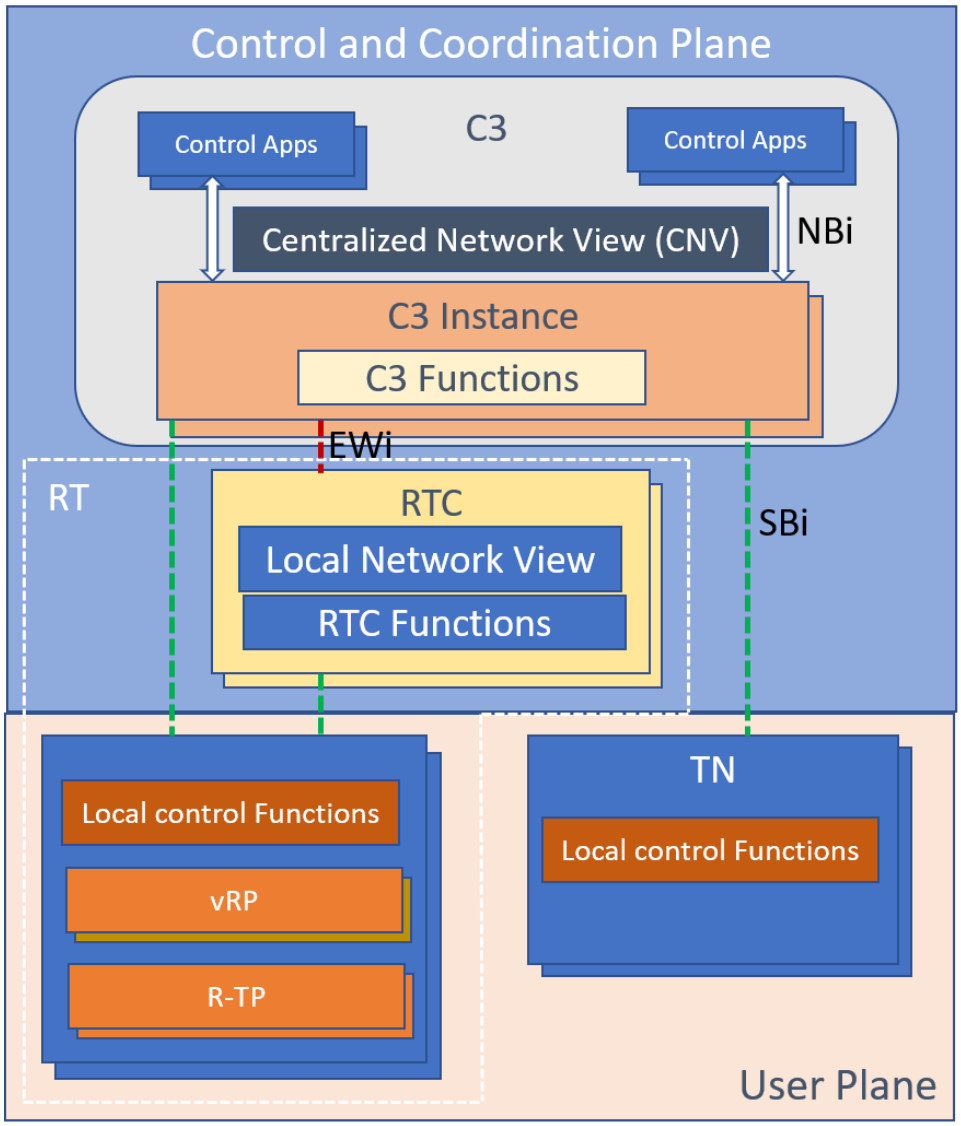

Fig. 4.4: Control and coordination functional architecture for HMN [2, 3]

Fig.4.4 shows on the top the control and coordination plane, besides the Radio Transceiver (RT) and Transport Node (TN) entities. RT comprises of *"Real-Time Controller (RTC)" [3]*, which is a part of the control and coordination plane, besides the legacy RAN user and control plane.

In COHERENT C3 and RTC are the main entities of control and coordination plane. C3's main functionality is to control and coordinate the network entities such as RTs and TNs of the RAN as shown in the Fig.4.4. C3 targets to achieve harmonization of RAN by orchestrating the network entities in the RAN. *"Centralized Network View (CNV)" [3]* is formed and maintained by continuously receiving the updates of various metrics and status reports from different lower layer entities of the RAN. Therefore, based on the CNV various SDN methods can be implemented in the C3 for control and coordination. Fig.4.4 shows the RTC instance for facilitating real-time or latency-sensitive control functions of RAN. RTC typically lies very near or within the RT. It receives the RAT specific reports and metrics in order to support delay sensitive RAT functionalities such as: resource scheduling, handover mechanisms, base station cooperation, Inter-cell Interference coordination etc..

Fig.4.4 as well shows the *"North-Bound interface (NBi)" [3]* within C3, which connects the C3 instance to the control applications. The typical control applications, which are non time-critical, controlled by C3 include, spectrum management, load balancing and traffic steering. For further detailed information regarding the functionalities of C3 and RTC, please refer to Section 5.2 in the COHERENT architecture [3].

In the next subsection, the abstraction methodology and the functional blocks involved in formulation of network graphs are described.

4.2.4 Abstraction and Network Graphs

Abstraction of network elements and network states play an essential role in facilitating C3 and RTC to achieve optimal control and coordination. Therefore, highly efficient representation of network elements and abstracted information is crucial. In this regard, COHERENT adopted the network graphs, which proved to be very efficient in the field of networking.

Network Graphs

The work presented in this sub-subsection including figures is derived from subsection - "3.2. COHERENT network graph and abstraction framework" of COHERENT deliverable "D3.1 - First report on physical and MAC layer modelling and abstraction [4] and Section - "2. COHERENT Framework" of COHERENT deliverable "D3.2 - Final report on physical and

MAC layer modelling and abstraction [13]". The work described in these deliverables is a cooperative work of various project partners where the author made significant contributions to the project results.

In wireless networks, modeling and abstraction of various properties and states of the network is mostly accomplished by network graphs. A network graph provides a very good and abstract depiction of the network by utilizing the information from various entities in the network. In the literature a rich flavor of various graph modeling techniques is available, which can be found in the reference [77]. Abstraction in conjunction with depiction of network graphs optimizes the storage and effective usage of the abstracted information in network graphs by C3/RTC for the effective control and coordination.

The basic constituents of a network graphs are nodes and edges. The network elements are represented in the network graph as nodes. While the network information between the nodes are represented by the edges. In HMNs, varied types of network elements are available such as: macro, small-cell, pico etc. base stations, UEs, D2D pairs etc. In the following, some examples of nodes and edges are given in the context of 5G and Beyond HMN.

- *Nodes*: The nodes can be divided into different categories. In LTE, the important categories are:
  - Base station or eNodeB: Macro, Micro, Pico, Femto
  - Relays
  - User Equipment (UE)
  - Machines
  - IoT Devices

  Moreover, the properties of above mentioned entities vary depending on the following scenarios:
  - Radio access technology (RAT)
  - Quality of service or (Channel quality indicator - CQI)
  - Transmit powers
  - Carrier frequency

  - Bandwidth
  - Resource allocation
  - Spectrum mask
  - Subscriber class
  - Noise floor

- *Edges*: The edges between the nodes depend on the modeling of the application scenario, measurement details and the level of abstraction. In general, an edge can exist between each node in the network. In the PHY layer, edges may represent the channel conditions among the nodes, while the edges in MAC-layer may reflect the status of resources. Additionally, edges can be marked at various RAN layers (PHY, MAC, RLC, RRC, PDCP etc.). The edges are as well technology dependent.

An example of a network graph is shown in Fig.4.5. This network graph shows interference at UE locations, which is originating from base stations. At the *nodes* or vertices the base stations in a serving area are depicted. At the *edges*, serving and interfering links are named. In this example, a particular nomenclature is used in specifying the edges. It starts with specific alphabets, in this example D stands for downlink. Furthermore, D is followed by the index of the base station transmitting, the receiving UE index and the base station index serving the UE [4, 13]. The other variant of the network graph can include th edge link connecting an UE to a serving base station. In this case these serving edges are denoted as, D followed by the base station index serving the UE and UE index. The other variation can be simply omit non-relevant information by leaving out specific edges unconnected. In this example, the edge between base station 5 and UE 5 is left unconnected. Hence, this example provides a glimpse of the potential possibilities of variations possible in formulation of network graphs, which can provide only the necessary information so that the control and coordination plane can make highly optimized decisions. In the next subsection, a brief overview of different application based abstraction procedures is presented.

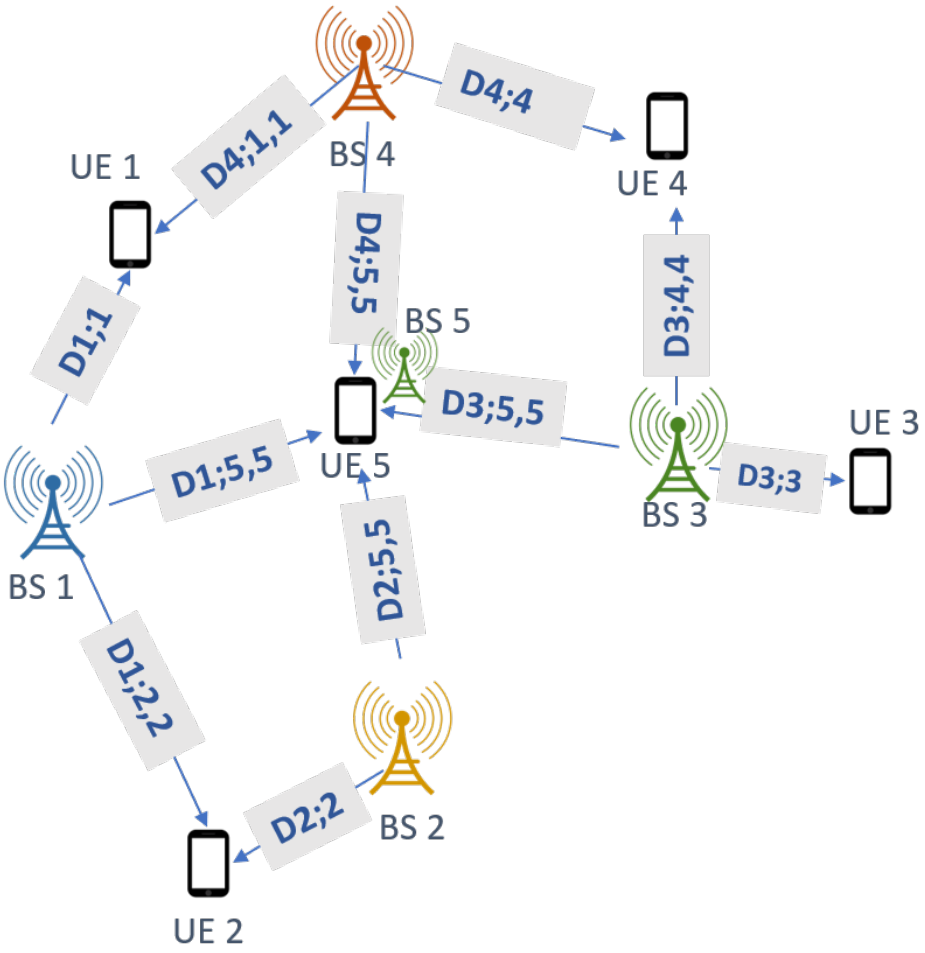

Fig. 4.5: An example downlink Network Graph showing interference [2, 4]

Overview of abstraction procedure

The work presented in this subsection including figures is derived from subsection - "3.2.4. Overview of abstraction procedure" of COHERENT deliverable "D3.1 - First report on physical and MAC layer modelling and abstraction [4]". The work described in this deliverable is a cooperative work of various project partners where the author made significant contributions to the project results.

To construct the network graphs for abstraction, firstly the relevant nodes and edges for the targeted applications or services need to be identified. In order to identify the relevant nodes, a service or application based modeling needs to be achieved. Secondly, the information received from the identified nodes in the network needs to be abstracted based on the model and the metrics which can quantify and qualify the targeted services or applications. The abstracted

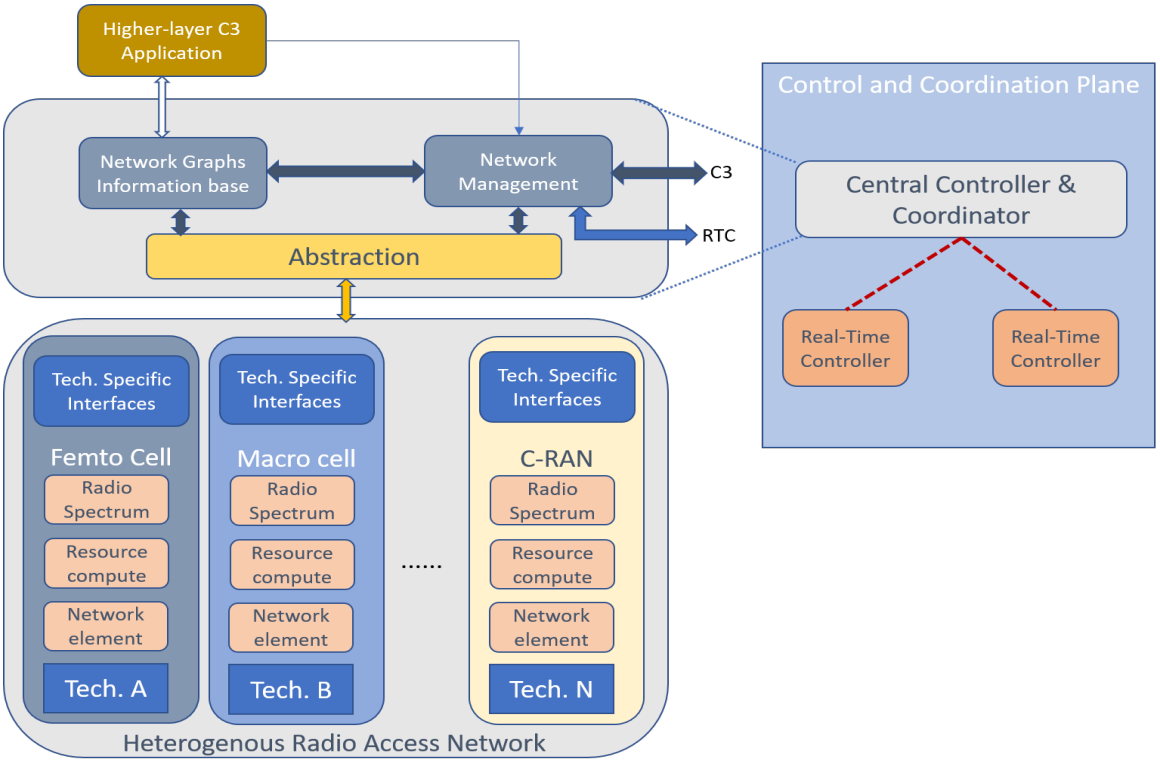

Fig. 4.6: Abstraction flow for the formulation of network graph in C3 instance [4]

information is therefore represented using the edges of the network graph. In essence, application or service based network modeling and abstraction of the network information play a significant role in the construction of optimized network graphs, which helps in shrinking the storage space besides significantly reducing the processing latency at C3 or RTC.

The abstractions can be generally classified into two major categories which are, RAT agnostic and RAT dependent abstractions. RAT agnostic abstractions are foreseen for control functions in C3, while the RAT dependent abstractions are for time-critical control functions in the RTC. Fig.4.6 depicts the flow of network information from various RATs, which constitute the HMN. It is shown in the figure, how the RAT specific information from each of the RATs are interfaced with control and coordination plane, which consists of a C3 instance. The RAT agnostic abstraction of the network information within the C3 instance is achieved by resource virtualization and abstraction block, which is then stored in the network graphs information base. The network management entity within the C3, as shown in the figure, interfaces with other C3 and RTC instances and the services for control and coordination of the network. Furthermore, Fig.4.7 shows the abstraction flow in case of time critical applications which are handled by

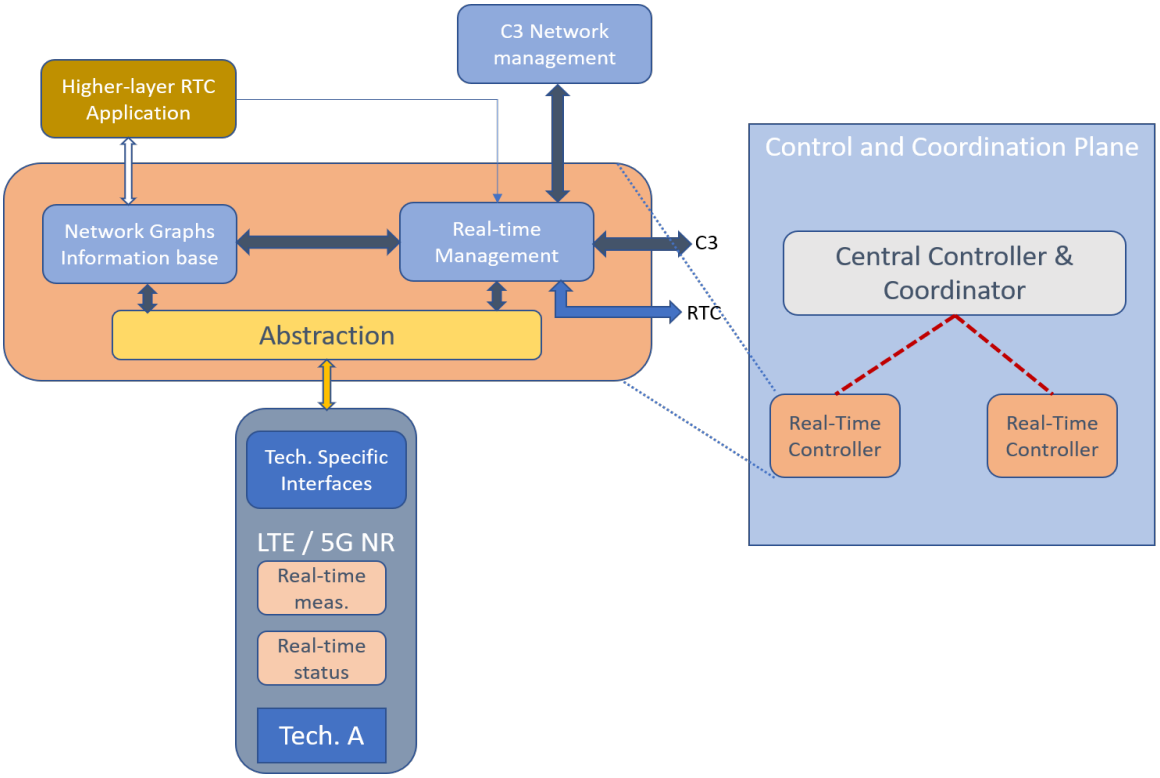

Fig. 4.7: Abstraction flow for the network graph in RTC instance [4]

RTC. It is as well shown that RTC instance constitutes the real-time management instance, which handles the delay sensitive control functions. This instance interfaces with the network graphs information base, RTC application and C3 as well, as shown in the figure.

Hence in this section the following aspects: the key concepts for COHERENT Architecture, COHERENT Architecture with Control and Coordination plane, importance of Abstractions, Network Graphs and framework for generation of Network Graphs, are presented in detail. In the next section, the application of COHERENT concepts and framework in a 5G and Beyond C-RAN / DAS HMN scenario is presented.

4.3 C-RAN / DAS in HMN

4.3.1 Motivation and Goals

This subsection is derived from author's self-published work "Probability of coverage based analysis of distributed antenna system and its implementation on LTE based real-time-testbed" published in "2017 9th International Congress on Ultra Modern Telecommunications and

Control Systems and Workshops (ICUMT)" [10]. From subsection "4.4.2 Distributed antenna systems for throughput improvement" of COHERENT deliverable "D3.2 - Final report on physical and MAC layer modelling and abstraction [13]"

Fig.4.8 shows a typical 5G and Beyond HMN scenario, where C-RAN / DAS is coexisting with a regular collated antennas system (CAS) or a conventional base station. In C-RAN / DAS, central unit (CU) is the entity where the data processing for all UEs connected to the distributed RRHs is done. Usually in C-RAN / DAS, the RRHs perform radio transmission and reception functionality. However, depending on the use case requirements RRHs can perform some additional functionality of PHY baseband processing in order to decrease the baseband data rate on the fronthaul links. As shown in the figure, CU is connected to a regular CAS eNodeB via LTE defined X2 interface and it is connected as well to C3 / RTC for COHERENT based control and coordination in HMN.

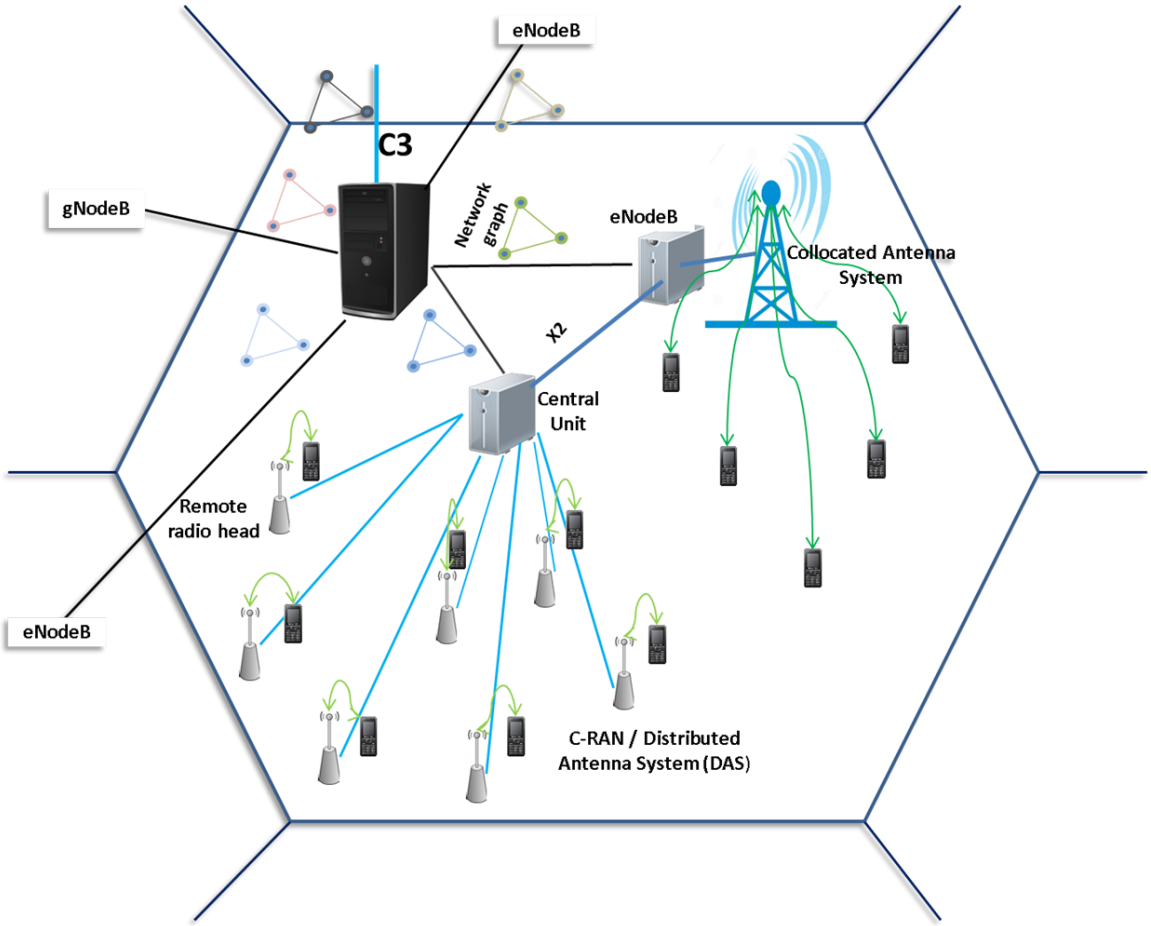

Fig. 4.8: C-RAN / DAS in 5G and Beyond HMN: Coexistence with LTE CAS

Fig.4.8 also shows the general concept of *"paired selection transmission technique" [10, 13]*

in C-RAN / DAS, where each RRH serves the nearest set of UEs. Motivated by some real-life environments such as stadiums and shopping malls, where the UEs are almost stationary or having low mobility requirement but the requirement on sum rate is very high, one can use some effective methods to achieve (UE, RRH) pairing so that the scheduling resources the (UE, RRH) pairs are reused. Typically the resources of distant UE-RRH pairs, i.e., where the SINR is high enough to decode the PHY channels [13], can be reused. Therefore, to achieve high sum rate in these scenarios using ST, a set of RRHs within a serving area can reuse the space, time and frequency resources thereby causing tolerable intra-cell interference but significantly improving the throughput density [13]. In this view, the targeted goals for C-RAN / DAS in COHERENT are improving throughput density, or the ratio of total throughput achieved per the coverage area, using rapid frequency reuse, in various RRH deployments besides analyzing the effect of transmission power and interference on the *reliability* [13].

C-RAN / DAS networks emit considerably very less transmit power, because of very less coverage. Therefore, in HMN scenarios the UEs which are at the edge of C-RAN coverage area are highly vulnerable to very high interference from high power downlink signals transmitted by neighboring macro or small cell eNodeBs. 3GPP LTE has provided schemes to address inter-cell interference in HetNets [82]. The initial scheme for Inter-Cell Interference Coordination (ICIC) is based on fractional frequency reuse, where the allocated RBs of the cell edge UEs belonging to neighboring cells are orthogonal, while the RB allocations of the UEs quite nearer to the eNodeB are reused with a factor of 1. In 3GPP LTE Release 10, [82, 83], a new scheme for interference coordination called enhanced inter-cell interference coordination (eICIC), where interference coordination or techniques in power, frequency and time domain are standardized. However, these techniques are applicable only when neighboring cells work on the same RAT, which is LTE. Therefore in 5G and Beyond HMN in order to achieve efficient control and coordination of radio resources and functions in interference limited scenarios, the need arises to employ ICIC techniques at C3 and RTC to meet the non-real time and real-time requirements of homogeneous RAT or heterogeneous RAT cases.

4.3.2 Generation and Usage of Network Graphs

Network graph, which is denoted by $G(V, E)$ [13], where V stands for the set of nodes or vertices and E stands for the set of edges, is constructed as follows:

This following description is derived from subsection "4.2.1.3 Generation and usage of Network graphs" of COHERENT deliverable "D3.2 - Final report on physical and MAC layer modelling and abstraction [13]". The work described in this deliverable is a cooperative work of various project partners where the author made significant contributions to the project results.

- **Nodes**: In this use case, nodes represent radio transmission entities of the heterogeneous network. Therefore, nodes belong to the set of the graph vertices V, which can represent RRHs, CU, eNodeBs or UEs.
- **Edges**: The edges, defined by $(v, v')\forall v, v' \in V$, are connections between the nodes or vertices of the network graph. When the graph is directed, the ordered pair of vertices (v, v') represents the direction of the edge, which is from the node v towards v'.
- **Properties**: Each edge constitutes a property depending on the application and set of abstractions depicted by the network graph. A property represented at an edge is defined as $f_{v,v'}$. For any set of K abstracted parameters or physical measurements, $p^{(j)}_{v,v'}\forall j \in \{1, 2, .., K\}$, the property is defined as: $f_{v,v'} = \{p^{(1)}_{v,v'}, ..., p^{(K)}_{v,v'}\}$, $\forall\ v, v' \in V$. In case empty property set, i.e., $f_{v,v'} = \phi$, the connection between (v, v') doesn't exist because no relevant property exist.

Fig.4.9 shows an example of network graph derived from the scenario with one C-RAN / DAS base station and one macro base station coexisting. In the figure, the main focus of this network graph is the interference characterization at the cell edge UEs paired to the C-RAN / DAS. The UE4, which is not affected by the interference from macro base station is clearly evident from the network graph as unaffected.

Fig.4.10 shows the entities involved in the generation of network graphs within the COHERENT framework. In COHERENT, the network graph is generated by Network Information Function (NIF) entity. The NIF generates the network graphs based on the atomic/complex parameters updated by a relevant entities. Furthermore, the generated network graphs is given

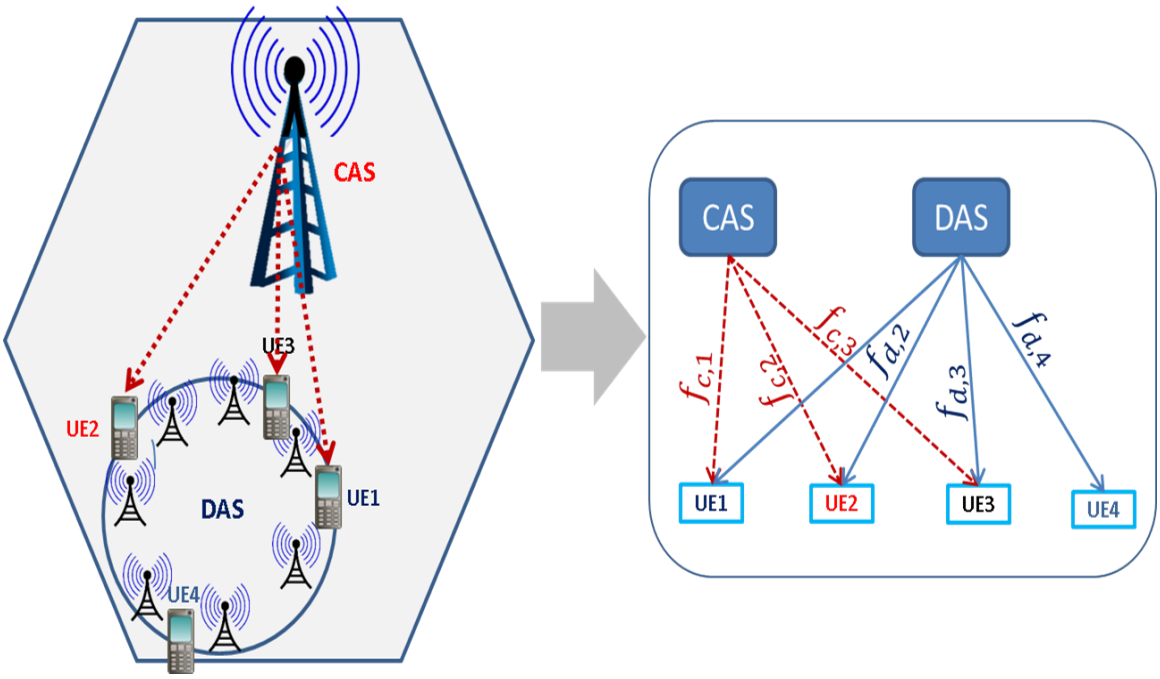

Fig. 4.9: C-RAN / DAS in 5G and Beyond HMN: NG representation based on definition

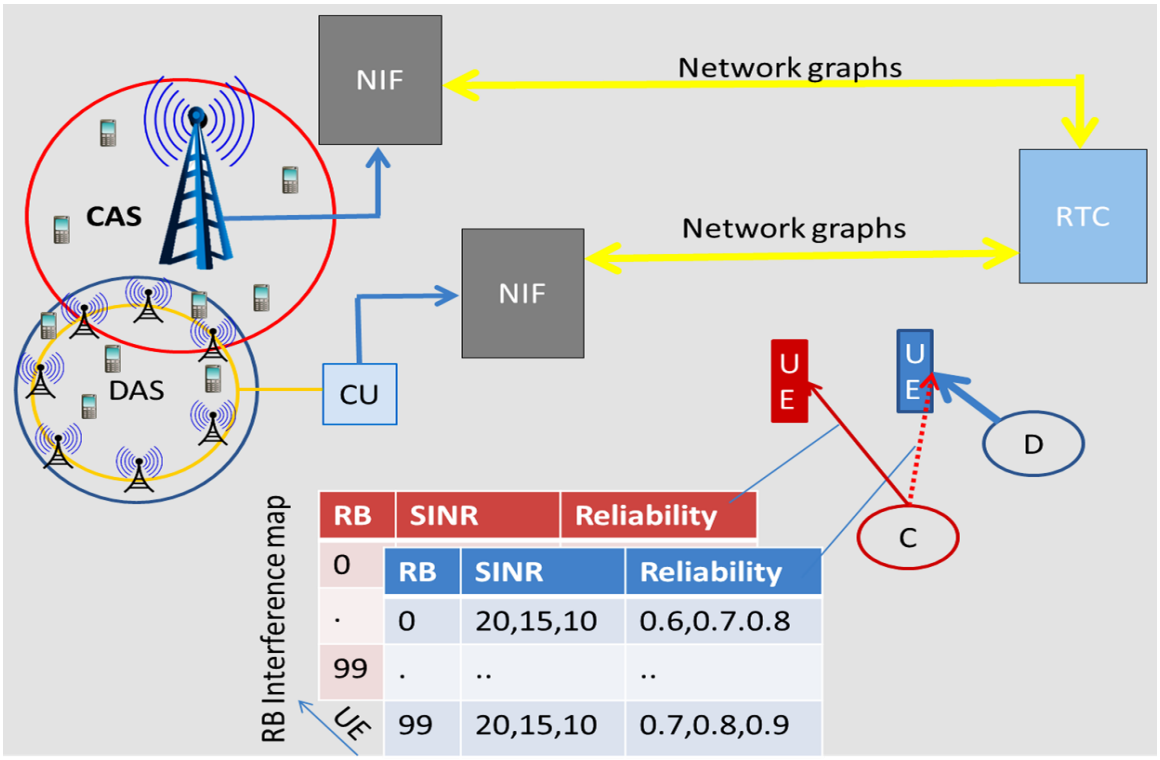

Fig. 4.10: C-RAN / DAS in 5G and Beyond HMN: Generation of NG in NIF for the communication from RTC to CU and CAS eNodeB

as an input to the control application together with the use case requirements. In the figure, we can see that the CU and CAS eNodeBs communicate directly with NIF. Based on the targeted applications, which are pairing and efficient scheduling in ICIC, which are real-time applications, the RTC in conjunction with C3 will process the network graphs. Furthermore in Fig.4.10, an example network graph is presented, where the RB wise interference map for each UE, which is generated at the RTC and communicated back to CU and CAS eNodeB via NIF. This interference map is based on $reliability$ of targeted SINR at each UE location provides information for the efficient scheduling of resources to the UEs which are affected by high interference.

Therefore, for efficient control and coordination of interference in HMN with C-RAN / DAS, it is required to various RAT specific information such as UE location, LTE measurement reports such as Channel Quality Indicator (CQI), Channel State Information (CSI) etc., besides C-RAN / DAS specific measurements such as Pathloss measurements details w.r.t. the relevant RRHs, UE-RRH pairing information, RB based SINR information with Reliablity, which is shown in Fig.4.10.

4.3.3 Abstracted Parameters

This subsection is derived from author's self-published work in subsection "4.4.2 Distributed antenna systems for throughput improvement" of COHERENT deliverable "D3.2 - Final report on physical and MAC layer modelling and abstraction [13]"

For the improvement of throughput density using efficient (UE, RRH) pairing and interference coordination such as ICIC [13], it is required to have the measurements or lower layer information for abstractions such as: CQI, SINR, Scheduling information, HARQ retransmissions rate of every user etc.. These lower layer information can comprehensively identify and characterize the UEs having bad coverage due to shadowing and UEs suffering with high interference in the network. The following tables, Table 4.1 and Table 4.2, represent the set of exposed and controlled parameters respectively for selection transmission C-RAN / DAS scheme. The exposed parameters are the necessary parameters for the required applications. In this work, the applications are pairing and efficient scheduling of resources with ICIC. A shown in Fig.4.10, the abstraction flow comprises of exposed parameters which are sent from CU towards NIF and the control parameters. The control parameters are the RAT specific parameters which are sent

back from C3 / RTC to CAS eNodeB and CU.

This following tables are derived from author's self-published work in subsection "4.4.2.5 Abstracted parameters" of COHERENT deliverable "D3.2 - Final report on physical and MAC layer modelling and abstraction [13]"

Table 4.1: Exposed Parameters [13]

Parameter	Direction	Granularity	Deployment
Reliability	UL/DL	UE, RB	RTC
SINR measured	UL/DL	RRH, UE, RB	RTC
CQI	DL	RB	RTC
UE radial distance	DL/UL	RB	RTC
Transmission power	DL/UL	RRH, UE, RB	RTC
Pathloss	DL/UL	RRH, UE	RTC

Table 4.2: Controlled Parameters [13]

Parameter	Description	Direction	Deployment
(UE, RRH)	Pairing	UL /DL	RTC
RB interference map	Interference per RB	UL / DL	RTC
Transmission power	Transmit power	UL /DL	RTC
UE radial distance	UE position	RB	RTC
Transmission power	Transmission power	RRH, UE, RB	RTC
Targeted SINR, Reliability	Reliability for SINR at UEs	UE	RTC

4.3.4 Simulation Results

This subsection is derived from author's self-published work in subsection "4.4.2.7 Results" of COHERENT deliverable "D3.2 - Final report on physical and MAC layer modelling and abstraction [13]"

One of the important measure of UE and RRH pairing in C-RAN / DAS selection transmission is monitoring the *reliability* of the UE, k, w.r.t. all the RRHs, r_j, based on the $SINR_{k,r_j}$ values at the UE locations, where $SINR_{k,r_j}$ represents the Signal to Noise and Interference Ratio (SINR) at UE k when RRH r_j is transmitting and all other RRHs are interfering. This

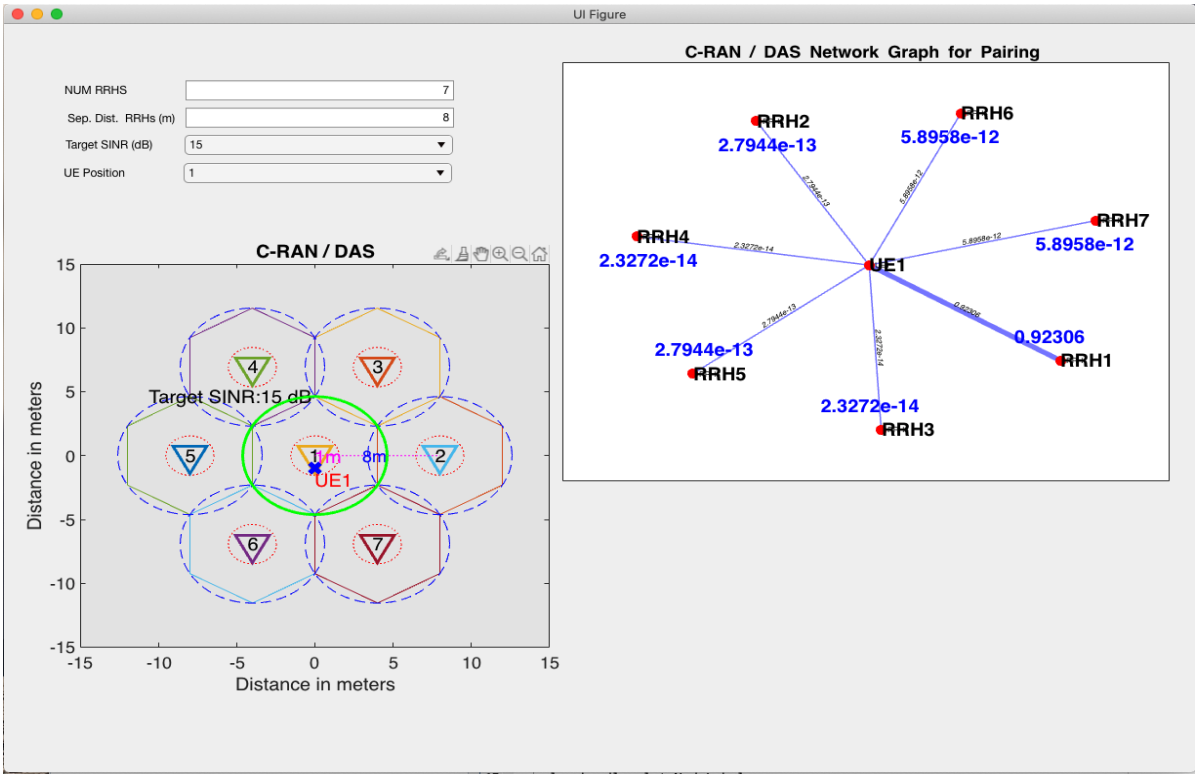

Fig. 4.11: MATLAB based GUI for generation of NGs in C-RAN / DAS

work employs a statistical metric called $reliability$, which is derived in Chapter 2. $reliability$ ensures, based on the channel model, the probability of achieving the minimum targeted SINR at UE location. Hence monitoring the $reliability$ is important to achieve reliability and fairness among UEs in the C-RAN / DAS system.

In the MATLAB based simulation model, a single cell of 12 meters radius is considered. Within the serving area, as set of RRH deployments, based on the number of RRHs distributed in the serving area, is configured, which are 7, 19, 37, 61 and 91 RRHs. These specific numbers are generated based on the optimum circular packing of RRHs in the hexagonal area described in detail in Chapter 2. Furthermore, a MATLAB based Graphical User Interface (GUI) [13] is developed that generates network graphs based on the $reliability$. Fig.4.11 shows the GUI, where the figure on the left shows the RRH distribution, which is 7 RRHs in this case. The symbol **x** shows where the UE is located. The drop-down menu within the GUI has the following fields: $NUM\ RRHS$ represents the number of RRHs desired in the cellular area, $Sep.\ Dist\ RRHs\ (m)$ represents the separation distance between each pair of RRHs, which is twice the RRH coverage radius, $Target\ SINR\ (dB)$ represents the targeted or required SINR

level at UE location, $UEPosition$ are different random UE positions generated. The plot on the right side provides the formulated Network Graph, which is a representation of the derived reliability in Chapter 2, based on the parameters mentioned above.

Pairing

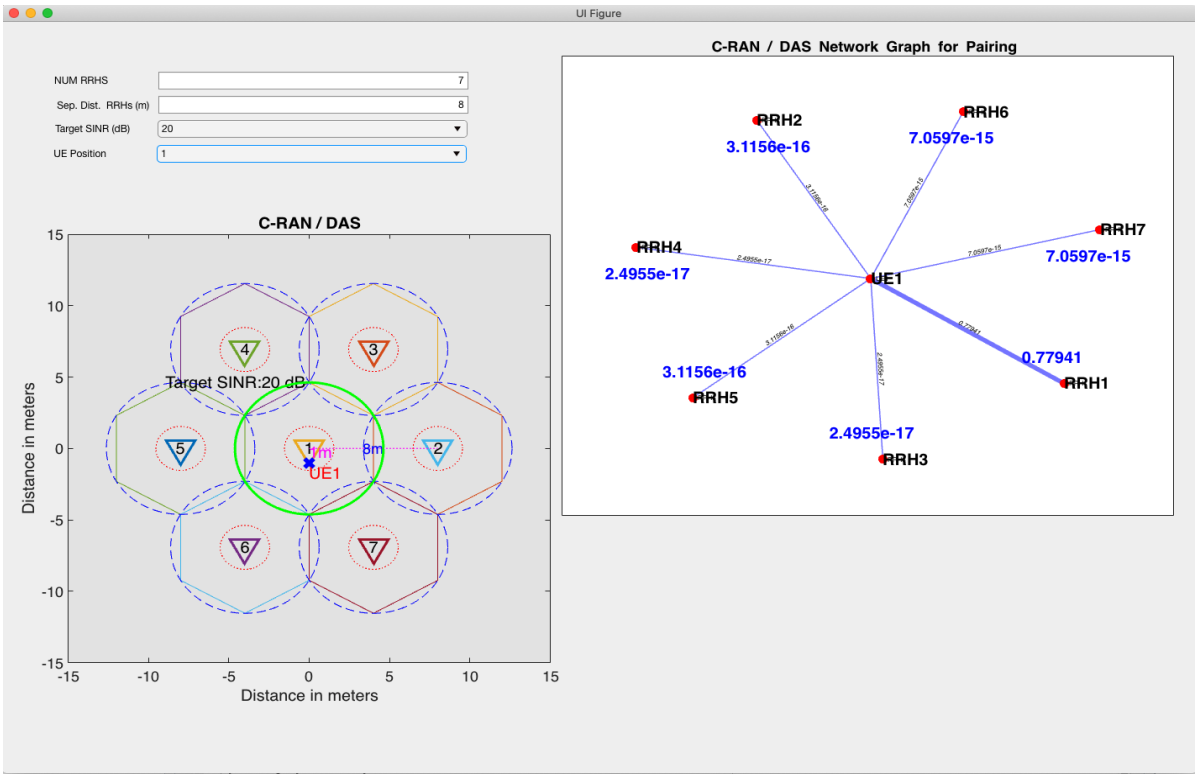

Fig. 4.12: NG formulated for pairing of $UE1$, for a targeted SINR of 20 dB

In order to monitor the $reliability$ of each UE within the coverage area, the exposed parameters Table 4.1 are regularly sent to NIF entity. NIF entity formulates the NGs based on the exposed parameters. Different NGs are formulated by NIF based on the goals required by CU. In this case, we present the NGs formulated in order to achieve efficient pairing with RRH. In Fig.4.11, the generated NG, which is on the right side of the figure. It shows that at the position $UE1$, which is positioned at 1 m, that is about 1/4th of the RRH radius. In this scenario, all the RRHs are transmitting the same power of -30 dBm and all RRHs reuse the time frequency resources. For the targeted SINR of 15 dB, the achievable $reliabilities$ if the UE2 is paired to different RRHs around $UE2$ is depicted in the NG. It is clear from the NG that the best choice is pairing $UE1$ to $RRH1$, as it has a $reliability$ of 0.9.

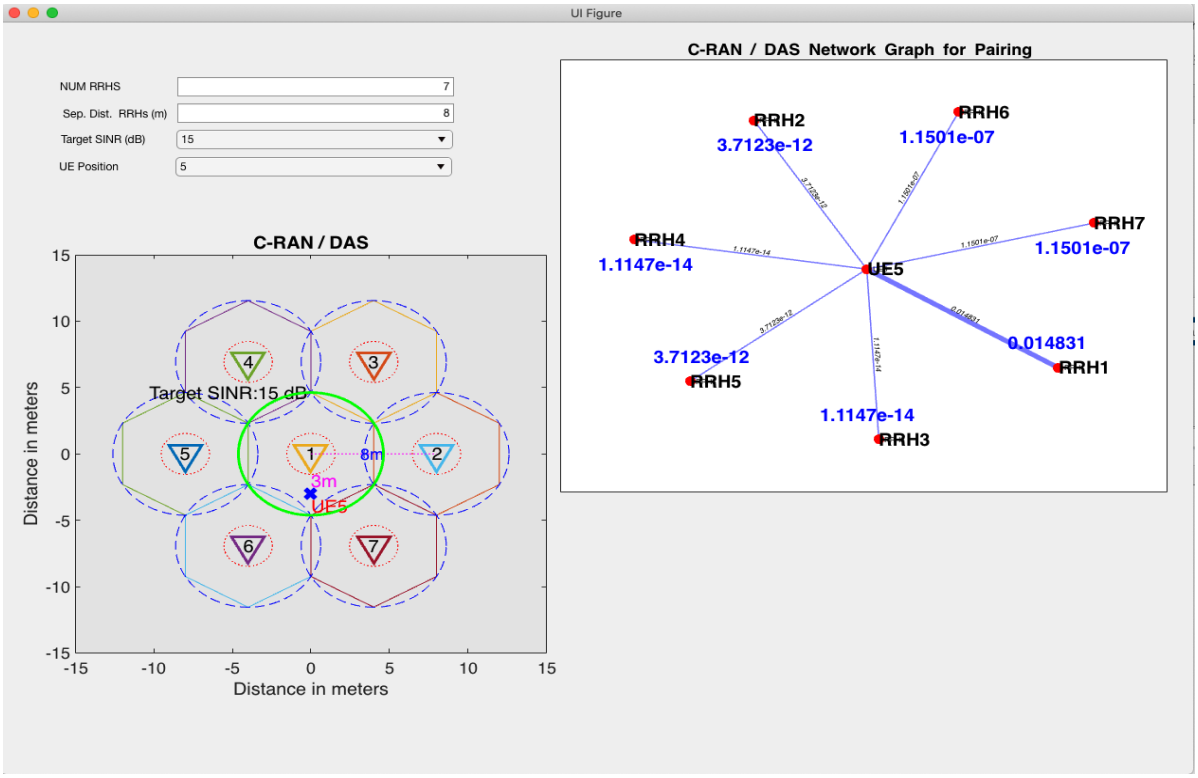

Fig. 4.13: NG formulated for pairing of $UE5$, for a targeted SINR of 15 dB

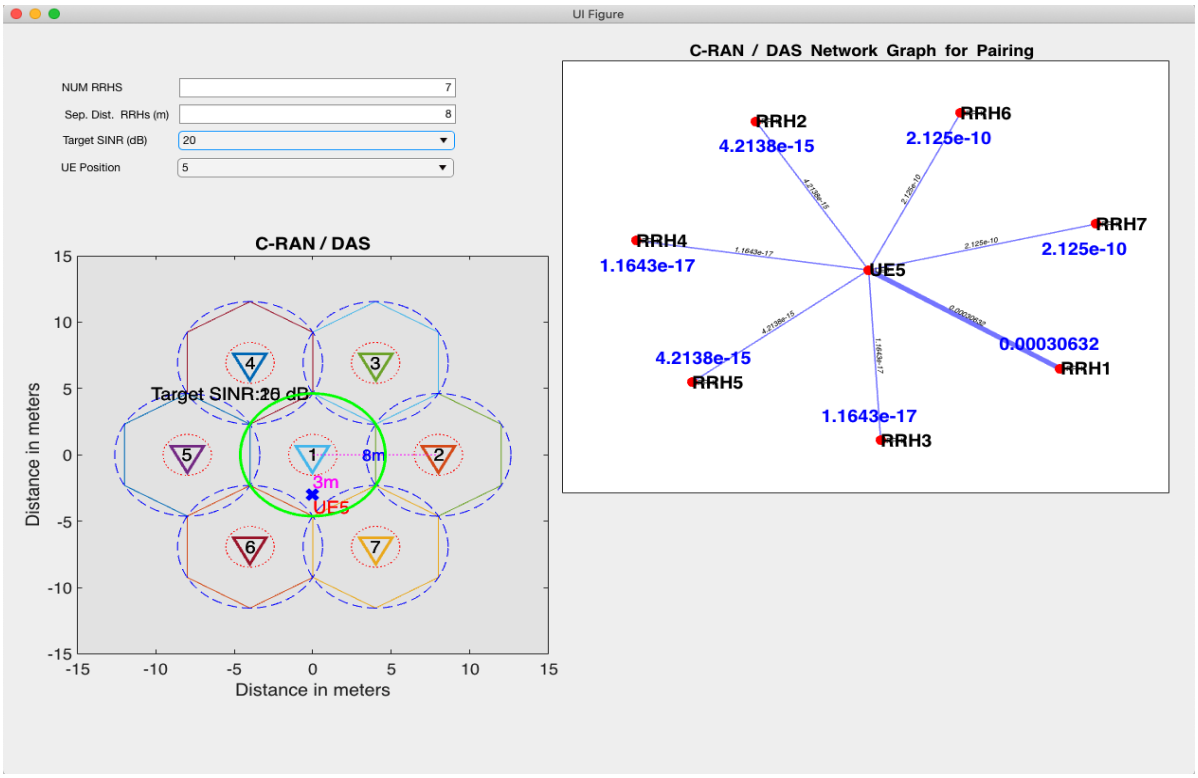

Fig. 4.14: NG formulated for pairing of $UE5$, for a targeted SINR of 20 dB

Fig.4.12 shows the NG formulated for $UE1$ with a targeted SINR of 20 dB at that position. In this case, the decision to pair is still with $RRH1$ because of $reliability$ of 0.8 shown on the edge of the NG. Fig.4.13 shows the NG formulated for $UE5$, which is around 3 m almost at the RRH coverage edge, with a targeted SINR of 15 dB at that position. In this case, the decision to pair is still with $RRH1$ even though the $reliability$ is very less. Fig.4.14 shows the NG formulated for $UE5$, the same location as before, with a targeted SINR of 20 dB at that position. In this case, the decision to pair is still with $RRH1$ even though the $reliability$ is extremely low.

Efficient Scheduling

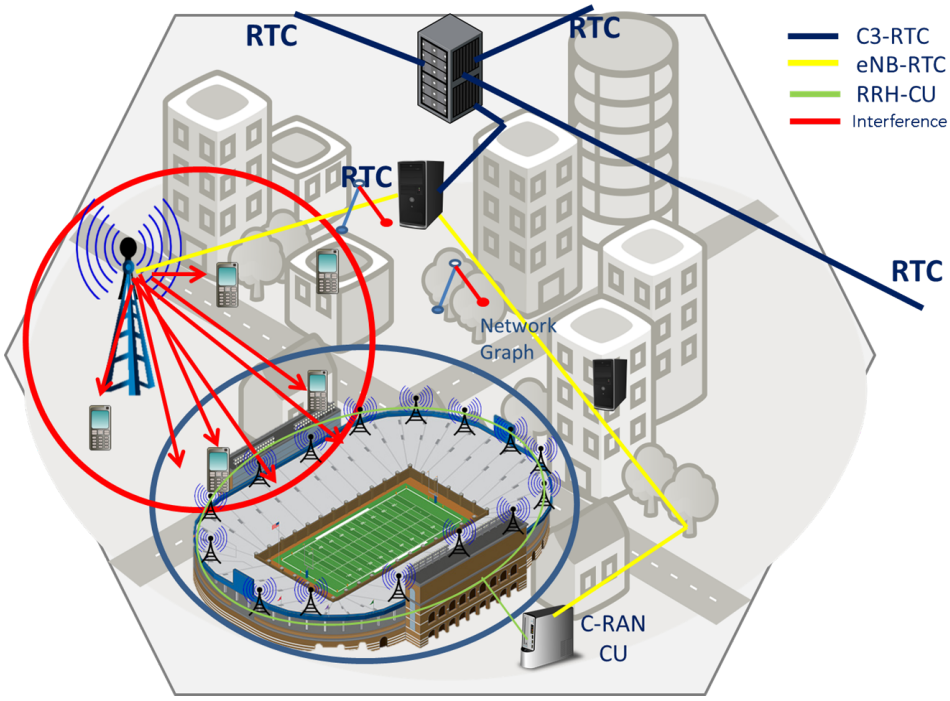

Fig. 4.15: C-RAN / DAS in HMN: Efficient scheduling of resources in Interference scenario

Fig.4.15 represents a typical real-life deployment scenario of C-RAN / DAS in HMN. In the figure, we can see the C-RAN / DAS being deployed in a stadium, where a high throughput density is required. These scenarios are called in 5G systems as *Hotspot* scenarios. As usually stadium lies near to the city or urban environment, the interference in the downlink, on the UEs covered under C-RAN / DAS, is very high from the neighboring macro and small cells. In this scenario, the CU requires the information from RTC, which has the information about the transmit powers of the neighboring eNodeBs over the RBs. Hence, the CU sends the Table 4.1 to

NIF. Then the NIF formulates the similar set of NGs describing RB, SINR and reliability maps, with requirements.

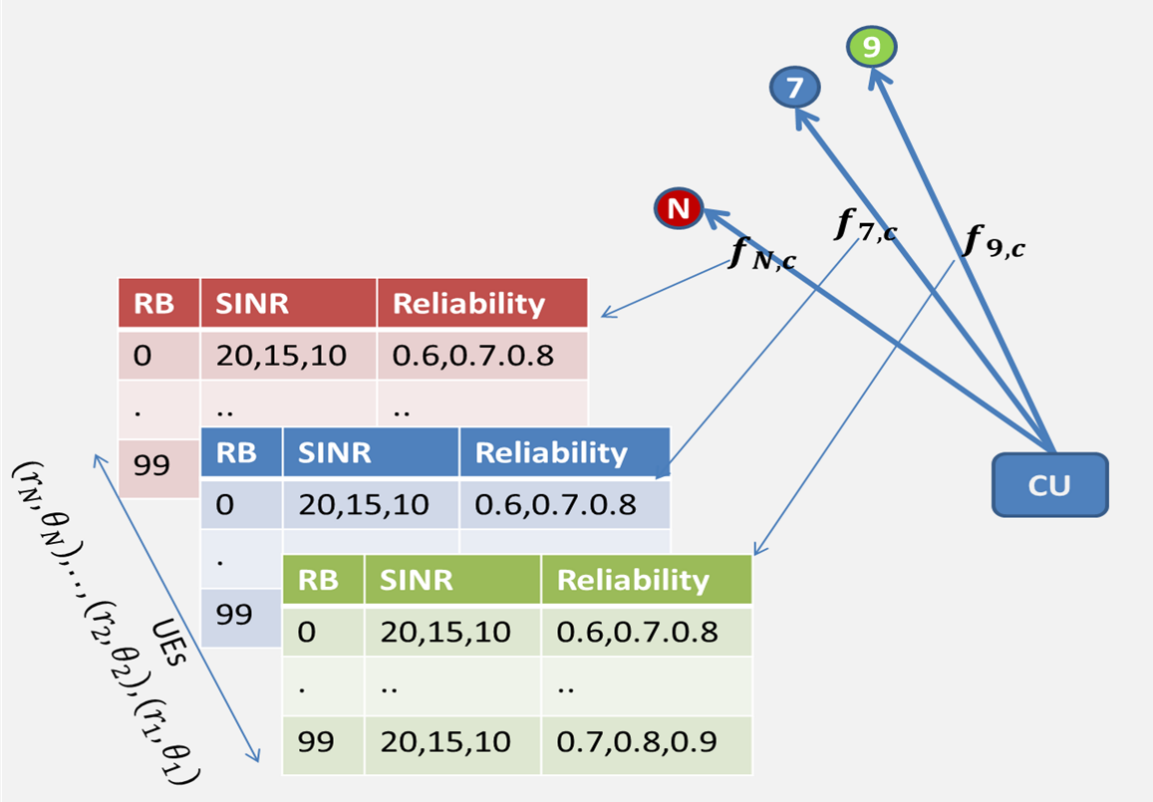

Fig. 4.16: NG for efficient scheduling

Fig.4.16 represents the NG formulated by NIF with the RB-wise information at different UE positions that are at the RRH edge, which are highly probable to suffer interference in DL from the neighboring eNodeBs. We can see from the figure that the UE positions and RB-wise information of $reliability$ required for each UE for different targeted SINRs and UE position is presented at each edge of the NG.

"Hence, Network graphs provide graphical representation of the required information for RTC / C3 in conjunction with the CU. The necessary parameters and abstraction metrics will be provided by the MAC and PHY layers towards the C3/RTC. C3 / RTC would in return provide the information like interference level on different RBs due to inter-cell interference, coverage information etc. back to MAC for efficient scheduling. In this way, the requirements will start from the lower layers and will flow towards RTC / C3 and back. The network graph will be generated by the NIF for RTC / C3 with the interference measurement information collected from each eNodeBs. The RBs affected by the cell edge users due to severe interference will be

identified and a decision to arbitrate the RBs reservation for the cell edge users will be provided by C3 / RTC. In this regard, the SINR / CQI reports of the UEs of both the cells will be collected at the C3 / RTC to coordinate the interference." [13]

4.4 Conclusion

In this chapter, firstly, the scope of the challenges that arise due to coexistence of manifold cellular systems and varied new and existing technologies, and the need for efficient control and coordination of radio resources, in 5G and Beyond Heterogeneous Mobile Networks is presented. Secondly, a brief summary of COHERENT solution for the challenges in HMN, which consists of the design of a *novel* system level architecture for RAN, control and coordination methodology, and abstractions using network graphs is presented.

Thirdly, an overview of the key aspects of COHERENT's novel *flexible* and *programmable* software defined networking (SDN) based system level architecture for 5G and Beyond HMN is presented. The main focus of COHERENT architecture is the efficient control and coordination of radio access functions in the 5G and Beyond Radio Access Network (RAN).

Fourthly, the challenges encountered by C-RAN / DAS in pairing and scheduling of resources in HMN, with focus on ultra-dense eMBB use case scenarios are analyzed. Various realistic scenarios of HMN with C-RAN / DAS deployments, and the need for control and coordination in these scenarios are presented. Based on the COHERENT architecture, the methodology for control and coordination using RTC and C3 in this scenario is formulated and explained. Furthermore, the abstraction of required parameters for the two challenges are formulated, and the network graph generation methodology and the control framework are presented. Lastly, based on the simulation models the network graphs for pairing are generated at different UE locations. For the case of efficient scheduling, the need for interference based network graphs is explained and the required abstracted and exposed parameters are given.

Therefore, in view of multidimensional requirements of 5G and Beyond use cases and the challenges that arise due to coexistence of various cellular systems and technologies, the novel *flexible* and *programmable* architecture and the control and coordination methods via network graphs based abstractions are shown to have the potential to provide viable solutions for key aspects of C-RAN / DAS in 5G and Beyond HMNs.

5 Real-time C-RAN / DAS Testbed and Measurement Results

This chapter begins with a detailed description of the design and implementation of real-time C-RAN / DAS testbed. Subsequently, in view of the practical deployment of C-RAN / DAS in real-time LTE systems, the measurement scenarios and the methodology employed, in order to validate the theoretical $reliability$ analysis presented in this thesis, is described. The work presented in this chapter is done by the author himself as part of COHERENT H2020 5G-PPP project funded by European Commission during July 2015 - March 2018. In this regard, this chapter consists of author's published work extracted from COHERENT project deliverables "D6.2 - Final Report on Technical Validation", Section 8 "Distributed Antenna System - Evaluation Results", as cited in reference [12], deliverable "D3.2 - Final report on physical and MAC layer modelling and abstraction", section 4.4.2 "Distributed antenna systems for throughput improvement", cited in reference [13], and deliverable "D3.1 - First report on physical and MAC layer modelling and abstraction", section 5.3 "Distributed antenna system", cited in reference [4].

5.1 System Design

This section describes the system design aspects of the real-time C-RAN / DAS testbed, which is built up to achieve validation of some of the research work presented in this thesis. The implementation of this testbed is done on a real-time Software Defined Radio (SDR) platform [42]. The general working principle of SDR is that the programmable or configurable communication processing of transmitter and receiver functional blocks run on a programmable devices such as Digital Signal Processors (DSPs). Therefore the testbed comprises of DSP cores, ARM processor cores and Radio Fequency (RF) front-end. The communication interface between radio frequency (RF) front-end and DSP is a digital baseband interface.

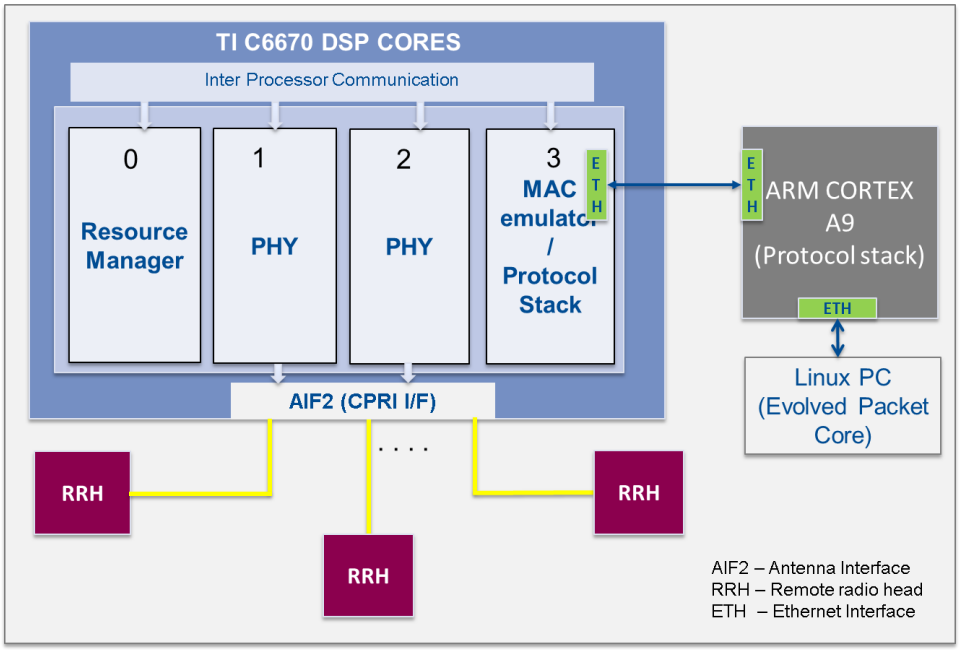

Fig. 5.1: Hardware blocks and Software Partition on DSP [5]
(*This figure is copied from author's published work "Reliability Analysis of Centralized Radio Access Networks in Non-Line-of-Sight and Line-of-Sight Scenarios", published in "IEEE Access", year 2019 [5]*)

Fig.5.1 shows an overview of the hardware and software components involved in building the central unit (CU) of C-RAN / DAS. The LTE based C-RAN / DAS testbed is built upon a complete SDR based LTE eNodeB solution having physical (PHY), medium-access-control (MAC), Protocol Stack (PS) layers and evolved packet core (EPC). PHY layer SDR based LTE eNodeB solution is provided by a company called mimoOn GmbH, Duisburg, Germany, which was a partner in one of the research projects. MAC, PS and EPC are provided by HCL technologies, Munich, which also was a partner in a research project. In this work, primarily the set of feasible adaptations, at PHY and MAC layers for C-RAN / DAS functionality at CU, are addressed, analyzed, implemented and validated.

LTE PHY layer signal processing blocks of the transmitter and receiver are implemented on Texas Instruments (TI) C66x generation DSP. TI's TMS320C6670 [6] is a highly efficient DSP having four cores developed specifically for prototyping small cell LTE eNodeB physical (PHY) layer. Fig.5.1 shows an overview of software partitioning on the DSP cores. The PHY transmitter and receiver processing blocks run on the cores 1 and 2, while the resource manager, which shares the DSP resources such as: memory, hardware interrupts, co-processors, queues etc., among the cores runs on core 0. MAC emulator is a software which emulates MAC functionality by sending

the PHY level configuration to the cores 1 and 2, on every millisecond and receives the decoded channels information from PHY. With the MAC emulator code one can set a different PHY configuration over many subframes, in order to validate the PHY functionality. A subframe in LTE is a block of 14 or 12 OFDM symbols. The duration of one subframe is 1 ms, this duration is also called total transmission interval (TTI).

Fig.5.1 also shows the hardware module called Antenna Interface 2 (AIF2), which is a part of the TMS320C6670 DSP. AIF2 module interfaces the DSP to the Remote Radio Heads (RRH) or RF front-end. For transmission, AIF2 receives the baseband IQ time domain signals from the DSP's FFT co-processor and converts the IQ baseband signals into common public radio interface (CPRI) baseband signals, which are then transmitted via optical cables to the RRHs. In the receiver, AIF2 receives the digital baseband signals from analog to digital converted (ADC) in the RRH via CPRI and translates them back to IQ time domain signals. The IQ time domain signals are then interfaced directly with the FFT co-processor module within the DSP for further processing.

The MAC and protocol stack (PS) layer run on ARM CORTEX A9 processor. DSP interfaces with ARM via Gigabit Ethernet interface. A task handler is implemented on the DSP core 3 to facilitate the transmission and reception of PHY level configurations and decoded messages between DSP and ARM. The Evolved Packet Core (EPC) runs on a Linux PC, which can be connected to internet to facilitate a complete end-to-end solution. The PS running on ARM board communicates with EPC via Gigabit Ethernet interface.

In the following subsections a brief overview of DSP, AIF2 and RF front-end capabilities and the relevant functionalities which were instrumental in building up this testbed is presented.

5.1.1 TMS320C6670 DSP

This subsection is extracted from Texas Instruments's - TMS320C6670 Data Manual [6]

Texas Instrument's (TI's) TMS320C6670 DSP is a multicore fixed-point processor for small cell LTE eNodeB physical (PHY) layer processing. The C6670 provides a programmable platform for implementing eNodeB functionality of various wireless standards including WCDMA / HSPA / HSPA+, GSM, LTE and WiMAX. Therefore, implementation of the processing blocks on a DSP facilitates high level of flexibility to analyze, modify, append new features and mea-

surements. In this subsection the details about TMS320C6670 DSP's functional blocks, as shown in Fig.5.2, in view of LTE based DAS implementation is presented.

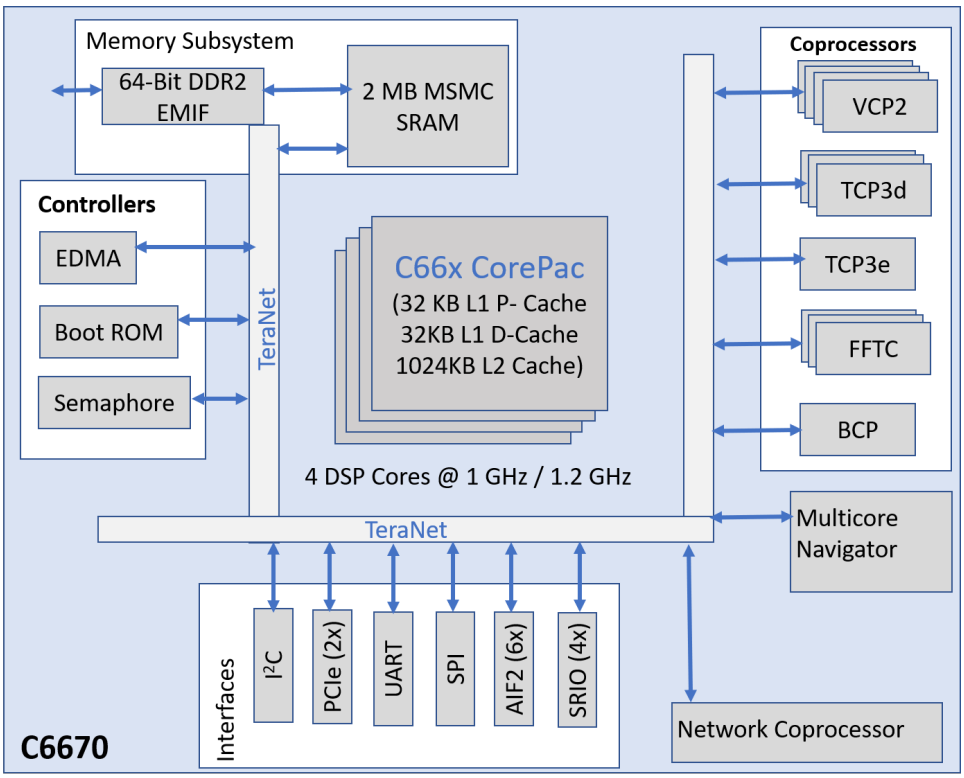

Fig. 5.2: TMS320C6670 relevant functional blocks [6]
(*This figure is extracted from "Texas Instruments's - TMS320C6670 Data Manual" [6]*)

TMS320C6670 DSP consists of 4 DSP cores, shown in Fig.5.2 as CorePacs, where each core can be clocked at at 1.00 GHz and 1.2 GHz. This DSP belongs to the latest generation of DSPs having combination of fixed-point and floating-point instruction set architectures. The performance of the DSP is 153.6 GMACS / 76.8 GFLOPS @ 1.2GHz. Each DSP core has internal memory of 32 KB L1-P, where L1P stands for internal program memory, and 32 KB L1D, where L1-D is for data memory. The L1-P and L1-D memories are usually used to store frequent program code or as cache memory. Furthermore, each core has 1024 KB internal memory called L2, which can be either used as cache or for storing frequently used program or tables. There is 2 MB of on chip shared memory, called as MSMC in the figure, available to all the 4 cores and controllers, which is primarily used for sharing data for multi-core programming. This DSP has the following hardware co-processors available for LTE processing [6]:

- Three enhanced Turbo decoders (TCP3d), for LTE's Physical Uplink Shared Channel

PUSCH) decoding, which supports up to 548 Mbps data rate.

- One enhanced Turbo encoders (TCP3e), which supports up to 500 Mbps for LTE.
- Four Viterbi decoders (VCP2), for Physical Downlink Control Channel (PDCCH) decoding, which support more than 38 Mbps 40-bit block size
- Three Fast Fourier Transform (FFT) co-processors, which supports all LTE FFT sizes. The FFT co-processor can perform one 2048 point FFT in 4.8 μs
- Bit Rate co-processor [84], which includes encoding, rate matching / dematching, code block segementation, multiplexing etc. for Physical Downlink Shared Channel (PDSCH) and PUSCH encoding and decoding. It supports up to 914 Mbps for LTE.

This DSP supports the following peripherals for LTE processing [6]:

- Six-lane SerDes based antenna interface (AIF2), which converts IQ baseband time domain data to CPRI operating up to 6.144 Gbps
- Hyperlink which supports. connections to other KeyStone Archtitecture devices providing resource scalability
- Gigabit Ethernet (GbE) Switch Subsystem
- 64-Bit DDR3 Interface with Speeds up to 1600 MHz
- SPI Interface
- Sixteen GPIO pins
- Eight 64-Bit Timers.

Apart from these, it has Multicore Navigator [85] HW module, which has 8192 multipurpose HW queues with Queue Manager. As shown in Fig.5.2, the Multicore Navigator interfaces with most of the hardware co-processors with the DSP cores using HW queues. Network Co-processor HW module interfaces the Ethernet based translation of messages with the DSP.

IAF Dual TMS320C6670 board

The following text is derived from IAF GmbH's - Dual 6670 AMC data sheet [7]

Fig.5.3 shows the functional block diagram of Dual 6670 Advanced Mezzanine Card (AMC) module, which hosts the C6670 DSP described previously. Dual 6670 AMC module [7] hosts two high performance TMS320C6670 from TI and one Xilinx Spartan-6 FPGA, apart from modules supporting various interfaces to communicate with other devices. The compact single width / full height AMC module is designed for the development future generation radio communication technologies by IAF GmbH, Braunschweig, Germany.

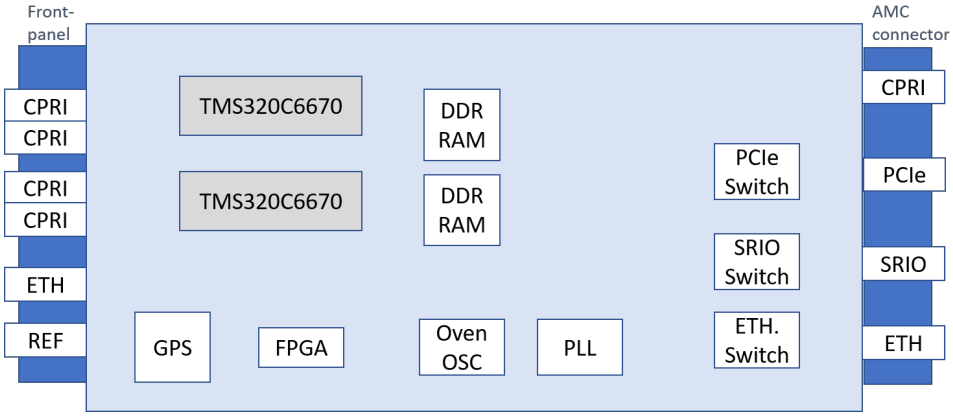

Fig. 5.3: Functional block diagram of Dual 6670 AMC module [7]
(*The following figure is extracted from "IAF GmbH's - Dual 6670 AMC data sheet" [7]*)

As shown in Fig.5.3, the Dual 6670 module has 4 x AIF2 / CPRI Small Form-factor Pluggable (SFP) connectors on the front panel to facilitate the CPRI baseband interface towards RF frontend. Towards backend, one can as well direct the CPRI, PCIe, SRIO and Ethernet signals over the AMC connector. In the current system design, the PHY and MAC Emulator processing of C-RAN / DAS is compiled and loaded onto one of the DSP on this module.

5.1.2 Antenna Interface 2 (AIF2)

This subsection is derived from Texas Instruments's - Antenna Interface 2 (AIF2) user's guide [8]

Antenna Interface2 (AIF2) [8] is a peripheral module within the TMS320C6670 DSP, which supports transfers of baseband IQ data between DSP processors and a high-speed serial interface. The main relevant features supported by AIF2 are:

- Baseband standards
  - Open Base Station Architecture Initiative (OBSAI)
  - Common Public Radio Interface (CPRI)
- Wireless Communication standards
  - GSM, WiMax, WCDMA, LTE
- Six baseband links
  - 6 GHz SerDes
  - Link Rates: OBSAI $\{2x, 4x, 8x\}$, CPRI $\{2x, 4x, 5x, 8x\}$
- Antenna Carriers (AxC)
  - Maximum AxC per Link: CPRI - Maximum 124 AxC + 4 control streams
  - AxC Offset, which is required for synchronization is supported
  - Programmable AxC which can be deleted in run state is supported
- Timing and Synchronization
  - Radio Timer: Programmable even on OFDM symbol boundaries
  - Physical Interface Timer: 10 ms frame count for CPRI timing
  - Timer Synchronization with external timer
  - System Events generation
- Data Transfers and Formats
  - Autonomous Direct Memory Access (DMA)
  - Big Endian and Little Endian
  - IQ or QI programming order
  - 16-bit I and 16-bit Q
- PHY

  - 8b10b line encoding / decoding

- CPRI
  - CPRI bit interleaving and AxC Container packing/unpacking
  - CPRI Synchronization

AIF2 has three basic layers, as follows:

- PHY layer, which consists of SerDes (SD), Receiver MAC (RM), CPRI Input (CI), Re-transmitter (RT), CPRI Input (CO), Transmitter MAC (TM).
- Protocol layer, which consists of Protocol Detector (PD), Protocol Encoder (PE) and Data Buffer (DB).
- Direct Memory Access layer, which consists of AIF2 DMA, Packet based DMA (PKT-DMA)

Please refer to TI's AIF user guide [8] for a detailed description of AIF2 Hardware blocks, their functionalities and configuration.

LTE Frame timing

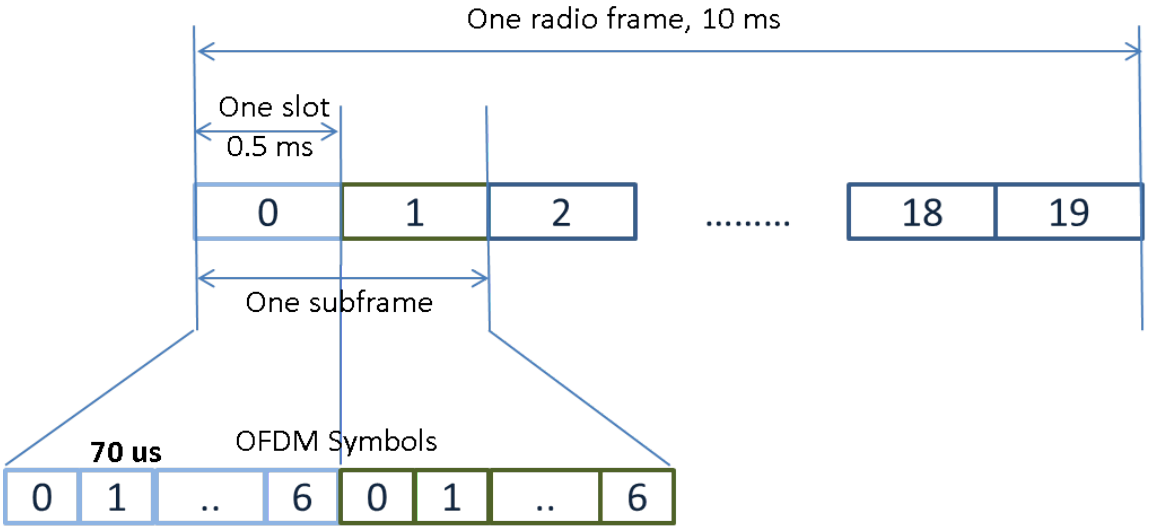

Fig. 5.4: LTE frame timing

Fig.5.4 shows the one frame in LTE. LTE radio frame is of 10 ms duration, which is further divided into 20 slots each of 0.5 ms duration. One subframe, which is 1 ms in duration, is of 2 slots. When the sampling rate is 30.72 MHz, the number of samples in one radio frame is around 307200, and 15360 samples per one slot. Each slot has 7 OFDM symbols in an Normal cyclic prefix case and 6 OFDM symbols in Extended cyclic prefix case. In a Normal cyclic prefix case, the first OFDM symbol has 160 samples of cyclic prefix and other OFDM symbols have 144 samples of cyclic prefix at 30.72 MHz sampling rate.

CPRI LTE Sample packing

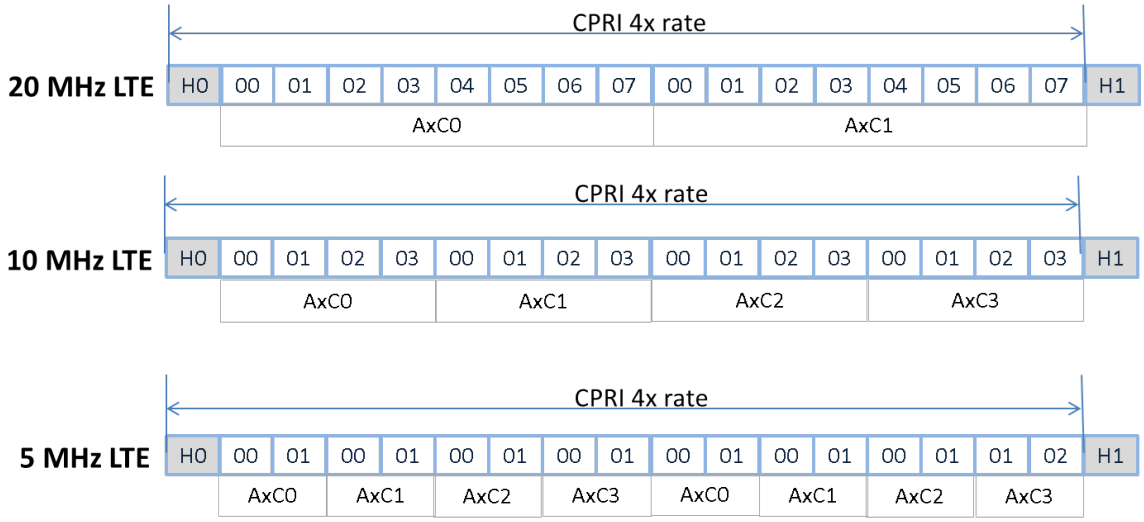

Fig. 5.5: CPRI 4x Basic Frame Vs. LTE Bandwidth [8]
(*The following figure is extracted from "IAF GmbH's - Dual 6670 AMC data sheet" [7]*)

Fig.5.5 shows CPRI sample packing based on LTE data from different antenna carriers (AxC) in the case 4x CPRI link rate. Different AxC can be from different antennas as in multiple-input-multiple-output (MIMO), or can from be UL and DL data as in TDD frame. The figure shows that for 20 MHz LTE case, which has a sampling rate of 30.72 MHz, two AxC's can be accommodated in a CPRI 4x Basic Frame. Similarly, it shows the CPRI sample packing for the case of LTE bandwidth's of 10 MHz and 5 MHz respectively.

Fig.5.6 shows the CPRI basic frame when the link rate is reduced to 2x, then only 1 AxC can be accommodated in the 20 MHz bandwidth case, because of the reduction in link rate. Furthermore, we can see that more number of AxCs can be accommodated in the case of lesser LTE bandwidths.

Fig. 5.6: CPRI 2x Basic Frame Vs. LTE Bandwidth [8]
(*The following figure is extracted from "IAF GmbH's - Dual 6670 AMC data sheet" [7]*)

LTE Bandwidth	Sample Rate	2x	4x	5x	8X	FFT Size
1.4 MHz	1.92 MHz	16	32	40	64	128
3.0 MHz	3.84 MHz	8	16	20	32	256
5 MHz	7.68 MHz	4	8	10	16	512
10 MHz	15.36 MHz	2	4	5	8	1024
15 MHz	23.04 MHz	1	2	3	4	1536
20 MHz	30.72 MHz	1	2	2	4	2048

Fig. 5.7: Table showing CPRI number of AxCs per link Vs. LTE Bandwidth [8]
(*The following table is extracted from "IAF GmbH's - Dual 6670 AMC data sheet" [7]*)

Fig.5.7 shows the complete picture of the number of AxCs that can be accomodated in the case of various CPRI link rates and LTE banwidth configurations. The FFT size and sampling rates for each LTE bandwidths is also shown.

Hence, AIF2 provides very efficient, flexible and fast interfacing of IQ baseband data, from multiple antennas for various LTE bandwidths, with RRHs via CPRI basis frames. This module is very much suitable for C-RAN / DAS in interfacing with many distributed RRHs using CPRI baseband standard.

5.1.3 Radio Front-end

This subsection is derived from Fraunhofer HHI's website - SDR RADIO FRONTEND [9]

The Radio front-end / RRH is the key component of the DAS. The RRH is connected to AIF2 using an optical fiber. The RRH can be remotely configured via the ethernet interface. As shown in Fig.5.8, the RRHs are provided by Fraunhofer Institute of Telecommunications, Heinrich Hertz Institute (HHI), Berlin, Germany, as a part of a collaborative research project. This RRH supports a very high range of frequencies ranging from 70 MHz up to 6 GHz. The RRH supports 2x2 Multiple Input Multiple Output (MIMO) or multi-antenna transceivers with 12-bit DACs and ADCs, which can be used in FDD or TDD operation. The tunable baseband bandwidth is between 200 kHz and 56 MHz which supports the largest LTE bandwidth of 20 MHz. As shown in Fig.5.8, the compact hardware is uTCA compliant with AMC form-factor, which supports optical, e.g. CPRI, as well as high-speed ethernet interface to facilitate real-time baseband processing.

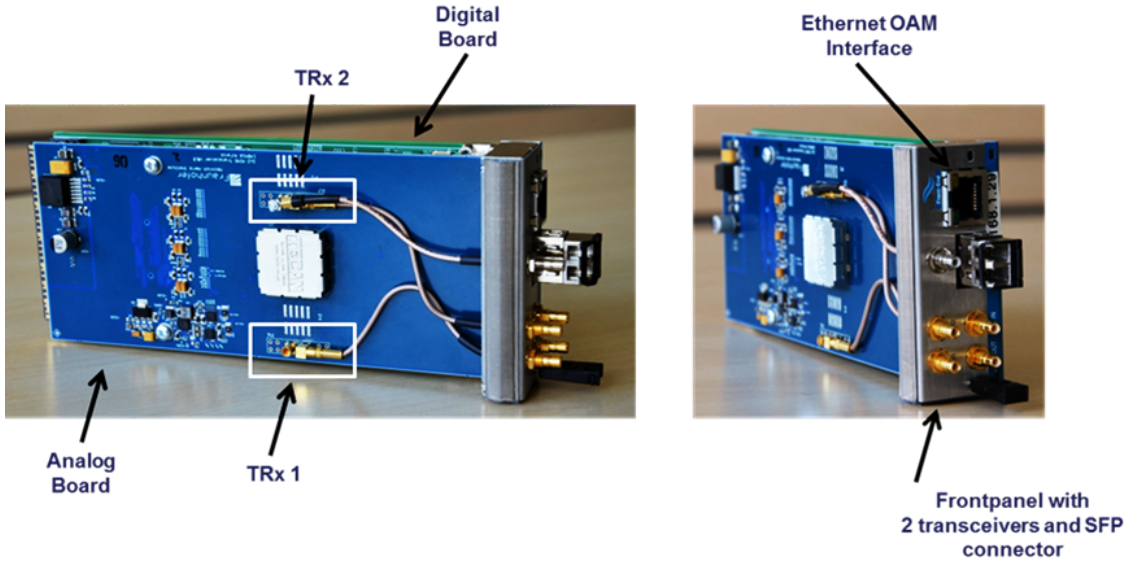

Fig. 5.8: Front panel of HHI's Radio Front-end [9]
(*This figure is extracted from "Fraunhofer HHI's website - SDR RADIO FRONTEND" [9]*)

Fig.5.9 describes the idea of SDR RRH, which has 2x2 MIMO transceiver blocks that can be stacked to form various sets of multiple antennas. The figure also shows how the FPGA interfaces with ADC and DAC to convert the baseband data into CPRI frames. The CPRI frames are forwarded to CU via Small Form-factor Pluggable (SFP) port.

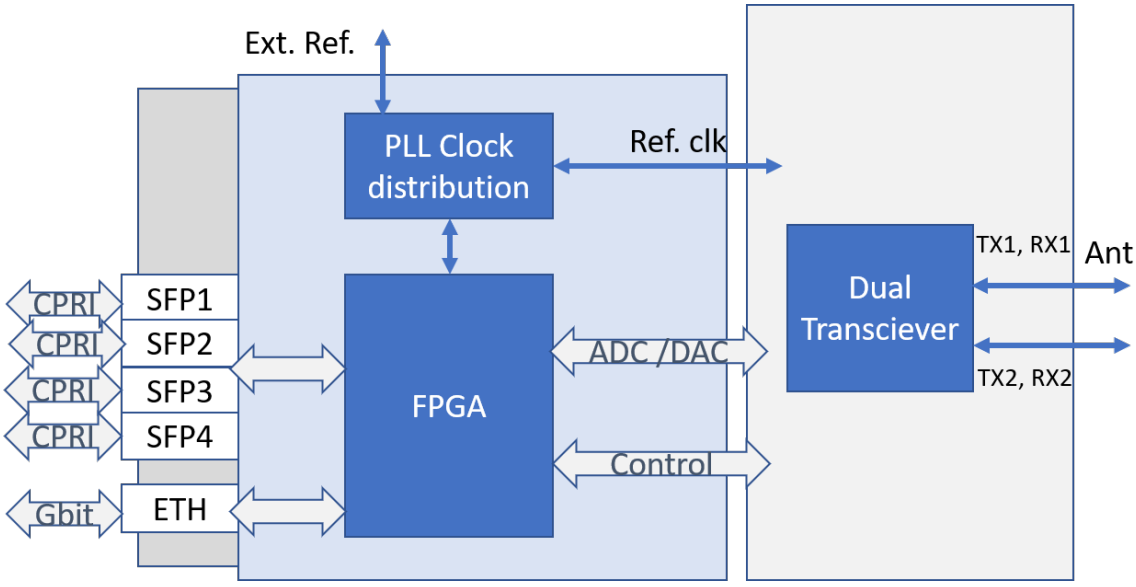

Fig. 5.9: Block diagram of SDR Transceiver [9]
(*This figure is extracted from "Fraunhofer HHI's website - SDR RADIO FRONTEND" [9]*)

Fig.5.10 shows the Graphical User Interface (GUI) used for configuring the following parameters on RRH:

- Transmitter frequency for the range between 70-6000 MHz.
- Receiver frequency for the range between 70-6000 MHz.
- Transmitter Power Amplifier (PA) attenuation for the 2 chains, which can be set between 0-89 dB.
- Receiver Automatic Gain Control (AGC) selection from three modes: AGC off, AGC Fast Attack, AGC Slow Attack.
- Receiver Low Noise Amplifier (LNA) gain settings for the 2 chains, between 0-70 dB.

The main features of SDR based RRH from HHI [9] can be summarized as:

- CPRI 4.1 standard
- Baseband optical SFP interface
- 2x2 MIMO transceiver with variable RF signal bandwidth

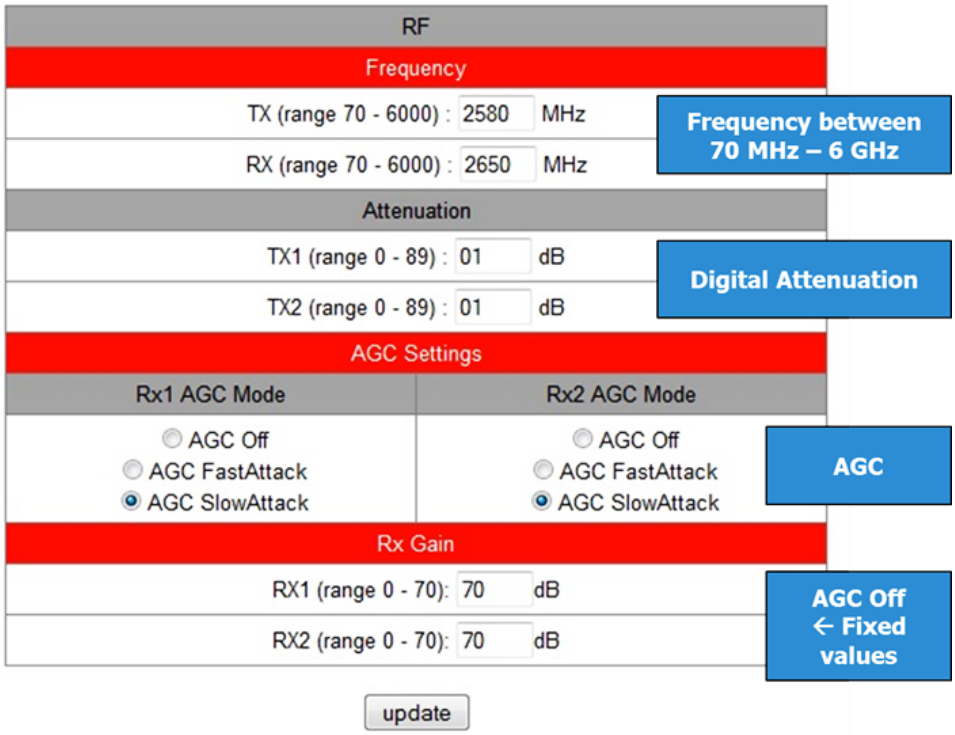

Fig. 5.10: GUI for Radio Front-end Configuration [9]
(*This figure is extracted from "Fraunhofer HHI's website - SDR RADIO FRONTEND" [9]*)

- 70 MHz - 6 GHz carrier frequency range
- Various reference clock sources
- Both Frequency division duplexing and time division duplexing features are supported
- RF filter with variable bandpass widths
- Maximal RMS output Power of 0 dBm at 2.6 GHz

Although DSP is capable of processing for many users in the current work, for the sake of simplicity an use case with only 2 UEs per subframe scheduled is selected for investigation. The current LTE testbed is fully functional to attach many commercial UEs and to communicate with them.

5.2 Adaptations in LTE for C-RAN / DAS

In the first subsection 5.2.1, a brief introduction to LTE PHY downlink channels and their structure in a LTE subframe is outlined. In the subsequent subsection 5.2.2, the analyzed

software modifications in the LTE DL processing chain in order to facilitate the functionality of C-RAN / DAS is described. Furthermore, the implementation details of these software modifications is presented. In the last subsection 5.2.3, the analyzed adaptations in LTE UE procedures for C-RAN / DAS are presented in detail.

5.2.1 Introduction - LTE PHY Downlink

This subsection is derived from 3GPP LTE PHY layer specifications, "E-UTRA; Physical channels and modulation (3GPP TS 36.211 V9.0.0)" [86] and "E-UTRA; Multiplexing and channel coding (3GPP TS 36.212 V9.2.0)" [87]

In the downlink, various physical channels were specified by 3GPP LTE Rel. 9 standard, which transport user plane and control plane data from eNodeB to UEs. In this subsection, a brief description of the physical downlink channels [86, 87] is presented.

Synchronization Channel (PSS and SSS): In order to achieve time and frequency synchronization at UE, eNodeB transmits Primary Synchronization Signal (PSS) and Secondary Synchronization Signal (SSS) with a periodicity of 50 ms. PSS is generated using frequency-domain Zadoff-chu sequences, which belong to constant amplitude zero auto-correlation (CAZAC) sequences. As shown in Fig.5.11, PSS sequence is mapped on to 6th OFDM symbol of slot 0 and slot 10 in each radio frame. Three different Zadoff-chu sequence of length 63 is chosen for PSS which map to three physical layer identities. The length 63 frequency domain sequence is mapped on to 72 subcarriers or 6 RBs centered around DC.

Secondary synchronization signal (SSS) are generated using different cyclic shifts of a single length-31 m-sequences, which have orthogonal properties. SSS are mapped onto 5th OFDM symbol on slot 0 and slot 10. SSS sequences are changed between slot 0 and slot 10, which helps the UE to identify the slot 0 or slot 10 precisely in order to determine the frame boundary. Likewise to PSS, the SSS symbols are mapped onto the middle 72 subcarriers centered around DC.

PSS transports physical layer identity, $(N_{ID})^{(2)}$, which can take values, 0,1 and 2, while SSS carries physical layer cell identity group $(N_{ID})^{(1)}$, which can take 168 values between 0 and 167. After successful decoding of PSS and SSS by the UE, the cell ID is computed using the expression, $N_{ID})^{cell} = 3 * (N_{ID})^{(1)} + N_{ID}^{(2)}$. Apart from decoding the cellID, the synchronization

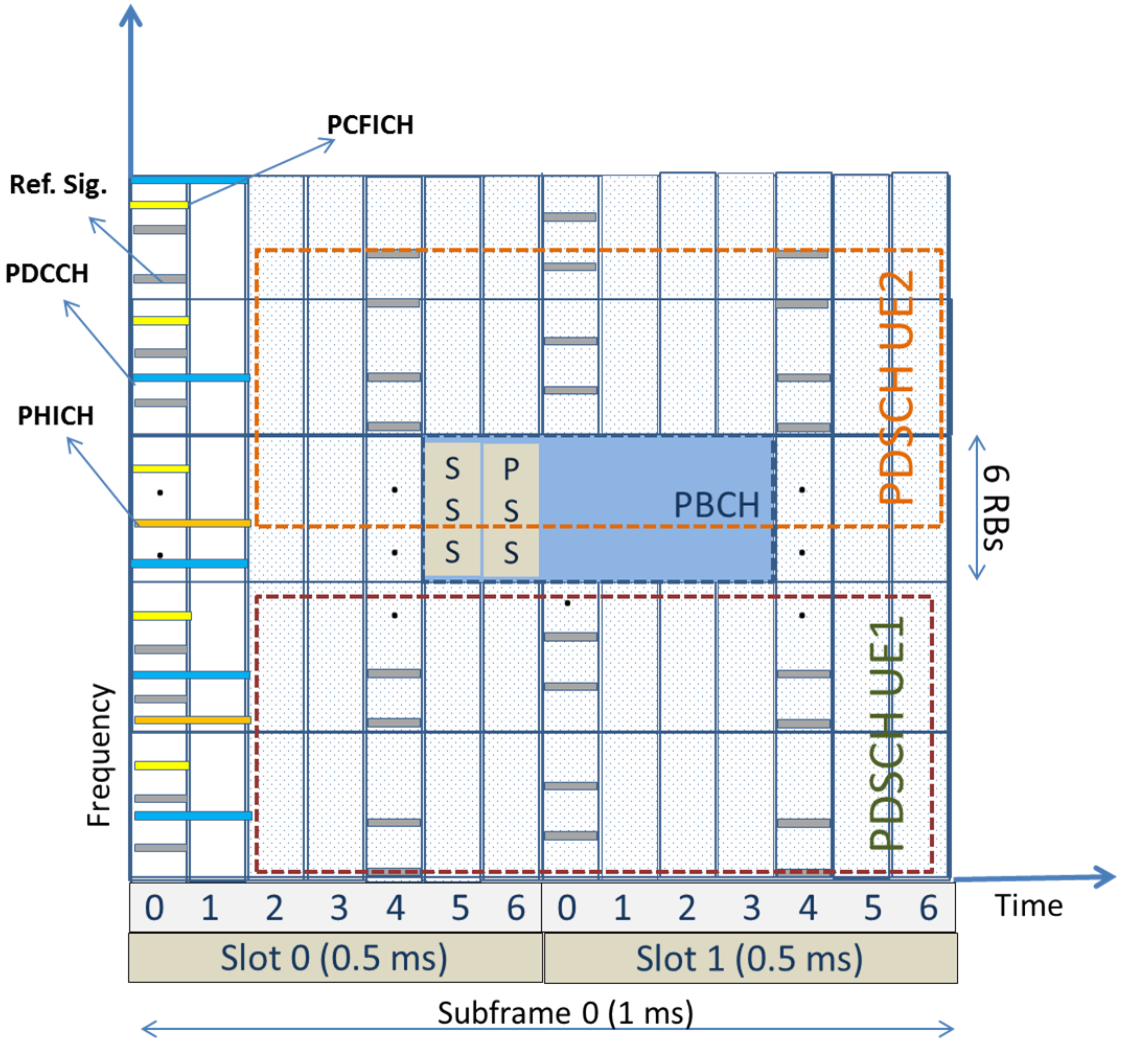

Fig. 5.11: LTE PHY Downlink Channels structure in a subframe

channels serve in estimating the carrier frequency offset and phase noise.

Cell Specific Reference Signals: The eNodeB transmits reference signals on specific OFDM symbols in every subframe, which are generated using orthogonal m-sequences. These signals serve to estimate the downlink channel at the UE. The channel estimates are then used to equalize the channel effects from the DL control and data channels by the UE. Typically in single antenna transmission scenario as shown in Fig.5.11, the OFDM symbol 0 and 4 in each slot consist of reference signals. Within these OFDM symbols, in frequency domain, every 6^{th} subcarrier is mapped with the reference signal. The start position of the subcarrier is determined by evaluating this expression $N_{ID}^{cell} mod\ 6$. After successful decoding of the reference signals, UE calculates the channel estimates and by interpolating them over time and frequency axes. In case of

transmission using 2 antennas, an interleaved pattern of mapping of references signals is used such that reference signals from both the antennas do not overlap.

Physical Broadcast Channel (PBCH): Master Information Block (MIB) is the minimum required system information broadcasted by the eNodeB to all the UEs within its coverage. MIB consists of downlink channel bandwidth, PHICH configuration and the 8 MSB bits of the system frame number (SFN). As shown in Fig.5.11, PBCH is mapped onto the middle 72 subcarriers around the DC, such that the UEs can extract the PBCH without the knowledge of the system bandwidth. The MIB data in PBCH is spread over 4 system frames or 40 ms, but located always on slot 1 of each system frame. After successful decoding of the PBCH, the UE can configure its sampling rate and FFT sizes based on the decoded MIB. Decoding PBCH configure the UE to decode the System Information Blocks (SIBs) as well, which prepares the UE for initial attach to the network.

Physical Control Format Indicator Channel (PCFICH): Control Format Indication (CFI) takes values, 1, 2 and 3, which indicates the number of OFDM symbols currently configured to carry control channels in the current subframe. CFI value is at first, channel coded with 1/16 code rate to 32 bits. Afterwards, these 32 bits are scrambled and QPSK modulated. As shown in Fig.5.11, the QPSK modulated symbols are mapped always on the OFDM symbol 0 of the subframe. After successful decoding of PCFICH channel, the UE knows the time domain span of control channels and at which OFDM symbol the data is located.

Physical Hybrid ARQ Indicator Channel (PHICH): PHICH channel is used for transmitting ACK or NACK messages as a part of the Hybrid Automatic Repeat Request (HARQ) procedure. After successful decoding of PUSCH / UL data the eNodeB shares the ACK with the UE and with a failed decoding a NACK. For a SISO case, HARQ indication (HI) value is a single bit, which can take either 1 or 0. PHICH is mapped onto the control symbols, which is indicated by the CFI decoded from PCFICH.

Physical Downlink Control Channel (PDCCH) : Downlink Control Information (DCI) provides UL / DL scheduling information to the UE. DCI represents different information at various bit fields. In case of DL resources being scheduled in that subframe to an UE, the DCI provides the Resource Indication Value (RIV), which gives exact physical RBs allocated where the DL data called as Transport Block (TB) is found. Many DCIs for various UEs can be sent

on the PDCCH channel, which is accomplished by mapping of encoded and modulated DCIs's through Control Channel Elements (CCEs). The modulation format used in PDCCH is QPSK. The number of CCEs that can be used to map a single DCI can be 1, 2, 4 or 8, where 8 CCEs has the highest reliability of being detected. Fig.5.11 shows the PDCCH being mapped in the first two OFDM symbol, here in this example the CFI value is 2.

Physical Downlink Shared Channel (PDSCH): The UE specific data together with some signaling and higher layer information is transmitted in predefined lengths of data called as transport blocks. TB is at first segmented into code blocks, which are scrambled and then channel coded at the eNodeB using turbo codes. The encoded data is further rate-matched to the number of bits proportional to the available sub-carriers for PDSCH. The rate-matched is mapped into modulation symbols, which can be QPSK, 16 QAM or 64 QAM modulated. These symbols are further layer-mapped and precoded for MIMO transmission modes. The available transmission modes are, SISO, MIMO schemes which are: closed-loop spatial multiplexing, open-loop spatial multiplexing, Cyclic-delay diversity and Transmit diversity schemes. The MAC decides the TB size, modulation and coding scheme (MCS) and the transmission modes based on the channel quality indicator (CQI) reported by the UE. The PDSCH data is not mapped in the control region but immediately after last OFDM symbol of the control channels. Fig.5.11 shows the mapped PDSCH data for 2 UEs starting from OFDM symbol 2 in slot 0 in time-domain, while some RBs of the total bandwidth are allocated to UE1 and UE2. We can see from the figure, that for some subframes there could be PBCH and Synchronization Channels mapped on to 6 RBs around DC. In these subframes, PDSCH data is not mapped on these RBs allocated to PBCH, PSS and SSS. In this figure, we can see how the PDSCH data from 2 UEs are mapped onto different RBs. Apart from UE specific data and higher layers data, PDSCH is also used to broadcast various SIBs and paging information.

5.2.2 Adaptations - LTE PHY Downlink

This subsection is derived from author's published work in IEEE conferences [10, 32], IEEE Access Journal [5] and in COHERENT deliverables D3.1, D3.2 and D6.2 [4, 12, 13]

In LTE PHY Downlink channels, the only data channel that transports UE data from eNodeB to UE is PDSCH. Apart from PDSCH, the other PHY DL channels does not require any

other processing modifications for C-RAN / DAS functionality. Therefore, in this subsection, the necessary adaptations required for PDSCH processing blocks to support C-RAN / DAS functionality will be analyzed.

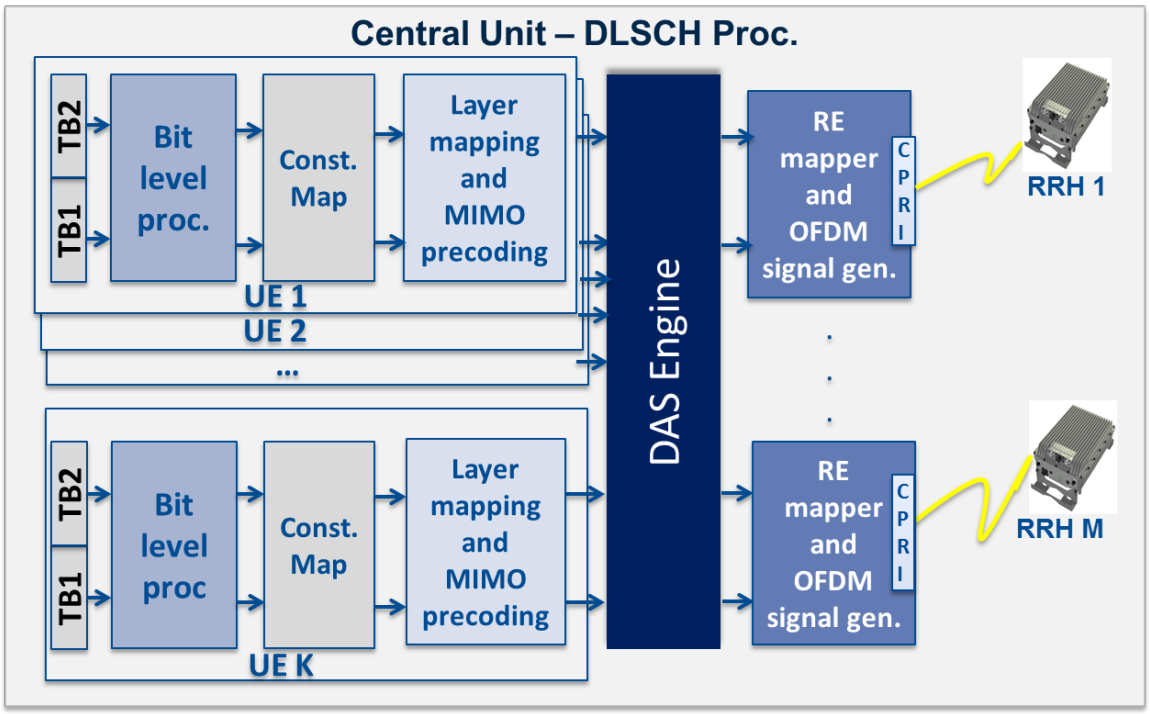

Fig. 5.12: PDSCH processing chain adaptations for DAS [10]
(*This figure is copied from author's published work, "Probability of coverage based analysis of distributed antenna system and its implementation on LTE based real-time-testbed", published in "2017 9th International Congress on Ultra Modern Telecommunications and Control Systems and Workshops (ICUMT)" [10]*)

After the subframe configuration for PDSCH channel and TB data for all UEs are received by the PHY, the PHY layer processes the PDSCH for each UE scheduled in that subframe. Fig.5.12 shows the PDSCH processing chain details besides providing the adaptations for C-RAN / DAS. As shown in the figure, the major processing blocks in PDSCH processing are: Bit level processing, Constellation Mapper, Layer mapping and MIMO precoding, DAS Engine, and Resource Element (RE) Mapper and OFDM signal generation.

As shown in Fig.5.13, Bit level processing starts with Cyclic Redudancy Check (CRC) calculation of the TB and then the CRC is attached to TB. Output of TB with CRC is segmented into a number of code blocks (CBs) of definite sizes as defined by 3GPP LTE [87]. Then, for each CB channel coding is applied using Turbo codes. The rate macther module matches the number of bits in TB to the number of Resource Elements (RE) scheduled for the TB. There are 12 REs

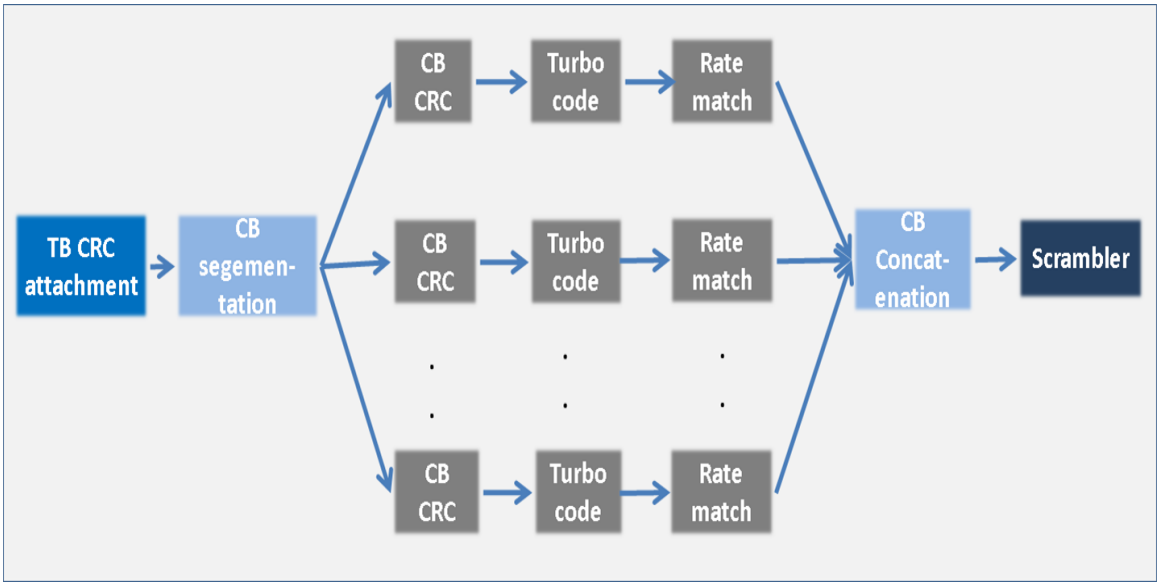

Fig. 5.13: PDSCH bit level processing

in 1 RB. Each of the channel coded CB is rate-matched, and the outputs of all the rate-matched CBs are concatenated back. The output of the CB concatenation module is scrambled to prevent from burst errors.

The scrambled data is passed through the Constellation Mapper module as shown in Fig.5.12, which maps the bits to constellation points depending on the modulation such as: QPSK, 16 QAM and 64 QAM. The constellation points are mapped to different layers depending on the transmission mode, which is single-input-single-output (SISO), Transmission diversity or space-frequency block coding (SFBC) and multiple-input-multiple-output (MIMO). The MIMO or SFBC precoding is done over the layers.

As shown in Fig.5.12, the PHY processing threads perform the PDSCH processing from TB until MIMO precoding for all UEs. In the standard LTE system, all the UEs are scheduled onto different non overlapping RBs. Hence in a standard LTE system, the MIMO precoded constellation points from all the UEs can be mapped symbol wise onto the same buffer, because of the non-overlapping RB allocation in LTE. This non-overlapping RB allocation PDSCH data in case of 2 UEs, UE1 and UE2, is shown in Fig.5.11.

DAS Engine

In the C-RAN / DAS the major modification required is the scheduling of overlapping RB allocation, in order to achieve frequency reuse at RB level among different (UE, RRH) pairs. In this regard, a new software module called, DAS Engine, is designed and implemented. This module receives the data from the MIMO precoder for each UE and does the required processing and forwarded it into RE mapper for each RRH.

Mapper

In a standard LTE eNodeB, there is one mapper module that maps all the control channels and data channel for each UE into the same time-frequency grid, as shown in Fig.5.11. This one time-frequency grid, is implemented as single buffer for each layer in the LTE eNodeB.

In oder to accomodate the overlapping RB allocation and to send different time-frequency grids to different RRHs, the mapper implementation is modified such that the the time-frequency mapping is done separately for each RRH. This modification is one of the major adaptations for C-RAN / DAS.

5.2.3 Adaptations - LTE Procedures

This subsection is derived from author's published work, "Probability of coverage based analysis of distributed antenna system and its implementation on LTE based real-time-testbed", published in "2017 9th International Congress on Ultra Modern Telecommunications and Control Systems and Workshops (ICUMT)" [10] and COHERENT deliverable "D6.2 - Final Report on Technical Validation" [12]

According to the 3GPP LTE standard [88], the UE must perform certain procedures, like cell search, cell selection, decoding of system information, random access and UE attach procedure, before it can transmit and receive data. Here, a summary, of the analysis about deployment of C-RAN / DAS in a LTE System, in view of modification of LTE procedures such as: cell search, cell selection, random access and multi-user scheduling of resources, is presented.

Cell selection and attach procedure

In a typical LTE system, each cell is uniquely identified based on physical layer cell identity (cellID) number. The cellID is broadcasted by eNodeB to all the UEs in the coverage area using Primary Synchronization sequence (PSS) and Secondary Synchronization Sequence (SSS) channels in the downlink. A UE within the coverage area sets its Radio Frequency (RF) carrier frequency to various carrier frequencies determined by the operator allowed bands according to E-UTRA absolute radio frequency channel number (EARFCN) defined in [89, 90]. By scanning various allowed carrier frequecnies, UE tries at first to decode PSS channel. 3GPP LTE utilizes Zadoff-Chu sequences, which have excellent auto-correlation properties in frequency domain, are used to generate the PSS. After detection of the PSS signals, UE measures the received signal strength indicator (RSSI) of each cell, which are scanned. This procedure is called cell search procedure in LTE. After completion of cell search, the cell with the greatest RSSI value will be selected by the UE. The selection of the cell by the UE is called as camp on the cell, which is defined in LTE as cell selection procedure [88]. In C-RAN / DAS, because of multiple RRHs distributed but connected to the same eNodeB, each RRHs require unique identifiers. The RRH unique identifiers can be called as sub-cellIDs. Therefore, using the cell-search and selection procedures defined by 3GPP LTE, it is feasible to transmit different sub-cellIDs from different RRHs so that the cell selection procedure in a typical LTE cell can be applied for RRH selection.

RSSI based RRH pairing

Received signal strength indicator (RSSI), is defined in the 3GPP LTE standard [89] as the sum total signal power of each resource element (RE) including interference and noise. RE, which is spans 1 subcarrier in frequency and 1 OFDM symbol in time, is the smallest discrete part of the LTE frame. The cell selection procedure of LTE is based on RSSI values, which is a good metric of the observed SINR at the UE location w.r.t. different RRHs. RSSI can be applied for finding (UE,RRH) pairs. The cell attach procedures defined in 3GPP LTE - RRC protocol specification [91]. In C-RAN / DAS the UE attach procedures can be applied for RRH attach.

LTE based multi-user scheduling of resources in DAS

In multiple access systems, efficient scheduling of radio resources is the key to achieve the sum-rate improvement. The LTE system considered here is a Frequency Division Duplexing (FDD) system, where the uplink (UL) and downlink (DL) transmissions are in different frequencies separated by a duplexing distance. In mult-user LTE system, the scheduling of radio resources is done based on the resource block (RBs), which spans 180 KHz in frequency and 0.5 ms or 1 slot in time. A typical LTE sub-frame with normal cyclic prefix (CP) consists of 14 OFDM symbols or 1 ms in time and 50 RBs or 600 REs for 10 MHz bandwidth. Therefore, the 50 RBs are scheduled to multiple UEs based on many factors such as, channel quality indicator (CQI), modulation and coding scheme (MCS), quality of service (QOS) etc. In C-RAN / DAS after formulation of (UE,RRH) pairs, the frequency reuse options can be explored within the serving area based on the $reliability$ analysis presented in this thesis. After finding the frequency-reuse (UE,RRH) pairs, overlapping RB allocations within the serving area can be scheduled to the reuse (UE,RRH) pairs. This is one of the major adaptations required at the MAC layer so that overlapping RB allocations can be scheduled. This adaptation and the corresponding handling of this adaptation in PHY layer is as well implemented in the C-RAN / DAS real-time testbed.

5.3 Implementation and Validation

In this section, firstly, a brief description of the existing software implementation of LTE eNodeB and secondly, the implementation of the adaptations in LTE PHY DL processing chain in order to support C-RAN / DAS functionality, are presented. The details of the necessary adapations in LTE are described in Subsection 5.2.2.

The Fig.5.14 shows an overview of PHY DL processing architecture CU C-RAN / DAS. MAC-PHY interface is the communication interface between higher layers and PHY. The PHY sends every millisecond a subframe indication, to request the MAC to send subframe configuration and UE data. MAC sends the subframe configuration and data for all the UEs scheduled in that subframe. The subframe configuration message contains the payload and configuration for each of DL channel. This is done at every 1 millisecond boundary. The other interface is towards the AIF2, where OFDM symbol timing based interrupts are received from

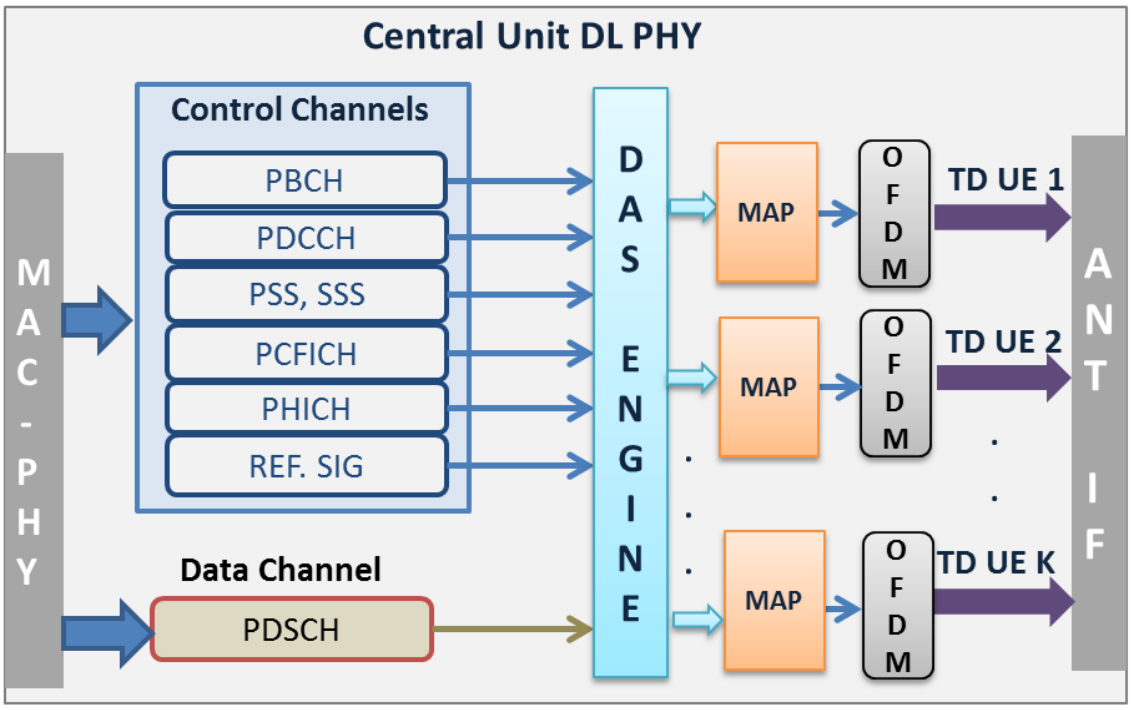

Fig. 5.14: Central Unit DL PHY processing Architecture

AIF2. The mapper then maps the data for the symbol and forwards it to IFFT module, which converts the frequency to time domain OFDM signal. The FFT Co-processor performs the IFFT and forwards it to the AIF2.

5.3.1 DAS Engine

In the C-RAN / DAS the major modification required is the scheduling of overlapping RB allocation, in order to achieve frequency reuse at RB level among different (UE, RRH) pairs. In this regard, a software module called *DAS Engine* is designed and implemented. As shown in Fig.5.15 shows the functional layout of *DAS Engine*. The input to this module are processed control and data channels of all the UEs, besides the common system information. The UE-wise inputs are: the processed control channels, which are PDCCH and PHICH, the output of MIMO precoder of the processed TBs. The system information are the general information for all the UEs, which comprises of PBCH, PSS, SSS, Reference Signals and PCFICH.

DAS Engine can perform different joint precodings between a set of RRHs for beamforming or multi-user MIMO functionalities. Therefore, the output of *DAS Engine* is rather RRH specific than UE specific as depicted in Fig.5.15. Because of memory and timing limitations of the

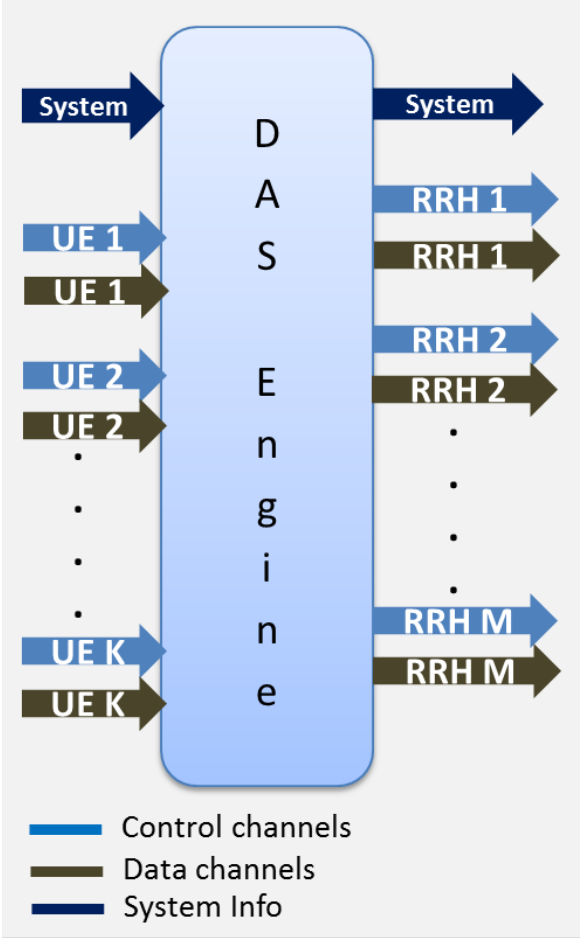

Fig. 5.15: DAS Engine Functional layout

existing LTE implementation, we have implemented the Pairing in Selection Transmission scheme of C-RAN / DAS. The Selection based Pairing scheme multiplexes data of different UEs with the RRHs, according to the Pairing methods used. In our implementation, we have implemented a fixed pairing method.

5.3.2 Mapper

In a standard LTE eNodeB, there is one mapper module that maps the control channels and data channel for each UE and the system information into the same time-frequency grid, as shown in Fig.5.11. In the time axis, we have the OFDM symbols, which are implemented to be 14. In the frequency axis, we have set of 1201 REs, for 20 MHz bandwidth or 100 RBs. This single time-frequency grid for each layer is implemented as single buffer for in a LTE eNodeB.

In C-RAN / DAS for each RRH, we have to implemented separate time-frequency grid in

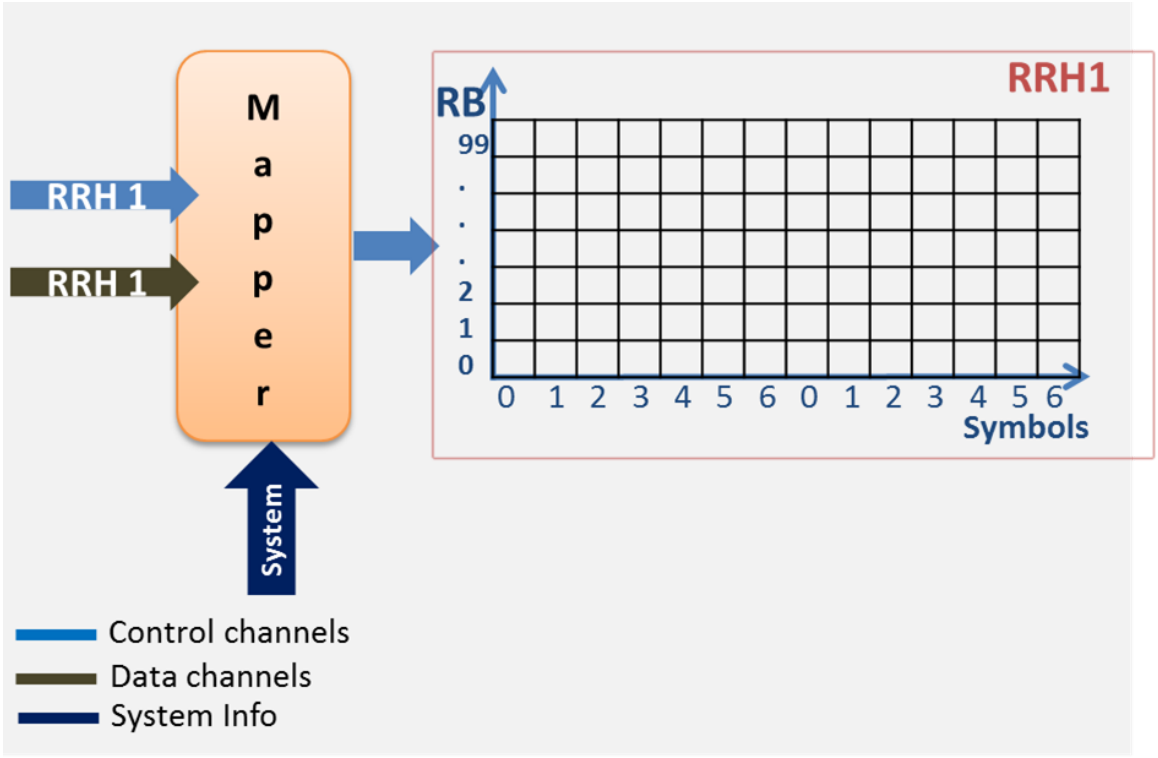

Fig. 5.16: Mapper Functional layout

order to facilitate flexible overlapping resource allocation among RRHs. As shown in Fig.5.16, the input to *Mapper* comes from the *DAS Engine*. The input to the mapper primarily consists of RRH specific, control and data channels, besides the system information. With this information, the mapper maps all the required data on to the subframe grid shown in the figure. In order to get this functionality, the existing LTE mapper implementation is modified such that the the time-frequency mapping is done separately for each RRH. This modification is one of the major adaptations for C-RAN / DAS, which involves a lot of memory allocation on the DSP and external memory in order to facilitate multiple RRHs. Hence, in this work CU is implemented to support only 2 RRHs to decrease the implementation time and to avoid real-time debugging issues. Concerning the huge memory requirement to support 2 RRHs, the complete memory layout of the existing LTE PHY implementation has been adapted completely, which consumed considerable amount of time to verify the whole LTE functionality after this adaptation.

5.3.3 AIF2

In subsection 5.1.2, we have described in detail the architecture and functional blocks of Antenna Interface2 module, which converts the baseband IQ signals from-and-to DSP to-and-from CPRI baseband signals in order to transmit and receive them to distributed RRHs. Because of the support of multiple RRHs, the AIF2 driver on the DSP is adapted to support the second CPRI link. The CPRI, LTE and AIF2 functional blocks are configured for the second CPRI link to support the second RRH. TI C6670 DSP consists of Antenna Interface Module (AIF2), which transmits and receives baseband IQ signal from and to the DSP and packs them into common public radio interface (CPRI) packets. The initial version of AIF2 driver was supporting a single RRH, in this work the driver has been extended to support the second RRH. This adaptation was tested very carefully, each block by block, until all the required configurations were set correctly and verified.

5.3.4 Validation

After implementing the modules described above, the individual components are verified using unit tests. After verification of the standalone modules, these modules are integrated into the existing DL threads. After integration, the existing LTE DL control framework, which is implemented on the TI's OS using software threads and finite state machines, has been carefully debugged and validated. The timing requirements from MAC and AIF2 are verified very carefully so that the real-time requirements of LTE symbol, subframe and radio frame boundaries are met. All safe debugging methods such as: Real-time tracing, memory overwrite protection and unit test based module by module verification, are employed to get the stable running CU eNodeB with 2 RRHs.

The *MAC Emulator* module is then configured with various LTE DL test cases, and the validation is achieved by testing the output of RRHs with a Keysight's MXA signal analyzer with 89600 VSA software. Long term stability tests are performed to ensure a stable LTE standard complaint real-time functionality.

5.4 Testbed and Measurement setup

The work presented in this section is derived from author's published work in "Reliability Analysis of Centralized Radio Access Networks in Non-Line-of-Sight and Line-of-Sight Scenarios" published in "IEEE Access", year 2019 [5] and COHERENT deliverables D3.1, D3.2, D6.1 and D6.2 [4, 11–13]

In this section, the details of the developed the C-RAN / DAS testbed along with LTE test configurations is presented. In addition, the measurement and validation methodology practices followed to validate some of *reliability* analysis proposed in this thesis is described.

5.4.1 Testbed

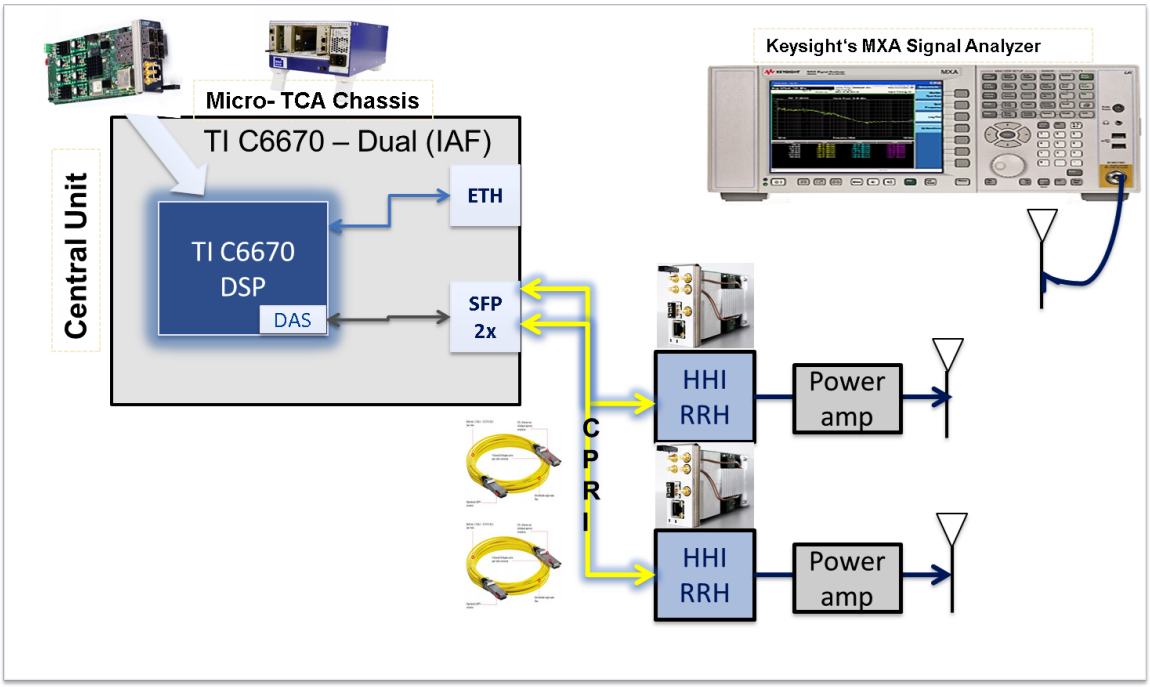

Fig. 5.17: LTE based DAS eNodeB setup with 2 RRHs [11]
(*This figure is copied from author's published work in COHERENT deliverable "D6.1 - Draft report on Technical Validation" [11]*)

Fig.5.17 shows the block diagram representation of the implemented C-RAN / DAS testbed. As described in Section 5.1, the central unit's PHY processing is ported on the TI C6670 DSP, which is located on a Dual C6670 AMC module. The Dual C6670 AMC module along with HHI's RF AMC module is hosted inside a Micro-TCA chassis. Fig.5.18 shows the Micro-TCA

chassis with the different AMC modules used in the implementation. The second HHI's RF module is also hosted in a second Micro-TCA chassis, which is set to move flexibly, in order to facilitate measurements. The CU PHY interfaces with the RF module using CPRI via optical cable. Fig.5.18 shows the all form-factor plugged (SFP) interface on the frontend of Dual C6670 AMC module, which provides the translation between optical and baseband signals and vice-versa. Each of the RF module is connected to a power amplifier (PA). The output of PA is connected to an antenna. On the receiver side, Keysight's MXA signal analyzer with 89600 VSA software is used to analyze the real-time LTE analysis of the downlink channels.

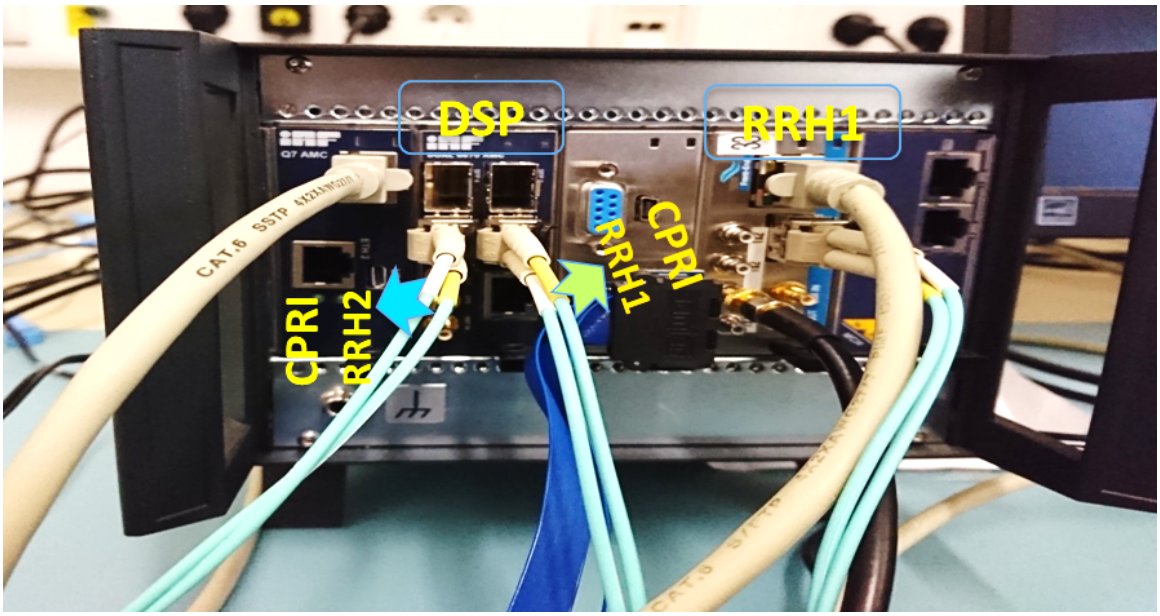

Fig. 5.18: Micro-TCA Chassis with AMC modules and interfaces [12]
(*This figure is copied from author's published work in COHERENT deliverable "D6.2 - Final report on Technical Validation" [12]*)

As detailed in section 5.1, the CU PHY processing is implemented on TI's C6670 DSP. The hardware components, which are described in Section 5.1, are hosted inside a micro-TCA chassis provided by IAF GmbH. In our design, the micro-TCA chassis is primarily used to supply power and cooling to the AMC modules. As shown in Fig.5.18, TI's DSP is located on one of the AMC boards on the left. The four SFP connectors on the frontend are also shown in the figure. Heinrich Heine Institute's, Berlin (HHI's) RRH board is the other AMC board, which is shown in the right-hand side of the Fig.5.18. As shown in the figure, the CPRI cables are the only interconnection between each SFP port and RF board. The two RF frontends are labeled as *RRH1* and *RRH2*. *RRH1* is located in the same Micro-TCA chassis as of CU, due to

the limitation in the available Micro-TCA chassis. In principle RRH1 can be located further away from the CU. It is as well shown in the figure, that the only interconnection between CU and each RRH is an optical cable.

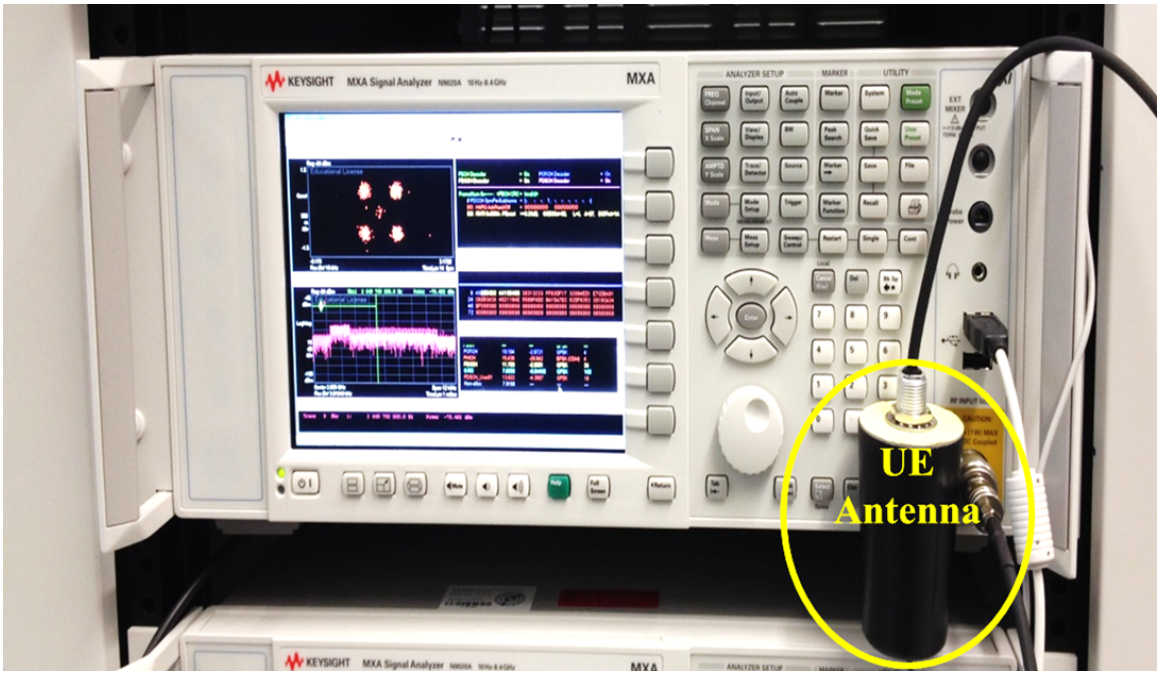

Fig. 5.19: Keysight's MXA Measurement equipment with 89600 VSA software [12]
(*This figure is extracted from author's published work in COHERENT deliverable "D6.2 - Final report on Technical Validation" [12]*)

Fig.5.19 shows the Keysight's N9020A MXA signal analyzer [92], along with 89600 vector signal analyzer (VSA) software for LTE PHY layer analysis. The VSA software provides in-depth analysis of decoding, system performance and quality of all the LTE DL and UL channels. The signal analyzer receives the signals from the RRHs and down-coverts the RF signal in DL to baseband IQ signal. The VSA software then analyses the IQ baseband signal and gives the details of all the decoded channels, the performance and quality of the decoded channels. Hence, the VSA software along with the signal analyzer can reliably validate the real-time stability of the CU implementation, as well as provide in-depth analysis of the quality of the decoded signals with reference to LTE compliance requirements [14].

5.4.2 Measurement setup

Fig.5.20 shows the lab setup of C-RAN / CU, where one of the Micro-TCA chassis hosts the central unit (CU) and *RRH1*. The second RRH, *RRH2*, is hosted by the second Micro-TCA

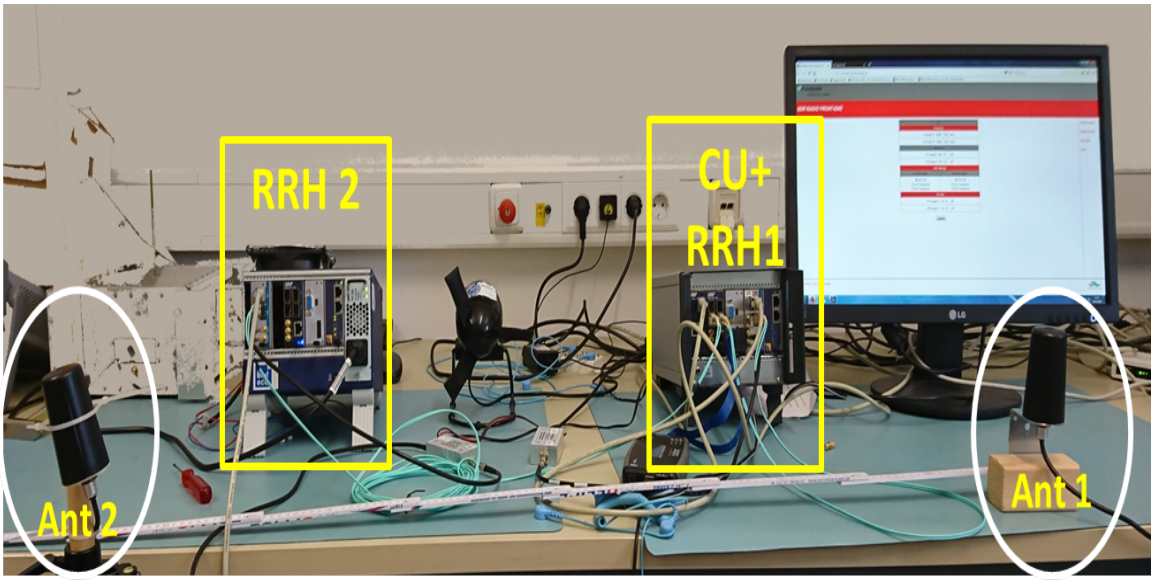

Fig. 5.20: LTE based C-RAN / DAS Central Unit with 2 RRHs [12]
(*This figure is extracted from author's published work in COHERENT deliverable "D6.2 - Final report on Technical Validation" [12]*)

chassis. It is also shown that long CPRI cables are interconnected the RRHs with the CU. *Ant1* and *Ant2* are connected to the output of respective PAs, which are connected to the RRHs.

Fig.5.21 shows the indoor lab environment, where the trials are performed. Also in this Figure, a pictorial representation rays emitted by the RRHs in the DL towards the UEs is shown. It also depicts the unwanted or interfering signals at the *UE1* originating from the non-serving *RRH2* because of the rays traveling in all directions due to omni-directional antennas used.

5.5 Measurement Scenarios and Results

The presented work in this section, including the figures and tables, is derived from author's self-published work in Section 8 "Distributed Antenna System - Evaluation Results" in COHERENT deliverable [12]

In this section, a detailed description of our measurement trials, the LTE configuration details of the test scenarios, validation methodology and results are presented. The main measurement methodology in this work is primarily targeted to understand the effects on the performance of C-RAN / DAS due to, variation of the distance between the RRHs, position of RRHs and variation of power levels of RRHs. In order to achieve validation of the theoretical investigations using commercial LTE tester with real-time test-bed, various measurements have been done

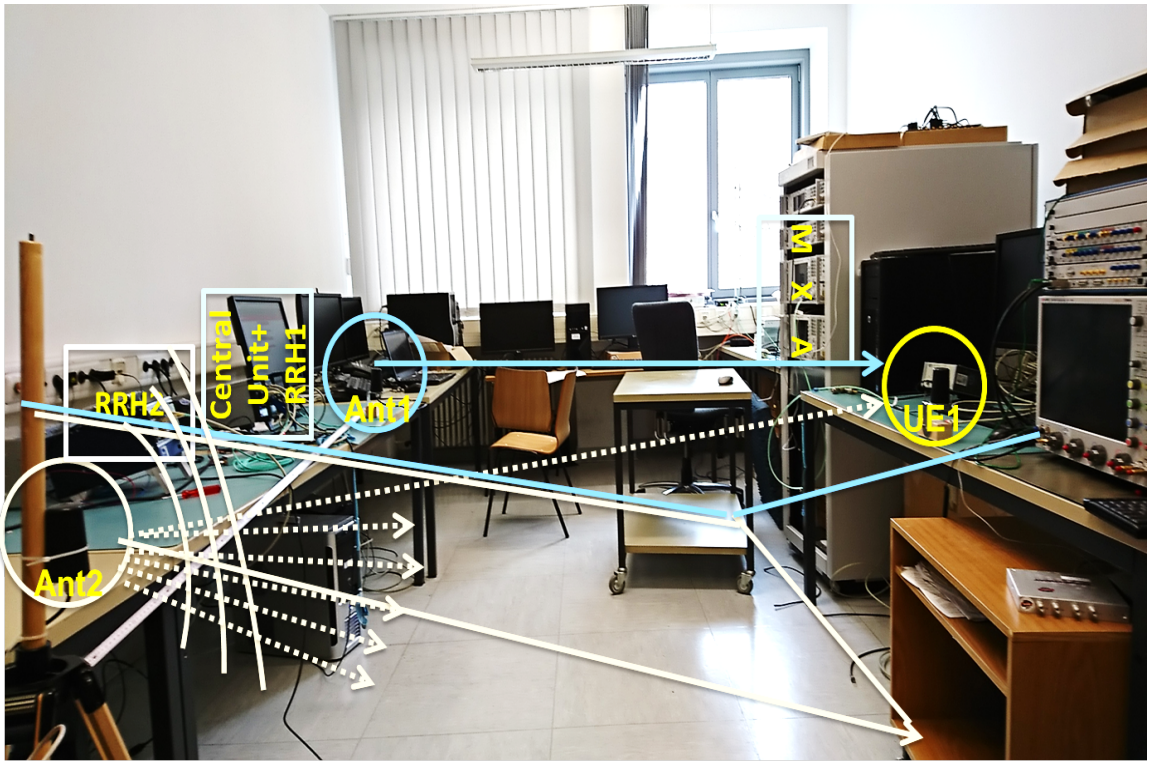

Fig. 5.21: Indoor lab layout. Pictorial representation of signals transmitted from RRH1 and RRH2 [12]
(*This figure is copied from author's published work in COHERENT deliverable "D6.2 - Final report on Technical Validation" [12]*)

focusing on attaining reliable throughput and performance by rapid frequency reuse at different UE locations of a C-RAN / DAS based on *reliability*. As *reliability*, which is derived in Chapter 2, depends on the RRH and UE locations, power being transmitted by RRHs and SINR requirements at UE locations, the validation is accomplished by performing various measurements varying these parameters. Furthermore, these measurements are intended to understand the effect of these parameters on the PHY layer performance in C-RAN / DAS.

Table 5.1 provides the LTE parameters configured on the MAC Emulator for our trials at the CU. In order to emulate the worst case deployment scenario, both the UEs are configured with the same full allocation of 50 RBs, which implies overlapping RB allocation. The performance of the received signal quality for DL channels is measured by Keysight's MXA signal analyzer in terms of error vector magnitude (EVM).

The Error Vector Magnitude is defined in LTE Table 6.5.2.5-1 [14], as a measure of the difference between the reference or ideal modulated constellation points and the equalized

Table 5.1: LTE configuration parameters [12]

(*This table is extracted from author's published work in COHERENT deliverable "D6.2 - Final report on Technical Validation" [12]*)

Parameters	**Values**
Carrier frequency DL	2.655 GHz
Channel Bandwidth DL	10 MHz / 50 RBs
No. of UEs	2
No. of RRHs	2
No. of antennas per RRH	1 (SISO)
No. of RBs scheduled in DL for $UE1$	50 RBs / all RBs
No. of RBs scheduled in DL for $UE2$	50 RBs / all RBs
MCS configured	9 (QPSK), 11 (16 QAM)
Max. Tx. Power RRH1	-8 dBm
Max. Tx. Power RRH2	-8 dBm
RNTI of UE1	10
RNTI of UE2	20
FSPL at 1m	41 dB
FSPL at 2m	47 dB
FSPL at 3m	50 dB

modulation constellation points of the received signal, which is called as error vector. The percentage RMS of the EVM is calculated as the square root of the ratio of the mean error vector power to the mean reference (ideal constellation points) power, which is expressed as a percentage. As given in Table 5.2, the minimum required EVM for different modulation schemes: QPSK is 18.5%, 16 QAM is 13.5% and 64QAM is 9%. Since SINR (dB) = -20log10(EVM), these EVM requirements correspond to 14.6 dB, 17.4dB and 20.9 dB for QPSK, 16 QAM and 64 QAM modulation schemes respectively.

In the following subsections, an overview, of the measurement scenarios investigated in this work, in addition to their practical importance in C-RAN / DAS, is presented. Also, a description of the measurement methodology in each scenario and the discussion of measured results is presented. Here, the measurement results of the performed trials in 4 scenarios, as well as the practical view of these scenarios, is presented.

In each of our trials, at first, the performance, transmit powers and received power levels of

Table 5.2: 3GPP LTE EVM Requirements [14]

(*This table is extracted from 3GPP LTE specification "E-UTRA; Base Station (BS)conformance testing (3GPP TS 36.141 v. 9.8.0)" [14]*)

Modulation scheme	**min. EVM in (%)**	**min. SINR in dB**
QPSK	18.5	14.6
16 QAM	13.5	17.4
64QAM	9	20.9

each RRH is validated and confirmed with the commercial LTE test equipment before performing different trials. In this regard, the received power from each RRH is measured independently, i.e. one at a time, to make sure that the pathloss according to FSPL is matched. Table 5.1 gives the Free Space Path Loss (FSPL) values for the distances measured. After the validation, based on FSPL values and EVM requirements, the right TX attenuation values to be set at each RRH are determined and fixed, in order to ensure the same transmit power at each RRHs. After this step, the variation of SINR at the UE location is achieved by adding additional TX attenuation at RRHs using the GUI provided by HHI as shown in Fig.5.10.

After making sure of equal transmit power levels at each RRHs, the SINR level at the $UE1$ is varied by attenuating the power level of $RRH2$. The location and power of $RRH1$ is mostly fixed in all our investigations. $RRH2$'s power and position, in addition to $UE1$ position, are varied in our trials.

In the next subsection, a brief overview of the measurements accomplished in various trials in 4 practical scenarios is described. Scenario 1 and Scenario 2 represent scenarios in C-RAN / DAS, where the UEs are quite close to the distributed RRHs. In these scenarios, the impact of the variation of RRH placement and RRH transmit power on system performance is studied. Scenario 3 and Scenario 4 depict the worst case scenario in DAS, where a UE is located equidistant to RRHs so that the UE may suffer from extremely high interference. In these scenarios, the variation of transmitted power of RRHs and its effect on frequency reuse and EVM measurements is measured and the results are presented.

In the next subsections, the measurement results and the analysis of these scenarios is presented. Furthermore, in these scenarios, a fair comparison between the simulation results based on *reliability* and EVM based measurement results is made.

5.5.1 Measurement Scenario 1

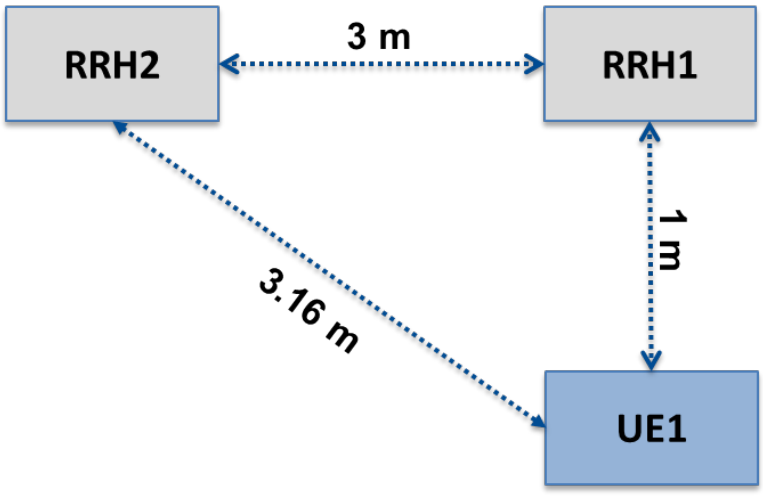

Fig. 5.22: RRHs and UE positions in Measurement scenario 1 [12]
(*This figure is extracted from author's published work in COHERENT deliverable "D6.2 - Final report on Technical Validation" [12]*)

Table 5.3: Scenario 1: CRC and EVM measurement results [12]

(*This table is extracted from author's published work in COHERENT deliverable "D6.2 - Final report on Technical Validation" [12]*)

SINR (dB)	CRC	EVM meas. (%)	Min. EVM Req.
14	Pass	49.3	18.6
17	Pass	26.8	18.6
20	Pass	20.4	18.6
23	Pass	14.5	18.6
26	Pass	11.7	18.6
29	Pass	8.4	18.6
32	Pass	5.9	18.6
35	Pass	3.9	18.6
38	Pass	3.4	18.6
41	Pass	1.6	18.6

In the scenario 1, as shown in Fig.5.22, both the RRHs are separated by 3 m, while $UE1$, which is actually the Keysight's MXA, is positioned at a distance of 1 m directly facing its serving RRH, *RRH1*. With these positions fixed, in each of the trials, the TX attenuation at $RRH2$ is modified in 3 dB steps in order to achieve variation of SINR level at $UE1$ location. In

this scenario, Table 5.3 provides the EVM and CRC values observed in each of the trials. The screen shots of EVM values of various decoded DL channels together with constellation plots observed on commercial LTE test equipment in each trial are captured and stored for analysis.

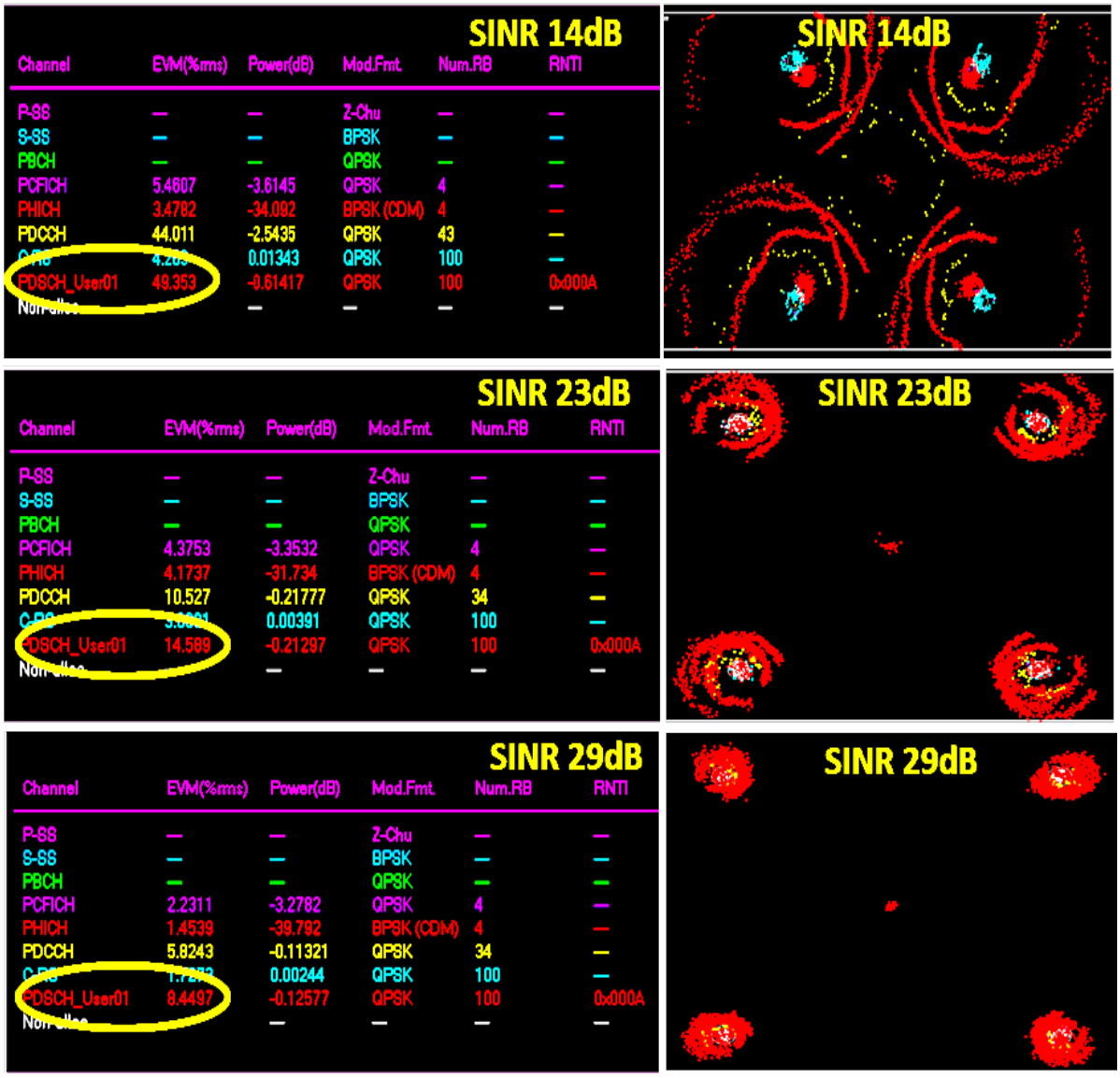

Fig. 5.23: Scenario 1: EVM measurements and constellation diagrams [12]
(*This figure is extracted from author's published work in COHERENT deliverable "D6.2 - Final report on Technical Validation" [12]*)

Fig.5.23 shows some of the captured snapshots from the commercial LTE test equipment. In each snapshot, the DL decode information, EVM values of each DL channel and constellation diagram is given by the VSA software running on the commercial LTE test equipment. The snapshots in the figure shows the measurement results for some of the SINR values achieved in the trials. The constellation plots show the effect of interference on the QPSK constellation at

low SINR values and how the constellation points gets better aligned with the increase in SINR.

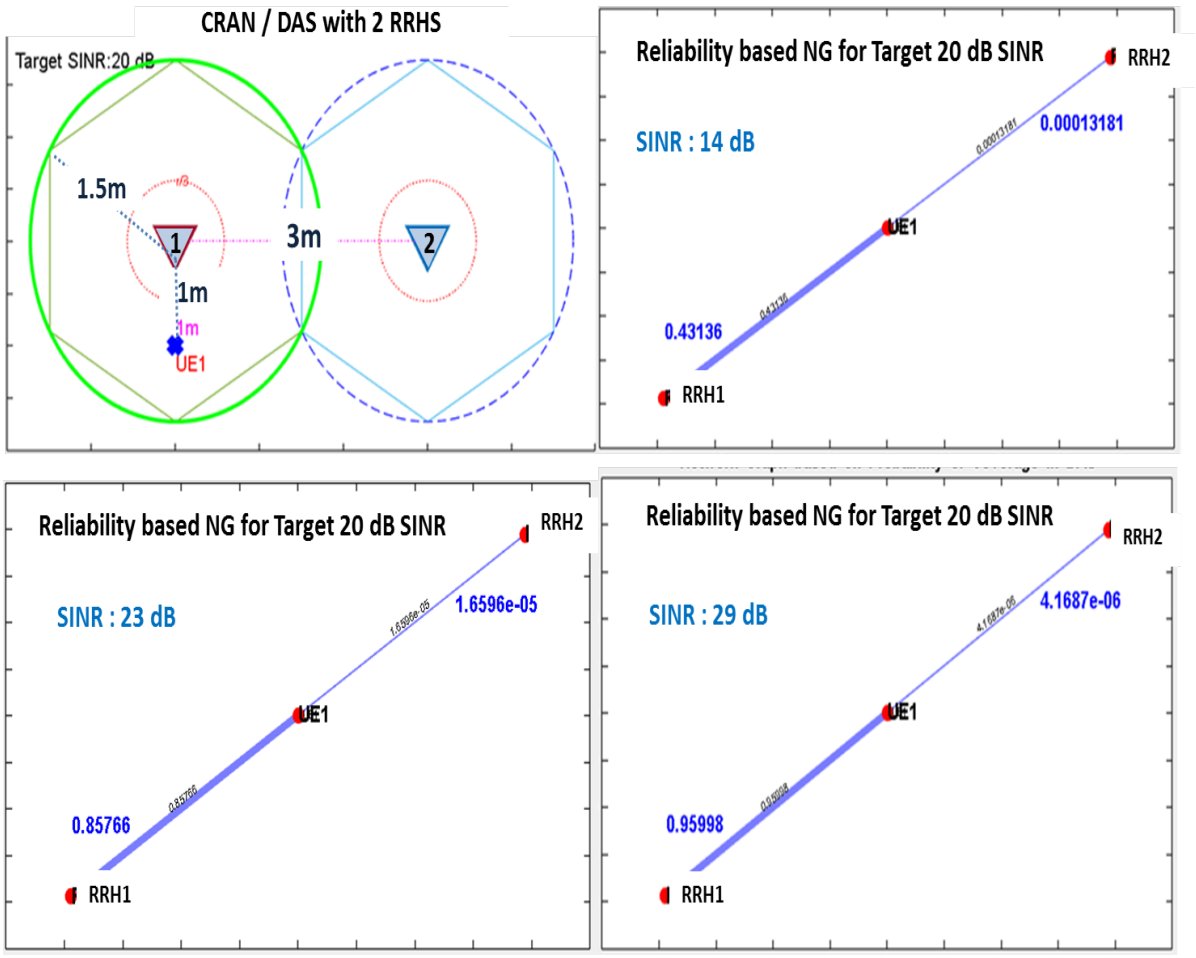

Fig. 5.24: Scenario 1: NG showing Reliability for 20 dB SINR at UE position with varying SINR level experienced at UE location [12]
(*This figure is extracted from author's published work in COHERENT deliverable "D6.2 - Final report on Technical Validation" [12]*)

It is interesting to note that, although the measured EVM values are very bad at SINR levels below 20 dB, the cyclic redundancy check (CRC) check of the sent Transport Block (TB) of PDSCH is passed, which represents correct decoding of PDSCH. This is primarily because of the channel coding techniques or Forward Error Correction (FEC) techniques such as, channel coding, channel interleaving and scrambling techniques performed in the PDSCH processing chain. However, in these cases, the EVM results are not conformed to the LTE EVM requirements for QPSK, which limits the EVM results of QPSK modulation to be below 18.6%. From these trials, the minimum required SINR level to meet the LTE requirements for QPSK in this scenario is observed to be 23 dB.

Fig.5.24 shows the Network Graphs generated using the $reliability$ metric implemented for this scenario on MATLAB. In this figure it is shown that the NGs are formulated targeting a minimum required SINR level of 20 dB. To make a fair comparison with the measured EVM results, the same cases of SINR levels as shown from the snapshots of EVM measurement, i.e. Fig.5.23 are simulated.

In case of minimum SINR level of 23 dB, which is determined from the LTE conformance requirements, it is shown in Fig.5.24 that the $reliability$ at the $UE1$ location is simulated to be around 0.85, which is adequate for making a decision for pairing of $UE1$ with $RRH1$. For SINR of 30 dB the $reliability$ is around 0.95. Therefore, in all the trials done in this scenario, the simulation results and measurement results almost map linearly to one another.

5.5.2 Measurement Scenario 2

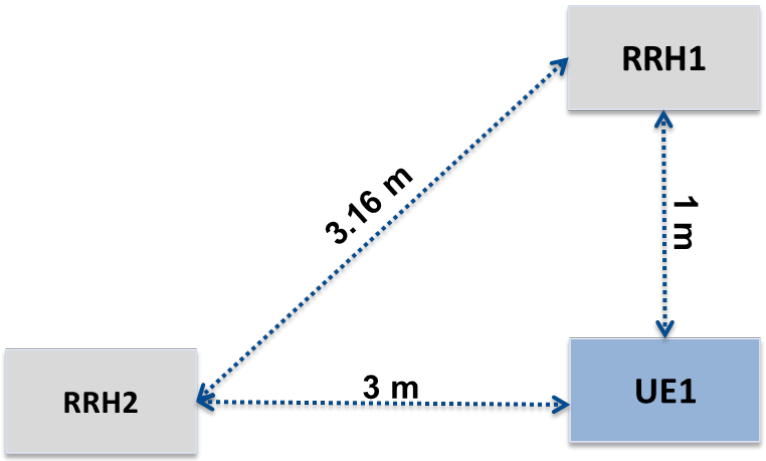

Fig. 5.25: RRHs and UE postions in Measurement scenario 2 [12]
(*This figure is extracted from author's published work in COHERENT deliverable "D6.2 - Final report on Technical Validation" [12]*)

In the scenario 2, which is shown in Fig.5.25, *RRH2* is set to a position, which is 3 m directly opposite to *UE1*. Hence the separation distance between RRHs is around 3.16 m. Compared to scenario 1, in this scenario, the placement of $RRH2$ is varied and its effect on EVM results at $UE1$ is observed.

After performing different trials based on the methodology described in subsection 5.5.1, the observed EVM values are tabulated in Table 5.4. Fig.5.26 shows VSA measurement snapshots of DL decode info, EVM and constellation diagram for different SINR values in this scenario. In

Table 5.4: Scenario 2: CRC and EVM measurement results [12]

(*This table is extracted from author's published work in COHERENT deliverable "D6.2 - Final report on Technical Validation" [12]*)

SINR (dB)	**CRC**	**EVM meas. (%)**	**Min. EVM Req.**
10	Pass	42.6	18.6
13	Pass	23.5	18.6
16	Pass	17.8	18.6
19	Pass	12.8	18.6
22	Pass	10.1	18.6
25	Pass	7.7	18.6
28	Pass	3.5	18.6
31	Pass	2.3	18.6

this scenario, from the observed EVM values, the minimum required SINR at the UE location to meet the LTE requirements for QPSK is around 16 dB.

Even though the interference power in this scenario logically should be higher, the observed interference power at $UE1$ is lower to that of scenario 1, which is mainly because of the indoor lab environment. This is because of the obstruction to LOS from $RRH2$ to $UE1$, the intensity of LOS component of interference is lower in this scenario compared to scenario 1, which has helped to improve the system performance at lower SINR value. In this case, the indoor lab channel has effected positively on the received interference power from $RRH1$.

Fig.5.27 shows the Network Graphs generated using the $reliability$ implemented on MATLAB for this scenario. We can see from this theoretical simulation results that for the SINR of 16 dB the $reliability$ at the $UE1$ location is around 0.78, which is high enough for making a decision for pairing of UE with $RRH1$. For SINR of 31 dB the $reliability$ is around 0.99. These results maps almost linearly to the EVM results in Table 5.4.

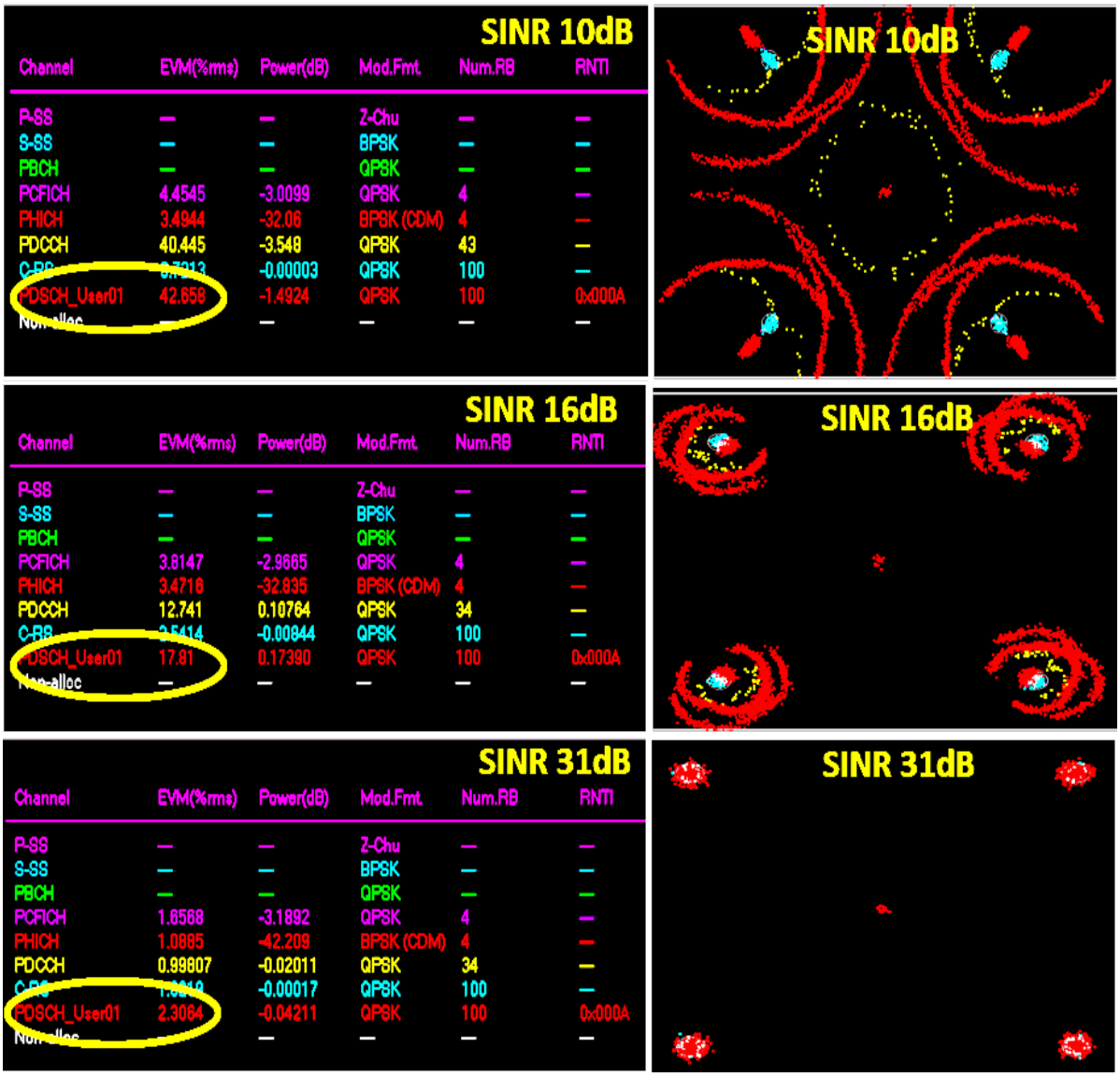

Fig. 5.26: scenario 2: EVM measurements and constellation diagrams [12]
(*This figure is extracted from author's published work in COHERENT deliverable "D6.2 - Final report on Technical Validation" [12]*)

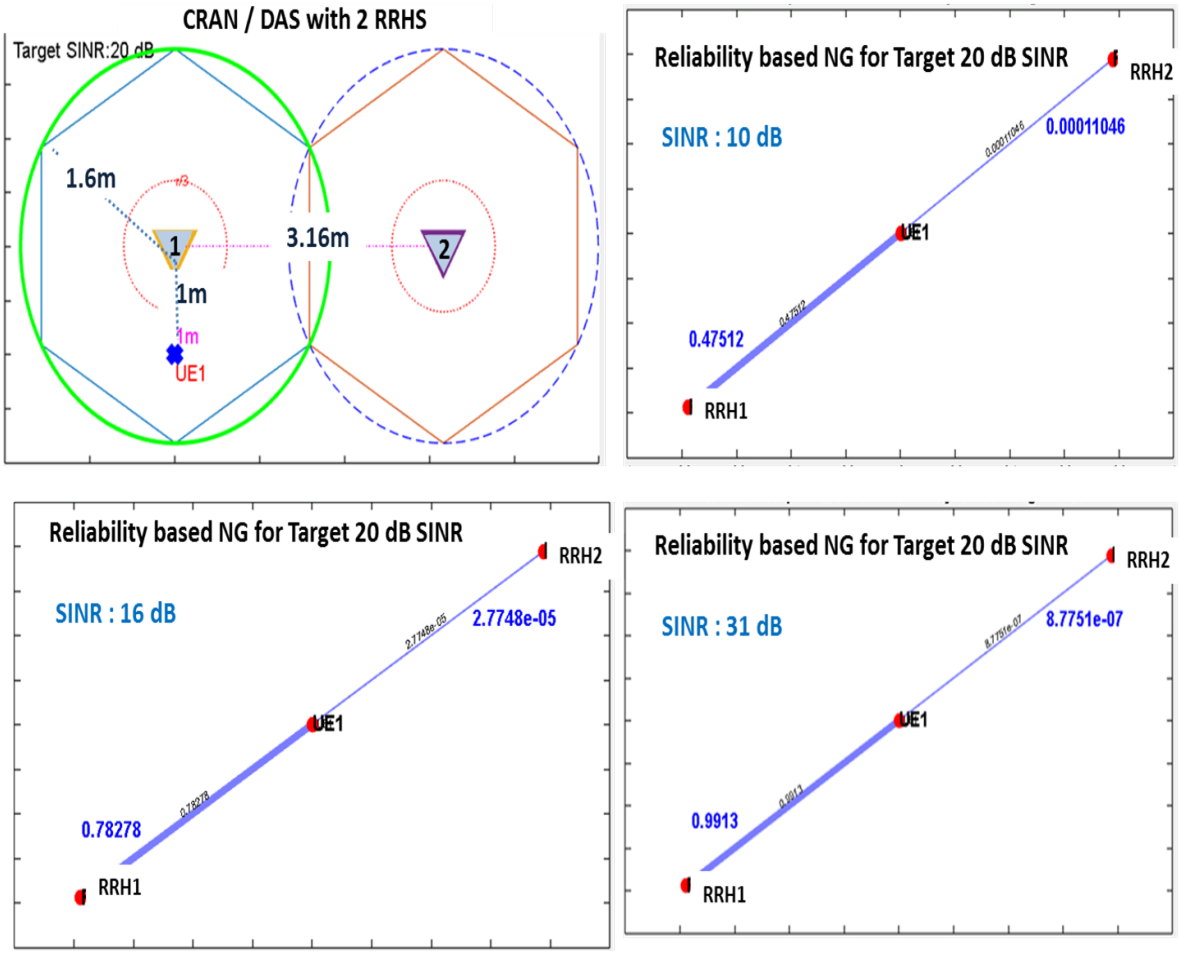

Fig. 5.27: Scenario 2: NG showing Reliability for 20 dB SINR at UE position with varying SINR level experienced at UE location [12]
(*This figure is extracted from author's published work in COHERENT deliverable "D6.2 - Final report on Technical Validation" [12]*)

5.5.3 Measurement Scenario 3

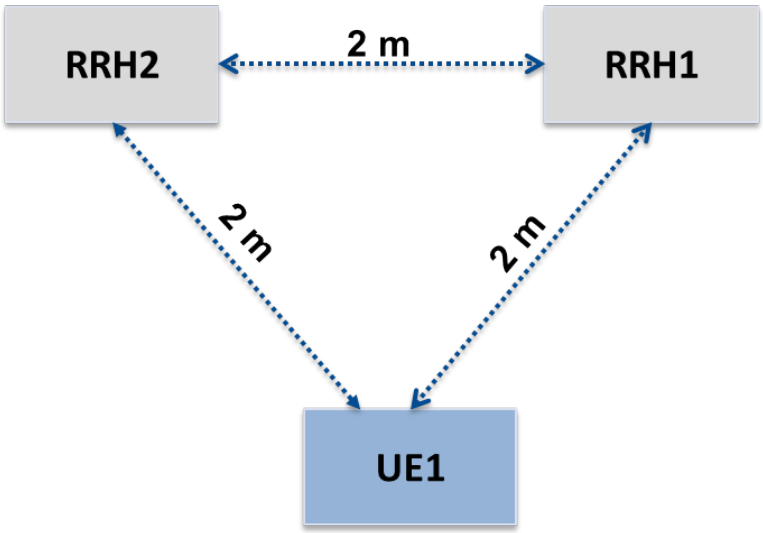

Fig. 5.28: RRHs and UE positions in Measurement scenarios 3 and 4 [12]
(*This figure is extracted from author's published work in COHERENT deliverable "D6.2 - Final report on Technical Validation" [12]*)

Table 5.5: Scenario 3: CRC and EVM measurement results [12]

(*This table is extracted from author's published work in COHERENT deliverable "D6.2 - Final report on Technical Validation" [12]*)

SINR (dB)	CRC	EVM meas. (%)	Min. EVM Req.
0	Fail	NA	18.6
3	Fail	NA	18.6
6	Fail	NA	18.6
9	Pass	41.7	18.6
12	Pass	31.8	18.6
15	Pass	21.3	18.6
18	Pass	16	18.6
21	Pass	11.7	18.6
24	Pass	8.1	18.6
27	Pass	6.5	18.6
30	Pass	5.4	18.6

Fig.5.28 shows the measurement scenario where the two RRHs are 2 m apart. The two RRHs are positioned equidistant to the UE, which is the LTE measurement equipment. This implies that both the RRHs are 2 m apart from each other and equidistant to UE. As mentioned

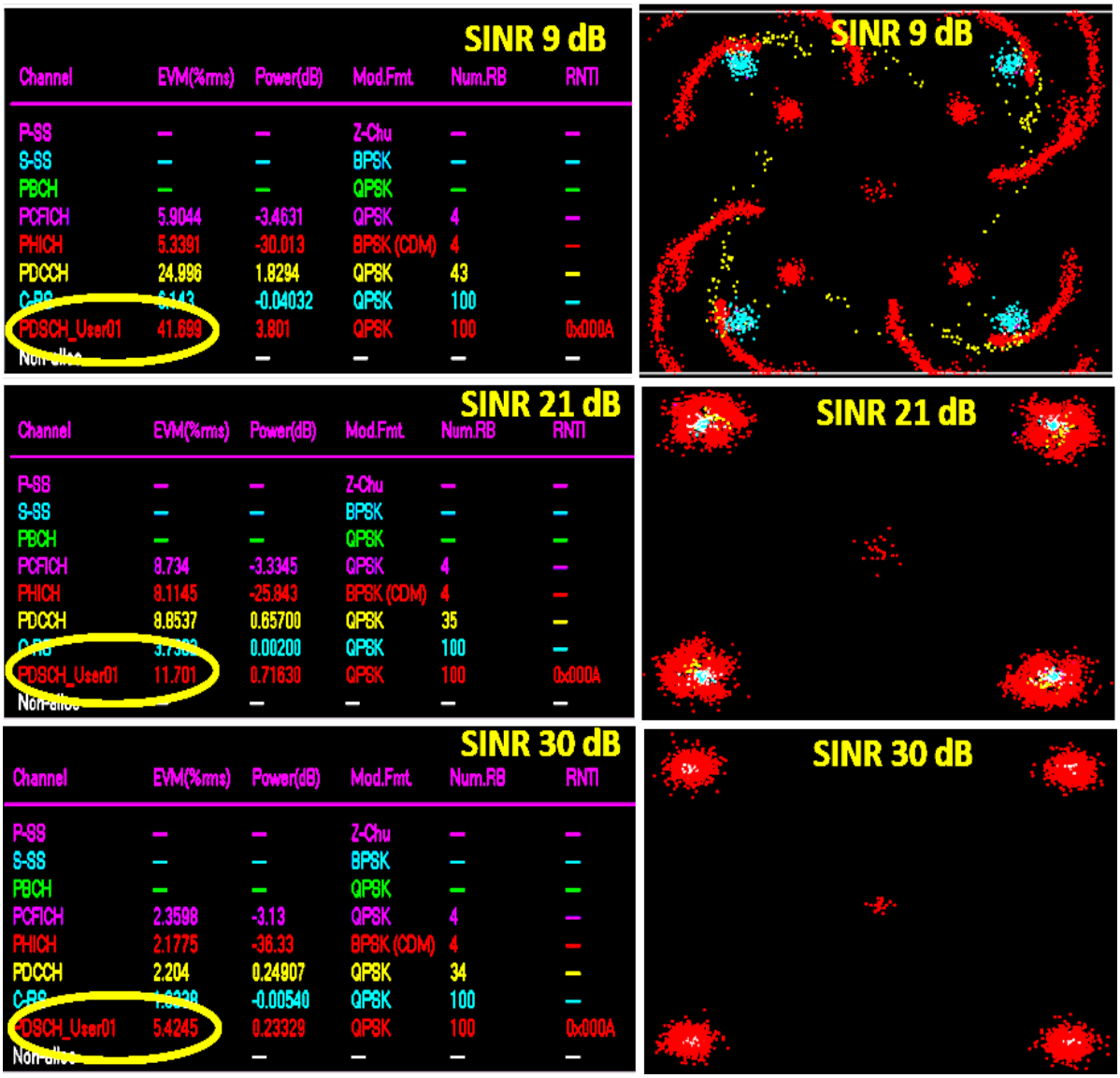

Fig. 5.29: Scenario 3: EVM measurements and constellation diagrams [12]
(*This figure is extracted from author's published work in COHERENT deliverable "D6.2 - Final report on Technical Validation" [12]*)

in the other scenarios, the transmit power level of *RRH1* is kept constant and the transmit power level of *RRH2* is varied in order to vary the SINR at UE location. This scenario can be classified as the classical cell-edge UE problem. In these scenarios, the received power from the serving / paired RRH, which is $RRH1$, and the received interference power from the neighboring RRH, which is $RRH2$, are equal. Hence, this case is the worst case scenario of frequency reuse application.

Here in scenario 3, the QPSK modulation is configured in the MAC Emulator of the testbed,

with the Modulation and Coding Scheme (MCS) values mentioned in Table 5.1. The MCS values and TB sizes are give in 3GPP LTE specification [50]. The measured EVM results of all the channels including PDSCH and the constellation diagram is shown in Fig.5.29.

From the measurement results presented in Table 5.5, we can see that the CRC check fails for SINR levels less than 9 dB. These results show the effect of very high interference on the UE. Trials with SINR level $\geq$ 9 dB, the CRC check passed but the EVM requirements are not met. Hence the measured SINR levels should be above 18 dB to meet the LTE requirement for QPSK modulation scheme in this scenario.

5.5.4 Measurement Scenario 4

Table 5.6: Scenario 4: CRC and EVM measurement results [12]

(*This table is extracted from author's published work in COHERENT deliverable "D6.2 - Final report on Technical Validation" [12]*)

SINR (dB)	**CRC**	**EVM meas. (%)**	**Min. EVM Req.**
0	Fail	NA	13.5
3	Fail	NA	13.5
6	Fail	NA	13.5
9	Fail	NA	13.5
12	Pass	36.8	13.5
15	Pass	27.6	13.5
18	Pass	19.6	13.5
21	Pass	13.5	13.5
24	Pass	9.5	13.5
27	Pass	7.5	13.5
30	Pass	5.4	13.5

Similarly the measurement trails are done in the scenario shown in Fig.5.28 for 16 QAM modulation scheme. The LTE subframe configuration has been set with MCS of 11, according to Table 5.1. By following the same methodology as described in scenario 3, the observed EVM results in case of 16 QAM is tabulated in Table 5.6. The observed screenshots of the measurement equipment for some SINR levels are shown in Fig.5.30. The minimum required SINR in this scenario, in order to meet the LTE EVM requirement for 16 QAM, which is less

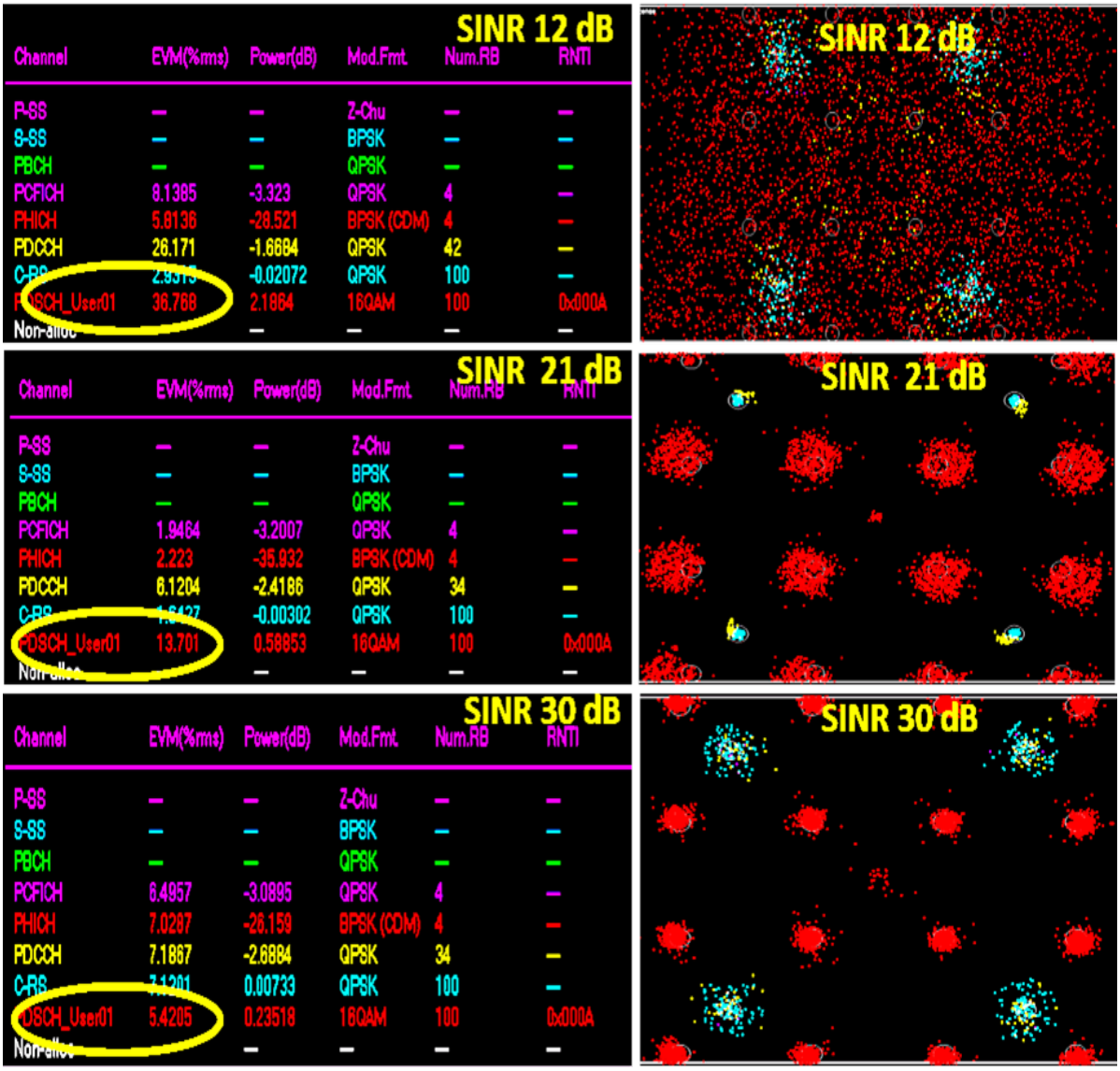

Fig. 5.30: scenario 4: EVM measurements and constellation diagrams [12]
(*This figure is extracted from author's published work in COHERENT deliverable "D6.2 - Final report on Technical Validation" [12]*)

than 13.5%, is observed to be 21 dB.

Fig.5.31 shows the Network Graphs generated using the $reliability$ implemented on MATLAB in scenarios 3 and 4. The necessary parameters for the MATLAB based GUI for the scenarios 3 and 4 were given to generate the network graphs. From these theoretical network graph abstractions, for the targeted SINR of 21 dB the $reliability$ at the $UE1$ location is should be 0.8 theoretically. The $reliability$ of 0.8 is high enough for making a decision for the pairing of $UE1$ with $RRH1$. For SINR of 30 dB the $reliability$ is around 0.97. It is observed that, these

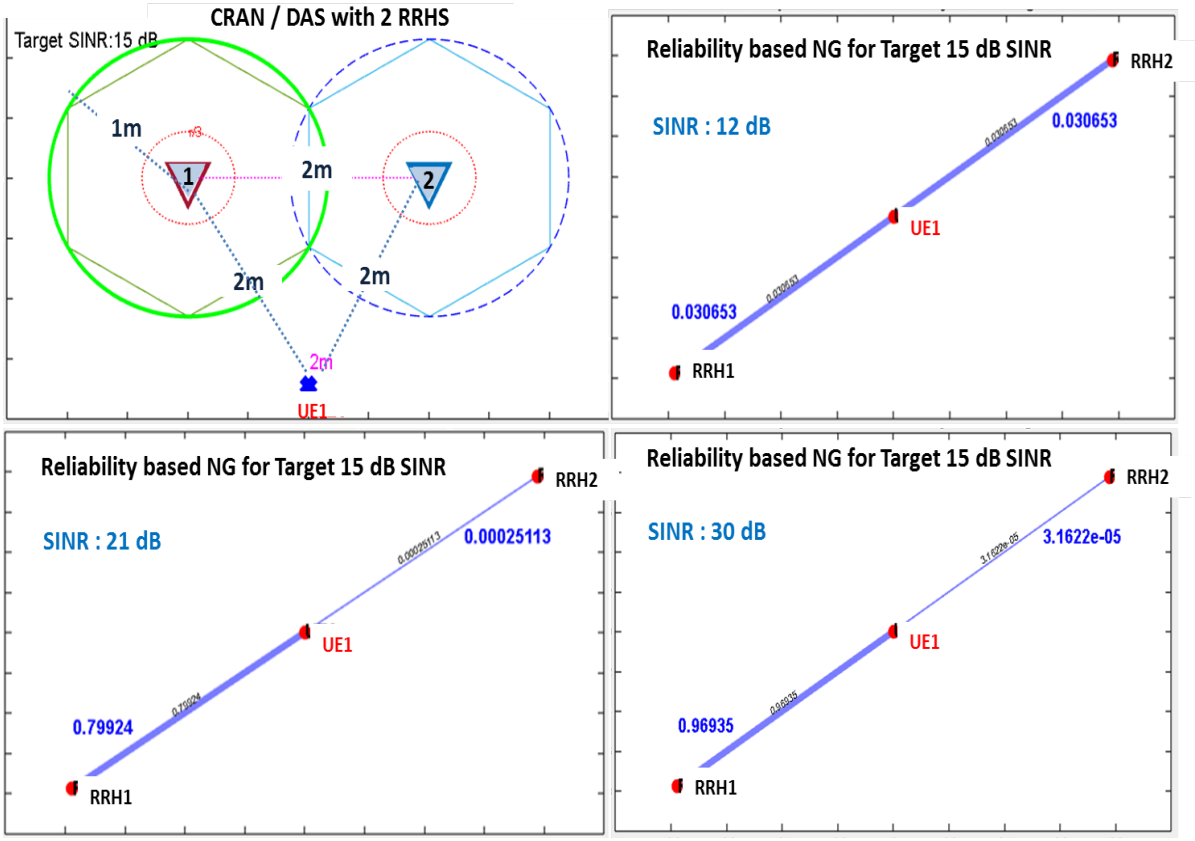

Fig. 5.31: Scenarios 3 and 4: NG showing Reliability for 15 dB SINR at UE position with varying SINR level experienced at UE location [12]
(*This figure is extracted from author's published work in COHERENT deliverable "D6.2 - Final report on Technical Validation" [12]*)

theoretical results of Network Graph map almost linearly to the measurement results in Table 5.5 and Table 5.6. Since the $reliability$ depends not directly on the modulation scheme but on the targeted SINR and channel model, the theoretical value of $reliability$ is the same for scenario 3 and scenario 4. Nevertheless, the modulation scheme is dependent on the targeted SINR which is derived from Bit Error Rate (BER) and EVM requirements for the modulation scheme.

Hence in all the scenarios, measurement results correspond very much to the mathematically derived SINR based $reliability$ presented in this thesis. Therefore by measuring EVM using standard LTE measurement device, we can validate the SINR based $reliability$ derived in this thesis.

5.6 Conclusion

In this chapter, the system design, LTE adaptations, implementation and validation, and measurement results of a real-time C-RAN / DAS testbed is presented. The real-time testbed is designed and implemented on a DSP based SDR platform. After implementing the necessary DAS adapatations within the LTE processing blocks, the testbed has been successfully validated with Keysight's commercial LTE tester. The goal of the work presented in this chapter is firstly, to design and implement the real-time LTE based DAS testbed and secondly, to validate the $reliability$ based analysis presented in this thesis. In this regard, different scenarios for the trials have been conceptualized and observed. In these scenarios, RRHs and UE postions, transmit powers and modulation schemes were varied in overlapping RB allocation for 2 UEs. The measurement results were observed on Keysight's VSA software running on Keysight MXA N9020A signal analyzer. The $reliability$ derived in this thesis is validated by 3GPP LTE defined metric called Error vector magnitudes (EVM). The EVM measurements are calculated and displayed on Keysight's 89600 VSA software. The maximum EVM values for each modulation is set by 3GPP for LTE conformance testing, which provides the minimum required SINR values for each modulation scheme. The description and measurement results for each scenario were described in detail. From the analysis of CRC and EVM measurement results in different scenarios, it is observed that most of the measurement results map nearly linear to the theoretical $reliability$ based simulation results. This nearly linear mapping provides the validation of $reliability$ analysis given in this thesis. From the measurement results, the minimum required SINR at UE location for QPSK modulation is 18 dB and for 16QAM an SINR is 21 dB to meet the LTE conformance. These minimum required SINR requirements serve to derive the required $reliability$ at the UE locations. As comprehensively presented in this thesis, the $reliability$ then serves to reliably pair RRHs and UEs, finding frequency-reuse pairs, efficient power and scheduling allocations in C-RAN / DAS.

6 CONCLUSIONS AND FUTURE WORK

6.1 Conclusions

In this thesis, novel aspects of C-RAN / DAS systems were addressed, modeled, analyzed, simulated and validated with an objective to meet the very challenging requirement set on *Area traffic capacity* (10 Mbit/s/m^2) in 5G and Beyond eMBB *hotspot* scenario.

Driven by the key design principles of 5G and Beyond systems, *reliability* and *flexibility*, a novel C-RAN / DAS lower layer framework, which includes system model, novel RRH distribution and derived expressions for *reliability*, is comprehensively presented. In this regard, a novel *flexible* distribution of RRHs based on the optimum method of hexagonal packing of circles is presented. By means of mathematical expressions and simulation results, it is shown that this *novel* distribution achieves *flexibility* by offering an easier way of analyzing and controlling the required number of RRHs, system throughput and the total transmit power in C-RAN / DAS. Furthermore, through simulations it is shown that C-RAN / DAS has the potential to save more than 25 dB of total transmit power compared to conventional cellular systems, in case of same cell-edge coverage in both the systems.

A lower layer definition of *reliability*, which is the probability of achieving a minimum required SINR at a UE location, is shown to be utilized in the derivation of *reliability* in Rayleigh and Rician fading channel models. The derived *reliability* in NLOS and LOS scenarios were verified and proven using MATLAB models to have sufficient accuracy. In LOS scenarios the accuracy is validated within the constraint set of equidistant interferers. Through simulation resu lts, it is shown how the intensity of LOS component of interferers and desired signals effects the *reliability*, besides explaining the significance of these results in realistic C-RAN / DAS deployment scenarios like stadiums and shopping malls.

The key challenges in C-RAN / DAS systems in eMBB *hotspot* scenario investigated

in this work are: efficient pairing of UEs and RRHs, effective and low complexity solution of achieving frequency reuse, and fair DL power allocation among the RRHs within a reuse RRH group. (UE, RRH) pairing based on the measured pathloss is chosen, which is shown to achieve rapid frequency reuse by dense deployment of RRHs. With regard to frequency reuse, an efficient and low complexity method of finding frequency reuse RRH groups in C-RAN / DAS is presented, taking into consideration the UE requirements on *reliability* and *throughput*. In this regard, a *novel* expression for the minimum reuse distance is derived, which is shown to significantly reduce the overhead of collecting all the distance measurements and the computational complexity. Using MATLAB simulation model, it is shown how the reuse distance varies based on the UE locations and UE requirements. The advantage of using this novel reuse distance is that, it helps to analyze and exploit the reuse opportunities that arise due to different requirements of UEs in order to find the best fitting set of dynamic reuse RRH groups in a given scenario.

Within a reuse RRH group, the problem of optimal downlink (DL) power allocation among RRHs is formulated. In this work, the intention to meet *fairness* and *reliability* for all the users is shown by employing a *novel* utility function, which is based on *reliability*. The existence, uniqueness, and fairness for the cooperative game based on *novel* utility function are proven in detail using mathematical analysis of validation of all Nash conditions. In this regard, two theorems are postulated and proven to show the existence of a unique Nash Bargaining Solution (NBS). Accordingly, iterative Nash bargaining algorithms are developed, which are validated to converge to Pareto-optimal solution in 5-10 iterations. Subsequently, via simulation results, it is shown that C-RAN / DAS has the potential to achieve multifold throughput improvement based on the mean number of reuse RRHs. In some simulated scenarios, upto 50 fold throughput improvement is observed. This demonstrates the ability of C-RAN / DAS to meet the challenging requirements of eMBB *hotspot* scenario.

With an aim towards understanding the challenges encountered by C-RAN / DAS in 5G and Beyond Heterogeneous Mobile Networks (HMN), a detailed outline of the scope of demanding requirements that arise due to coexistence of manifold cellular systems and varied new and existing technologies, and the need for efficient control and coordination of radio resources, is elucidated. Consequently, a comprehensive set of solutions comprising of, a *novel* system level architecture for RAN, control and coordination methodology, and abstractions using network

graphs, is presented in detail. Different aspects of the novel *flexible* and *programmable* SDN based system level architecture, which was jointly achieved under COHERENT project, for 5G and Beyond HMN are described. Focusing on the challenges encountered by C-RAN / DAS in pairing and scheduling of resources in HMNs, various realistic scenarios and the methodology for control and coordination using RTC and C3 in these scenarios are presented. Furthermore, the abstractions of required parameters in these scenarios are formulated using the network graph generation methodology and the control framework. In various scenarios, the generated network graphs for pairing using simulation models are shown. In case of efficient scheduling, the need for interference based network graphs is explained and the required abstracted and exposed parameters are outlined. Therefore, in view of the multidimensional requirements of 5G and Beyond use cases and the challenges that arise due to coexistence of various cellular systems and technologies, the novel *flexible* and *programmable* architecture and the control and coordination methods via network graphs based abstractions are shown to have the potential to provide viable solutions for some key aspects of C-RAN / DAS in 5G and Beyond HMNs.

In order to validate the *novel* aspects described in this thesis, a SDR based real-time C-RAN / DAS testbed is implemented and validated using a commercial LTE test equipment, which is presented in detail. The validity of *reliability* is shown to have achieved by observing the error vector magnitude (EVM) measurements of LTE Physical Downlink shared Channel (PDSCH) on Keysight N9020A MXA signal analyzer along with 89600 VSA software, which is a commercial LTE test equipment. Different scenarios based on the placement of RRHs and UE locations as well as different transmit powers and modulation schemes have been investigated. In these trials, the measurement results that are captured on VSA software are presented with analysis. Almost linear mapping of the simulation results based on *reliability* to the measurement results has been achieved. From the measurement results it is observed that, in case of QPSK modulation an SINR above 18 dB and for 16QAM an SINR above 21 dB at the UE location is required to meet the conformance requirements of LTE, and these required SINR values in turn map to the targeted SINR requirements in the *reliability* expression. Additionally, a MATLAB based GUI has been implemented to generate Network graphs based on *reliability*. Therefore, the validation using the real-time testbed and commercial LTE test equipment demonstrates the feasibility of implementing the algorithms and solutions presented in this thesis in commercial C-RAN / DAS deployments.

Hence, by means of extensive theoretical analysis based on $reliability$ framework and the proposed solutions for 5G and Beyond eMBB *hotspot* scenarios, simulation models and real-time testbed based measurements validated by commercial LTE test equipment, it is shown that C-RAN / DAS technology has the potential to meet the challenging capabilities of multifold increase in *throughput* and *Area traffic capacity* via dense deployment of RRHs and rapid frequency reuse while maintaining $reliability$ and $fairness$ among UEs.

6.2 Future Work

Based on the analysis presented in this thesis, some further interesting and promising research directions in C-RAN / DAS for 5G and Beyond are described below:

- As the validation of the work presented in this thesis is achieved via real-time LTE testbed and commercial LTE test equipment, demonstrating the results could greatly motivate the industry to consider MAC and PHY layer solutions for implementation in C-RAN / DAS commercial deployments in order to monitor and control UE requirements reliably and fairly. This could be achieved with a direct partnership with industry or with a joint collaboration research project.

- Extension of the *reliability* framework to other 5G use cases: URLLC, where the requirements are very low *latency* and very high *reliability*; and mMTC, where very high *connection density* and very low *energy efficiency* are required. In these scenarios, it is very interesting to see the applicability of the *reliability* analysis presented in this thesis and the additional challenges which need to be addressed in C-RAN / DAS .

- The control and coordination of resources based on the COHERENT framework presented in this thesis can be implemented in a system level testbed. By emulating C-RAN / DAS and macro base stations radiating very high power scenario in a system level testbed, one can validate and measure the improvement in system performance, besides understanding its impact on system latency and control overhead. Furthermore, it is interesting to explore the improvement in latency by usage of graph theory on the generated network graphs in pairing and resource allocation.

- Other potential research area is the extension of reliability analysis considering multiple antennas at RRHs and the corresponding gain in system performance, reliability, spectral efficiency and diversity improvement, in comparison with single antenna RRHs. In this regard, the reliability based analysis for mulitple antennas CAS including sectoring, beamforming and spatial multiplexing techniques can be used as a baseline performance. Further, this analysis could be extended to cooperative communication aspects of RRHs such as Coordinated Multi-Point (CoMP) and RRH clustering, which are proven to be very effective to cell-edge UEs.

LIST OF PUBLICATIONS

Journals

(A) D. Peethala, T. Kaiser and A. J. H. Vinck, ”Reliability Analysis of Centralized Radio Access Networks in Non-Line-of-Sight and Line-of-Sight Scenarios,” in IEEE Access, vol. 7, pp. 18311-18318, 2019. doi: 10.1109/ACCESS.2019.2896410.

Conferences

(B) D. Peethala, N. Zarifeh and T. Kaiser, ”Probability of coverage based analysis of distributed antenna system and its implementation on LTE based real-time-testbed,” *2017 9th International Congress on Ultra Modern Telecommunications and Control Systems and Workshops (ICUMT)*, Munich, 2017, pp. 226-231.

(C) S. D. V. Peethala, T. Kreul and T. Kaiser, ”Real-time Testbed for Validating Distributed Antenna Scenarios,” *WSA 2016; 20th International ITG Workshop on Smart Antennas*, Munich, Germany, 2016, pp. 1-4.

(D) T. T. Nguyen, A. Kabbani, S. Peethala, T. Kreul and T. Kaiser, ”Experiments on spectrum sensing algorithms of pilot-added OFDM signals with a cognitive LTE-A system,” *2015 IEEE 20th International Workshop on Computer Aided Modelling and Design of Communication Links and Networks (CAMAD)*, Guildford, 2015, pp. 303-307.

(E) A. Kabbani, A. R. Ali, H. Cao, A. B. Güven, Y. Gao, S. Peethala, and T. Kaiser, ”Implementation Aspects of a DSP-Based LTE Cognitive Radio Testbed,” *Int. Conf. Cognitive Radio Oriented Wireless Networks (CROWNCOM)*, Qatar, April 2015, by Springer.

Standardization

(F) European Telecommunications Standards Institute, "Broadband Radio Access Networks (BRAN); Study of central coordination of WAS/RLANs operating in the 5 GHz frequency band," *European Telecommunications Standards Institute*, TR 103 494 V. 1.1.1. [Online]. Jan. 2018. Available: https://www.etsi.org/deliver/etsi_tr/103400_103499/103494/01.01.01_60/tr_103494v010101p.pdf [Accessed: Nov. 4, 2019] - Contributed.

Public Deliverables

(G) A. Anttonen, T. Chen, T. Suihko, A. Mammela, S. D. Peethala et al., "First report on physical and MAC layer modelling and abstraction," *COHERENT Deliverable D3.1*, July 2016. [Online]. Available: http://www.ict-coherent.eu/coherent/wp-content/uploads/2016/10/COHERENT_D3_1_PU_v1.0.pdf [Accessed: Nov. 4, 2019].

(H) N. Zarifeh, M. Alissa, S. D. Peethala et al., "Final report on physical and MAC layer modelling and abstraction," *COHERENT Deliverable D3.2*, Dec. 2017. [Online]. Available: http://www.ict-coherent.eu/coherent/wp-content/uploads/2018/03/COHERENT_D3.2_V1.0.pdf [Accessed: Nov. 4, 2019].

(I) K. Katsalis, N. Nikaien, D. Peethala et al., "Draft report on technical validation," *COHERENT Deliverable D6.1*, Jan. 2017. [Online]. Available: http://www.ict-coherent.eu/coherent/wp-content/uploads/2018/03/Coherent_D6.1_v1.0.pdf [Accessed: Nov. 4, 2019].

(J) M. Savela, T. Chen, S. D. Peethala et al., "Final Report on Technical Validation," *COHERENT Deliverable D6.2*, June 2018. [Online]. Available: http://www.ict-coherent.eu/coherent/wp-content/uploads/2018/08/COHERENT_D6_2_final.pdf [Accessed: Nov. 4, 2019].

Book Chapters

(K) A. Kabbani, A. R. Ali, H. Cao, A. B. Güven, Y. Gao, S. Peethala, and T. Kaiser, ”Implementation Aspects of a DSP-Based LTE Cognitive Radio Testbed.” In: M. Weichold , M. Hamdi , M. Shakir, M. Abdallah, G. Karagiannidis, M. Ismail (eds) ”Cognitive Radio Oriented Wireless Networks: 10th Internation Conference, CROWNCOM 2015.” vol 156. Springer, Cham, Oct. 2015. Online ISBN: 978-3-319-24540-9.

BIBLIOGRAPHY

[1] Recommendation ITU-R M.2083-0, "IMT Vision – Framework and overall objectives of the future development of IMT for 2020 and beyond," Tech. Rep., ITU-R, https://www.itu.int/rec/R-REC-M.2083, Sep 2015.

[2] COHERENT D2.1, "Use cases and architecture," Tech. Rep., 5G PPP, http://www.ict-coherent.eu/coherent/wp-content/uploads/2016/08/COHERENT_D2_1_v1.0.pdf, Jan. 2016.

[3] COHERENT D2.2, "System architecture and abstractions for mobile networks," Tech. Rep., 5G PPP, http://www.ict-coherent.eu/coherent/wp-content/uploads/2016/10/COHERENT_D2_2_PU_v1.0.pdf, July 2016.

[4] COHERENT D3.1, "First report on physical and mac layer modelling and abstraction," Tech. Rep., 5G PPP, http://www.ict-coherent.eu/coherent/wp-content/uploads/2016/10/COHERENT_D3_1_PU_v1.0.pdf, July 2016.

[5] D. Peethala, T. Kaiser, and A. J. H. Vinck, "Reliability analysis of centralized radio access networks in non-line-of-sight and line-of-sight scenarios," *IEEE Access*, vol. 7, pp. 18311–18318, 2019.

[6] Texas Instruments, "TMS320C6670 Data Manual (sprs689d)," Tech. Rep., Texas Instruments, http://www.ti.com/lit/ds/symlink/tms320c6670.pdf, Mar 2012.

[7] IAF, "Dual 6670 amc - data sheet," Tech. Rep., IAF GmbH, https://www.iaf-bs.de/content/products/flyer_dual_6670_amc_v4.pdf, April 2015.

[8] Texas Instruments, "Antenna Interface 2 (aif2) - User's Guide (sprugv7e)," Tech. Rep., Texas Instruments, http://www.ti.com/lit/ug/sprugv7e/sprugv7e.pdf, Feb 2015.

[9] Fraunhofer HHI, "SDR RADIO FRONTEND," Tech. Rep., Fraunhofer Henrich Hertz Institute, https://www.hhi.fraunhofer.de/fileadmin/PDF/WN/SDR/FraunhoferHHI_WN_SDRRadioFrontEnd.pdf, April 2015.

[10] D. Peethala, N. Zarifeh, and T. Kaiser, "Probability of coverage based analysis of distributed antenna system and its implementation on lte based real-time-testbed," in *2017 9th International Congress on Ultra Modern Telecommunications and Control Systems and Workshops (ICUMT)*, Nov 2017, pp. 226–231.

[11] COHERENT D6.1, "Draft report on technical validation," Tech. Rep., 5G PPP, http://www.ict-coherent.eu/coherent/wp-content/uploads/2018/03/Coherent_D6.1_v1.0.pdf, March 2016.

[12] COHERENT D6.2, "Final report on technical validation," Tech. Rep., 5G PPP, http://www.ict-coherent.eu/coherent/wp-content/uploads/2018/08/COHERENT_D6_2_final.pdf, June 2018.

[13] COHERENT D3.2, "Final report on physical and mac layer modelling and abstraction," Tech. Rep., 5G PPP, http://www.ict-coherent.eu/coherent/wp-content/uploads/2018/03/COHERENT_D3.2_V1.0.pdf, Dec 2017.

[14] European Telecommunications Standards Institute, "E-UTRA; Base Station (BS) conformance testing (3GPP TS 36.141 v. 9.8.0)," Tech. Rep., European Telecommunications Standards Institute, https://www.etsi.org/deliver/etsi_ts/136100_136199/136141/09.08.00_60/ts_136141v090800p.pdf, July 2011.

[15] Yang Yang, Jing Xu, Guang Shi, and Cheng-Xiang Wang, *5G Wireless Systems: Simulation and Evaluation Techniques (Wireless Networks)*, Springer, 2017.

[16] M. Shafi, A. F. Molisch, P. J. Smith, T. Haustein, P. Zhu, P. De Silva, F. Tufvesson, A. Benjebbour, and G. Wunder, "5g: A tutorial overview of standards, trials, challenges,

deployment, and practice," *IEEE Journal on Selected Areas in Communications*, vol. 35, no. 6, pp. 1201–1221, June 2017.

[17] NOKIA, "5G use cases and requirements," Tech. Rep., NOKIA, `https://www.ramonmillan.com/documentos/bibliografia/5GUseCases_Nokia.pdf`, Dec 2016.

[18] S. Ali, A. Ahmad, R. Iqbal, S. Saleem, and T. Umer, "Joint rrh-association, sub-channel assignment and power allocation in multi-tier 5g c-rans," *IEEE Access*, vol. 6, pp. 34393–34402, 2018.

[19] M. Mohammadi, H. A. Suraweera, and C. Tellambura, "Uplink/downlink rate analysis and impact of power allocation for full-duplex cloud-rans," *IEEE Transactions on Wireless Communications*, vol. 17, no. 9, pp. 5774–5788, Sept 2018.

[20] A. Checko, H. L. Christiansen, Y. Yan, L. Scolari, G. Kardaras, M. S. Berger, and L. Dittmann, "Cloud ran for mobile networks-a technology overview," *IEEE Communications Surveys Tutorials*, vol. 17, no. 1, pp. 405–426, Firstquarter 2015.

[21] R. Heath, S. Peters, Y. Wang, and J. Zhang, "A current perspective on distributed antenna systems for the downlink of cellular systems," *IEEE Communications Magazine*, vol. 51, no. 4, pp. 161–167, April 2013.

[22] W. Choi and J. G. Andrews, "Downlink performance and capacity of distributed antenna systems in a multicell environment," *IEEE Transactions on Wireless Communications*, vol. 6, no. 1, pp. 69–73, Jan 2007.

[23] Y. Lin and W. Yu, "Downlink spectral efficiency of distributed antenna systems under a stochastic model," *IEEE Transactions on Wireless Communications*, vol. 13, no. 12, pp. 6891–6902, Dec 2014.

[24] Lin Dai, Shidong Zhou, and Yan Yao, "Capacity analysis in cdma distributed antenna systems," *IEEE Transactions on Wireless Communications*, vol. 4, no. 6, pp. 2613–2620, Nov 2005.

[25] X. You, D. Wang, B. Sheng, X. Gao, X. Zhao, and M. Chen, "Cooperative distributed antenna systems for mobile communications [coordinated and distributed mimo]," *IEEE Wireless Communications*, vol. 17, no. 3, pp. 35–43, June 2010.

[26] Z. Liu and L. Dai, "A comparative study of downlink mimo cellular networks with co-located and distributed base-station antennas," *IEEE Transactions on Wireless Communications*, vol. 13, no. 11, pp. 6259–6274, Nov 2014.

[27] P. Chow, A. Karim, V. Fung, and C. Dietrich, "Performance advantages of distributed antennas in indoor wireless communication systems," in *Proceedings of IEEE Vehicular Technology Conference (VTC)*, June 1994, pp. 1522–1526 vol.3.

[28] NGNM Alliance, "5G White Paper," Tech. Rep., NGNM, `https://www.ngmn.org/fileadmin/ngmn/content/images/news/ngmn_news/NGMN_5G_White_Paper_V1_0.pdf`, Feb 2015.

[29] J. Ordonez-Lucena, P. Ameigeiras, D. Lopez, J. J. Ramos-Munoz, J. Lorca, and J. Folgueira, "Network slicing for 5g with sdn/nfv: Concepts, architectures, and challenges," *IEEE Communications Magazine*, vol. 55, no. 5, pp. 80–87, May 2017.

[30] F. Z. Yousaf, M. Bredel, S. Schaller, and F. Schneider, "Nfv and sdn—key technology enablers for 5g networks," *IEEE Journal on Selected Areas in Communications*, vol. 35, no. 11, pp. 2468–2478, Nov 2017.

[31] L. Wang H. Chang, "A simple proof of thue's theorem on circle packing," Tech. Rep., National Taiwan University, `https://arxiv.org/pdf/1009.4322.pdf`, Sep 2010.

[32] S. D. V. Peethala, T. Kreul, and T. Kaiser, "Real-time testbed for validating distributed antenna scenarios," in *WSA 2016; 20th International ITG Workshop on Smart Antennas*, March 2016, pp. 1–4.

[33] Y. Qian, M. Chen, X. Wang, and P. Zhu, "Antenna location design for distributed antenna systems with selective transmission," in *2009 International Conference on Wireless Communications Signal Processing*, Nov 2009, pp. 1–5.

[34] J. Zhang and J. G. Andrews, "Distributed antenna systems with randomness," *IEEE Transactions on Wireless Communications*, vol. 7, no. 9, pp. 3636–3646, September 2008.

[35] E. Park, S. Lee, and I. Lee, "Antenna placement optimization for distributed antenna systems," *IEEE Transactions on Wireless Communications*, vol. 11, no. 7, pp. 2468–2477, July 2012.

[36] European Telecommunications Standards Institute, "E-UTRA; base Station (BS) conformance testing (3GPP TS 36.141 version 9.2.0)," Tech. Rep., European Telecommunications Standards Institute, `https://www.etsi.org/deliver/etsi_ts/136100_136199/136141/09.02.00_60/ts_136141v090200p.pdf`, Feb 2010.

[37] J. Sanchez-Garcia and D. R. Smith, "Capture probability in rician fading channels with power control in the transmitters," *IEEE Transactions on Communications*, vol. 50, no. 12, pp. 1889–1891, Dec 2002.

[38] I. A. Stegun M. Abramowitz, *Handbook of Mathematical Functions*, New York:Dover, 1 edition, 1964.

[39] K. T. Truong and R. W. Heath, "The viability of distributed antennas for massive mimo systems," in *2013 Asilomar Conference on Signals, Systems and Computers*, Nov 2013, pp. 1318–1323.

[40] A. A. M. Saleh, A. Rustako, and R. Roman, "Distributed antennas for indoor radio communications," *IEEE Transactions on Communications*, vol. 35, no. 12, pp. 1245–1251, December 1987.

[41] H. Kim, S. Lee, and I. Lee, "Sum rate based transmission selection schemes in distributed antenna systems," in *2013 IEEE 77th Vehicular Technology Conference (VTC Spring)*, June 2013, pp. 1–5.

[42] Y. Lin and W. Yu, "Downlink spectral efficiency of distributed antenna systems under a stochastic model," *IEEE Transactions on Wireless Communications*, vol. 13, no. 12, pp. 6891–6902, Dec 2014.

[43] C. Yang, J. Li, and Z. Tian, "Optimal power control for cognitive radio networks under coupled interference constraints: A cooperative game-theoretic perspective," *IEEE Transactions on Vehicular Technology*, vol. 59, no. 4, pp. 1696–1706, May 2010.

[44] G. Scutari, D. P. Palomar, and S. Barbarossa, "Asynchronous iterative water-filling for gaussian frequency-selective interference channels: A unified framework," in *2006 IEEE 7th Workshop on Signal Processing Advances in Wireless Communications*, July 2006, pp. 1–5.

[45] Zhu Han, Zhu Ji, and K. J. R. Liu, "Fair multiuser channel allocation for ofdma networks using nash bargaining solutions and coalitions," *IEEE Transactions on Communications*, vol. 53, no. 8, pp. 1366–1376, Aug 2005.

[46] S. Koskie and Z. Gajic, "A nash game algorithm for sir-based power control in 3g wireless cdma networks," *IEEE/ACM Transactions on Networking*, vol. 13, no. 5, pp. 1017–1026, Oct 2005.

[47] A. B. MacKenzie and S. B. Wicker, "Game theory in communications: motivation, explanation, and application to power control," in *GLOBECOM'01. IEEE Global Telecommunications Conference (Cat. No.01CH37270)*, Nov 2001, vol. 2, pp. 821–826 vol.2.

[48] F. A. Khan, H. He, J. Xue, and T. Ratnarajah, "Performance analysis of cloud radio access networks with distributed multiple antenna remote radio heads," *IEEE Transactions on Signal Processing*, vol. 63, no. 18, pp. 4784–4799, Sept 2015.

[49] C. Pan, H. Zhu, N. J. Gomes, and J. Wang, "Joint precoding and rrh selection for user-centric green mimo c-ran," *IEEE Transactions on Wireless Communications*, vol. 16, no. 5, pp. 2891–2906, May 2017.

[50] European Telecommunications Standards Institute, "Physical layer procedures (release 9) (3gpp ts 36.213 v9.2.0)," Tech. Rep., European Telecommunications Standards Institute, `https://www.etsi.org/deliver/etsi_ts/136200_136299/136213/09.02.00_60/ts_136213v090200p.pdf`, June 2010.

[51] Guocong Song and Ye Li, "Cross-layer optimization for ofdm wireless networks-part i: theoretical framework," *IEEE Transactions on Wireless Communications*, vol. 4, no. 2, pp. 614–624, March 2005.

[52] H. E. E. O. M. Elfadil, M. A. I. Ali, and M. Abas, "Fractional frequency reuse in lte networks," in *2015 2nd World Symposium on Web Applications and Networking (WSWAN)*, March 2015, pp. 1–6.

[53] T. D. Novlan, R. K. Ganti, A. Ghosh, and J. G. Andrews, "Analytical evaluation of fractional frequency reuse for ofdma cellular networks," *IEEE Transactions on Wireless Communications*, vol. 10, no. 12, pp. 4294–4305, December 2011.

[54] J. E. Suris, L. A. DaSilva, Z. Han, and A. B. MacKenzie, "Cooperative game theory for distributed spectrum sharing," in *2007 IEEE International Conference on Communications*, June 2007, pp. 5282–5287.

[55] Guilin Wang, Haojun Zhang, Yanqin Zhu, Qijin Ji, and Haifeng Shen, "Nash bargaining between friends for cooperative data distribution in a social peer-to-peer swarming system," in *2013 International Conference on Machine Learning and Cybernetics*, July 2013, vol. 04, pp. 1490–1495.

[56] L. Zhou, "The nash bargaining theory with non-convex problems," *Econometrica*, vol. 65, pp. 681–685, May 1997.

[57] J. E. Suris, L. A. DaSilva, Z. Han, and A. B. MacKenzie, "Cooperative game theory for distributed spectrum sharing," in *2007 IEEE International Conference on Communications*, June 2007, pp. 5282–5287.

[58] Zhu Han, Zhu Ji, and K. J. R. Liu, "Fair multiuser channel allocation for ofdma networks using nash bargaining solutions and coalitions," *IEEE Transactions on Communications*, vol. 53, no. 8, pp. 1366–1376, Aug 2005.

[59] J. Nash, "Two-person cooperative games," *Econometrica*, vol. 21, no. 12, pp. 128–140, 1953.

[60] H. Boche and M. Schubert, "A generalization of nash bargaining and proportional fairness to log-convex utility sets with power constraints," *IEEE Transactions on Information Theory*, vol. 57, no. 6, pp. 3390–3404, June 2011.

[61] Chi Wan Sung, "Log-convexity property of the feasible sir region in power-controlled cellular systems," *IEEE Communications Letters*, vol. 6, no. 6, pp. 248–249, June 2002.

[62] H. Boche and S. Stanczak, "Convexity of some feasible qos regions and asymptotic behavior of the minimum total power in cdma systems," *IEEE Transactions on Communications*, vol. 52, no. 12, pp. 2190–2197, Dec 2004.

[63] M. Schubert and H. Boche, "Nash bargaining and proportional fairness for log-convex utility sets," in *2008 IEEE International Conference on Acoustics, Speech and Signal Processing*, March 2008, pp. 3157–3160.

[64] D. Fudenberg and J. Tirole, *Game Theory*, Cambridge, MA: MIT Press, 1991.

[65] S. Boyd and A. Mutapcic, "Subgradient methods," Tech. Rep., Stanford University, `https://see.stanford.edu/materials/lsocoee364b/02-subgrad_method_notes.pdf`, April 2008.

[66] S. E. E. Ayouibi M. Maternia, "5g ppp use cases and performance evaluation models," Tech. Rep., 5G PPP, `https://5g-ppp.eu/wp-content/uploads/2014/02/5G-PPP-use-cases-and-performance-evaluation-modeling_v1.0.pdf`, April 2016.

[67] J. G. Andrews, S. Buzzi, W. Choi, S. V. Hanly, A. Lozano, A. C. K. Soong, and J. C. Zhang, "What will 5g be?," *IEEE Journal on Selected Areas in Communications*, vol. 32, no. 6, pp. 1065–1082, June 2014.

[68] F. Boccardi, R. W. Heath, A. Lozano, T. L. Marzetta, and P. Popovski, "Five disruptive technology directions for 5g," *IEEE Communications Magazine*, vol. 52, no. 2, pp. 74–80, February 2014.

[69] P. Demestichas, A. Georgakopoulos, D. Karvounas, K. Tsagkaris, V. Stavroulaki, J. Lu, C. Xiong, and J. Yao, "5g on the horizon: Key challenges for the radio-access network," *IEEE Vehicular Technology Magazine*, vol. 8, no. 3, pp. 47–53, Sept 2013.

[70] A. Gupta and R. K. Jha, "A survey of 5g network: Architecture and emerging technologies," *IEEE Access*, vol. 3, pp. 1206–1232, 2015.

[71] D. C. Cox and H. Lee, "Physical relationships," *IEEE Microwave Magazine*, vol. 9, no. 4, pp. 89–94, Aug 2008.

[72] X. Zhang and J. G. Andrews, "Downlink cellular network analysis with multi-slope path loss models," *IEEE Transactions on Communications*, vol. 63, no. 5, pp. 1881–1894, May 2015.

[73] C. Prehofer and C. Bettstetter, "Self-organization in communication networks: principles and design paradigms," *IEEE Communications Magazine*, vol. 43, no. 7, pp. 78–85, July 2005.

[74] European Telecommunications Standards Institute, "Broadband Radio Access Networks (BRAN); Study of central coordination of WAS/RLANs operating in the 5 ghz frequency band," Tech. Rep., European Telecommunications Standards Institute, ETSI TR 103 494, V1.1.1, `https://www.etsi.org/deliver/etsi_tr/103400_103499/103494/01.01.01_60/tr_103494v010101p.pdf`, Jan. 2018.

[75] Ericsson Technical White paper, "5g systems – enabling industry and society transformation," Tech. Rep., Ericsson, `https://www.ericsson.com/assets/local/news/2015/1/what-is-a-5g-system.pdf`, Jan 2015.

[76] F. Ahmed et al., "Distributed graph coloring for self-organization in lte networks," *Journal of Electrical and Computer Engineering*, 2010.

[77] P. Cardieri, "Modeling interference in wireless ad hoc networks," *IEEE Communications Surveys Tutorials*, vol. 12, no. 4, pp. 551–572, Fourth 2010.

[78] OpenFlow, "https://www.opennetworking.org/sdn-resources/openflow," .

[79] IETF RFC 6241, "Network configuration protocol (netconf)," Tech. Rep., IETF, `https://tools.ietf.org/html/rfc6241`, June 2011.

[80] IETF RFC 5415, "Control and provisioning of wireless access points (capwap) protocol specification," Tech. Rep., IETF, `https://tools.ietf.org/html/rfc5415`, Mar. 2009.

[81] IETF RFC 5412, "Lightweight access point protocol," Tech. Rep., IETF, `https://tools.ietf.org/html/rfc5412`, Feb 2010.

[82] 3rd Generation Partnership Project, "E-UTRA; Further advancements for e-utra physical layer aspects (3GPP TR 36.814 v9.2.0)," Tech. Rep., 3rd Generation Partnership Project, https://portal.3gpp.org/desktopmodules/Specifications/SpecificationDetails.aspx?specificationId=2493, Mar. 2017.

[83] European Telecommunications Standards Institute, "E-UTRA; Physical layer procedures (3GPP TS 36.213 version 10.1.0 release 10)," Tech. Rep., European Telecommunications Standards Institute, https://www.etsi.org/deliver/etsi_ts/136200_136299/136213/10.01.00_60/ts_136213v100100p.pdf, April 2011.

[84] Texas Instruments, "Bit Rate Coprocessor (BCP) - User's Guide (sprugz1a)," Tech. Rep., Texas Instruments, http://www.ti.com/lit/ug/sprugv7e/sprugv7e.pdf, May 2015.

[85] Texas Instruments, "Multicore Navigator - User's Guide (sprugr9h)," Tech. Rep., Texas Instruments, http://www.ti.com/lit/ug/sprugv7e/sprugv7e.pdf, April 2015.

[86] European Telecommunications Standards Institute, "E-UTRA; Physical channels and modulation (3GPP TS 36.211 v9.0.0)," Tech. Rep., European Telecommunications Standards Institute, https://www.etsi.org/deliver/etsi_ts/136200_136299/136211/09.00.00_60/ts_136211v090000p.pdf, Jan. 2010.

[87] European Telecommunications Standards Institute, "E-UTRA; Multiplexing and channel coding (3GPP TS 36.212 v9.2.0)," Tech. Rep., European Telecommunications Standards Institute, https://www.etsi.org/deliver/etsi_ts/136200_136299/136212/09.02.00_60/ts_136212v090200p.pdf, June 2010.

[88] European Telecommunications Standards Institute, "E-UTRA; Physical layer procedures (3GPP TS 36.213 v9.2.0)," Tech. Rep., European Telecommunications Standards Institute, https://www.etsi.org/deliver/etsi_ts/136200_136299/136213/09.02.00_60/ts_136213v090200p.pdf, June 2010.

[89] European Telecommunications Standards Institute, "E-UTRA; Physical layer; measurements (3GPP TS 36.214 v9.2.0)," Tech. Rep., European Telecommunications

Standards Institute, https://www.etsi.org/deliver/etsi_ts/136200_136299/136214/09.02.00_60/ts_136214v090200p.pdf, June 2010.

[90] European Telecommunications Standards Institute, "E-UTRA; User Equipment (UE) radio transmission and reception (3GPP TS 36 101 v9.2.0)," Tech. Rep., European Telecommunications Standards Institute, https://www.etsi.org/deliver/etsi_ts/136100_136199/136101/09.02.00_60/ts_136101v090200p.pdf, June 2010.

[91] European Telecommunications Standards Institute, "Radio Resource Control (RRC) Protocol specification (release 9) (3gpp ts 36.331 v9.12.0)," Tech. Rep., European Telecommunications Standards Institute, https://www.etsi.org/deliver/etsi_ts/136300_136399/136331/09.12.00_60/ts_136331v091200p.pdf, December 2012.

[92] Keysight, "N9020A MXA Signal Analyzer," https://www.keysight.com/de/pdx-x202266-pn-N9020A/mxa-signal-analyzer-10-hz-to-265-ghz?pm=spc&nid=-32508.1150426&cc=DE&lc=ger, Online; accessed Dec. 13, 2018.

DOI: 10.17185/duepublico/74939
URN: urn:nbn:de:hbz:464-20211111-144029-2